THE PHOTOCHEMISTRY OF COBALT(III)-AMINOACIDATO COMPLEXES

A thesis

submitted in partial fulfilment

of the requirements for the degree

of

Doctor of Philosophy in Chemistry

at the

University of Canterbury

by

Shane G. Telfer

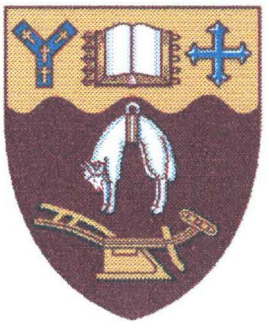

University of Canterbury

March, 1999

Education is an admirable thing. But it is well to remember from time to time that nothing that is worth knowing can be taught.

Oscar Wilde

SYNOPSIS

The photodecarboxylation reaction of Co(III)-aminocarboxylato complexes has been examined from several angles. Firstly, the currently accepted mechanism for the formation of $[Co(bpy)_2(CH_2NH_2)]^{2+}$, following the UV photolysis of $[Co(bpy)_2(gly)]^{2+}$ (bpy = 2,2'-bipyridine, gly = glycinate), has been tested. A Co(II)-bound α-aminoalkyl radical, with a lifetime of around 10^{-4} s, has been proposed as a reaction intermediate. This assertion was tested with the use of a radical clock, derived from chelated cyclopropylglycine. If a Co(II)-bound aminocyclopropylmethyl radical is formed, it will ring-open with rate constant $k \geq 10^7$ s^{-1} (298 K). This rate constant has been estimated on the basis of transition-state theoretical calculations and published data for related radicals.

The cyclopropyl group actually survived photolysis, and was found as cyclopropanecarboxaldehyde. This result implies that either the rate determining step has been wrongly assigned, or the proposed mechanism is incorrect.

Carbonyl compounds were also detected following the photolysis of $[Co(bpy)_2(aa)]^{2+}$ complexes, where aa = alaninate, valinate, phenylglycinate, and aminoisobutyrate. It was proposed that a Co–C–N metallacycle is formed briefly, but decomposes to give a Co(I) complex and an iminium ion. Hydrolysis of the latter fragment would account for the carbonyl compounds.

Secondly, some novel Co–C–N metallacycles have been prepared via the photodecarboxylation reaction. Cobalt(III) complexes with N,N-bis(2-pyridylmethyl)aminoacidate (amino acid = glycine, alanine, and cyclopropylglycine) ligands with 1,10-phenanthroline (phen) filling the remaining coordination sites, were prepared. Upon UV photolysis in aqueous solution, all three complexes yielded Co–C–N metallacycles which were sufficiently stable to allow characterisation by conventional

^{1}H NMR, ^{13}C NMR, and UV-vis techniques. The solid state structure of the photolysis product of the glycinate derivative was determined by X-ray crystallography. These organometallic products eventually decompose, giving carbonyl compounds, free bis(2-pyridylmethyl)amine (bpa), free phen and the Co(II) ion. A peroxo-bridged Co(III) dimer, $[Co(phen)(bpa)(O_2)Co(phen)(bpa)]^{4+}$, crystallised from this mixture, and was characterised by X-ray crystallography.

Thirdly, the UV photolysis reactions of a series of $[Co(bpy)_2(aa)]^{2+}$ in DMSO solution were investigated. Carbonyl compounds are also produced in this solvent. The formation of *trans*(N)-$[Co(aa)_2(bpy)]^{+}$ complexes was also observed. This was ascribed to secondary (thermal) chemistry between dissolved molecular oxygen and some of the photolysis products: free amino acid, free phen, and Co(II). This same mixture gave rise to the $[Co(bpy)_3]^{3+}$ ion in aqueous solution. This difference was rationalised on the basis of the equilibria of the various $[Co^{II}(aa)_x(bpy)_y]^{(2-x)+}$ complexes in the different solvents, and the potentials at which they are oxidised.

ACKNOWLEDGMENTS

I would like to take this opportunity to thank a number of people who have made my time in the Chemistry Department a stimulating experience.

Foremost, Dr Richard Hartshorn: supervisor *par excellence*. I am extremely grateful to have benefited from Richard's expansive knowledge and his passion for teaching. Thanks Richard for creating an excellent atmosphere for learning chemistry.

Special mention must be made of the academic staff who have assisted me in broadening the scope of this thesis beyond the traditional boundaries of inorganic chemistry. The "open-door" policy of the academic staff was truly invaluable.

I would also like to thank some of my fellow students. Mark Rees and James Butchard, whose interesting and articulate conversations have made the last three years both socially and intellectually rewarding. Mark was also instrumental in the development of the theoretical component of this thesis. Andy Phillips' willingness to share his knowledge of organic chemistry was greatly appreciated.

Finally, I thank my parents for a world of opportunties.

TABLE OF CONTENTS

ABBREVIATIONS

aa	amino acidate
aib	aminoisobutyrate
ala	alaninate
bpa	bis(2-pyridylmethyl)amine
bpy	2,2'-bipyridine
COSY	2D ^{1}H NMR correlation spectroscopy
cpg	2-cyclopropylglycinate
DFT	density functional theory
DMSO	dimethylsulfoxide
dpa	N,N-(2-pyridylmethyl)-L-alaninate
dpc	N,N-(2-pyridylmethyl)-2-cyclopropylglycinate
dpg	N,N-(2-pyridylmethyl)glycinate
edda	ethylenediamine-N,N'-diacetate
eddp	ethylenediamine-N,N'-dipropionate
edta	ethylenediamine-N,N,N',N'-tetraacetate
EI	electron impact (in mass spectrometry)
en	1,2-diaminoethane
FAB	fast atom bombardment (in mass spectrometry)
gly	glycinate
ida	iminodiacetate
iod	2-amino-4-iodo-butyrate
pdda	1,3-propanediamine-N,N'-diacetate

LMCT	ligand to metal charge transfer
pgly	2-phenylglycinate
phen	1,10-phenanthroline
pro	prolinate
TEMPO	2,2,6,6-tetramethyl-1-piperidinyloxy free radical
TMPS	sodium trimethylsilylpropanesulfonate
tren	tris(2-aminoethyl)amine
UV	ultra violet frequency light
val	valinate
vis	visible (light)

CHAPTER ONE

INTRODUCTION

> "If our black and nervous civilisation, based on coal, shall be followed by a quieter civilisation based on the utilisation of solar energy, that will not be harmful to progress and to human happiness."
>
> Giacomo Ciamician, 1912.[1]

Photochemistry - the study of the interaction between light and matter. The subject is vast, and is propelled by a range of motivations: by *intellectual curiosity*, from the Beer-Lambert law to the ultra-violet catastrophe; by *practical applications*, to the point of "whiter-than-white" washing powders; and by a desire to *understand the natural world*, "how does a firefly glow?".

The various sections of this thesis, although covering some rather diverse aspects of chemistry, are linked by a common thread: the photochemistry of cobalt(III) complexes which contain amino acids as ligands. The general field contains elements of the three broad motivations for investigating photochemical questions from above, however, the primary motivation in this instance has been intellectual curiosity.

This chapter presents an introduction to the field of photochemistry, with a particular emphasis on transition metal photochemistry. A background to the 'dark' chemistry of Co(III) complexes is then given, before the photochemistry of these compounds is outlined. The focus is then narrowed down to the photochemistry of Co(III) complexes which have amino acids as ligands, and an overview of previous work in this field is presented.

The photochemistry of transition-metal complexes

What is the nature of the interaction of light with matter?

The energy levels in matter are quantised, that is, they can take only certain, discrete values. The absorption of a photon, or a "packet" of light energy, can induce a change in the *electronic* energy level of a molecule. If the energy of an incident photon corresponds to the energy difference between the two electronic levels, absorption can occur. Each photon which is absorbed can directly activate only one molecule. Transitions usually take place from the lowest electronic energy level of a molecule, the *ground state*, and the molecule ends up in a higher energy level, or *excited state*. For electronic transitions, the energy difference corresponds to light in the ultra-violet to visible (200 - 900 nm) range.

For an effective electronic transition, there must be an interaction between the electric field vector of the light and the electric dipole of the molecule. The probability of absorption, which can be expressed in quantum mechanical terms, is related to the observed intensity of the absorption *via* the experimentally measurable extinction coefficient (ε). This relationship is expressed by the well-known Beer-Lambert law.

$$A = \varepsilon\, cl = \log \frac{I_0}{I} \qquad (1.1)$$

The spectrophotometrically measured absorbance is related to the concentration of the absorbing species (c), the path length of light through the solution (l), and the extinction coefficient (or molar absorptivity coefficient) (ε). I is the intensity of light transmitted, and I_0 is the intensity of the incident light.

Selection rules are a convenient way to summarize the quantum mechanical conditions which govern the absorption of a photon. Firstly, the spin multiplicity may not change during an electronic transition. Spin forbidden transitions may find intensity in some cases, however, for example for heavy atoms which have significant spin-orbit coupling. Secondly, transitions between orbitals of the same parity are 'Laporte-forbidden'. In reality, many transitions which are formally Laporte-forbidden, for example d-d transitions in coordination compounds, attain moderate intensity owing to the coupling of electronic and vibrational motions.

Electronic transitions for coordination compounds

A large variety of electronic transitions are possible for coordination compounds.[2] Two of those which are encountered most frequently, d-d transitions and ligand-to-metal charge transfer transitions (LMCT), are outlined presently.

Ligand-field, or d-d transitions, involve the transition of an electron within the non-degenerate set of d orbitals which are localised predominantly on the central metal atom. They are Laporte-forbidden and can be spin-forbidden. They are characterised by molar absorptivity coefficients in the range $\varepsilon \approx 10^1 - 10^2$ $Lmol^{-1}cm^{-1}$. The energies corresponding to these transitions are very sensitive to the symmetry around the metal centre, and the nature of the donor atoms. Ligand-field excited states have a tendency to undergo substitution reactions due to the changes in the metal-ligand force constants.[2]

LMCT excitations formally involve the transfer of electron density from an molecular orbital localised primarily on a ligand, to one localised on the metal. The transitions are usually spin- and Laporte-allowed, and have $\varepsilon \approx 10^3 - 10^6$ $Lmol^{-1}cm^{-1}$. The energy of this transition is loosely related to the ionisation energy of the ligand and the reduction potential of the metal ion. Inner-sphere redox processes can be induced by the radial shift of electron density, whilst ligand substitution can be activated by the population of anti-bonding orbitals.[2]

Deactivation processes

Electronically excited states of coordination compounds, as for any compound, can be deactivated by many different pathways (Fig 1.1).

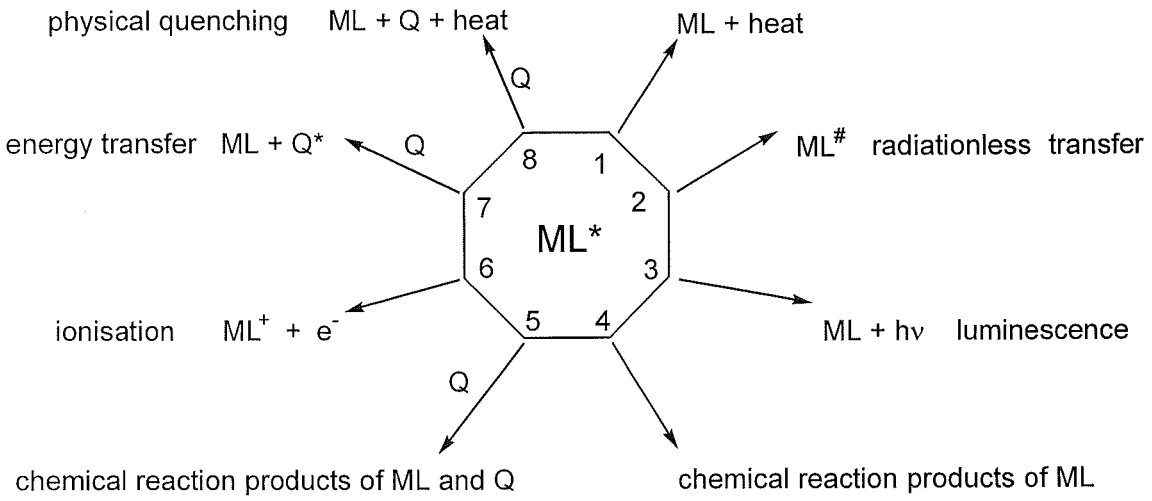

Figure 1.1. Some possible deactivation processes for excited states.

Deactivation pathways of the excited state can be classified as either photo*physical* or photo*chemical* processes, depending on whether a chemical change is induced in the complex. The efficiency of a particular primary process is quantified by a quantum yield, which is defined as:

$$\phi = \frac{\text{number of molecules undergoing that process}}{\text{number of photons absorbed by the reactant}} \qquad (1.2)$$

Photophysical deactivation processes

One of the most important photophysical deactivation processes is radiationless transfer (2) which refers to the transition between two distinct excited states. Internal conversion is the transition to another electronic state of the same multiplicity, while intersystem crossing populates an electronic state which has a different spin. The nascent excited states are usually "hot", that is, vibrationally excited. These processes are significant in that they may allow the population of excited states which are not directly attainable by optical absorption. The new excited state will decay *via* one of the processes in Fig 1.1. The intersystem crossing process is spin forbidden, however the presence of a heavy atom facilitates the conversion. For coordination compounds, the kinetics of internal conversion and intersystem crossing are very similar; $k_{ic} \approx 10^{12}$ s^{-1}, and $k_{isc} \approx 10^{9}$ - 10^{13} s^{-1}.[2]

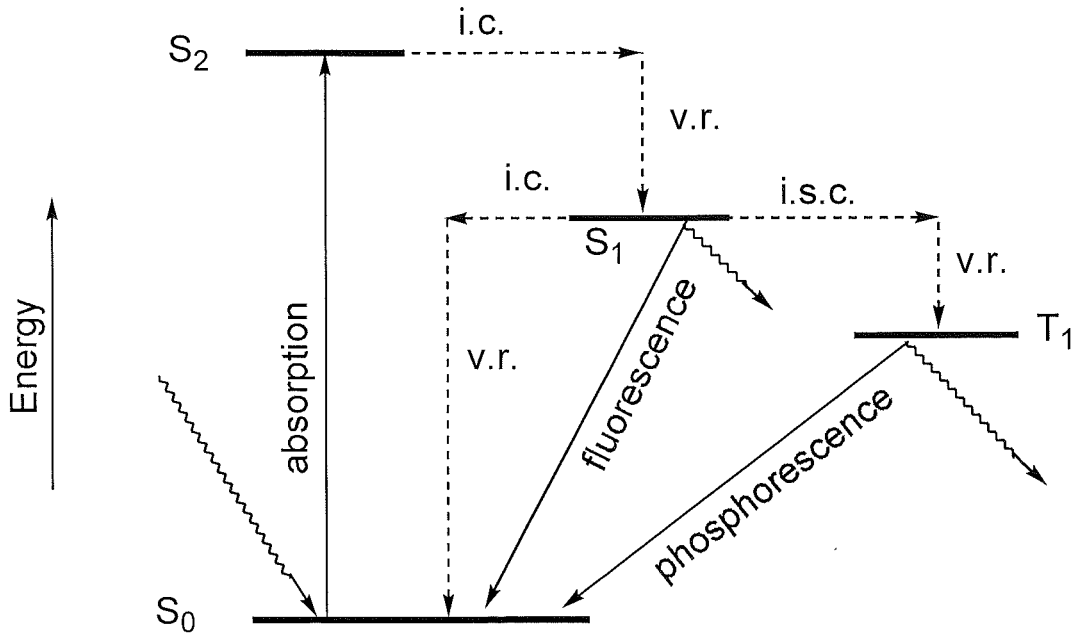

Figure 1.2. A selection of intramolecular photophysical processes. The full arrows correspond to radiative processes, the dashed arrows to non-radiative processes. Internal conversion (i.c.), intersystem crossing (i.s.c.), and vibrational relaxation (v.r.) are abbreviated. S represents a singlet state, and T a triplet state.

The term luminescence (3) covers the phenomena of fluorescence and phosphorescence. Fluorescence is an emission of radiation from a singlet excited state. The emitted radiation is of lower energy than the absorbed radiation due to the fact that the excited state must shed some excess vibrational energy before it emits the fluorescent light. Phosphorescence is a radiative transition from a triplet state to the ground state. Generally, intersystem crossing must occur to populate this triplet state. This transition, and the emission, are both facilitated by the presence of a heavy atom. These processes are summarised in Fig 1.2.

Photochemical deactivation processes

Excited states have molecular structures and thermodynamic properties which may differ markedly from the ground state. The excited state may be able to make use of its excess energy to undergo reactions which are not available to the ground state molecule. For instance, excitation can be associated with significant radial and angular distortions which may promote bond cleavage. If photochemical processes are to compete with physical deactivation of the excited state, paths of low activation energy must be followed. The photochemical reactions of transition-metal complexes have been reviewed in detail by Sima.[2] The following section contains a few representative examples, which cover the most important categories of photochemical reactions.

Outer-sphere redox reactions

Outer sphere redox reactions can take place between the excited state and a suitable quencher (Eqtn 1.3). The excited state is often both a more powerful reductant (since an electron has been promoted to a high-energy orbital), and oxidant (because there is now a "hole" in a low-energy orbital) than the ground state. A redox reaction may take place if there is a suitable oxidising or reducing species in the surrounding medium.

$$A^* + Q \rightarrow A^{\pm} + Q^{\mp} \qquad (1.3)$$

A well-studied example is the redox quenching of an excited state of $[Ru(bpy)_3]^{2+}$ by hydrated Fe^{3+} cations (Eqtn 1.4).[3] The reduction potentials ($E_0(*[Ru(bpy)_3]^{3+}/[Ru(bpy)_3]^{2+}) = -0.86$ V, $E_0(Fe^{3+}/Fe^{2+} = +0.77$ V)) indicate that the process is quite exergonic.

$$*[Ru(bpy)_3]^{2+} + Fe^{3+} \rightarrow [Ru(bpy)_3]^{3+} + Fe^{2+} \qquad (1.4)$$

Photoredox elimination and addition processes

The redox properties of the excited state can also activate the complex to photoredox *elimination* and *addition* reactions. These result in a change in the oxidation state of the central metal ion along with a change in the coordination number of the complex. Often the products are transient species which react further in secondary (thermal) reactions to give the observed products. Photoaddition reactions stem from an increase in the Lewis acidity of the metal upon excitation. An example is the oxidative addition of $CHCl_3$ to $[Pt^{II}Cl_2(bpy)_2]$, which proceeds *via* a MLCT excited state (Eqtn 1.5).[4]

$$[Pt^{II}Cl_2(bpy)_2] \xrightarrow{h\nu, CHCl_3} [Pt^{IV}Cl_4(bpy)_2] \qquad (1.5)$$

Intramolecular redox processes

Redox processes can also take place in an *intramolecular* fashion, whereby an electron is (formally) exchanged between the central metal atom and a coordinated ligand. LMCT states, populated either by direct excitation, or *via* non-radiative transitions from other excited states, are frequently responsible for these inner-sphere redox processes. The primary products, a reduced metal centre and an oxidised ligand, are often quite reactive and will undergo secondary thermal reactions. The photochemical reactivity of $[CuCl_4]^{2-}$ illustrates these points (Eqtns 1.6 and 1.7).[5]

$$[CuCl_4]^{2-} \xrightarrow{h\nu} [CuCl_3]^{2-} + Cl\cdot \qquad (1.6)$$

$$Cl\cdot + Cl\cdot \rightarrow Cl_2 \qquad (1.7)$$

Photochemical isomerisation reactions

The excess energy of an excited state can be channelled into photochemical isomerisation processes. Many different classes of isomerisations have been reported, including transformations between linkage isomers, optical isomers, geometrical isomers, and tautomers. The processes are often mediated by transients formed *via* inner-sphere redox pathways. A large amount of interest has focussed on the linkage isomerisation reaction of the $[Co(NH_3)_5(NO_2)]^{2+}$ complex (Eqtn 1.8).[6] The NO_2^- ligand can coordinate *via* the nitrogen atom ("nitro"), or *via* an oxygen atom ("nitrito"). The photochemical transformation between these two forms has been proposed to occur following the photoinduced formation of a Co(II)-ligand radical pair, followed by re-oxidation of the metal centre.

$$\left[Co^{III}(NH_3)_5(NO_2)\right]^{2+} \xrightarrow{h\nu} \left[Co^{II}(NH_3)_5\right]^{2+}, \dot{N}O_2 \longrightarrow \left[Co^{III}(NH_3)_5(ONO)\right]^{2+} \quad (1.8)$$

Photosubstitution reactions

Photosubstitution reactions of transition-metal complexes comprise a large subset of the photochemical reactions observed for these compounds. The term photosubstitution refers to the ligand exchange between the primary and secondary coordination spheres, with preservation of the oxidation state and coordination number of the metal ion. Aquation is the most common outcome from the photosubstitution avenue, as most photochemical studies have been performed on aqueous solutions. The interested reader is directed to a full review of this topic.[2]

Developments in the field of transition-metal photochemistry

In a 'state-of-play' article in 1990, Moggi and Balzani noted that "after an induction period which lasted up to the early 1960s, the photochemistry of coordination compounds has exhibited an autocatalytic development for about two decades and continues to be a rapidly growing field".[7] A review of the research themes which have

developed within the domain of transition-metal photochemistry, and the practical applications which emerged, provides an illuminating background to this subject. The whirlwind approach taken here is aimed at providing a taste of the directions which the field has taken, with reference to notable publications for the reader who is further interested.

Improvements in experimental technology, for instance light sources and filters, stimulated the general field of photochemistry in the early part of this century. The first reports of the light-induced chemical transformations of coordination compounds appeared in the 1920s, and by the 1950s a large collection of papers concerning photosubstitution and photoredox reactions had been published.[7] Around this time, developments in crystal field theory, and later ligand field theory, allowed the interpretation of electronic absorption spectra. Much of the work focused on Co(III) complexes, which displayed a dramatic dependence of reactivity on wavelength, and on Cr(III) complexes which were found to exhibit strong luminescence. The photo-induced substitution reactions of carbonyl complexes had found applications in synthesis by this time.

The realisation that excited states exhibit different chemical reactivity to ground states, and the success of the "localised" molecular orbital approach in the description of the electron density distribution in coordination compounds, propelled further developments in the field. The oft-cited monograph from Balzani and Carassiti[8] systematised progress up to 1970.

Following the observation that electron transfer could quench the excited state of $[Ru(bpy)_3]^{2+}$, the study of *inter*molecular interactions between the excited state and the surrounding medium began to dominate the field. Owing to their reversible redox behavior, polypyridyl complexes of Ru(II) and Os(II) were found to be excellent molecules for light-induced electron-transfer processes. This knowledge was applied to

the development of materials which are able to convert and store solar energy. Approaches to this problem have focused on the use of solar energy to drive 'uphill' reactions which can store energy for later use as fuels. Of most note is the redox decomposition of water into H_2 and O_2. This process can be photocatalysed by coordination compounds which have suitable redox properties.[2]

In 1983, an entire issue of the Journal of Chemical Education was devoted to the topic of inorganic photochemistry.[9] The discussions were focused on topics such as intermolecular deactivation processes (for example energy and electron transfer), solar energy conversion schemes, and bioinorganic photochemistry. This decade also saw the scope of transition-metal photochemistry widened to include, for example, pulsed techniques,[10] which allowed the spectroscopic identification of transient species, the application of photochemistry in synthesis,[2] and the development of theoretical approaches.[11]

The themes of the 1990s are perhaps best illustrated by the regular specialist issues of the Journal of Coordination Chemistry.[12] Sykora and Sima have written an extensive account of developments up to 1990, with particular attention paid to the properties of excited states and their chemical reactivity.[2] Since that time, the development of photochemical aspects of supramolecular transition-metal chemistry has been a popular topic,[13] with the exciting potential of molecular-level mechanical machines and logic gates controlled by photochemical stimuli. This was also the subject of an earlier monograph.[14] Other topics which have generated considerable recent interest include metal-to-ligand charge transfer photochemistry,[15] the medicinal applications of transition-metal photochemistry, and further research in the field of transition-metal luminescence.[12]

The chemistry of Co(III) complexes - an overview

History

Like most great discoveries in science, the observation that "$CoCl_3$" and NH_3 combined to from a stable compound was probably greeted with a sigh of "Hmmmm.....that's funny", rather than the fabled "Eureka".* In 1852, Fremy[16] established that the air oxidation of a Co(II) salt in aqueous ammonia gave a stable Co(III) salt which was associated with six molecules of ammonia, formulated as $CoCl_3.6NH_3$. This was indeed a puzzling find, given that both components appeared to have their valencies satisfied. Furthermore, a range of similar compounds could be isolated: $CoCl_3.5NH_3$; $CoCl_3.4NH_3$; and $CoCl_3.3NH_3$.

Enter Alfred Werner, who re-formulated these compounds in the way familiar to present-day chemists. Werner proposed that metals possess two types of valency; a primary valency (oxidation state), and a secondary valency (coordination number).[17] The primary valency of the cobalt is three, and the secondary valency six, and the compounds can be described as $[Co(NH_3)_6]Cl_3$, $[Co(NH_3)_5Cl]Cl_2$, and so on. Significantly, these secondary valencies were associated with a certain geometrical arrangement, thus predicting the existence of geometrical isomerisation. Some years on, Werner himself was able to close the door on opposing theories by resolving the octahedral $[Co(en)_2(NH_3)X]^{2+}$ ($X = Cl^-, Br^-$) complex into its predicted optical isomers.

* This is an adaptation of a quote from Isaac Asimov.

The properties of Co(III) complexes

Following their role as the raw materials for the foundation of coordination chemistry as a scientific discipline, Co(III) complexes have served as workhorses for the development of many general theories in this field. These include many stereochemical and ligand substitution investigations. Co(III) complexes are amenable to such studies as, in general, they have well-defined octahedral geometries, and ligand-exchange reactions occur at slow, easily measurable rates. Two other general features of Co(III) complexes, which have proved to be of considerable value in this thesis, are outlined below.

Diamagnetism and NMR spectroscopy

The Co(III) ion has six d electrons, and an overwhelming majority of its complexes are octahedral and low-spin, with a $(t_{2g})^6$ configuration. That is, the six d electrons are housed in the t_{2g} set of d orbitals. Hence, most Co(III) complexes are diamagnetic and are amenable to characterisation by NMR spectroscopy. Both ^1H and ^{13}C NMR spectroscopy have found widespread application not only for the identification of ligands bound to the cobalt centre, but also as a probe of the geometrical arrangements of the ligands.

Electronic structure and UV-vis spectroscopy

For strict octahedral symmetry (eg $[Co(NH_3)_6]^{3+}$), the $(t_{2g})^6$ electronic configuration will give rise to two spin-allowed d-d transitions. These correspond to the transitions from the $^1A_{1g}$ ground state, to the $^1T_{1g}$ and $^1T_{2g}$ upper states. The energy of the absorption bands are of diagnostic value for the coordination sphere around the cobalt atom. In general, the position of these bands correlate directly with the strength of the ligands (although the symmetry of the complex can upset this simple relationship). More powerful ligands, high in the spectrochemical series, shift the absorption bands to high energies. If the symmetry around the cobalt centre is reduced from strictly octahedral,

(as in a mixed ligand complex) the lower energy $^1T_{1g}$ band is expected to be split. Such splitting is rarely seen as two fully resolved peaks, especially if the ligands occupy similar positions in the spectrochemical series. As a general rule, a reduction in symmetry correlates with a rise in intensity of the absorption bands.

Synthesis of Co(III) complexes

The classic route to Co(III) complexes is the oxidation of a Co(II) salt in the presence of the desired ligand(s).[18] This is often done in aqueous solution, with oxidants such as hydrogen peroxide, molecular oxygen , or lead dioxide.

Another popular method is to prepare a Co(III) intermediate compound, which has ligands which are sufficiently labile to undergo substitution reactions. Typically, chloro ligands are employed for this purpose. The departing ligand can also be a bidentate unit, the most notable example being the carbonato (CO_3^{2-}) ligand. Indeed, it is possible to substitute all three carbonato ligands in $[Co(CO_3)_3]^{3-}$ to yield a new Co(III) complex.[18]

Co(III) has a particular affinity for nitrogen donor atoms, as will become apparent throughout this thesis. Other common ligands include H_2O, halides, and carboxylates. In addition to mononuclear complexes, hydroxo (OH^-), peroxo (O_2^{2-}), and amido (NH_2^-) groups often function as bridging units to form dinuclear Co(III) complexes.

An overview of the photophysics and photochemistry of Co(III) complexes

Far less is known about the photo*physical* behavior of Co(III) complexes than is known regarding their photo*chemical* characteristics. Assessment of the excited state dynamics of these complexes is hampered by their lack of radiative emission, since luminescence gives the best handle on the nature of the excited state(s). In fact, only

one Co(III) complex, $[Co(CN)_6]^{3-}$ has been reported to luminesce.[19] Excited state absorption spectra, recorded following the near-UV excitation of several Co(III)-amine complexes, have been reported. Unfortunately, a coherent picture of the excited states could not be formed.[20] Transient absorption spectra following LMCT excitation of two Co(III) complexes with mixed pyridyl and amine donors have been published more recently.[21] Non-radiative excited state decay processes, which eventually returned the complex to its $^1A_1$ ground state, were proposed to account for the short (<1 ps) lifetime of the ^{1}LMCT state.

The photo*chemistry* of Co(III) complexes is dominated by two processes: aquation and redox decomposition. Although the details of which excited state is actually the "reactant" are often unknown, some patterns to the observed photochemical reactivity have emerged.[22] The most well-studied families of complexes are the $[Co(NH_3)_5X]^{z+}$ and $[Co(CN)_5X]^{z-}$ ions where X represents an monodentate ligand.

Photoredox reactions can be induced by irradiation in the LMCT bands. The LMCT excited state is formally a Co(II) species, and the primary photoproducts are a Co(II) complex and an oxidised ligand fragment. Secondary (thermal) reactions of these primary photoproducts may lead to overall reaction stoichiometries which disguise the nature of the original photochemical reaction. Generally photoredox reactions have a high quantum yield, for example, $\Phi = 0.16$ for the LMCT excitation of $[Co(NH_3)_6]^{3+}$. Chelating ligands also display this type of photochemistry, with a quantum yield of $\Phi = 0.13$ for $[Co(en)_3]^{3+}$.[23]

Photoredox reactions can also be initiated by radiationless transfer from a ligand-field excited state to a charge-transfer excited state. Such processes are often invoked to explain the observation of redox decomposition products following irradiation in a d-d band. Likewise, spin-forbidden triplet LMCT states, which are situated at low energies, can also be populated by this mechanism and may influence the observed photochemistry.

Photoaquation reactions are the dominant photochemical processes following ligand field excitations. There is no direct correlation between the ligand released in the photochemical process, and that which is released during thermal aquation. Photoaquation processes for the $[Co(NH_3)X]^{z+}$ class of complexes tend to have low quantum yields which are strongly dependent upon the excitation wavelength. $[Co(CN)_5X]^{z-}$ complexes generally have much higher quantum yields which are uniform over the ligand-field wavelengths. The difference in photochemistry between these sets of complexes is thought to be due to the difference in the nature of the low-lying excited states.[2]

The photochemistry of Co(III)-aminocarboxylato complexes

One class of Co(III) complexes which undergo some very interesting photochemical transformations are those with aminocarboxylato ligands. A review of this chemistry is given presently which, for convenience, is divided into two sections. Although this disrupts the actual chronological sequence, the first part covers the photochemistry of Co(III) complexes with *bidentate* aminoacidato ligands. The second section deals with the inclusion of these units in *polydentate* aminocarboxylato ligands.

Background

Most of the early contributions to this field of research came from Poznyak's laboratory. This work culminated in a landmark review article, entitled "*Photochemical Reactions of Ligands in Transition Metal Complexes*".[24] At the heart of this paper is the concept that photochemical reactions can induce changes in a coordinated ligand without altering other aspects of the complex (in the wider sense). A general model for this type of photochemical reactivity was proposed. The initial step was based on Adamson's

radical-pair model whereby the absorption of light leads to homolysis of the metal-ligand bond and the formation of a radical pair, usually *via* a LMCT excited state (Eqtn 1.9).

$$\left[L_nCo^{III}X\right]^{z+} \xrightarrow{h\nu} \left[L_nCo^{II}, X^{\bullet}\right]^{z+} \qquad (1.9)$$

If the ligand X is a collection of atoms (or groups of atoms) represented by ABC, the ABC• radical can fragment. Recombination of the new radical with the metal centre will generate a new complex (Eqtn 1.10).

$$\left[L_nCo^{II}, ABC^{\bullet}\right]^{z+} \longrightarrow \left[L_nCo^{III}(AB)\right]^{z+} + C^{\bullet} \qquad (1.10)$$

The photochemistry of Co(III) complexes with bidentate aminoacidato ligands

Up to the late 1980s, the photochemistry of Co(III)-aminoacidato complexes was primarily the domain of Poznyak's group.[24] One remarkable discovery was the formation of a stable organometallic product *via* the photoelimination of carbon dioxide (Fig 1.3).

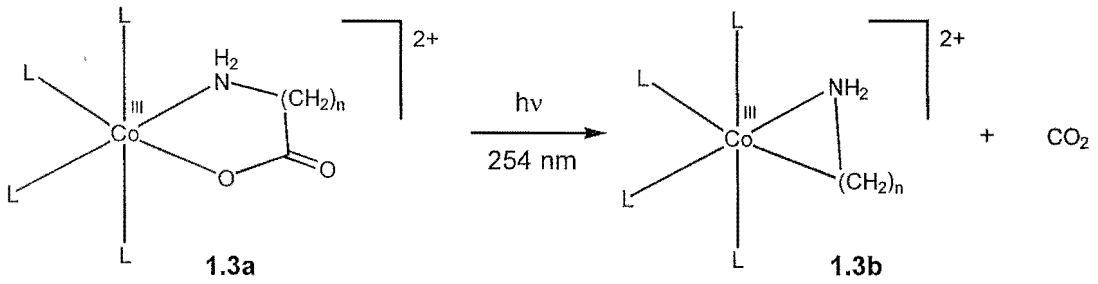

Figure 1.3. The formation of a complex containing a three-membered chelate ring from the photodecarboxylation of a glycinate ligand.

The observation of a three-membered Co–C–N chelate (**1.3b**, n = 1), resulting from the photo-contraction of a five-membered glycinate chelate ring (**1.3a**, n = 1), was especially startling. When the four remaining coordination sites are occupied by two bipyridine (bpy) ligands, the complex **1.3b** is relatively stable, and has been characterised by X-ray crystallography.[25] The ligating carbon atom is likely to be strongly electron donating. The π-acidic bpy ligands are thought to stabilise the complex by accommodating some of this electron density.

The photolysis reaction proceeds in the same manner upon replacement of the bpy by ethylenediamine ligands (**1.3a**, $L_4 = (en)_2$). However, the three-membered rings which result from photolysis of glycinato chelates (**1.3a**, n = 1) are considerably less robust with en co-ligands. This precluded the isolation of these photolysis products in the solid state.[24]

Stable four- and five-membered chelates, originating from β- and γ-amino acids (**1.3a**, n= 2, and n = 3 respectively), were also produced by this route. However, the stability of these chelates is less affected by the nature of the ancilliary ligands.[26]

In the decade following the publication of the review article detailed above, several more literature reports concerning the photodecarboxylation of Co(III)-aminoacidato complexes have appeared. The UV photolysis reactions of series of complexes containing optically active aminoacidato ligands (L-alaninate, L-valinate, and L-aspartate), with amine ancilliary ligands, has been detailed.[27] The photolysis products were poorly characterised, however the authors reached the conclusion that, following photodecarboxylation, a rapid racemisation occurred over the two asymmetric centres (the residual chiral carbon of the amino acid fragment, and the configuration of the chelate rings).

Natarajan and Natarajan[28] have used flash photolysis to investigate the kinetics of the formation of the metallacycle **1.4b**, following the UV excitation of the glycinato complex **1.4a**. A first-order rate constant of $k = 4 \times 10^3\ s^{-1}$ was deduced. A critical examination of their assignment of the rate determining step forms the basis of the first section of this thesis.

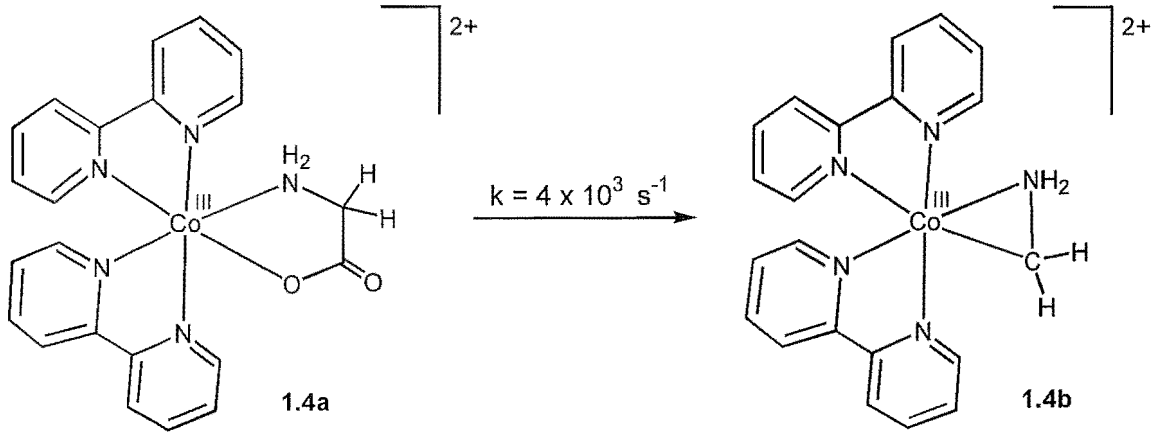

Figure 1.4

The generality of photochemical reactions of *ligands* in transition-metal complexes has been extended by the observation of the loss of SO_2 from a Co(III)-bound sulfinato ligand (**1.5a**).[29] Interestingly, a peroxo complex was the final product (**1.5b**), presumably formed *via* incorporation of dissolved molecular oxygen. The ligating carboxylato unit survived photolysis, and ended up *trans* to the tertiary nitrogen of the tren ligand in the product. Neither the isomerisation mechanism, nor the photolysis mechanism, were discussed in any detail.

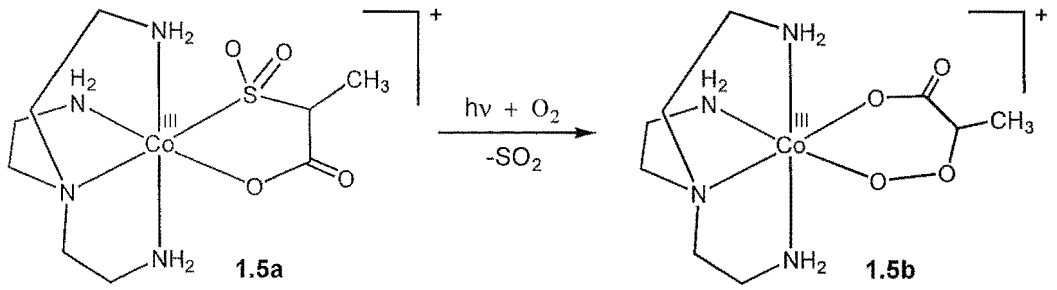

Figure 1.5. The photochemical reaction of a sulfinato ligand.

Photochemical reactions of Co(III) complexes with polydentate aminocarboxylato ligands

The photolysis of *polydentate* aminocarboxylato complexes of Co(III) has also been the subject of extensive investigation. The work in this field up to 1989 has been reviewed by Pavlovskii and Poznyak,[30] with many of the results discussed originating from the authors' own laboratory. Complexes of tetradentate ligands, with a bidentate diamine or di-imine ligand filling the remaining coordination sites, have received the most attention, however, it was the photochemistry of the $[Co(edta)]^-$ complex which sparked the proceedings in this area.

In the early 1970s, it was found that irradiation of the LMCT bands of $[Co(edta)]^-$ (**1.6a**) gave predominantly redox decomposition products: CO_2, formaldehyde, and the Co(II) ion.[31] Some photophysical aspects of the LMCT excitations were discussed in this early work. Endicott postulated that the ^{1}LMCT state is too short-lived to exhibit significant reactivity. A ligand-centred excitation of the carbonyl group of the aminocarboxylato ligand (to a triplet state), followed by internal conversion to a reactive ^{3}LMCT state, was proposed to account for the observed photochemistry.[31c] Such photophysical investigations have since attracted little attention.

In contrast, Poznyak's group observed products other than those from redox decomposition processes following photolysis of frozen solutions (77K) of $[Co(edta)]^-$ (**1.6a**).[32] On the basis of UV-vis spectroscopy, these were assigned as complexes containing a three-membered Co–C–N chelate ring (**1.6b**). The product was unstable at room temperature. This reaction was re-visited by the same group more recently, with particular attention paid to the secondary (thermal) chemistry of the reaction products.[33]

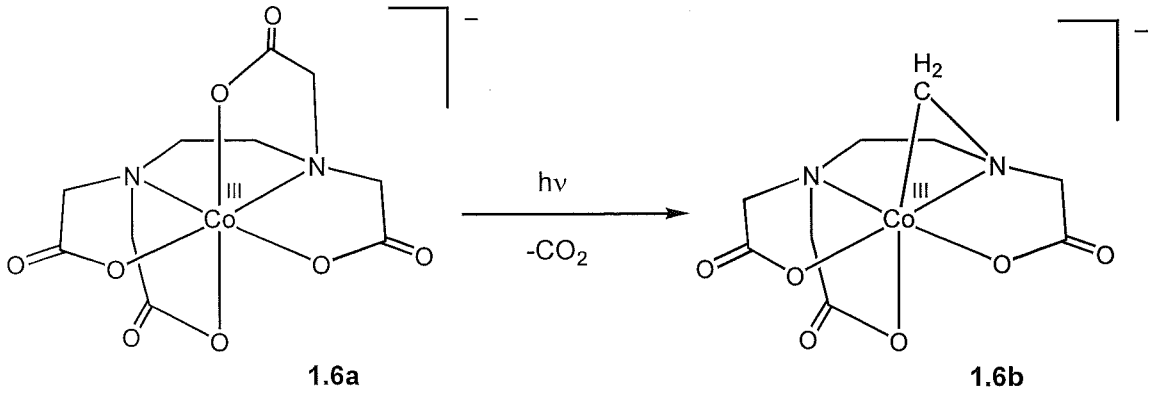

Figure 1.6. Photochemistry of the $[Co(edta)]^-$ complex.

The original observation of the metallacycle **1.6b** inspired these workers to search for stable analogues, including the bidentate examples discussed in the previous section. In terms of polydentate systems, four- and five-membered organometallic chelates have proved to be those most amenable to isolation. Numerous such compounds have been well characterised.[30]

Three polydentate complexes which contained *three*-membered Co–C–N chelates, formed by the photodecarboxylation of glycinato-type ligands, have been isolated (Fig 1.7). The first two examples were characterised by UV-vis spectroscopy, and, in the case of **1.7b**, ^{1}H NMR spectroscopy.[34,35] More recently, the photochemistry of **1.7e** was investigated, and the crystallised photolysis product (**1.7f**) was characterised by X-ray analysis.[36] These examples are discussed further in Chapter 4.

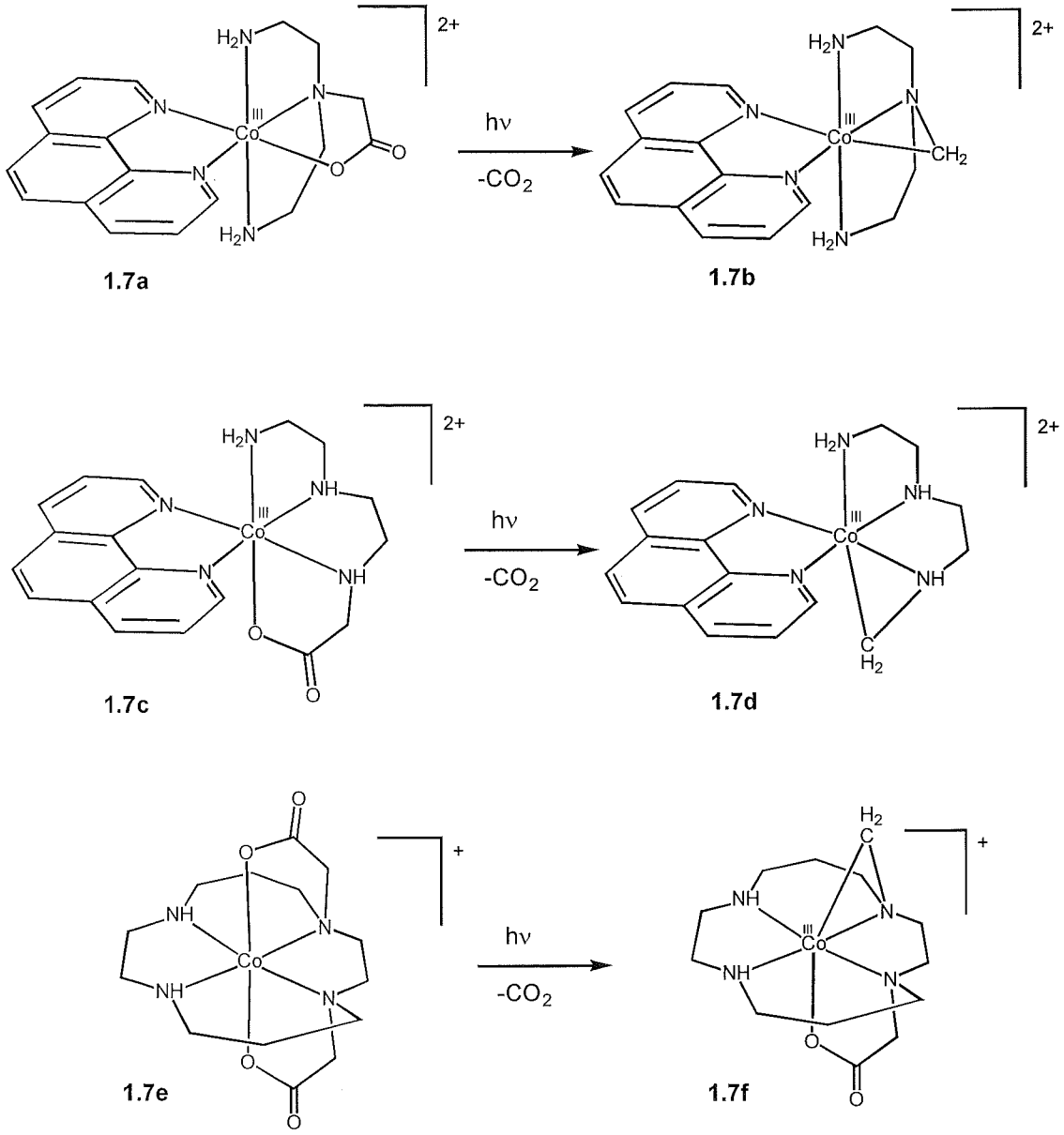

Figure 1.7. The literature examples of three membered aminomethylene (C–N) ligands which are part of a polydentate framework.

In the past decade, several further reports have appeared which detail various photochemical aspects of Co(III)-aminocarboxylato complexes. Photolysis of a Co(III)-ornithinetriacetato complex (**1.8a**),[37] was reported to induce decarboxylation and formation of an organocobalt species. This product was not able to be well-characterised owing to its thermal instability.

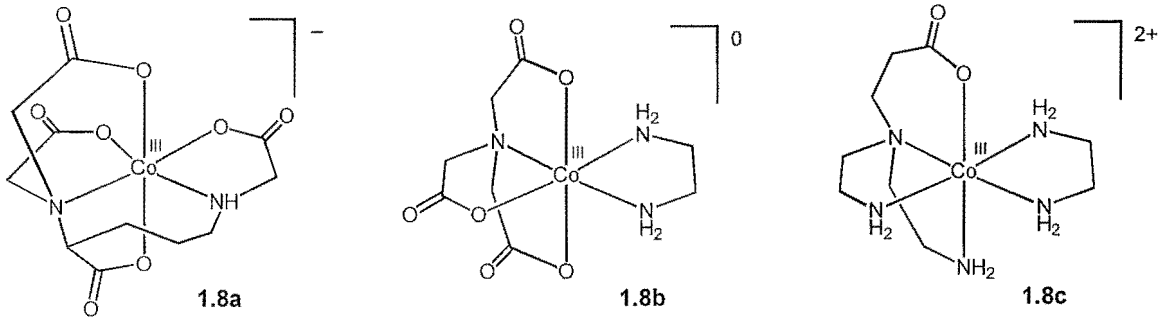

Figure 1.8. Some recent examples of polydentate aminocarboxylato complexes of Co(III) which have been investigated from a photochemical perspective.

Upon photolysis of the Co(III)-nitrilotriacetato complex (**1.8b**),[38] $[Co^{II}(edta)]^{2-}$ was observed. It was proposed that the edta ligand was formed as a result of coupling reactions between the decomposition products of an unstable organometallic complex. The propionato arm of the complex **1.8c** was very unreactive towards photodecarboxylation.[39] The reasons for this are discussed further in Chapter 4.

Two geometrical isomers of the thiodiacetato complex **1.9a** and **1.9b** undergo a photodecarboxylation reaction to give the same product (**1.9c**).[40] This provides a good example of the potential for geometrical isomerisation to accompany the photolysis reaction. The product, which contains a Co–C–S chelate, was characterised by X-ray crystallography.

A geometrical re-organisation which accompanied the photodecarboxylation reactions of a family of *amino*carboxylato complexes has recently been reported.[41] This report is detailed in Chapter 6.

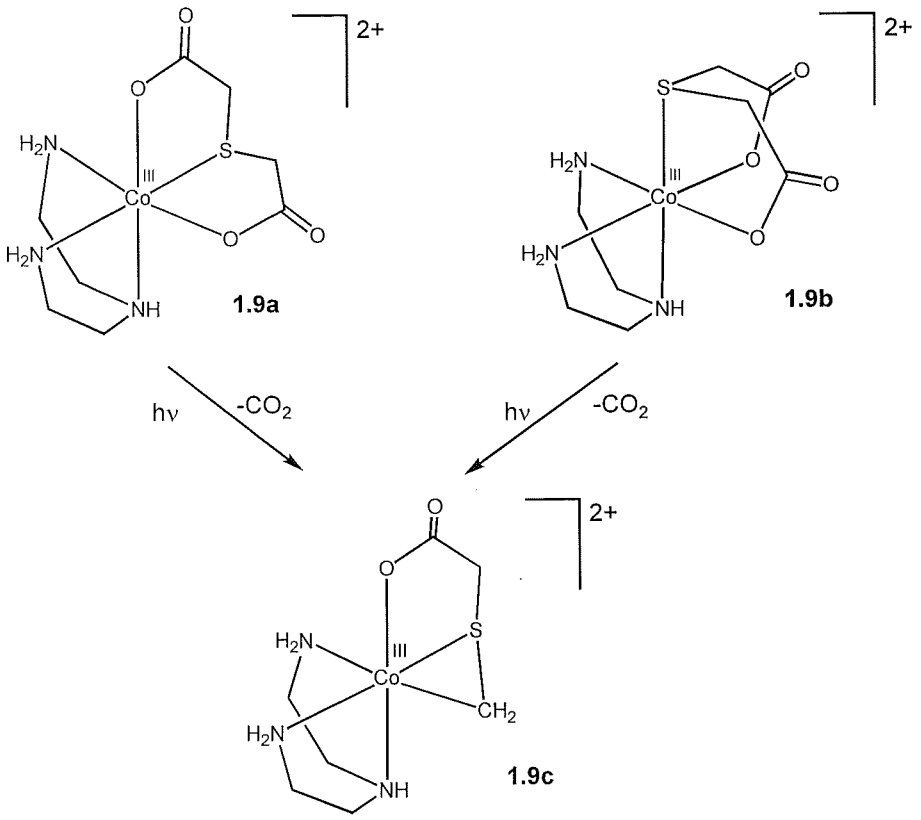

Figure 1.9. The photodecarboxylation of a thiodiacetato complex which yielded a complex with a Co–C–S chelate ring. Both geometrical isomers gave the *same* photolysis product.

The work described in this thesis

It can be seen from the preceding summary that the photochemical reactions of amino acids which are coordinated to Co(III) represents an interesting, yet relatively new and underdeveloped, field of chemistry. One of the more significant advances which has been brought about by this field of research is the production of novel complexes which are inaccessible by other means. It has also served as a lynchpin for the development of the more general field of the photochemical reactions of ligands in transition metal complexes. However, there remains considerable scope for further investigation in this field. For example, the mechanism of formation of organometallic products *via* the photodecarboxylation reaction has not been fully explored. Also, the potential for

producing novel complexes *via* reactions of the organometallic photoproducts has not been fully developed. Steps towards addressing these points form the basis of this thesis.

> "Chemistry is the science of change. It is ironic then that, although we have become so knowledgeable about the properties of reactants and products–about the beginnings and ends of chemical journeys–we remain more often than not unsure of just how these journeys are made."
>
> Anthony Downs and Timothy Green, 1999.[42]

The work in this thesis comprises an investigation into the photochemical reactivity of Co(III) complexes with aminocarboxylate ligands, with a particular emphasis on the reaction mechanism. Most attention has focused on the formation of three-membered Co–C–N chelate rings, which originate from five-membered aminoacidato chelates. Although there is also much scope for exploration of the excited state manifold of these complexes, this thesis is certainly photo*chemical* in its outlook, rather than photo*physical*. Light has been used primarily as a reagent: a tool for initiating a chemical reaction. It is the direction which the reaction takes following this point, ie the mechanism of the photochemical reaction, which is of prime interest. Besides this line of inquiry, this thesis is also concerned with extending the potential of these photodecarboxylation reactions in synthesis.

Chapter 2 deals with the deficiencies of the currently accepted photolysis mechanism for Co(III)-aminocarboxylato complexes. A method for testing this mechanism, which involves the introduction of a radical clock into the aminoacidato ligand, is devised.

Chapter 3 discusses the implementation of this test, and its implications for the currently accepted mechanism. The thermal instability of the organometallic photolysis products is discussed.

The development of a polydentate ligand system which can impart stability to the photolysis products is detailed in **Chapter 4**, with some consideration given to the secondary chemistry of the eventual decomposition products.

Chapter 5 discusses two approaches to obtaining further information regarding the photolysis mechanism.

The solvent-dependence of the photolysis reaction is detailed in **Chapter 6**, with particular emphasis given to the formation of secondary reaction products in the photolysate.

Chapter 7 contains a 'state-of-play' summary, some possible alternative mechanisms, and the outlook towards possible future directions for this field of investigation.

Where appropriate, each chapter includes a section which details the experimental results which are discussed in the text.

Appendix 1 contains a background to transition-state theory and *ab-initio* quantum mechanics, along with the raw data from the *ab-initio* calculations detailed in this study. A outline of crystallographic methods, and selected data for each structure, is presented in **Appendix 2**. This is followed by a list of the publications which are cited throughout the text.

CHAPTER TWO

THE PHOTOLYSIS MECHANISM OF $[Co(bpy)_2(aa)]^{2+}$ COMPLEXES

Inconsistencies in the published mechanism

Irradiation of the glycinatobis(2,2'-bipyridine)cobalt(III) ion ($[Co(bpy)_2(gly)]^{2+}$, 2.1a), with UV light has been shown to result in decarboxylation and formation of a complex containing a three-membered Co-C-N metallacycle **2.1d**. This complex, $[Co(bpy)_2(CH_2NH_2)]^{2+}$, is remarkably stable and has been characterised by X-ray crystallography.[25]

A mechanism for this reaction was proposed (Fig 2.1), wherein absorption of UV light induces ligand-to-metal charge transfer (LMCT) and homolysis of the cobalt-oxygen bond. This affords a Co(II)-bound aminoacyloxyl radical intermediate (**2.1b**). Decarboxylation of this radical is proposed to produce a coordinated aminoalkyl radical **2.1c**, which can re-oxidise the Co(II) centre, yielding the metallacycle **2.1d**.

Natarajan and Natarajan employed laser flash photolysis to study the kinetics of this reaction.[28] The data were consistent with first order kinetics, and a rate constant of 4×10^3 s^{-1} was calculated for the formation of the metallacycle (**2.1d**). This rate constant was tacitly assigned to the final step of the reaction sequence, cobalt-carbon bond formation.

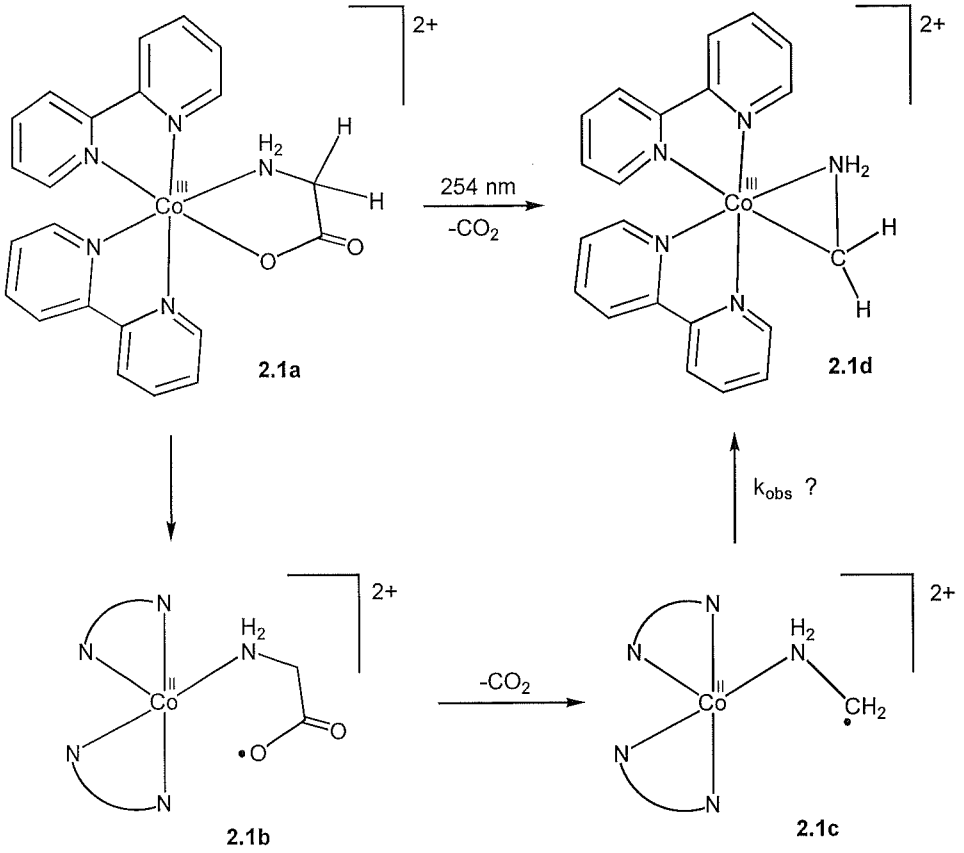

Figure 2.1. The mechanism which has been proposed for the photochemical formation of $[Co(bpy)_2(CH_2NH_2)]^{2+}$.

There are two striking anomalies in the assignment of this rate determining step.

Firstly, bimolecular reactions between Co(II) complexes and alkyl radicals have second order rate constants which are usually greater than 10^8 $M^{-1}s^{-1}$.[43] These reactions approach the diffusion-controlled limit in H_2O. It would be remarkable if a similar *intramolecular* reaction has a rate constant as low as 10^3 s^{-1}.

Secondly, the measured rates would imply that the cobalt(II)-aminoalkyl radical intermediate **2.1c** has a half-life on the order of milliseconds. Monodentate ligands on Co(II) are well known to undergo rapid ligand exchange reactions in aqueous solution. For example, $[Co(NH_3)_6]^{2+}$ has a half-life of less than 1 μs before one of the NH_3 detaches.[44] As such, one may expect that the aminoalkyl radical ligand will be displaced by aqua ligands on a microsecond timescale, which would effectively prevent formation of the metallacycle.

A radical clock to test the mechanism

Radicals are intermediates in the pathways of many reactions. *Radical clocks* have found widespread application in detecting these intermediates, estimating their lifetime, and providing relative values for the rate constants of their reactions.

The questions which were raised in the previous section regarding the photolysis mechanism of $[Co(bpy)_2(gly)]^{2+}$, centred around the proposed rate constant for Co–C bond formation. This section explores the potential for a radical clock to test the assertion that this step proceeds with a rate constant of around 10^3 s^{-1}.

An introduction to radical clocks

> "Most of the methods for measuring the lapse of time have, I believe, been the contrivance of monks and religious recluses who, finding time hang heavy on their hands, were at some pains to see how they got rid of it."
>
> William Hazlitt, 1839.

The fundamental operation of a radical clock is to divert a radical intermediate from its normal reaction course with a *well-calibrated* rearrangement reaction. Analysis of the product distribution provides information on the extent to which each reaction channel was followed. This allows the relative rates of the rearrangement reaction and the "normal" reaction to be established.

The archetypal radical clock is the cyclopropylmethyl radical (**2.2a**), which ring opens to the 3-butenyl radical (**2.2b**) with a rate constant of 1×10^8 s^{-1} at 298 K.[45]

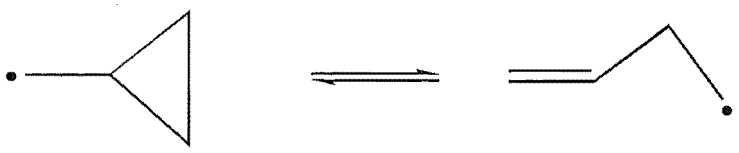

2.2a **2.2b**

Figure 2.2. The cyclopropylmethyl radical clock.

If cyclopropyl group is incorporated into a reactant, and a radical is generated on the *exo* carbon atom (as in **2.2a**), the cyclopropyl group will have an opportunity to rearrange. If this rearrangement is allowed to proceed, the "normal" reaction of the radical must be slower than the ring-opening reaction. If the rate constant of the rearrangement reaction is known, an upper bound for the rate constant for the "normal" reaction step can be set. Accordingly, this provides a minimum half-life for the radical in the usual course of events. Generally, the rate constant for ring opening of cyclopropyl methyl radicals is around 10^8 s^{-1} (*vide infra*). However, this value is sensitive to substitution at both the radical centre and on the cyclopropane ring.

If the option of rearrangement reaction is not exercised, that is, the rearrangement was too slow to compete with the normal course of the reaction, then a minimum rate constant can be estimated for the normal reaction. Thus, a maximum lifetime for the radical can be inferred. Alternatively, the absence of rearranged products may be a consequence of the complete absence of a radical from the reaction pathway.

Another prominent radical clock is the 5-hexenyl radical (**2.3a**) which cyclises to the cyclopentylmethyl radical (**2.3b**) at around 2.3×10^5 s^{-1} at room temperature.[46]

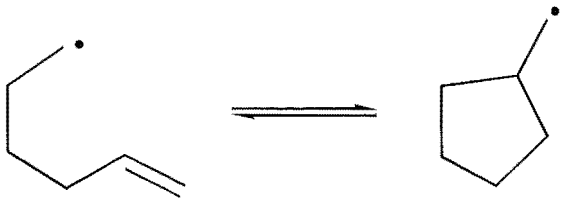

2.3a **2.3b**

Figure 2.3. The 5-hexenyl radical clock.

Two comprehensive literature reviews have appeared which summarise the scope of unimolecular radical clocks.[47] Accurately calibrated radical clocks which have rearrangement reactions spanning eight orders of magnitude (from 10^3 s^{-1} to 10^{11} s^{-1}) are available. These radical clocks have been employed to probe the reaction mechanisms, reaction rates, and radical lifetimes, for a large variety of reactions. A very recent example is now detailed.

The conversion of methylmalonyl-CoA (**2.4a**) to succinyl-CoA (**2.4b**), which is catalysed by a vitamin B_{12}-dependent enzyme, was widely accepted to proceed *via* radical intermediates.

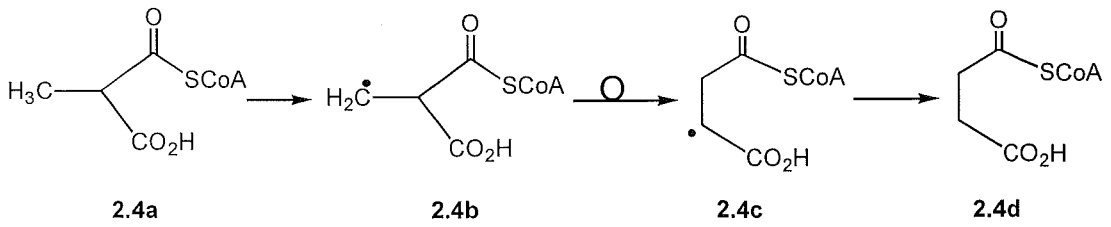

2.4a **2.4b** **2.4c** **2.4d**

Figure 2.4. A radical mechanism for the vitamin B_{12}-dependent conversion of methylmalonyl-CoA (**2.4a**) to succinyl-CoA (**2.4b**).

A method to test this assertion, which involved a cyclopropylmethyl radical clock, was devised by He and Dowd.[48] A phenyl-substituted cyclopropylmethyl group was attached to the substrate (**2.5a**). If formed, the 2-phenyl-substituted cyclopropylmethyl radical (**2.5b**) will have a lifetime of less than 10 ns before it rearranges to give **2.5c** ($k_c \approx 4 \times 10^{11}$ s^{-1}). This reaction will compete with the usual reaction of radical **2.5b** which would give the product **2.5d** (with a rate constant k_d).

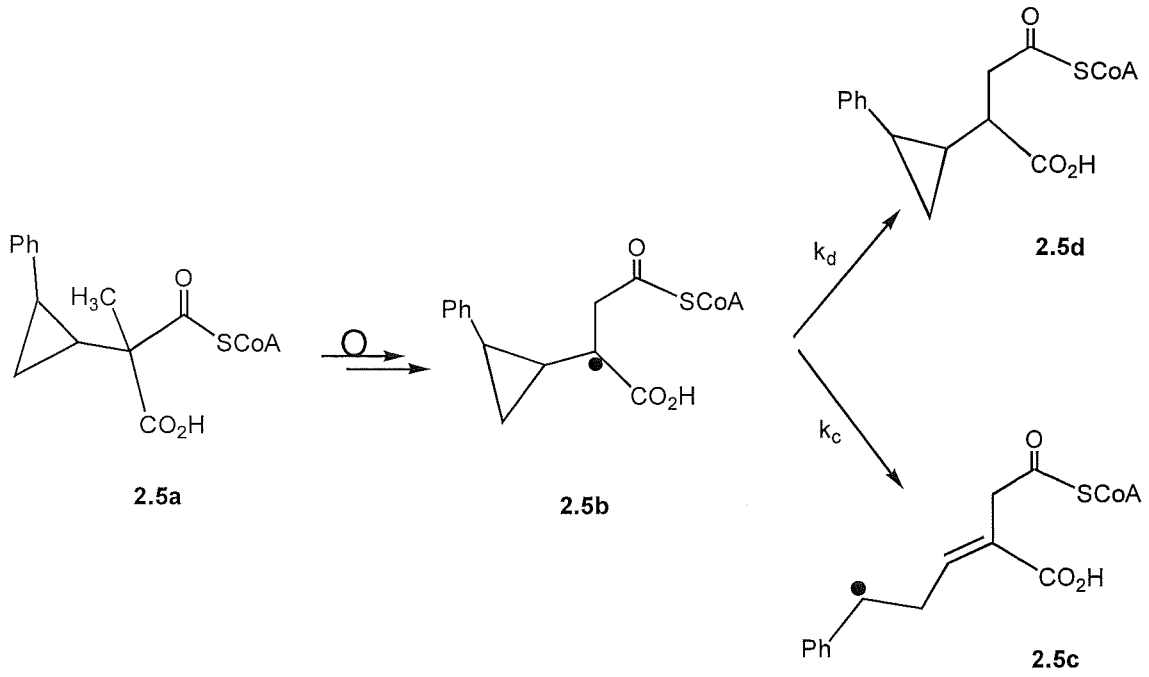

Figure 2.5. A radical clock test of the intermediacy of radicals in the enzymatic rearrangement of methylmalonyl-CoA (**2.5a**).

It was observed that the cyclopropyl ring remained intact during the enzymatic conversion of **2.5a** to **2.5d**, with no evidence of any ring-opened products. Any bimolecular reaction which would give the succinate **2.5d** from a radical intermediate **2.5b**, could not possibly occur on a time scale which would be competitive with ring opening (k_c). Hence, the intermediacy of radical **2.5b** is an impossibility. A control reaction was performed whereby the radical **2.5b** was generated by independent means. A ring-opened product derived from **2.5c** was isolated, demonstrating that rearrangement is the expected product if **2.5b** is formed.

Cyclopropylglycine as a radical clock

The mechanism proposed for the formation of a Co–C–N metallacycle following UV irradiation of $[Co(bpy)_2(gly)]^{2+}$ (Fig 2.1) is inconsistent with some other well-documented experimental results. This casts some doubt on the mechanism, or at least on the assignment of the rate determining step. The focus of the remainder of this chapter is the development of a test for this mechanism. The approach has been to devise a radical clock which can provide a relative estimate of the rate constant for Co–C bond formation for the Co(II)-bound aminoalkyl radical **2.1c**.

A precursor to a suitable radical clock would be chelated cyclopropylglycine (**2.6a**).

According to the published mechanism, UV irradiation of the $[Co(bpy)_2(cpg)]^{2+}$ complex **2.6a** would induce homolysis of the Co–O bond and decarboxylation, generating a Co(II)-bound aminocyclopropylmethyl radical **2.6b**. This is a radical clock which has two possible reaction avenues. Firstly, the radical could oxidise the cobalt centre, preserving the cyclopropyl group (**2.6c**). Alternatively, the radical could rearrange, destroying the cyclopropyl ring and forming ring-opened products (**2.6d**). The relative rates of these two competing processes will determine the eventual ratio of ring-opened and ring-closed products.

If $k_r > k_c$, ring-opened products will be formed in the photolysis, while if $k_r < k_c$, the cyclopropyl group will feature in the products. This latter outcome would also be expected if the radical **2.6b** is not formed at all.

The Co(II)-bound aminoalkyl radical **2.6c** is expected to react with the cobalt centre with $k_c \approx 10^3 - 10^4\ s^{-1}$, if Natarajan's assignment of the rate determining step is valid. This rests on the premise that the Co–C bond formation step for radical **2.6c** will not be significantly different from that of the unsubstituted radical (formed from

$[Co(bpy)_2(gly)]^{2+}$). In order to use the radical clock experiment to make any strong conclusions regarding the rate constant k_c, it is vital that k_r can be estimated with some certainty. Ideally, k_r will be much greater than k_c so that the ring opening reaction will be fast enough to divert the reaction from the proposed slow Co–C bond formation step. This point is addressed in the following section.

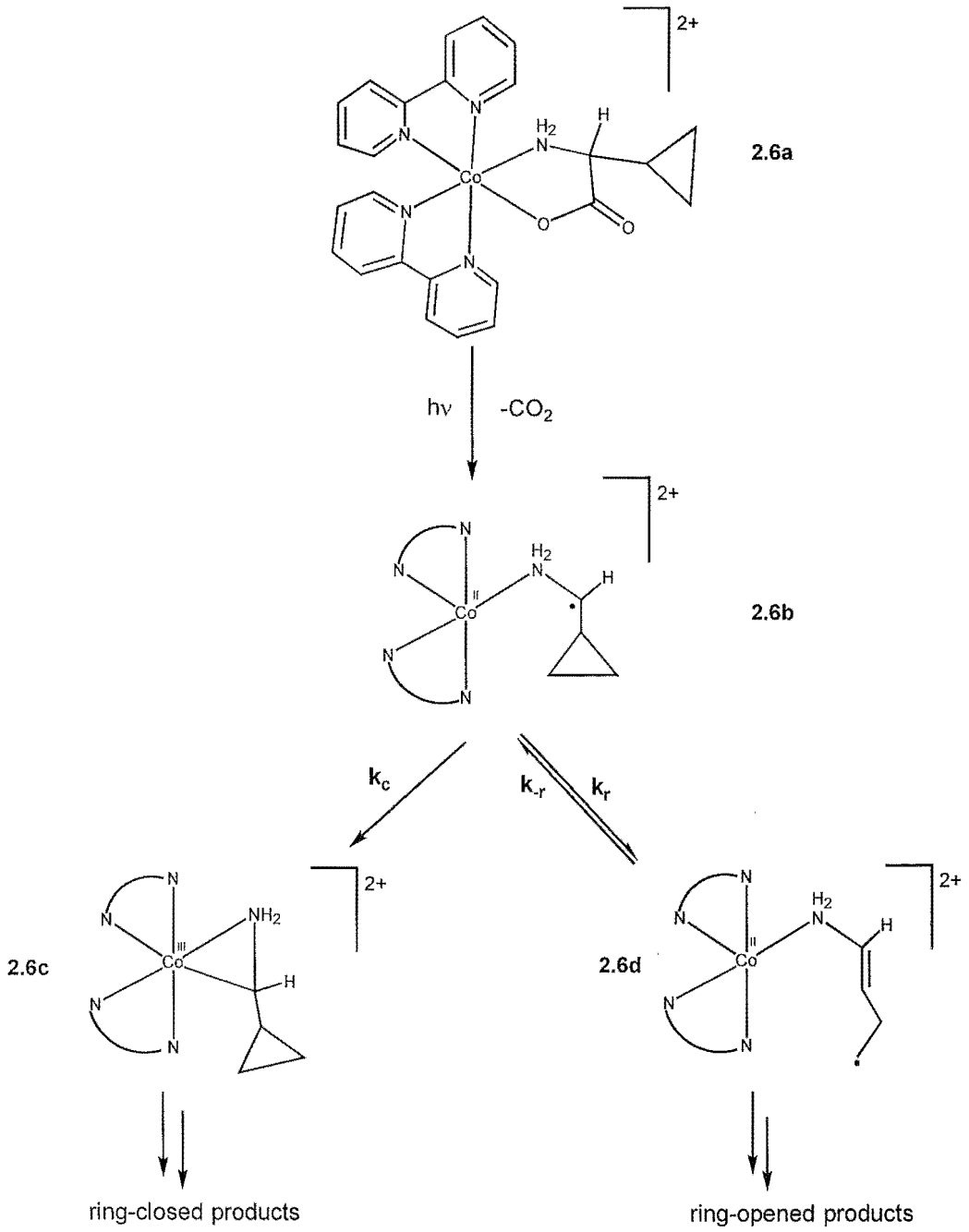

Figure 2.6. Two possible photochemical reaction pathways for the $[Co(bpy)_2(cpg)]^{2+}$ complex (**2.6a**).

Is cyclopropylglycine a viable radical clock?

From a practical perspective, estimation of a rate constant for the ring-opening of **2.6b** must be inferred from that of the *free* aminocyclopropylmethyl radical, rather than the coordinated radical. The presence of the cobalt centre would make any experimental or theoretical investigations especially difficult. The coordinated radical would be difficult to generate, and the paramagnetic Co(II) ion would seriously compromise any kinetic ESR study. The size of this system makes an accurate theoretical assessment a difficult proposition.

Prior to this study, no kinetic information was available for the rearrangement reaction of the free aminocyclopropylmethyl radical. However, numerous approaches, both theoretical and experimental, have been made to this problem for many related radicals (*vide infra*). This section presents an approach to obtaining a rate constant for the ring opening of the aminocyclopropylmethyl radical, and extends these results to make an estimate for the rate constant for the coordinated radical. This has been achieved by using the body of related literature in two ways.

(i) The methods of Radom[49] and of Newcomb[50,51,52] were adopted whereby transition state theory was utilised to calculate rate constants for the ring-opening reaction of the aminocyclopropylmethyl radical, and for its protonated analogue. The protonated analogue is expected to better represent the Co(II) system as the lone pair of the nitrogen centre is involvled in bonding in both cases. This is discussed in more detail later. Rate constants for both the forward and reverse reactions were calculated in order to establish whether an equilibrium would favour the ring-opened radical or the ring-closed form.

(ii) The rate constants reported for other α-substituted cyclopropylmethyl radicals have been analysed. The trends relating the nature of the substituent and the rate constants, have been used to predict the kinetics of the amine-substituted radical.

These two lines of investigation are brought together in the final section which discusses the implications for the radical clock experiment.

Transition state theory

Transition state theory (TST) is a well-established and accurate method of calculating rate constants from the molecular properties of a reacting system.[53,54,55,56,57]

This section will present the basic concepts of TST, with the calculation of rate coefficients for the rearrangement reactions of the aminocyclopropylmethyl radical (protonated and unprotonated) providing worked examples of its implementation. Appendix 1 contains an overview of TST, an introduction to *ab initio* quantum mechanics, and the background to the links between them.

Potential energy surfaces

The idea that atoms within molecules move according to forces derived from a potential field which is determined by electronic interactions is a basic concept in molecular dynamics. The potential surface - a "map" of energy as a function of nuclear coordinates - can be created *via* quantum mechanical calculations. The cartographer can then compute the trajectories (position and momenta) of all atoms at all times, and identify features such as minimum energy conformations. A chemical reaction can be thought of as the movement from one minimum to another on the potential surface, with the maximum point on the reaction pathway termed the transition state (TS). Within the topological metaphor, the chemical reaction involves traversing a mountain pass which

links two valleys. A two-dimensional slice of a potential energy surface, showing some pertinent features, is shown in Fig 2.7.

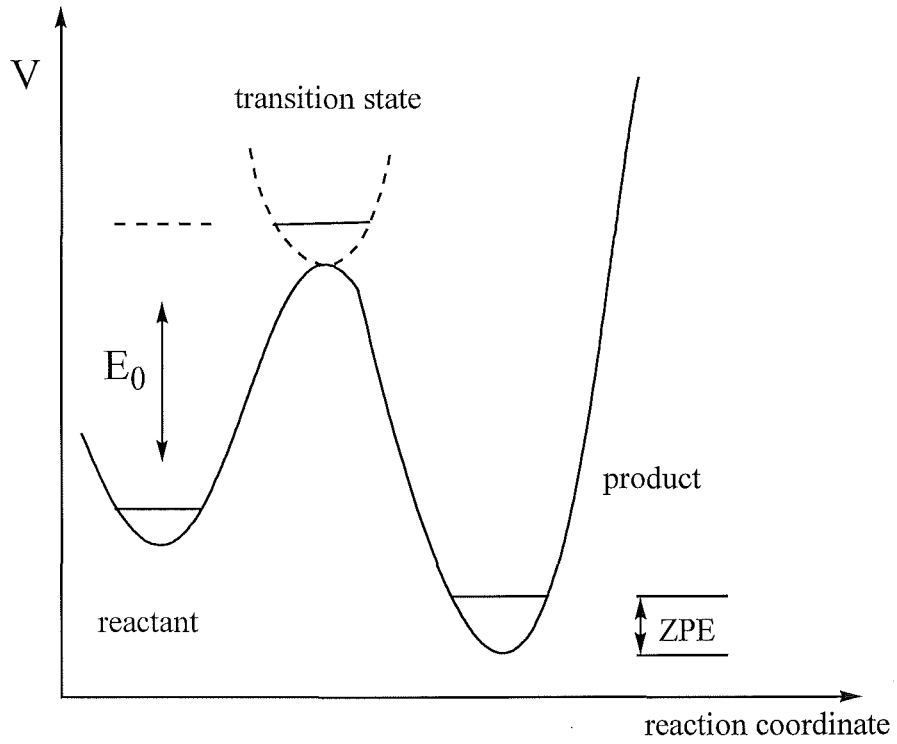

Figure 2.7. A slice of a typical potential energy surface. The reaction barrier (E_0) for the forward reaction is shown, along with the zero point energy correction (ZPE) for the product.

Transition state theory

A complete evaluation of all trajectories over a defined period of time, with a count of those which begin as reactants and end as products, will yield a reaction rate. However, such an evaluation of atomic motions on the potential surface would be an immense task. The primary assumption of TST is that there exists a *critical geometry*: all reactants whose trajectory leads them to adopt this conformation – the *transition state* – will become products. This greatly simplifies the mathematics, and yields a rate coefficient (for a unimolecular reaction) of the form:

$$k = \frac{kT}{h}\frac{Q^{\ddagger}}{Q}\exp\left(-\frac{E_0}{kT}\right) \qquad (2.1)$$

This formula is composed of the Boltzmann constant (k), Planck's constant (h), the temperature (T), the partition constants for the reactant (Q) and the transition state ($Q^{\ddagger}$), and the critical energy (E_0). This critical energy is the difference between the zero-point energies of the reactant and transition state, as shown in Fig 2.7. The power of the TST approach lies with the reduction from dealing with the entire potential energy surface, to the analysis of just two points - the reactant and the transition state.

Obtaining the required parameters - *ab initio* quantum mechanical calculations

The essential parameters for the calculation of rate constants with TST are:

(a) The reactant and transition state geometries and vibrational frequencies. These are required to evaluate the respective partition functions and ZPE corrections.

(b) The relative energy of the reactant and transition-state. Following ZPE corrections, these values will give the reaction barrier (E_0).

Realistically, these parameters cannot be measured experimentally. However quantum mechanical techniques are eminently well suited to the task of calculating these values. The advent of fast, relatively cheap personal computers, and the accessibility of software packages which perform *ab initio* calculations, have brought high-level theoretical approaches to the solution of such questions within the reach of non-specialists.

The following section summarises several recent publications concerning *ab initio* and TST calculations of cyclopropylmethyl radicals. Subsequently, the approach adopted in the present study for the aminocyclopropylmethyl radicals is discussed.

Previous theoretical estimates of the rate constants for the rearrangement of the cyclopropylmethyl radicals

The unsubstituted cyclopropylmethyl radical

High level calculations predict that the minimum energy conformation of the cyclopropylmethyl radical is a "bisected" structure, which allows the unpaired spin maximum overlap with two of the cyclopropyl C–C bonds (Fig 2.8).[49]

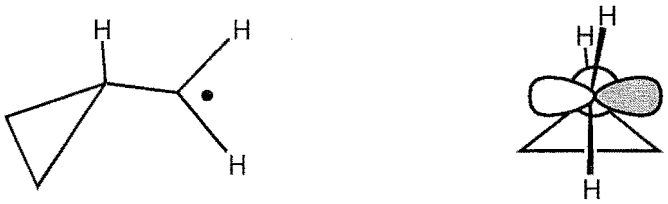

Figure 2.8. The bisected geometry of the cyclopropylmethyl radical.

Kinetics

The first report of an *ab initio* calculation of the ring opening reaction of the cyclopropylmethyl radical which gave results comparable to experimentally derived values, appeared in 1996.[50] It was demonstrated that the G2 level of theory, although computationally rather demanding, yielded an Arrhenius expression which is comparable to that found by low-temperature kinetic ESR measurements and competitive kinetic techniques (Table 2.1).[Y] The effects of incorporating methyl groups

[Y] It should be noted that a clerical error appeared in this paper. The correct values of the activation energy and reaction enthalpy at the G2 level of theory are 34.2 kJmol^{-1} and –14.6 kJmol^{-1} respectively.

in the ring carbons were examined, and were found to reproduce the experimental observation that the rate constant increases nearly additively with substitution. It was shown that the relative rates of ring-opening were not necessarily proportional to the heat of reaction (ΔH_{rxn}).

Table 2.1. Comparison of Various Theoretical Predictions with the Experimental Arrhenius Function for the Ring Opening of the Cyclopropylmethyl Radical.

Level of theory[a]	log A	E_{act} (kJmol^{-1})	k (s^{-1} 298 K)	Ref.
CBS-RAD(B3LYP, B3LYP)	13.2	31.2	5×10^7	49
G2	13.0	34.2	1×10^7	50
B3LYP/6-31G[b]	13.2	33.3	2×10^7	49
Experimental	13.2	29.5	1×10^8	45

[a] See appendix 1 for an explanation of this term.

[b] The B3LYP Arrhenius parameters were calculated from the data in ref 50 by adding the temperature correction of –2.9 kJmol^{-1} to the corrected zero-point energy, and using the relationship $E_{act}(T) = \Delta H^{\ddagger}(T) + RT$.

The influence of the level of theory on the calculated rate constant for the ring-opening reaction of the cyclopropylmethyl radical was detailed in a comprehensive publication from Radom's group.[49] The impact of the level of theory on the geometry, zero-point energy, and vibrational frequencies were discussed, and guidelines as to the requirements for a reliable rate constant calculation were prescribed. In essence, their conclusion was that the density functional hybrid method, B3LYP, in association with the 6-31G* basis set, provides an economical and reliable prediction of energies, and of geometry- and frequency-dependent quantities, including the Arrhenius frequency factor. The experimental results were best reproduced with the high level (read computationally demanding) CBS-RAD procedure.

Geometries of α-substituted cyclopropylmethyl radicals

Radicals which are mono-substituted at the radical centre (α-substituted) have two possible bisected conformations, termed *syn* or *anti* to describe the relative disposition of the cyclopropyl group and the α-substituent (Fig 2.9). Generally, the *anti* conformation is more stable since, although it eclipses the substituent with the methine H atom, it prevents the steric clash of the substituent with two of the cyclopropyl methylene hydrogens. The barrier to rotation about the *exo* C–C bond is low, hence the two forms can interconvert rapidly.[51]

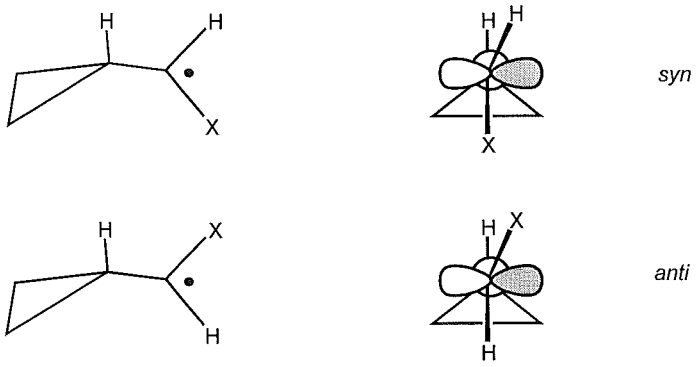

Figure 2.9. Two conformations of an α-substituted cyclopropylmethyl radical. Note that the radical centre will not necessarily be non-planar, as is pictured.

The reaction pathway of the unsubstituted cyclopropylmethyl radical is doubly degenerate by virtue of having two identical conformations of the transition state. However, substitution of the radical at the α-position removes this reaction degeneracy. There are now two possible transition states for the ring opening. One will lead to the *cis* double bonded product, and the other to the *trans* product (Fig 2.10).

It is expected that the *syn* transition state will suffer an energetic penalty due to the eclipsing of the substituent with one of the cyclopropyl C–C bonds, and the reaction pathway *via* the *anti* transition state will be favoured. It has been calculated that this energy difference amounts to about 4 $kJmol^{-1}$ for a methyl group (X = CH_3) , and 6 $kJmol^{-1}$ for an ester (X = CO_2Me) substituent.[52]

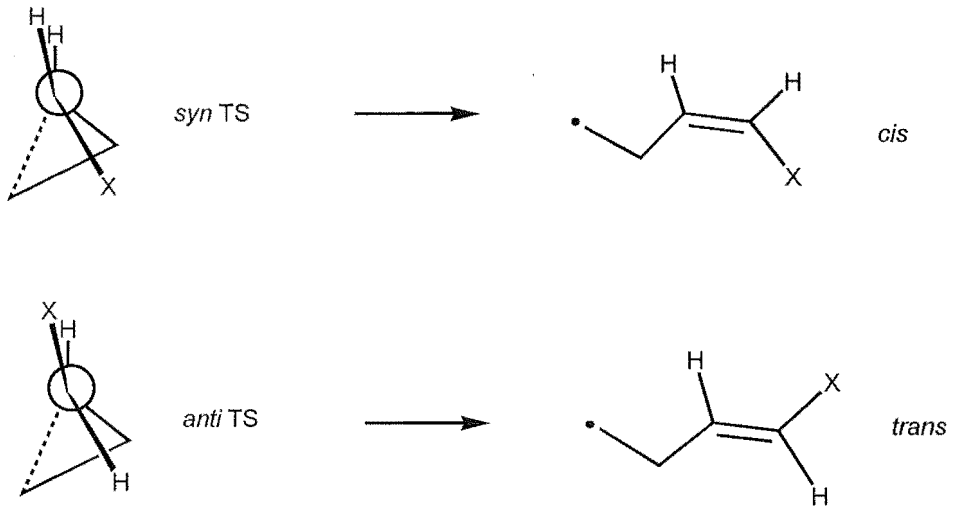

Figure 2.10. Two possible transition states for the ring-opening reaction of a α-substituted cyclopropylmethyl radical.

This removal of the reaction degeneracy will reduce the Arrhenius frequency factor as compared to the unsubstituted radical. If one of the channels is *totally* precluded by a large reaction barrier, the frequency factor will be reduced by log 2 (= 0.3). Often the reaction barrier difference is small enough so that both channels will operate. For example, for the methyl-substituted radical there is an approximate five-fold rate constant difference (with reaction *via* the *syn* transition state faster than *via* the *anti* transition state). In this case, the Arrhenius factor only drops by about 0.1 in comparison with the unsubstituted radical.[52] The kinetics are discussed further in the next section.

Previous calculations of rate constants of α-substituted cyclopropylmethyl radical

Newcomb's group have investigated the energetics of the ring-opening reactions of α-substituted cyclopropylmethyl radicals. The results of the theoretical investigations are tabulated below (Table 2.2). It has been demonstrated that the enthalpic contributions to the kinetics of the ring-opening reactions are well reproduced by high-level theoretical calculations. However, the accuracy of calculated *frequency factors* has

been established for only the unsubstituted radical. This lack of interest is a result of the empirical observation that this parameter is reasonably invariant with substitution.[58] The enthalpy of activation, therefore, will be primarily responsible for the differences in the rate constants.

Table 2.2. The Effect of Substitution at the Radical Centre on the Reaction Barrier of the Ring Opening of the Cyclopropylmethyl Radical.

Substituent		Level of theory	E_0 (kJmol^{-1})	Ref.
H		B3LYP/6-31G*	32.1	a
CH_3	*anti*	B3LYP/6-31G*	36.0	48
CH_3	*syn*	B3LYP/6-31G*	39.7	48
CO_2Me	*anti*	B3LYP/6-31G*	42.7	48
CO_2Me	*syn*	B3LYP/6-31G*	48.5	48
CH_3[b]	*anti*	PMP2/6-31G*//UHF/6-31G*	31.3	50
OCH_3[b]	*anti*	PMP2/6-31G*//UHF/6-31G*	38.2	50
Vinyl[b]	*anti*	PMP2/6-31G*//UHF/6-31G*	53.6	50

[a] Table 2.1. [b] The energies were not ZPE corrected.

A recent report from Newcomb's group described the use of DFT (B3LYP) in order to compute relative reaction barriers for a variety of methyl- and ester-substituted radicals. The results correlated impressively with experimental data.

Ab initio molecular orbital calculations were used to examine the influence of electronic effects on the reaction barrier by introducing vinyl and methoxy substituents to the spin–bearing carbon. Placing a vinyl substituent at the radical centre was predicted to increase the reaction barrier by 18.8 kJ/mol. The analysis of isodesmic reactions enabled the authors to conclude that the heightened barrier was a consequence of loss of

conjugation upon moving from the ground state to the TS.[⊕] A methoxy group exerted a lesser influence on the barrier height of the ring–opening reaction ($\Delta(\Delta E_0)$ = 3.3 kJ/mol), and methyl substitution on the radical centre was predicted to lower the reaction barrier slightly ($\Delta(\Delta E_0)$ = 3.5 kJ/mol) compared to the parent radical. The influence of these substituents is primarily inductive and scarcely differs between the ground and transition states.

These literature reports gave us confidence that the calculation of a rate constant for the system of interest in the present study - the aminocyclopropylmethyl radical - would yield a useful approximation for the rate constant for ring opening.

Computational methods

Although the calculations in the present study were initiated before the publication of Radom's paper[49] the recommendations in that report have subsequently shaped the approach taken in the present study to the theoretical determination of a rate constant for ring opening of the aminocyclopropylmethyl radical. In addition, only modest computer resources were available locally. The energy, geometry, and frequency

[⊕] The effect which substitution has on the reactant and transition state energies can be dissected with isodesmic reactions – reactions in which the reactants and products have the same number of each type of bond. This is more precise than the direct comparison of absolute energies as many sources of error cancel. Differences in reaction barriers are able to be rationalised in terms of the influence of substitution on the relative stabilities of the reactant and transition state. See: Hehre W.J., Radom L., Schleyer P.von R., Pople J.A., *Ab Initio Molecular Orbital Theory*; Wiley: New York, 1986.

calculations were performed at the B3LYP/6-31G* level. Such DFT methods accommodate electronic interactions better than simple Hartree-Fock techniques. Also, in many cases DFT provides a more economical return on computer time. The reader is directed to Appendix 1, and the references therein, for a more comprehensive account of DFT.

The calculations were executed by the Gaussian94 software package.[59] In practical terms, the calculations were initiated with the input of a tentative molecular geometry, an optimisation performed, and an energy for the stationary point obtained. A frequency calculation was then completed for this structure. The raw frequencies were scaled by a factor of 1.0013, and the zero-point energies by 0.9806, to account for known systematic errors.[60] The principle moments of inertia were obtained directly from the Gaussian94 output. The partition functions, and subsequently the rate constants, were evaluated at three different temperatures, and numerical differentiation of ln(k) with respect to T^{-1} yielded the Arrhenius parameters, A and E_{act}. The spin distribution and atomic coordinates for all the radicals and the transition states are given in Appendix 1.

The calculations for the aminocyclopropylmethyl radical

Geometry.

The calculated geometries for the reactant, transition state, and product for the radical, along with selected bond lengths, are displayed in Fig 2.11. Of the two possible conformations of the amine group with respect to the cyclopropyl group, the geometry (and energy) of the *anti* conformations of both the reactant and transition state were ascertained. Accordingly, this discussion will concentrate on the reaction of the *anti* conformation of the reactant, through the *anti* transition state.

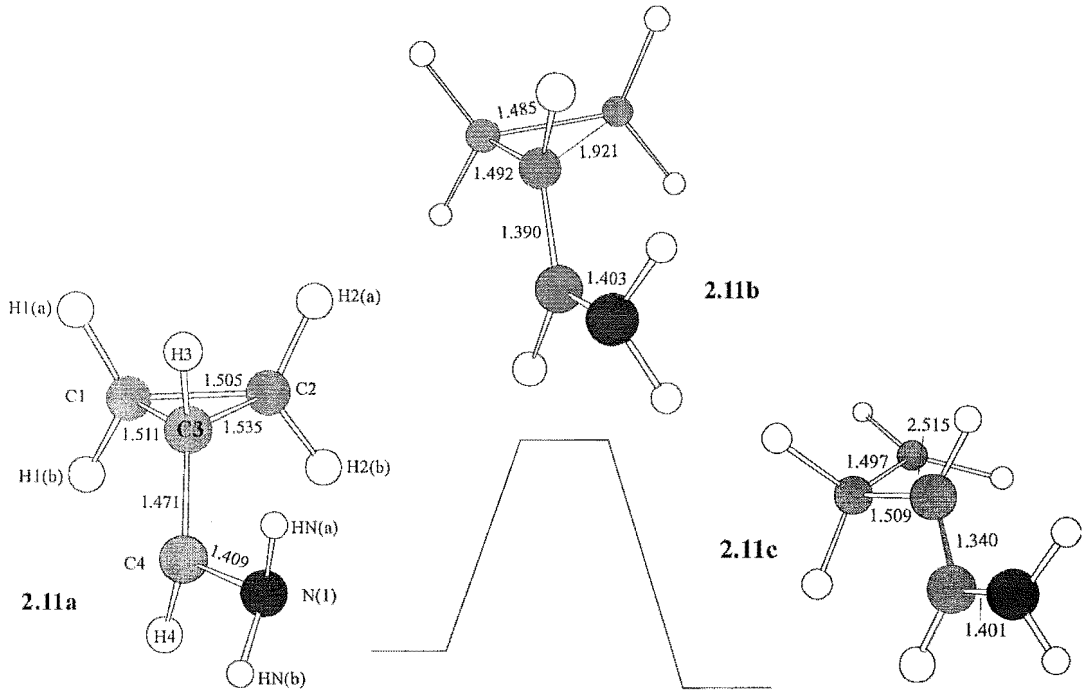

Figure 2.11. The calculated geometry of the aminocyclopropylmethyl radical (**2.11a**), its ring-opened product (**2.11c**), and the transition state for ring opening (**2.11b**).

The aminocyclopropylmethyl radical (**2.11a**) is predicted to have C_1 symmetry, with the geometry around the spin-bearing carbon (C4) marginally non-planar (sum of bond angles = 351.9°, RMS deviation from plane = 0.094 Å). This is in keeping with previous calculations on other aminoalkyl radicals.[61] The short C4–N1 bond length, and the spin density on the nitrogen centre are indicative of significant delocalisation of the unpaired electron. This is a well-documented[62,63] phenomenon for α-aminoalkyl radicals, and can be represented formally by two resonance forms (Fig 2.12).

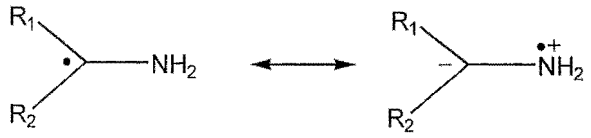

Figure 2.12. Delocalisation of the unpaired spin in aminoalkyl radicals.

Earlier, it was noted that, for the parent cyclopropylmethyl radical, the orientation of the radical centre allows the unpaired electron maximum overlap with the cyclopropyl C–C bonds, despite the energy penalty that results from the eclipsing of two hydrogen atoms. In the present example, the eclipsing interaction is diminished, with the substituents on C3 and C4 assuming an energetically favourable staggered disposition. This is due to the delocalisation of the unpaired electron towards N1, that is, *away* from the cyclopropyl group (dihedral angles: ∠N1–C4–C3–H3 = 50.3°; ∠H4–C4–C3–H3 = 163.1°). This will lead to a lessening of the interaction between the radical centre and the cyclopropyl ring. Thus, rotation around the C3–C4 bond will not be restricted, and the amine substituent will not be forced to eclipse H3. The interaction between the nitrogen and the unpaired spin is further enhanced by pyramidalisation of the spin-bearing carbon centre, bringing the nitrogen lone pair and the unpaired electron close in space. This pyramidalisation is possibly also induced by the "carbanion–esque" (ie partially sp^3 hybridised) character of this carbon atom.[64]

The transition state for this ring-opening process (**2.11b**) is close to planar for the atoms which are part of, or attached to, the incipient double bond (RMS deviation from plane for C1,C3, H3, C4, H4, N1 = 0.042Å, cf 0.028Å for the product).

The constant length of the C4–N1 bond suggests that the nitrogen lone pair remains partially delocalised throughout the reaction. In the enamine product this delocalisation can be depicted as an iminium resonance form (Fig 2.13).

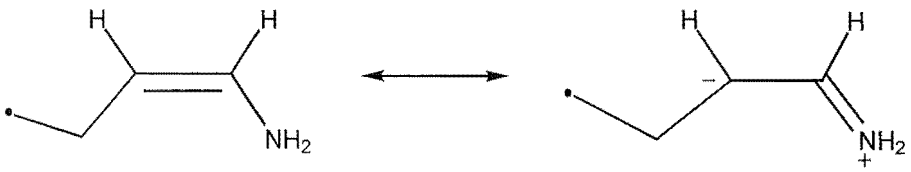

Figure 2.13. Two resonance forms of the ring-opened aminocyclopropylmethyl radical.

Partition functions

The raw data for the TST calculations for the ring opening of the aminocyclopropylmethyl radical are summarised in Table 2.3.

It is unsurprising that the rotational contributions to the partition functions from the reactant and transition state are roughly equal. The geometrical changes upon ring-opening are relatively minor and, because Q_{rot} increases with the square root of the moments on inertia, these changes will have a trifling effect on the value of this function. A corollary of this is that $Q^{\ddagger}_{rot}/Q_{rot}$ will be close to unity for both the forward and reverse reactions. Accordingly, the controlling influence on the overall partition functions will be Q_{vib}.

Table 2.3. Partition Function and Energy data for the Aminocyclopropylmethyl Radical Ring Opening and Closing.

	Q_{rot}[a]	Q_{vib}[a]	Energy[b]	ZPE correction[b]
2.11a	7.93×10^4	10.45	-211.8989623	0.113855
2.11b (TS)	8.60×10^4	7.09	-211.8821801	0.111146
2.11c	8.97×10^4	18.64	-211.9011211	0.111353

[a] Partition function data at 298 K. [b] Raw values in Hartrees. 1 Hartree is 2656.50 $kJmol^{-1}$.

The values of $Q^{\ddagger}_{vib}/Q_{vib}$ are dominated by low frequency vibrations (see Appendix 1). The lower value of this ratio for the reverse reaction, as compared to the forward reaction, is fostered by three vibrational modes in the ring-opened form which have frequencies less than 200 cm^{-1}. Such low-frequency motions are generally torsional, rather than bending or stretching modes, and arise from the relative "floppiness" of the ring-opened form.

The Arrhenius function.

The inclusion of an amine substituent at the radical centre is predicted to increase the activation energy by 6.3 $kJmol^{-1}$, leading to a twenty-fold drop in the rate constants compared to the unsubstituted radical (Table 2.4). The actual origin of this activation energy difference cannot be inferred with certainty from the absolute energies as these values are not accurate enough for direct comparison. It would be possible to make this comparison by analysing appropriate isodesmic reactions,[50] however this avenue was not pursued in the present study.

Table 2.4. Arrhenius Parameters for the Rearrangement of the Aminocyclopropylmethyl Radical.

	log A	E_{act} ($kJmol^{-1}$)	k (s^{-1}, 298 K)
2.11a→2.11b	13.1	39.7	1×10^6
2.11b→2.11a	12.4	49.6	5×10^3
Parent[a]	13.2	33.3	2×10^7

[a] Data for the forward reaction from Table 2.1.

A relatively large geometrical rearrangement must occur for the radical to reach the TS for ring opening. Not only does the C3–C2 bond have to lengthen and the C3–C4 bond shorten, C1, C3, H3, C4, H4, and N1 must come into the same plane. Compared to the unsubstituted cyclopropylmethyl radical, which has C3, H3, C4, and H4 already planar in its minimum energy conformation, a far more drastic manoeuvre is required to attain the TS configuration. However, this does not alter log A to any considerable degree, perhaps because some entropic compensation is earned because rotation around the *exo* bond, C3–C4, is hindered. This would allow the TS geometry to be formed more readily as it does not have to "freeze" out a rapid rotation. Comparison of the log A values for the ring-opening of the aminocyclopropylmethyl radical and its unsubstituted analogue, shows that $\Delta S^{\ddagger}$ is nearly invariant. This is entirely consistent with the empirical observations discussed later.

Ring opening of an ester-substituted cyclopropylmethyl radical was found experimentally to accelerate with increasing solvent polarity.[65] This radical rearranges faster than its unsubstituted parent, despite theoretical predictions to the contrary: calculations at the B3LYP/6-31G* level estimating a 30-fold drop in the rate constant upon ester substitution.[52] This was explained by favourable transition-state polarisation effects which may have been overlooked by theoretical procedure as no account is made for solvation effects (all species are presumed to be in the gas phase).

The transition state for the ring opening of the aminocyclopropylmethyl radical may similarly derive some stabilisation from the resonance delocalisation of the incipient double bond. Thus, the ring-opening rate constant for the aminocyclopropylmethyl radical presented above may substantially underestimate the true value, especially in polar media.

The ring-closing reverse reaction is predicted to have a rate constant three orders of magnitude smaller than that for the ring-opening. Again, the most significant contributor to this difference is the activation energy. This agrees with what one may expect intuitively: the formation of a cyclopropyl ring will be a thermodynamically difficult process. There is also a drop in the Arrhenius factor which reduces the rate constant by a factor of 0.5 compared to the ring-opening. In structural terms, this is due to the stiffening of the vibrational modes, and an entropic penalty due to the increased geometrical restrictions.

The calculations for the protonated aminocyclopropylmethyl radical

Geometry

The geometry of the *anti* conformation of the protonated aminocyclopropylmethyl radical (**2.14a**) broadly reflects that of its unprotonated analogue, with the proton adding in the position formerly occupied by the nitrogen lone pair.

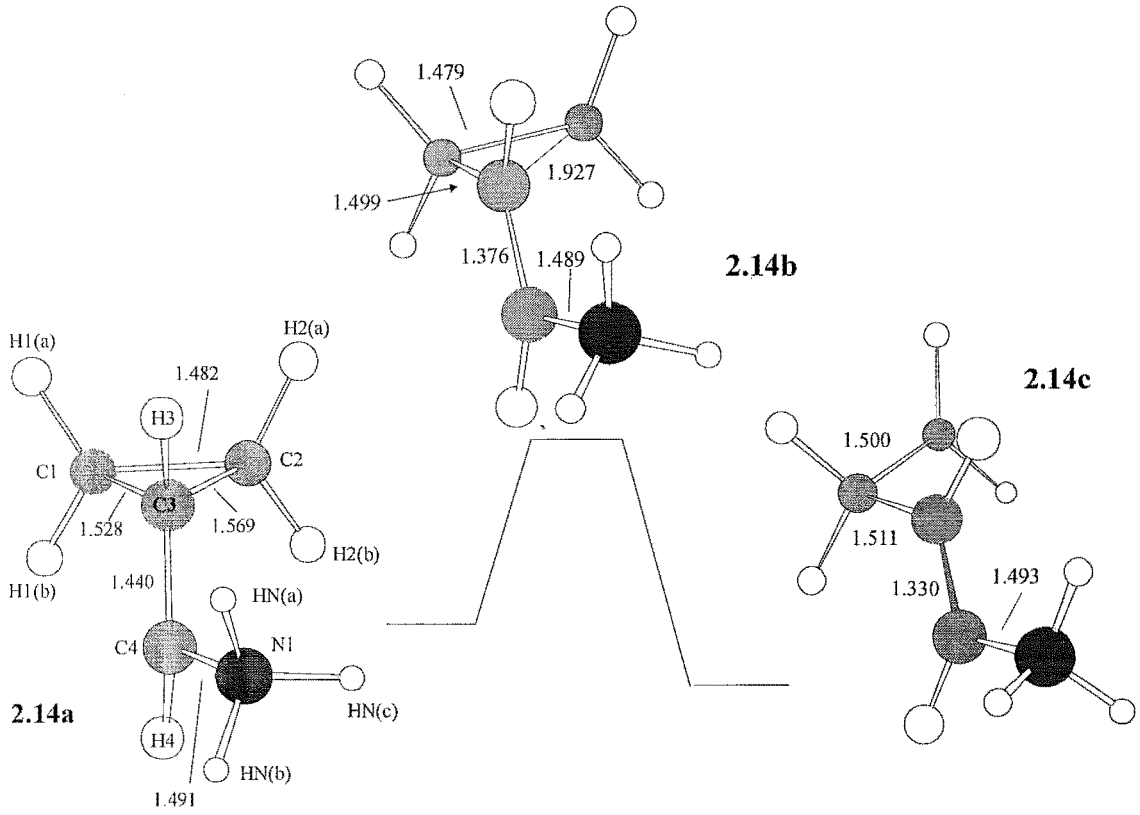

Figure 2.14. The calculated geometry of the protonated aminocyclopropylmethyl radical (**2.14a**), its ring-opened product (**2.14c**), and the transition state for ring opening (**2.14b**).

Protonation mitigates the ability of the lone pair to overlap with the radical centre, hence the lengthening of the C4–N1 bond and the absence of spin density on N1. The nitrogen centre may retain a weak inductive electron withdrawing effect. The radical centre C4 is marginally non-planar (bond angle sum = 354.6°, RMS deviation from plane = 0.076 Å), the *exocyclic* C3–C4 bond is 1.440 Å, and the dihedral angles are ∠N1–C4–C3–H3 = 34.27° and ∠H4–C4–C3–H3 = 173.8°. These structural parameters imply that:

(i) The radical has a significant interaction with the cyclopropyl bonds since the p orbital housing the unpaired spin bisects the cyclopropyl C–C bonds.

(ii) The radical centre pyramidalises to alleviate the unfavourable eclipsing of methine hydrogen H3 and the amine group, while allowing H4 to bisect H1b and H2b. This pyramidalisation also minimises the non-bonding interactions between the ammonium group and H3.

There is a difference of 0.041 Å in the bond lengths of the cyclopropyl bonds C3–C2 and C3–C1 as the overlap of the unpaired spin with these bonds is not symmetrical. Rotation about the C4–C3 bond favours overlap of the radical p orbital with the C3–C2 bond. This lengthens C2–C3, and develops some spin density on C2. The lengthening of the C3–C2 bond may be enhanced by a steric clash with the amine group which is *syn* to this bond.

Partition functions.

The near-unity value for $Q^{\ddagger}_{rot}/Q_{rot}$ for both the forward and reverse reactions ensures that the vibrational partition functions are again the major influence on the frequency factor. For the forward reaction, the frequency factor varies trivially from log[kT/h]. However, the higher value of Q_{vib} for the ring-opened form contributes to a five-fold reduction in this value for the reverse reaction. This can be ascribed to the low-frequency vibrational (torsional) modes in the more flexible ring-opened radical.

Table 2.5. Partition Functions and Energies Relating to the Rearrangement Reactions of the Protonated Aminocyclopropylmethyl Radical.

	Q_{rot}[a]	Q_{vib}[a]	Energy[b]	ZPE correction[b]
2.14a	8.56×10^4	14.77	-212.2540346	0.127968
2.14b (TS)	9.19×10^4	10.42	-212.2446752	0.126116
2.14c	9.96×10^4	36.06	-212.2557608	0.126104

[a] Partition function data at 298 K. [b] Raw data in Hartrees. 1 Hartree is 2656.50 kJmol^{-1}.

The Arrhenius function.

Theoretical calculations generally predict that the substitution at the radical centre leads to a heightened reaction barrier, roughly proportional to the steric bulk of the substituent (Table 2.2). In this case, since the ammonium substituent is reasonably compact, steric effects should not be exceptional. Hence, electronic effects are probably responsible for the unprecedentedly low activation energy.

Table 2.6. Arrhenius functions for the Rearrangement Reactions of the Protonated Aminocyclopropylmethyl Radical.

	log A	E_{act} (kJmol^{-1})	k (s^{-1}, 298 K)
2.14a→2.14c	13.1	21.9	2×10^9
2.14c→2.14a	12.2	29.0	1×10^7
Parent[a]	13.2	33.3	2×10^7

[a] Data for the forward reaction from Table 2.1.

The geometry and spin distribution can provide clues as to the reactivity of this radical. Both hint that the nitrogen centre does not have a significant interaction with the unpaired spin. Moreover, the shortening of the C(3)–C(4) upon substitution (1.440 Å *vs* 1.457 Å), the significant elongation of the C(3)–C(2) bond (1.569 *vs* 1.534 Å), and the development of spin density on C(2), all imply that the interaction of the unpaired spin with the cyclopropyl ring is significant. This delocalisation of spin density is consistent with a faster rate of rearrangement.

It is reasonable to expect that the ring-closing reaction of **2.14c** is accelerated by the orientation of the spin-bearing carbon C(2). The half-filled p orbital is directed towards C(3), rather than perpendicular to the C(2)–C(3) axis as in the unsubstituted case.

Sensitivity of the model to approximations and the potential for improvements

When using mathematics to model real systems, it is imperative to be mindful of the approximations one invokes, and the untoward perturbations which they may inflict. Several short-cuts have been taken in the present study, besides those inherent in the *ab initio* calculations and in transition-state theory. These will be now be outlined, and the scale of the influence on the calculated Arrhenius expressions will be estimated.

Low frequency vibrational modes (< 200 cm^{-1}), which correspond to torsional motions, are often better represented as hindered rotors than as harmonic oscillators, with a sinusoidal, rather than parabolic, potential.[57] In the case of the unsubstituted cyclopropylmethyl radical, a suspect low frequency torsion of the *exo*-methylene group was identified, treated as a hindered one-dimensional rotor, and associated with the rotational partition function.[49] In that case, the calculation of the internal rotational partition function used Truhlar's method wherein the rotational potential is given by a cosine function and an approximate analytical solution is derived.[66] Alternatively, the energy levels could be calculated by solving the one-dimensional Schrodinger equation for rotational motion using a reduced moment of inertia.[67]

In the present investigation, *all* vibrational modes were treated as harmonic oscillators for the evaluation of the vibrational partition functions. Any error associated with this approximation will be mitigated somewhat by the fact that the $Q^{\ddagger}_{vib}$ and Q_{vib} are treated in the same manner, leading to a partial cancellation of these errors in the TST expression. The best guess for the uncertainty introduced to the rate constant by this short-cut is about a factor of two or three. This estimate is based on a report regarding the addition of alkyl radicals to ethylene, a reaction closely related to the reverse reactions in the current study. It was found that treatment of three low-frequency torsions with the more accurate hindered rotor model generally *increased* the frequency factor two- or three-fold.[57]

Frequencies calculated at the B3LYP level were all scaled by an empirical factor which accounts for known systematic errors.[60] Again, the effect of any inaccuracies in the values of these frequencies will be quenched by the fact that a ratio of the vibrational partitions is used in the TST expression. Even the *complete elimination* of the lowest frequency mode, which makes the largest contribution to the frequency factor, of either the reactant or the transition state would only change the rate constant by a factor of 3! It is reasonable to assume that the errors arising from the calculated frequencies will be negligible.

The rotational partition functions impart little influence on rate coefficient and any errors in their calculated values will be of trifling significance, as discussed earlier. Moreover, the B3LYP method is known to predict molecular geometries very accurately.[49]

The energies of all species were calculated at the B3LYP/6-31G* level. This level of theory has produced impressive (ie comparable to experimental) results for other α-substituted radicals (Table 2.2). Although the B3LYP technique has gained a reputation for underestimating reaction barriers,[68,69] the reverse is certainly true for the cyclopropylmethyl radical. Indeed, some heart can be taken from Radom's observation that, for the parent radical, the B3LYP/6-31G* level of theory actually *overestimates* the reaction barrier by 3.8 kJ/mol.

Calculations with a more accurate method, or with an enlarged basis set, would enable the reaction barrier for ring opening of the aminocyclopropylmethyl radicals to be stated with more certainty. However, for the key reaction in the present study, the rearrangement of the protonated aminocyclopropylmethyl radical, a 5 $kJmol^{-1}$ increase in the reaction barrier would induce a mere six-fold reduction in the rate constant (298 K).

The calculations are likely to represent a *minimum* value for the real rate constants for the following reasons.

(i) The reaction from the *anti* conformation of the radicals has been calculated. These are more stable than the *syn* radicals,[51] hence the calculations represent the pathway of higher activation energy.

(ii) Ring opening *via* the *anti* transition state is likely to be a lower energy route to the product, as, in the transition state, the nitrogen substituent is not forced to be co-planar with a cyclopropyl C–C bond. Contribution *via* the *syn* transition state was neglected. However, if reaction through this transition state is possible, the real rate constants will be larger than calculated rate constants.

All the calculations were based on the presumption that the reacting species are in the gas phase. The shortcomings of this approach were highlighted earlier for an ester-substituted radical where the effects of transition-state polarisation were not fully accommodated. These may also apply to the amine-substituted radical. Where such effects are not in operation, such as the parent, methyl-substituted, or ammonium-substituted radicals, the gas-phase results should represent valid estimates for the solution rate constants.[52]

The errors which have been introduced through the various approximations will not detract from *relative* comparisons of the predicted rate constants for the forward and reverse reactions. Therefore, for both the amine substituted cyclopropylmethyl radical, and its protonated analogue, it can be stated with certainty that *the ring-opened form will dominate the ring-closed form in the event of any equilibrium.*

In an absolute sense, the calculated rate constants can be regarded as being reasonably reliable. The largest uncertainty is associated with the reaction barrier, and if this has

been underestimated, the true rate constants could be up to an order of magnitude slower than calculated. The influence other uncertainties, eg the harmonic oscillator approximation and the inference that the reaction will proceed from the *anti* conformation of the reactant *via* the *anti* transition state, will probably serve to *reduce* the calculated rate constant from its true value. In conclusion, allowing for an order of magnitude discrepancy introduced by an underestimate of the true activation energy, a minimum value for the rate constant for the ring opening of the protonated aminocyclopropylmethyl radical can be set at $10^8 s^{-1}$.

Rate constants of α–substituted cyclopropylmethyl radicals which have been measured experimentally

Rate constants for the ring-opening reaction of a variety of α-substituted cyclopropylmethyl radicals have been measured experimentally, usually by low-temperature ESR spectroscopy or by competitive kinetic techniques. This section reviews these experimental findings, and aims to establish trends which relate the effects of substitution with the observed rate constants. The final section of this chapter combines the earlier theoretical approach with this summary of experimental work in order to estimate a rate constant for the crucial reaction - the ring opening of the Co(II)-bound aminocyclopropylmethyl radical.

Relative contributions to the rate constants from A and E_{act}

Table 2.7. Experimental Arrhenius Parameters for the Ring-opening Reaction of α-Substituted Cyclopropylmethyl Radicals.

R	TS[c]	log A	E_{act} (kJmol^{-1})	k (s^{-1}, 298K)	Ref.
H		13.2	29.5	1×10^8	45
CH_3[a]		-	-	4×10^7	65
CH_3		13.1	32.2	4×10^7	58
S–Phenyl		-	-	$\geq 10^7$	70
Cyclopropyl		13.6	36.0	2×10^7	71
Phenyl	*anti*	14.0	52.7	6×10^4	71
CO_2Et		-	-	1×10^8	71
$CO_2{}^tBu$[b]	*anti*	13.7	44.8	7×10^5	71
$CO_2{}^tBu$[b]	*syn*	14.0	51.9	8×10^4	71

[a] Estimated from ref 65 by dividing their rate constants for the tagged (*trans*-2-(2,2-diphenylcyclopropyl)-cyclopropyl)methyl radicals by a factor of five. See also ref 52.

[b] These values should be regarded as a minimum limit. See text and ref 52.

[c] Conformation of the transition state, if stated.

The Arrhenius factors (A) for ring-opening of α-substituted cyclopropylmethyl radicals remain close to, or higher than, that of the unsubstituted radical. This implies that substitution of a (necessarily) bulkier group at the radical centre promotes the ring-opening reaction by increasing the entropy of activation. Differences in the Arrhenius factor, however, contribute less than an order of magnitude to the variation in the rate coefficient. The more influential parameter is the activation energy. This in turn will be controlled by the electronic and steric impact of substitution on both the reactant and the TS.

The effects of substitution - experimental findings

The introduction of mildly electron-donating alkyl groups (methyl, cyclopropyl) at the radical centre decreases the rate constant for ring opening. In these cases, both the *anti* and *syn* transition state conformations are accessible, however there is a kinetic retardation compared to the parent radical. This reflects the steric compression experienced by the *syn* form in aligning with a cyclopropyl bond in the TS which impedes reaction through this channel. Substituting a bulky, electron withdrawing thioether group at the radical centre was found to impart a moderate reduction in the rearrangement rate constant.[70]

Radical-stabilising substituents, such as phenyl and $^{t}BuCO_2$, retard the rate of ring opening at ambient temperatures.[71] Delocalisation of the unpaired spin is promoted by these substituents; an effect which is reduced in the TS, and lost completely in the product. Furthermore, the bulkiness of the substituents discourages the formation of the *syn* transition state. This selectivity is apparent from the high ratio of *trans* to *cis* isomers in the double-bonded product.[58] It was suggested that this steric effect might be tempered by the relief of non-bonding interactions of the substituent with the cyclopropyl ring.

It should be noted, however, that the ester groups can also stabilise the product by resonance delocalisation of the double bond, and that reactant radical stability will not control the kinetics entirely.[72] In the case of the ethyl ester, the notion that the TS is stabilised by polar effects has been invoked to explain the large rate constant, and it was suggested that several experimental factors may have led to an inaccurately low value for the tert-butyl ester. The placement of an amine substituent at the radical centre may induce similar polarisation effects, as discussed earlier.[52,65]

Broadly speaking, in the absence of polarisation effects, substitution at the radical centre has been shown experimentally to decrease the rate constant for ring-opening. This

abatement can be ascribed to both electronic and steric effects. Substituents which delocalise the unpaired spin, or which hinder the *syn* transition state, will retard the rate of ring-opening.

For the protonated aminocyclopropylmethyl radical, the substituent is unlikely to interact with the adjacent unpaired spin, and the size of the ammonium group is comparable to the methyl group. Hence, a reasonable approximation for the ring-opening rate constant would be around 10^7 s^{-1}.

What about the cobalt?

How closely will the estimations of rate constant that of the *protonated* aminocyclopropylmethyl rearrangement resemble the *Co(II)-bound* aminocyclopropylmethyl radical? The ultimate aim of both the TST calculations (10^8 - 10^9 s^{-1}) and the review of experimental data (10^7 s^{-1}), was to provide the foundation for a reliable rate constant for the protonated radical. This section discusses the replacement of a proton by $[Co^{II}(bpy)_2]^{2+}$ at the nitrogen centre, and the implications of all this for the cyclopropylglycine radical clock experiment.

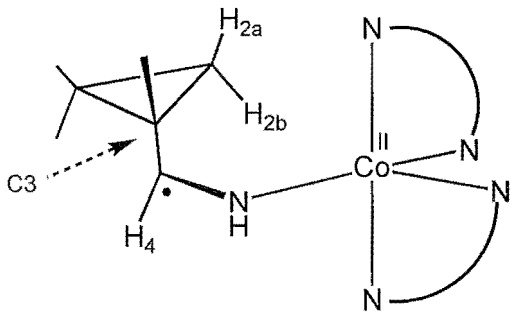

Figure 2.13. The *anti* conformation of the coordinated radical.

Steric effects

The nitrogen atom will coordinate to the cobalt centre *via* its lone pair of electrons, with a bond length of around 2 Å. The sphere of influence of the $[Co^{II}(bpy)_2]^{2+}$ is dependent on which conformation the radical adopts: in the *anti* form, H2b (3.5 Å), C4 (2.9 Å), and H4 (3.3 Å) will experience steric compression. This may induce lengthening of the C3–C2 bond, a widening of the Co–N1–C4 angle, and/or rotation around the C3–C4 axis. Realistically, the impact would be small, perhaps the C3–C2 bond elongation leading to a rate enhancement. The *syn* form of the radical will contact closely with H1a and H2a, perhaps elongating C3–C1 and C3–C2, maybe marginally accelerating the ring opening.

Unfortunately, no data exist for the analysis of steric effects comparable to the large $[Co(bpy)_2]^{2+}$ fragment. As discussed earlier, the steric bulk of this fragment could have: (i) an accelerating effect due to relief of non-bonding interactions with the cyclopropyl ring; or (ii) a decelerating effect caused by the reluctance to form the *syn* transition state. The calculated rate constant has fully allowed for this effect by considering only reactions *via* the *anti* channel.

A broad generalisation from both theoretical and experimental reports, is that the rate constant actually decreases with increasing substituent size. Given the large distance between the cyclopropyl ring/radical centre and the cobalt centre, the effect may be diminished somewhat in the present case. Regardless, the calculated rate constant, and that predicted by comparison with related experimental data, probably represent upper bounds to that of the Co(II) system.

Electronic effects

In electronic terms, the electropositive cobalt centre may boost the polarisation of the C4–N1 bond, making the radical centre more electron deficient, thereby further increasing the overlap of the unpaired spin with the cyclopropyl bonds. This could lead to a rate enhancement over the protonated radical. It is of note that the sulphur-substituted radical rearranges swiftly (Table 2.7). The electronic influence of this moiety may parallel that of the "$[(bpy)_2Co(NH_2)]^{2+}$" in the present study. Sulphur is somewhat more electronegative than nitrogen, however, the effect of the cobalt centre may well equalise their electron-withdrawing power.

The bottom line for the radical clock experiment

It appears that the rate constant for the protonated aminocyclopropylmethyl radical, based on the calculations and comparison with relevant experimental results, will serve as a good approximation for the Co(II)-bound analogue. The structural, steric, and electronic and differences should not have major implications for the rate constant for ring opening. Therefore, the best estimate for the ring-opening of the coordinated aminocyclopropylmethyl radical has an upper bound at 10^9 s^{-1} at room temperature, and a reasonable lower bound could be set at 10^7 s^{-1}. Furthermore, the rate constant for the reverse reaction should be around two orders of magnitude smaller than the forward reaction.

In summary: *if a coordinated aminocyclopropylmethyl radical is formed following the photolysis of* $[Co(bpy)_2(cpg)]^{2+}$, *it will ring-open with a rate constant* (k_r) *of between* 10^7 - 10^9 s^{-1}. *If an equilibrium is developed, the ring-opened product will dominate the ring-closed form.*

The reaction of the coordinated aminocyclopropylmethyl radical with the cobalt centre is proposed to occur with a rate constant (k_c) of 10^3 s^{-1}. Thus, the cyclopropylglycine ligand constitutes a viable radical clock as the ring-opening reaction of this radical will be fast enough to divert the photolysis reaction from its regular course.

A summary of Chapter 2

This chapter opened with a critique of the currently accepted mechanism for the photodecarboxylation of $[Co(bpy)_2(aa)]^{2+}$ complexes. It was pointed out that the assignment of the rate determining step is inconsistent with some well-established literature results. In itself, this is not a damning indictment, but a critical assessment of this mechanism is warranted. The potential for a radical clock to test the mechanism, whereby a radical rearrangement reaction is set up in competition with the proposed rate determining step of Co–C bond formation, was discussed. A complex of cyclopropylglycine constitutes an excellent precursor to such a clock. A theoretical investigation has demonstrated that the ring-opening reaction of the Co(II)-bound radical (formed by the photodecarboxylation of this complex) is likely to be considerably *faster* than the proposed bond formation with cobalt. This conclusion is supported by the ring-opening rates reported for other radicals. Therefore, if the currently accepted mechanism is correct, photolysis of the cpg complex should be diverted from its regular course by the ring-opening rearrangement, and the cyclopropyl group will not be present in the photolysis product. Furthermore, the ring-opened form of the radical will dominate the ring-closed form *if* an equilibrium is allowed to develop. The results of the experimental study of the cyclopropylglycinato complex are described in Chapter 3.

CHAPTER THREE

CHELATED CYCLOPROPYLGLYCINE AS A RADICAL CLOCK:

THE PRACTICE

Background

Several inconsistencies in the currently accepted mechanism for the photolysis of $[Co(bpy)_2(aa)]^{2+}$ complexes were detailed in Chapter 1. A method for testing this mechanism with a radical clock was introduced which involved the substitution of a cyclopropyl group at the α-carbon of the aminoacidato ligand. This chapter reports the results of photolysis of this complex of cyclopropylglycine. The outcome of these experiments is discussed in terms of the currently accepted photolysis mechanism.

The $[Co(bpy)_2(gly)]^{2+}$ complex yields a stable Co–C–N metallacycle following UV irradiation. As outlined in the introduction, this is a well-studied reaction. On the other hand, complexes of this type which have substituents at the α-position of the aminoacidato ligand have received relatively little attention. There is, however, evidence to suggest that alkyl substitution at this position compromises the stability of the photolysis product which contains a three-membered chelate ring. This literature report comes from Poznyak's group,[73] who investigated photolysis of the isopropyl-substituted complex, $[Co(bpy)_2(val)]^{2+}$. The changes in the UV-vis spectrum upon photolysis at 77K were consistent with the formation of a metallacycle. This product decomposed upon warming to room temperature, but the decomposition products were not identified.

Identification of the eventual products following photolysis of α-alkyl substituted complexes was required before undertaking the radical clock experiment. This chapter presents the synthesis and characterisation of a range of such complexes, along with the characterisation of their steady-state photolysis products. The results were useful particularly for analysis of the radical clock experiment.

Synthesis of $[Co(bpy)_2(aa)]^{2+}$ complexes

Cyclopropylglycine was prepared *via* a modification of a literature procedure,[74] furthering the work of Sargeson *et al.* This group detailed a templated synthesis, to yield a Co(III) complex of cyclopropylglycine (**3.1b**). The final step of their reaction sequence was the reduction of a chelated cyclopropyliminocarboxylato ligand (**3.1a**). We employed slightly more vigorous conditions to reduce the cobalt centre to the +2 oxidation state in the same step, thereby liberating cyclopropylglycine (**3.1c**). The amino acid was then purified by ion-exchange chromatography, and recrystallised to give a microanalytically pure product.

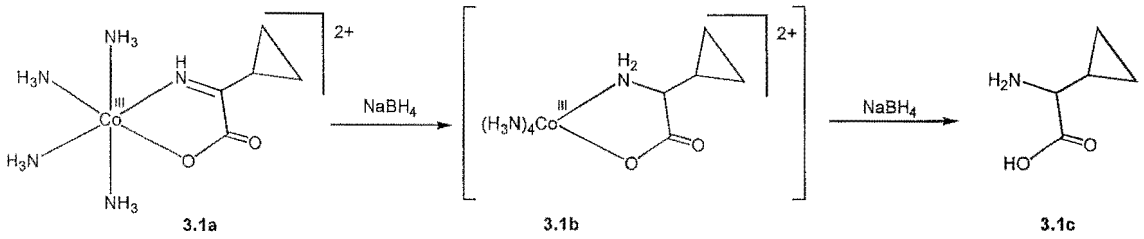

3.1a **3.1b** **3.1c**

Figure 3.1. The synthesis of cyclopropylglycine (cpg).

It was important to optimise the synthetic route to the $[Co(bpy)_2(aa)]^{2+}$ complexes, especially given the small amount of cyclopropylglycine which we were able to isolate, and its comparatively laborious preparation. The general method of Tatehata[75] was found to be superior to several alternatives which appear in the literature.[76,77,78] Tatehata prepared a series of $[Co(phen)_2(aa)]^{2+}$ complexes, *via* $[Co(phen)_2Cl_2]^+$ in methanol, and separated the reaction products by ion-exchange chromatography.

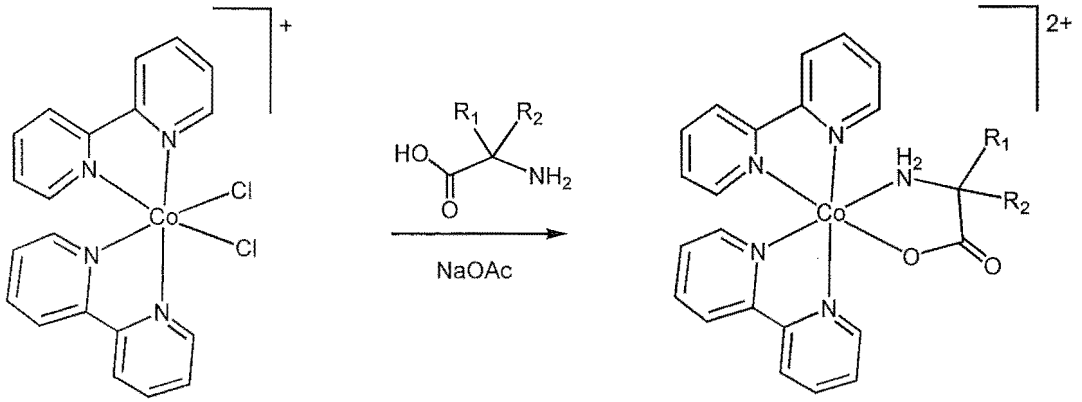

3.2a 3.2b

Figure 3.2. Preparation of the $[Co(bpy)_2(aa)]^{2+}$ complexes of ala ($R_1 = CH_3$, $R_2 = H$), val ($R_1 = CH(CH_3)_2$, $R_2 = H$), pgly (R_1 = phenyl, $R_2 = H$), aib ($R_1 = R_2 = CH_3$), and cpg (R_1 = cyclopropyl, $R_2 = H$).

This procedure was found to be more efficient than either using $[Co(bpy)_2(CO_3)]^+$ as a precursor, or *via* the PbO_2 oxidation of an aqueous solution of Co(II), an amino acid, and bipyridine. The formation of side-products, notably $[Co(aa)_2(bpy)]^+$ and $[Co(bpy)_3]^{3+}$, persisted however.

Characterisation of the $[Co(bpy)_2(aa)]^{2+}$ complexes

This range of complexes, where aa = ala, val, pgly, aib, and cpg, has been characterised by NMR, UV-vis, elemental analysis, and mass spectrometry. This represents the first such characterisation for these compounds (apart from the microanalysis and UV-vis of the $[Co(bpy)_2(ala)]^{2+}$).[77] In addition, the solid state structure of the cyclopropylglycinato complex was determined by X-ray crystallography.

$[Co(bpy)_2(aa)]^{2+}$ complexes of chiral amino acids have two diastereoisomers. These diastereoisomers result from the combination of the helicity of the three chelate rings (Δ,Λ) and the chiral centre of the amino acid (*R,S*). If an optically pure amino acid is used to prepare a complex, two diastereoisomers may form, eg Λ-$[Co(bpy)_2(S\text{-aa})]^{2+}$

and Δ-$[Co(bpy)_2(S\text{-aa})]^{2+}$. On the other hand, if racemic amino acid is used, the diastereoisomers will now each have an enantiomer. For example, the enantiomers of the above compounds, Δ-$[Co(bpy)_2(R\text{-aa})]^{2+}$ and Λ-$[Co(bpy)_2(R\text{-aa})]^{2+}$, will also be formed. This is illustrated in Fig 3.3 for the $[Co(bpy)_2(ala)]^{2+}$ complex.

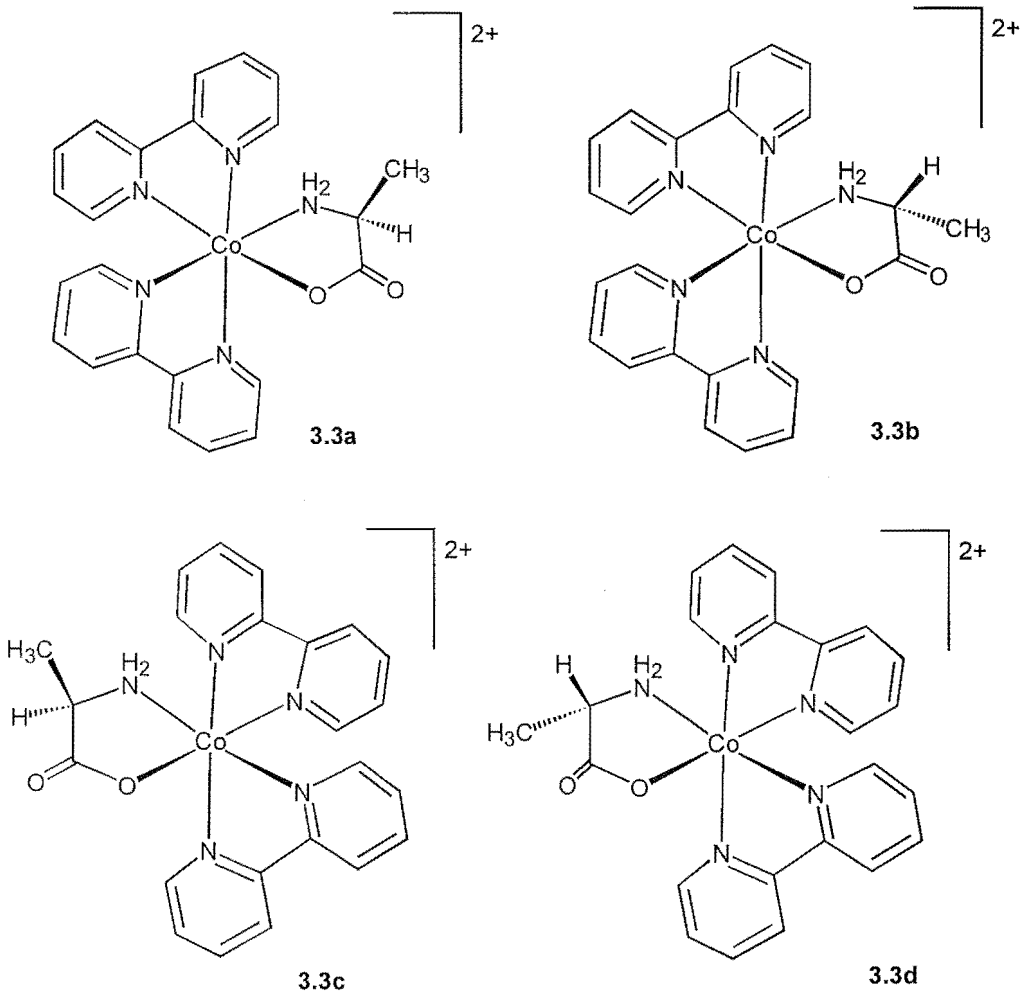

Figure 3.3. The four possible stereoisomers of the $[Co(bpy)_2(ala)]^{2+}$ complex.
3.3a = Λ-*S*; **3.3b** = Λ-*R*; **3.3c** = Δ-*R*; **3.3d** = Δ-*S*.

^{1}H NMR spectroscopy proved to be a useful tool for characterisation of these diastereoisomers, and the acquisition of 2D COSY spectra proved useful for the assignment of the peaks in these spectra. The 2D spectra were especially helpful in the cases where both diastereoisomers were present, as the signals often overlapped.

A preference for one diastereoisomer was noted in the preparation of all of the complexes: ala (3:1 ratio), val (9:1), cpg (5:2), and pgly (8:5). In the case of the $[Co(bpy)_2(val)]^{2+}$ and $[Co(bpy)_2(pgly)]^{2+}$ complexes, it was possible to purify one of the diastereoisomers by fractional crystallisation. However, both isomers persisted to some degree for the $[Co(bpy)_2(ala)]^{2+}$ and $[Co(bpy)_2(cpg)]^{2+}$ complexes. Alternative separation methods were not explored as, for the purposes of the photolysis experiments, the presence of two diastereoisomers was considered to be of little consequence.

A similar degree of stereoselectivity for the $[Co(phen)_2(S\text{-aa})]^{2+}$ complexes was noted by Tatehata, who postulated that the energy differences between the diastereoisomers was a result of repulsive interactions between the ortho proton of the diimine ligand and the α-substituent of the amino acid. On the basis of both CD spectra and ^1H NMR, he concluded that the major diastereoisomer had the Λ-S configuration.

We also examined molecular models in order to assess the influence of the anisotropic magnetic fields of the bipyridyl rings on the ^1H NMR chemical shifts of the chelated amino acid protons. This helped with the assignment of the ^1H NMR resonances to particular diastereoisomers. The chemical shift of the α-H of the chelated amino acid was most useful as it was found to exhibit significant variation between diastereoisomers. In the spectrum of the $[Co(bpy)_2(ala)]^{2+}$ complex, the α-H of the major isomer (3.85 ppm) was found to resonate at lower field than that of the minor isomer (3.36 ppm). A molecular model shows that for the Λ-*R*/Δ-*S* configuration, the α-H lies directly above the plane of one of the bipyridine rings. It is therefore exposed to a large shielding effect, and should resonate at higher field. This configuration was assigned to the minor isomer. In the case of the Δ-*R*/Λ-*S* isomer however, the α-H is significantly less influenced by the magnetic fields of the bipyridine ligands. The chemical shift of this proton is very close to those of the α-H atoms in the diastereoisomers of the $[Co(en)_2(ala)]^{2+}$ complex[79] (3.78 and 3.69 ppm), where such

ring currents are absent. Similar reasoning led to the assignment of the Δ-*R*/Λ-*S* configuration to the major diastereoisomers of the $[Co(bpy)_2(val)]^{2+}$, $[Co(bpy)_2(pgly)]^{2+}$, and $[Co(bpy)_2(cpg)]^{2+}$ complexes.

The X-ray crystal structure of $[Co(bpy)_2(cpg)](ClO_4)_2$

The X-ray crystal structure of the $[Co(bpy)_2(cpg)]^{2+}$ complex cation (Fig 3.4) unequivocally demonstrates the presence of a 3-membered cyclopropane ring in the complex, and is entirely consistent with the structure proposed on the basis of the other methods of characterisation.

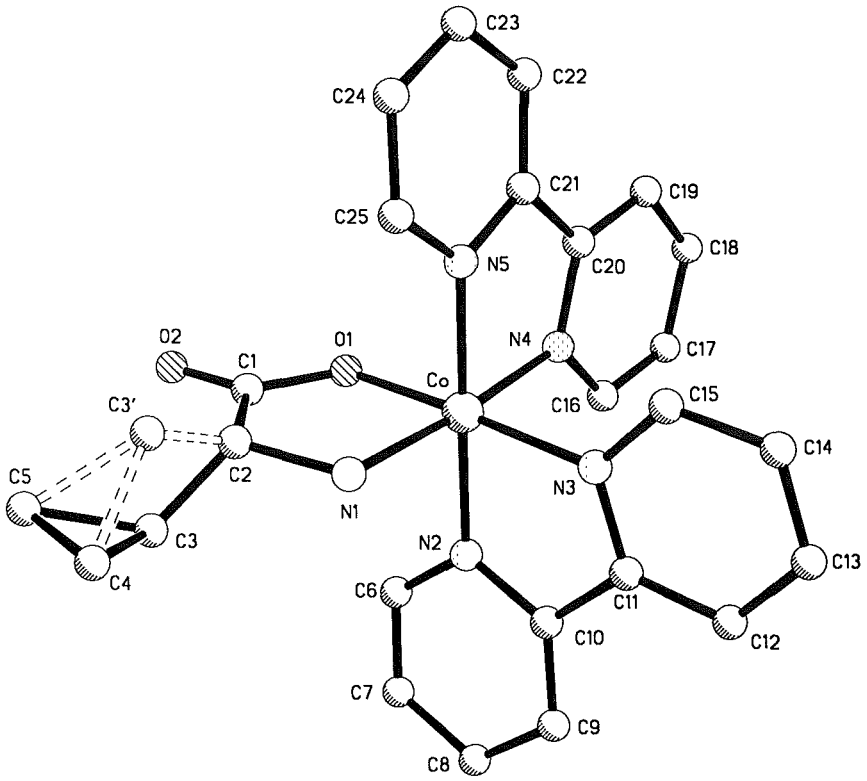

Figure 3.4. X-ray crystal structure of the $[Co(bpy)_2(cpg)]^{2+}$ cation. Hydrogen atoms are not shown. Selected bond lengths (Å) and angles (°): Co-O(1) 1.876(4); Co-N(1) 1.940(5); Co-N(2) 1.933(6); Co-N(3) 1.935(6); Co-N(4) 1.931(5); Co-N(5) 1.941(6); O(1)-Co-N(1) 86.6(2); N(2)-Co-N(3) 83.1(3); N(4)-Co-N(5) 82.8(2); C(4)-C(3)-C(5) 59.1(6); C(4)-C(3')-C(5) 51.2(19).

The geometry around the cobalt centre is slightly distorted from octahedral, and the bond lengths and angles are comparable to those of the $[Co(bpy)_2(gly)](ClO_4)_2$ [80] and $[Co(phen)_2(gly)](ClO_4)_2$ complexes.[81] According to the Cambridge Structural Database, these are the only other published structures of the type $[Co(di\text{-}imine)_2(aa)]^{2+}$. The Co-O bond length (1.876 Å) is somewhat shorter than the analogous glycinato complex (1.911 Å).

It became apparent during the refinement of the structure that there was pronounced disorder of the methine carbon of the cyclopropyl ring. This atom (C3) was modeled in two sites, giving two diastereoisomers; 85% in the Δ-*R*/Λ-*S* configuration and 15% as the Δ-*S*/Λ-*R* isomer. (It should be noted that this ratio of diastereoisomers is approximately that in the bulk material, as evidenced by ^{1}H NMR spectroscopy). There is considerable thermal displacement of C(2) perpendicular to the plane of the chelate which is probably an artifact of the disorder. This prevented the placement of the α-proton in a sensible position, hence it was disregarded in the refinement. In addition to the disorder within the complex ion, one of the perchlorate counter-ions is disordered unequally in two sites which differ only by rotation about one of the Cl-O bonds.

Steady state photochemistry of the $[Co(bpy)_2(aa)]^{2+}$ complexes

Steady state photolysis (254 nm) experiments were performed on D_2O solutions of this series of $[Co(bpy)_2(aa)]^{2+}$ complexes, and ^{1}H NMR spectroscopy was used to identify the photolysis products.

The changes in the ^{1}H NMR spectra upon irradiation of the $[Co(bpy)_2(aa)]^{2+}$ complexes indicated that a complex containing a Co–C–N metallacycle was not present. For example, 16 inequivalent bpy resonances would be expected for this complex (in

addition to the 16 signals from the starting material), whereas a simplification of the aromatic region in the spectrum was actually observed.

Carbonyl compounds were detected amongst the photolysis product; acetaldehyde, 2-methylpropanal, benzaldehyde, and acetone were identified following photolysis of the ala, val, pgly, and aib complexes respectively (Fig 3.5).

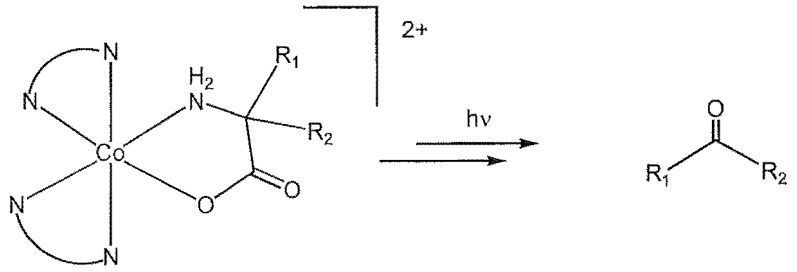

Figure 3.5

Free amino acid, $[Co(bpy)_3]^{3+}$, and free bipyridine were also identified by ^1H NMR spectroscopy. The hydrated forms of acetaldehyde and 2-methylpropanal were also present, as would be expected in aqueous solution. The relative concentrations of all the products were determined by reference to an added internal standard (TMPS), and their identities were confirmed by spiking the solution with authentic samples.

Addition of DCl to the neutral photolysates resulted in large increases in the integrals of the free bipyridine and free amino acid signals in the ^1H NMR spectra. The interaction of the paramagnetic Co(II) ion with the bipyridine and free amino acid is likely to reduce the intensity of their ^1H NMR peaks. However, this effect will be mitigated by the presence of acid, and the ^1H NMR signals were seen to increase correspondingly.

Comparison of the ^1H NMR integrals in the acidified samples against an internal standard accounted for most ($\approx$ 80%) of the $[Co(bpy)_2(aib)]^{2+}$ complex following irradiation. It was found that for a 0.10 M solution, the ratio of acetone to free

aminoisobutyric acid in the photolysate was approximately 1:3. There was a distinct increase in the fraction of acetone at lower concentrations. For example a 0.03 M solution of $[Co(bpy)_2(aib)]^{2+}$ gave a ratio of *circa* 1:1.7 (acetone:aib) following photolysis. Free bipyridine and $[Co(bpy)_3]^{3+}$ were present in roughly equal amounts, although the concentration of $[Co(bpy)_3]^{3+}$ increased gradually over time.

Unfortunately full materials balances could not be achieved for the other complexes. This is ascribed to a combination of: (i) volatility of the carbonyl compounds; (ii) persistent interactions with the paramagnetic Co(II) cation; (iii) poor signal to noise ratio in the NMR spectra at high concentrations of DCl; and (iv) aldol polymerisation of the aldehydes.

The photolysis of $[Co(bpy)_2(pgly)]^{2+}$ – the path which was not taken

It is worthwhile taking a brief digression to consider another possible outcome of the photolysis of the pgly complex (Fig 3.6). If a radical is generated at the α-carbon of the amino acid (**3.6b**), the unpaired spin could be delocalised into the phenyl ring (**3.6c**). This would introduce some spin density at the ortho position of the ring. This may lead to '*ortho*-metallation' whereby a bond may form between the *ortho* position of the phenyl ring and the cobalt centre, generating a five-membered chelate ring (**3.6d**). Such cyclometallated complexes are well-known for metals such as Pd and Pt, however this is a very rare structural motif for cobalt complexes.[82] If the cyclometallated complex **3.6d** is unstable at room temperature, it is an open question as to what the decomposition products might be (**3.6e**).

These possibilities were considered when the photolysis of the $[Co(bpy)_2(pgly)]^{2+}$ complex was monitored. However, the ^1H NMR spectrum of the photolysate did not display peaks which could be assigned to the putative complex **3.6d**. The eventual products (benzaldehyde, free pgly etc) were analogous to those observed following

photolysis of the other aminoacidato complexes. There is one circumstance which would give the observed product distribution *via* this alternative 'delocalisation' route. This would involve homolytic dissociation of the Co–C bond in **3.6d** to give a imine-substituted phenyl radical. Abstraction of a labile hydrogen atom by this radical, for example from the α-position of a molecule of **3.6a**, would give **3.6e** (with X = H). This possibility cannot be ruled out.

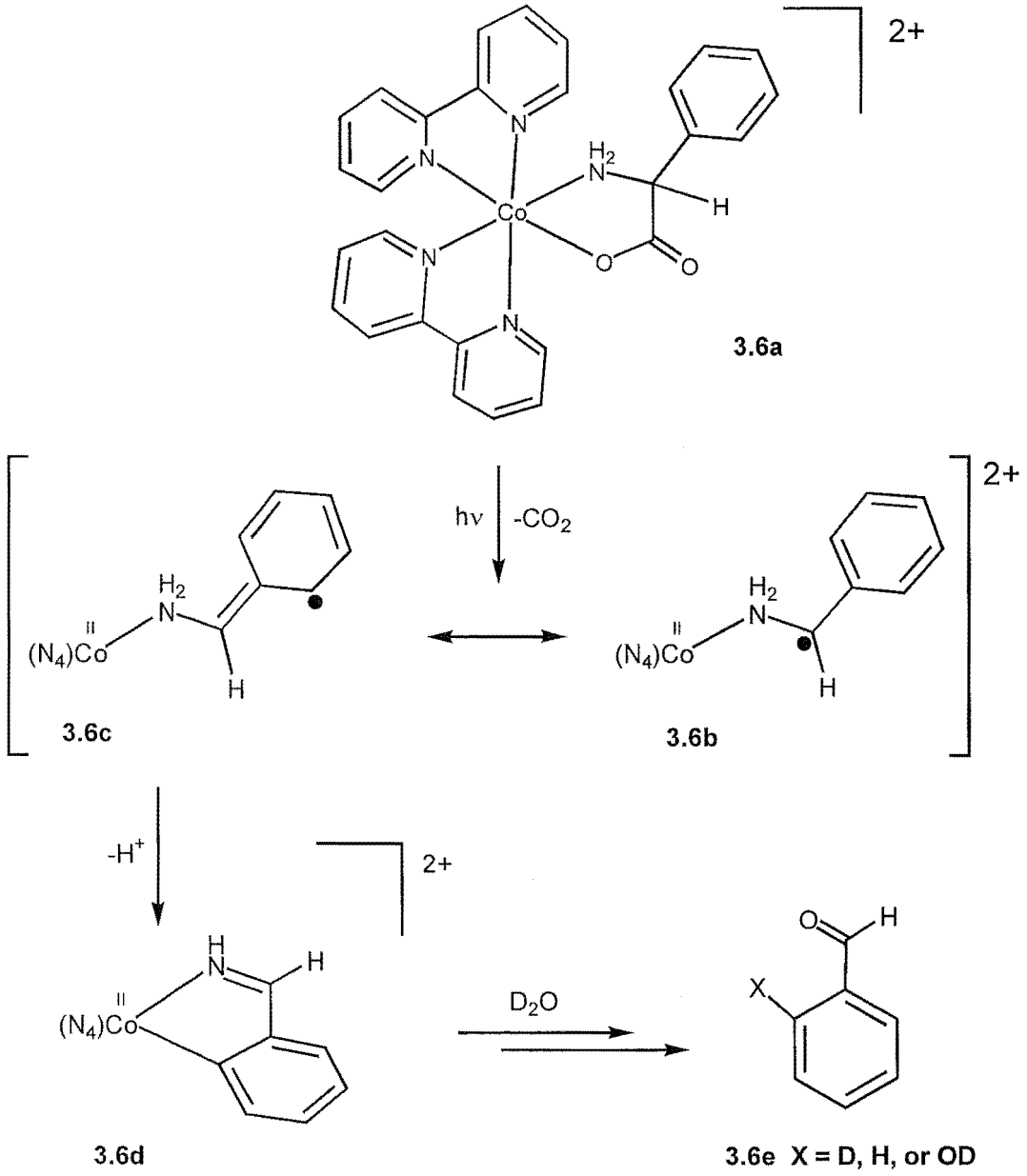

Figure 3.6. A possible photochemical pathway for the $[Co(bpy)_2(pgly)]^{2+}$ complex.

Steady-state photolysis of $[Co(bpy)_2(cpg)]^{2+}$ – the radical clock experiment

UV photolysis of a D_2O solution of $[Co(bpy)_2(cpg)]^{2+}$ (**3.7a**) gave a product distribution entirely analogous to the other $[Co(bpy)_2(aa)]^{2+}$ complexes. The products which were identified by ^1H NMR were: free cpg; $[Co(bpy)_3]^{3+}$; free bpy; and, most importantly, cyclopropanecarboxaldehyde (**3.7b**). No ring-opened products were detected by ^1H NMR spectroscopy.

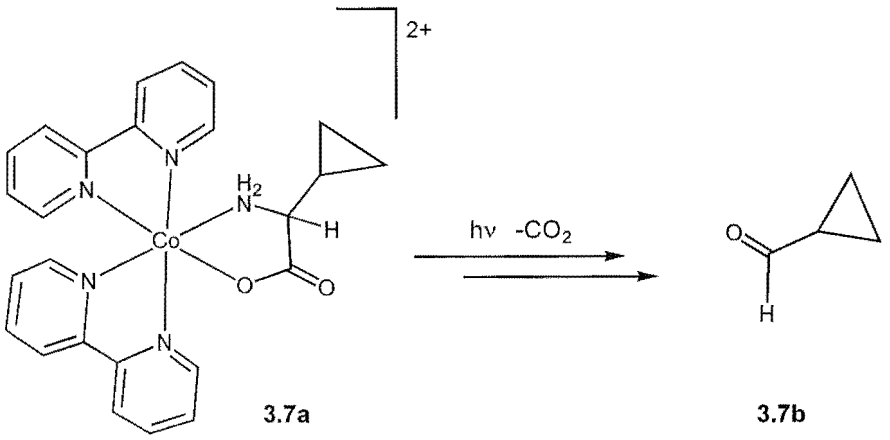

Figure 3.7. Cyclopropanecarboxaldehyde is produced following the UV photolysis of $[Co(bpy)_2(cpg)]^{2+}$.

A COSY spectrum was obtained in order to confirm the presence of the cyclopropanecarboxaldehyde. The coupling pattern shown by this spectrum was fully consistent with that expected for cyclopropanecarboxaldehyde; the methine proton displaying a correlation with both the cyclopropyl ring protons and the aldehyde proton. In addition, the aldehyde was extracted into $CDCl_3$ for comparison of the ^1H and ^{13}C NMR spectra with those previously published for this compound.[83] These spectra were identical to those published for authentic samples.

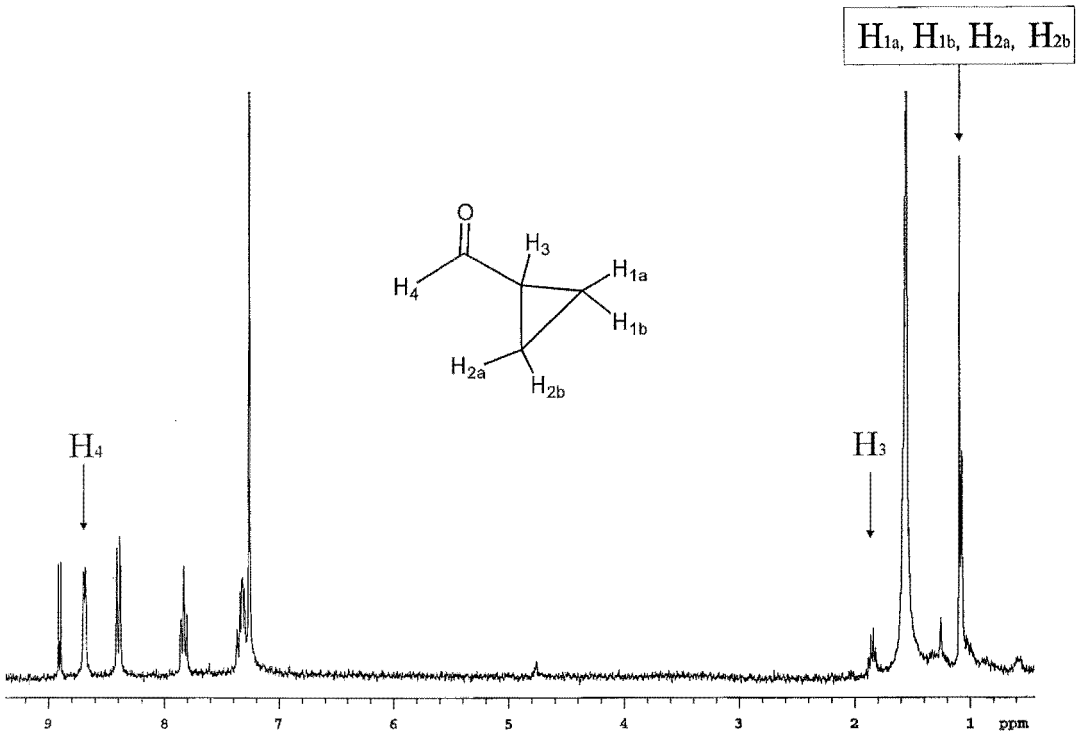

Figure 3.8. The ^{1}H NMR (300 MHz) spectrum of cyclopropanecarboxaldehyde extracted from the photolysate of $[Co(bpy)_2(cpg)]^{2+}$ by $CDCl_3$. The other five signals in the low field region are from free bpy (four multiplets) and $CHCl_3$ (singlet). The broad peak around 1.6 ppm is probably HOD.

The implications of the radical clock experiment for the currently accepted mechanism

On the basis of the currently accepted mechanism, photolysis of the $[Co(bpy)_2(cpg)]^{2+}$ (**3.9a**) complex is predicted to generate the radical **3.9b**. Bond formation between this radical and the cobalt centre has been proposed to occur with $k_c \approx 10^3 - 10^4$ s^{-1}. However, at this point another reaction channel is available to radical **3.9b**, whereby the cyclopropyl group can rearrange. This step is predicted to have a rate constant $k_r \approx 10^7 - 10^9$ s^{-1} (Chapter 2). As such, $k_r > k_c$, and the currently accepted mechanism implies that ring-opened products will form exclusively.

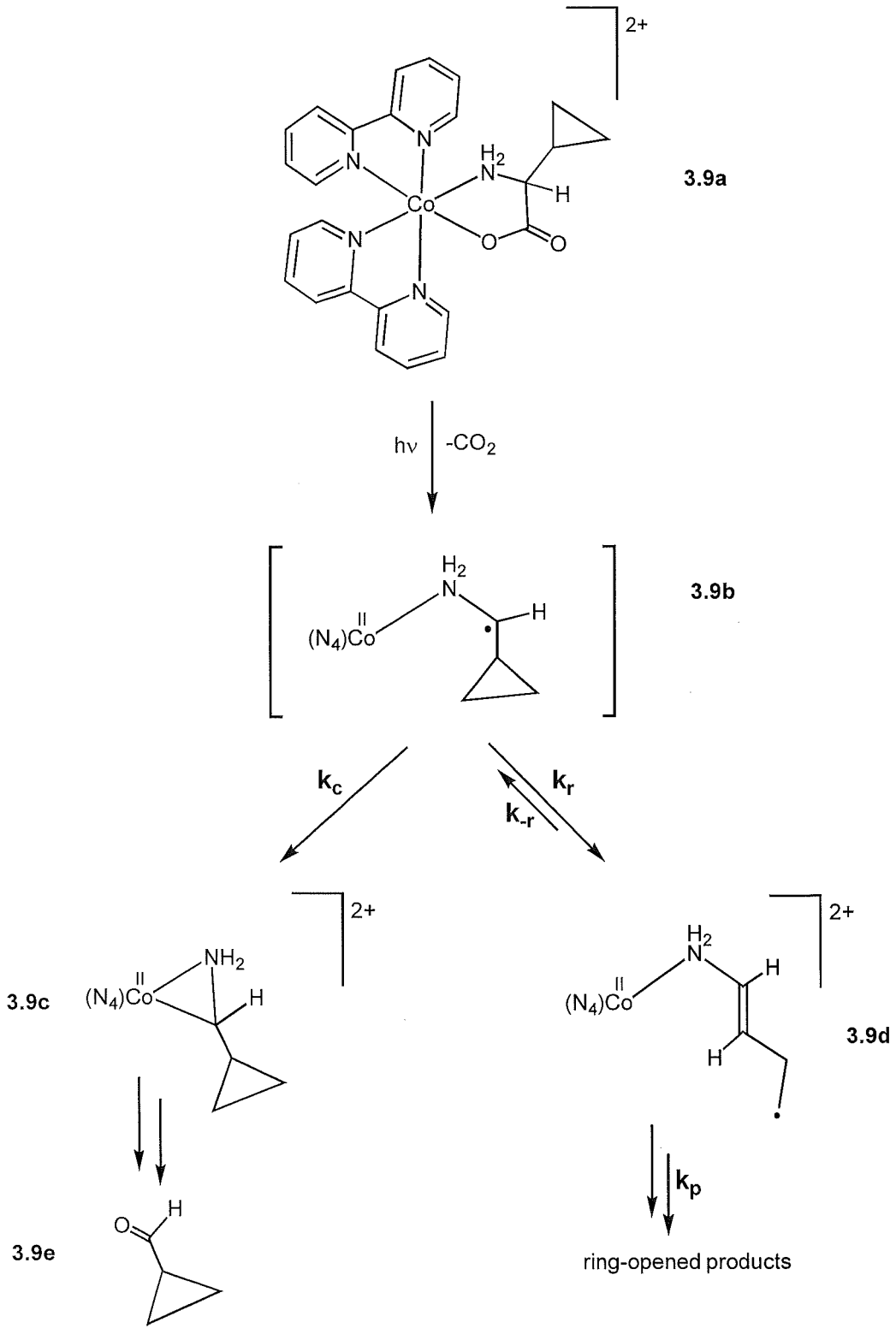

Figure 3.9. Two possible reaction pathways for the $[Co(bpy)_2(cpg)]^{2+}$ complex.

Ring-opened products should be detectable if around 10% of the molecules had followed that pathway from radical **3.9b**.[#] No ring opened products were actually detected, therefore k_c must be at least ten times faster than k_r. A lower limit for k_r was estimated at 10^7 s^{-1} (Chapter 2).

Therefore, *if the radical **3.9b** is formed, the rate constant of the reaction which removes it must be greater than* 10^8 s^{-1}. *Thus, if the reaction follows the proposed mechanism, this value represents a minimum value for* k_c. *This is more than four orders of magnitude greater than the value assigned to this rate constant in the original kinetic study.*

[#] It should be noted that the potential ring-opening reaction of **3.9b** is reversible, and the equilibrium constant, given by $K = k_r/k_{-r}$, will have a value of at least 100 (if one actually develops, see Chapter 2). This leads to one circumstance whereby the coordinated radical **3.9b** could have rearranged, but no ring-opened products would have been observed. This could arise if the sum of the rate constants of the reactions which remove the ring-opened radical (k_p) is more than 100 times *smaller* than k_c. This puts $k_p < 10^1$ s^{-1}, making this an extremely unlikely possibility.

How do the carbonyl compounds form?

The appearance of carbonyl compounds following photolysis of the α-substituted $[Co(bpy)_2(aa)]^{2+}$ complexes warrants an explanation. Similar behavior has been reported for photolysis of $[Co(edta)]^-$, [84] $[Co(gly)_3]$ and $[Co(ala)_3]$,[85] for which aldehydes were detected as photo-oxidation products of the aminocarboxylato ligands. Likewise, photolysis of cobalt(III)-polyamine complexes, for example $[Co(en)_3]^{3+}$, leads to ligand fragmentation and the production of carbonyl compounds.[8] No consideration was given in these reports to a mechanism for the formation of these carbonyl compounds. A decomposition route for the flash photolysis products of $[Co(bpy)(en)(gly)]^{2+}$ and $[Co(bpy)(en)(ala)]^{2+}$ has been advanced, although it was unsubstantiated by any empirical evidence.[28] Adaptation of this proposal to the closely related $[Co(bpy)_2(aa)]^{2+}$ complexes, does not lead to the prediction that carbonyl compounds will form from the photolysis products.

The carbonyl compounds clearly originate from the R_1R_2C–N fragment of the amino acid, following decarboxylation. However, the actual pathway to their formation is not immediately obvious.

Spectroscopic evidence implies that a complex containing a Co–C–N metallacycle is formed during the low-temperature photolysis of $[Co(bpy)_2(val)]^{2+}$, as touched upon in the introduction to this chapter. The metallacycle, however, did not survive when the frozen solution was warmed to room temperature. These observations suggest that substitution of an alkyl group on the α-C of the aminoacidato ligand will not *prevent* the formation of a metallacycle, rather it renders such chelates prone to thermal decomposition. On this basis, it is reasonable to propose that the carbonyl compounds which were observed following the photolysis of the $[Co(bpy)_2(aa)]^{2+}$ complexes, are

the thermal decomposition products of unstable metallacycles. A possible decomposition route is given in Fig 3.10.

The X-ray crystal structure of the $[Co(bpy)_2(H_2C–NH_2)]^{2+}$ ion (**3.10c**, $R_1 = R_2 = H$), which is the relatively stable photolysis product of the $[Co(bpy)_2(gly)]^{2+}$ complex, demonstrated that the C–N bond length in the metallacycle is 1.41 Å.[25] This is significantly shorter than a standard C–N single bond (1.50 Å), and implies that the bond order is greater than unity. The bonding within the three-membered chelate may therefore be better represented with a contribution from an additional resonance form; a trigonal bipyramidal Co(I) centre bound to an iminium ion (**3.10b**).

The decomposition of the metallacycles, can be represented by dissociation of the iminium ion (**3.10d**) from the Co(I) centre. Iminium ions are prone to hydrolysis and will yield the observed carbonyl compounds (**3.10e**).

Although somewhat speculative, the free amino acid, free bpy, and Co(II) ions which are observed following photolysis may result from bimolecular redox reactions between a $[(bpy)_2Co(I)]^+$ compound (which may also have solvent etc coordinated) and a molecule of starting material, $[Co(bpy)_2(aa)]^{2+}$ (**3.10a**). A reaction such as this would generate two molecules of Co(II), four molecules of free bpy, and one molecule of free amino acid.

$$\left[(bpy)_2 Co^{I}\right]^{+} + \left[Co(bpy)_2(aa)\right]^{2+} \rightarrow 2Co^{2+} + 2bpy + aa^{-} \qquad (3.1)$$

This idea is consistent with the observations that lowering the concentration of $[Co(bpy)_2(aib)]^{2+}$ led to an increase in the ratio of acetone to free amino acid. The bimolecular redox reaction which would generate the free ligands will be inhibited by dilution, hence other reactions of the Co(I) complex may prosper. For example, the reaction of the Co(I) complex with a deuteron to form a Co(III)-deuteride species may dominate when the concentration of $[Co(bpy)_2(aib)]^{2+}$ is low.[86]

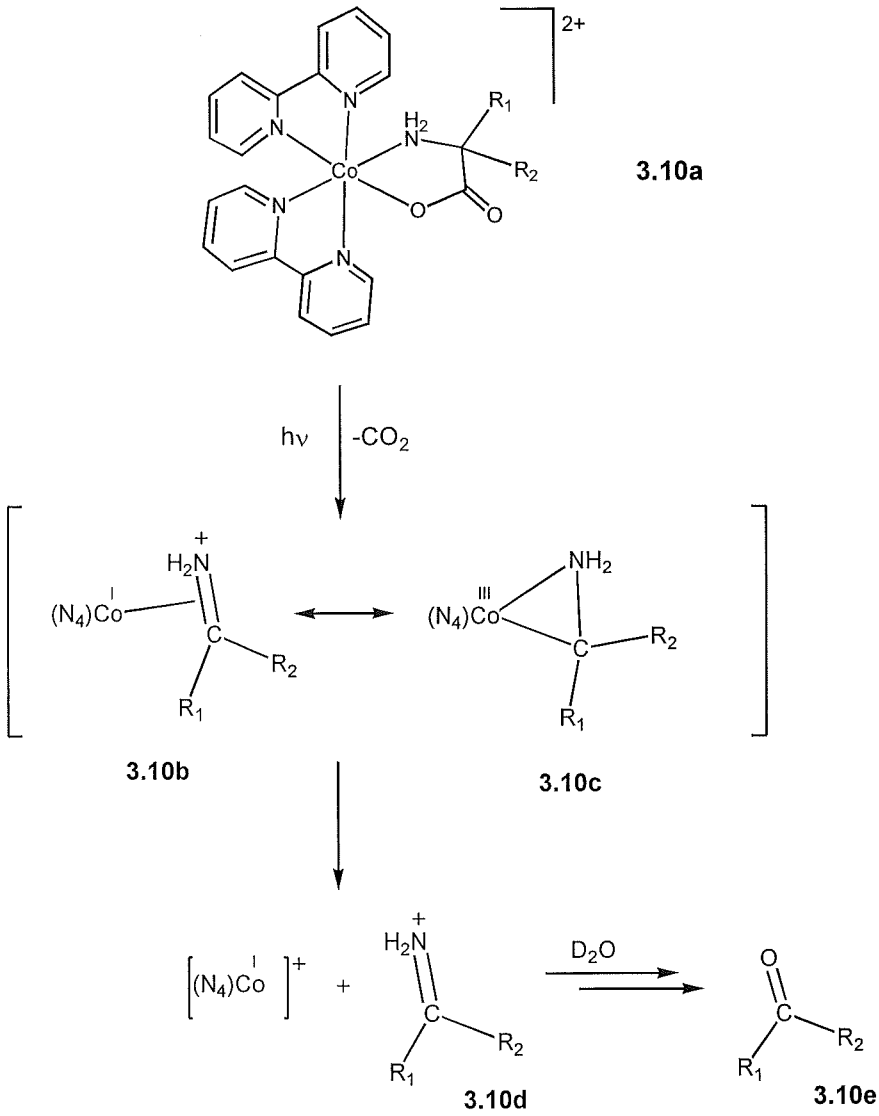

Figure 3.10. A suggested mechanism for the production of carbonyl compounds following photolysis of the $[Co(bpy)_2(aa)]^{2+}$ complexes.

The Co(I) decomposition pathway is represented by Eqtn 3.3. Co(III)-alkyl complexes are known to decompose *via* two other routes (Eqtn 3.1 and 3.2)

$$Co^{III}—R \rightarrow Co^{III} + R^- \quad (3.1)$$

$$Co^{III}—R \rightarrow Co^{II} + R^{\bullet} \quad (3.2)$$

$$Co^{III}—R \rightarrow Co^{I} + R^+ \quad (3.3)$$

Equation 3.1 represents heterolytic fission of the Co–C bond, which generates a carbanion and a Co(III) complex. In aqueous solution, the strongly basic carbanion would extract a proton from the solvent. For the specific case of an α-amino carbanion, which may be formed from decomposition of a Co–C–N metallacycle, a C-deuterated amine would be generated in D_2O. This should be easily detected by ^1H NMR. The absence of such amines implies that Eqtn 3.1 does not represent a significant decomposition pathway for the metallacycles in these systems.

The second alternative, homolytic cleavage of the Co–C bond (Eqtn 3.2), leads to the formation of a Co(II) complex and a radical. In this case, the fate of the radical fragment will vary depending the nature of the other species in the system. For instance, the radical will react rapidly with other radicals or will extract any loosely bound hydrogen atoms. In the present case, the α-amino radical could abstract a hydrogen atom from the α-position of another complex (reactant or metallacycle), or react with another molecule which has an unpaired electron, for example self-termination, or reaction with O_2. For an α-amino radical in D_2O, the potential products include amines (H abstraction), diamines (self-termination) and aldehydes (reaction with O_2). Again, any amine products would be detected by ^1H NMR spectroscopy, and their absence indicates that formation of a radical from the metallacycles, followed by hydrogen abstraction or self-termination, is not a significant process.

The reaction of aminoalkyl radicals with O_2 could also yield the observed carbonyl compounds. However, when the photolysis reaction of $[Co(bpy)_2(aib)]^{2+}$ was performed in de-oxygenated D_2O, the observed ratio of acetone to free amino acid was *unchanged.* Furthermore, Langford *et al* detected formaldehyde following the photolysis of $[Co(edta)]^-$ in degassed H_2O.[31c] Further evidence against this putative pathway was obtained by photolysing the $[Co(bpy)_2(aib)]^{2+}$ complex in the presence of the TEMPO radical trap. The rate constants for reactions of this radical trap with alkyl radicals are very large ($k_{298} \approx 10^9$ $M^{-1}s^{-1}$) and are relatively insensitive to the nature of

the alkyl radical.[47b] The product distribution was not altered, and no radical coupling products were detected by ^{1}H NMR spectroscopy. In addition, the retention of the cyclopropyl group in the photolysis of $[Co(bpy)_2(cpg)]^{2+}$ indicates that if an α-aminocyclopropylmethyl radical is formed in the decomposition reaction, it has a lifetime of less than about 10^{-8} s^{-1}.

In summary, observation of carbonyl compounds and the absence of alkylamines in the photolysate strongly suggests that the metallacycles decompose heterolytically to give a Co(I) complex and iminium ions.

Summary of Chapter 3

The UV photolysis of $[Co(bpy)_2(aa)]^{2+}$ complexes with alkyl substituents on the amino acid α-carbon results in the formation of (among other products) carbonyl compounds derived from the R_1R_2C–N fragment of the amino acid. Photolysis of the radical clock precursor, $[Co(bpy)_2(cpg)]^{2+}$ yielded cyclopropanecarboxaldehyde. The retention of the cyclopropyl group in the product demonstrates that if a cobalt(II)-bound aminoalkyl radical ever exists, either during the formation or decomposition of the metallacycle, it has a lifetime of less than 10^{-8} s. On the basis of these results, either the currently accepted mechanism for the photodecarboxylation of cobalt(III)-amino acid complexes is wrong or, at least, the rate determining step has been incorrectly assigned.

In contrast to the glycinato complex, photolysis of $[Co(bpy)_2(aa)]^{2+}$ complexes which have alkyl substituents on the α-carbon do not form *stable* photolysis products which contain a Co–C–N chelate. If such a complex is formed transiently, heterolytic cleavage of the Co–C bond could generate a Co(I) complex and an iminium ion. Hydrolysis of the iminium ion will generate the observed carbonyl compounds. The Co(I) fragment may undergo bimolecular redox reactions, or it can be protonated to give a Co(III)-hydride complex.

Experimental section

General

Materials

Reagent grade reagents and solvents were obtained from commercial sources and used without further purification for all syntheses unless stated. All ion-exchange resins and NMR solvents were purchased from Aldrich Chem. Co.

Measurements

^{1}H NMR spectra were recorded on a Varian Unity 300 MHz spectrometer at 23°C. For those recorded in dimethyl-d_6-sulfoxide (DMSO-d_6) the DMSO-d_5 line (δ 2.50 ppm) was used as a reference. Sodium trimethylsilylpropanesulfonate (TMPS, δ 0 ppm, singlet) was added as an internal reference for those recorded in D_2O. The signals are described as singlets (s), doublets (d), triplets (t), quartets (q) or multiplets (AB, ABX or m), and broad (br) where appropriate.

COSY, TOCSY, and nOe experiments used the standard pulse sequences and parameters available with the Varian 300 system.

A Varian XL-300 spectrometer was employed for the ^{13}C NMR spectra at 75 MHz, and all spectra were proton decoupled. The spectra were recorded at 23°C and referenced to the DMSO-d_5 peak (δ 39.5 ppm) or, in D_2O, to added dioxane (δ 67.4 ppm).

A GBC-920 spectrophotometer was used to record the UV-visible spectra in H_2O and the data are reported as λ_{max} (ε_{max}, $mol^{-1}dm^3cm^{-1}$). The abbreviation sh refers to a shoulder.

Elemental analyses were performed by the University of Otago Microanalytical Service.

FAB mass spectral data were obtained on a Kratos MS80RFA mass spectrometer equipped with an IonTech ZN11NF atom gun using xenon as the reagent gas and 3-nitrobenzyl alcohol as the matrix. Electron impact spectra were obtained at 70eV.

The results of the X-ray crystallography are collated in Appendix 2.

Preparation and isolation of 2-Cyclopropylglycine (cpgH) (3.1c)

Pentaammine(2-cyclopropyliminocarboxylato)cobalt(III) perchlorate was prepared by a slight modification of a literature method.[74] Lithium 5-bromo-2-oxoethanoatopentanoate (2.95 g, 13 mmol) in ethanol (40 mL) was added in portions over two hours to a warm (60°C) solution of $[Co(NH_3)_5(OH_2)](ClO_4)_3$ (7.40 g, 16 mmol) in water (60 mL). The reaction mixture was maintained at this temperature, with stirring, for two hours while the pH was kept at 5.25-5.5 by the addition of Na_2CO_3. The solution was then acidified to pH 2 with $HClO_4$ and cooled overnight. The red plate-like crystals and mother liquor were treated as described in the referenced article, to yield 2-oxo-2-cyclopropylethanoatopentaamminecobalt(III) perchlorate, and then pentaammine(2-cyclopropyliminocarboxylato)cobalt(III) perchlorate (1.91 g, 4.4 mmol, 34% from LiBKPA). 2-Cyclopropylglycine was liberated from the cobalt centre by reduction of the imine, and of the Co(III), by treating a buffered solution of this complex (1.1 g, 2.5 mmol, in a $Na_2CO_2/NaHCO_3$ buffer solution, pH 10, 90 mL) with an excess of $NaBH_4$ (0.25 g). The solution was acidified with dilute HCl to pH 3 after stirring for four minutes. A black by-product deposited with concomitant generation of H_2 gas. The reaction mixture was then filtered through Celite and the resulting pale pink solution loaded on to Dowex (H^+ form, 8 × 3 cm), washed with 0.1 M HCl (300 mL) then eluted with 0.5 M NH_3 solution. The fractions analysed by ^1H NMR after the solvent was removed on a rotary evaporator. Those which contained cyclopropylglycine were combined and recrystallised twice by layering a super-

saturated aqueous solution with isopropanol and cooling in a freezer. A hydrophobic white powder precipitated which was washed with isopropanol and ether, then air dried. Yield (82 mg, 59%). ^{1}H-NMR (dilute DCl): δ 0.50-0.85 (complex multiplet, cyclopropyl CH_2's, 4H), 1.15 (m, cyclopropyl CH, 1H), 3.11 (d, α-H, 1H, J = 10.7 Hz). ^{13}C NMR (D_2O): δ 5.38, 6.05 (cyclopropyl CH_2's), 14.06 (cyclopropyl CH), 61.40 (α-C), 175.97 (COO). Anal. Calcd for $C_5H_9NO_2$: C, 52.16; H, 7.88; N, 12.17. Found: C, 51.94; H, 7.88; N, 11.96. EI-MS (m/z): 116 ($[C_5H_{10}NO_2]^+$).

Preparation of the $[Co(bpy)_2(aa)]^{2+}$ complexes

General method

The $[Co(bpy)_2(aa)]^{2+}$ complexes were prepared by a slight modification of the method of Tatehata (Fig 3.2).[75] The amino acid (2.92 mmol) was added to a suspension of doubly recrystallised $[Co(bpy)_2Cl_2]Cl{\cdot}3H_2O$[87] (0.5 g, 2.92mmol) in dry methanol (30 mL), and the mixture warmed at 45-50°C with stirring. After 30 mins, sodium acetate (0.2 g) was added, and the solutions cooled to rt with stirring. The resulting orange solution was diluted with distilled H_2O (300 mL) and loaded on to SP Sephadex C25 (Na^+ form, 3 × 20 cm). An orange band eluted with 0.2 M NaCl, preceded by a red-orange band and followed by a yellow band. The orange eluate was concentrated on a rotary evaporator and de-salted on Sephadex G-10. This solution was concentrated once more and the addition of a saturated $NaClO_4$ solution prompted the precipitation of an orange solid. Recrystallisation from hot dilute $HClO_4$ gave orange crystals suitable for the microanalyses and UV-vis spectra. The yield varied widely but generally was in the region 40-60%.

$[Co(bpy)_2(ala)](ClO_4)_2 \cdot H_2O$

Two diastereoisomers were found in the crude product and a COSY spectrum aided the assignment of the peaks in the ^1H NMR spectra. In DMSO-d_6, the signal of the α-H in the minor isomer was presumed to be fully obscured by the residual H_2O peak. This resonance could be observed by obtaining a spectrum in D_2O. ^1H NMR of Λ-*S*/Δ-*R* (major) isomer (DMSO-d_6): δ 1.17 (d, CH_3, 3H, J = 6.8 Hz), 3.85 (q, α-H, 1H), 5.82 (br t, NH, 1H), 7.11-7.18 (d, 2H, bpy H and NH), 7.59-7.73 (br m, 3H), 8.15-8.21 (m, 2H), 8.38-8.45 (m, 3H), 8.68-8.73(m, 2H), 8.90 (m, 2H), 8.98-9.05 (m, 2H), 9.18 (d, 1H). ^1H NMR of Λ-*S*/Δ-*R* (minor) isomer (DMSO-d_6): δ 1.38 (d, 3H, CH_3, J = 7.3 Hz), 3.36 (α-H, partially obscured by H_2O), 6.17 (br m, NH, 1H), 6.63 (br m, NH, 1H). Most of the bipyridine resonances overlapped those of the major isomer, however the following peaks could be seen clearly; δ 8.49 (d, 1H, J = 5.4 Hz), 9.28 (d, 1H, J = 5.4 Hz). ^{13}C NMR of Λ-*S*/Δ-*R* isomer (DMSO-d_6): δ 19.34 (CH_3), 52.06 (α-C), 124.95 (2C), 125.72, 126.36, 128.89, 129.14, 130.01, 130.19, 142.31 (2C), 142.98, 143.41, 148.85, 150.99, 152.73, 153.58, 156.37, 156.52, 157.19, 157.26, 182.12 (COO). ^{13}C NMR Λ-*R*/Δ-*S* isomer (DMSO-d_6): δ 18.74 (CH_3), 51.82 (α-C), 182.48 (COO). Only nine bipyridine signals were identifiable, the remainder obscured by the peaks of the major isomer,: δ 125.12, 125.72, 129.25, 129.71, 143.09, 149.69, 151.42, 156.58, 157.10. Anal. Calcd. For $[CoC_{23}H_{22}N_5O_2](ClO_4)_2 \cdot H_2O$: C, 40.85; H, 3.58; N, 10.36. Found: C, 40.80; H, 3.30; N, 10.04. UV-vis: 482 nm (92). MS (FAB): (m/z) 558.1 ($[Co(bpy)_2(ala)(ClO_4)]^+$, 7%), 459.1 ($[Co(bpy)_2(ala)]^+$, 15%), 303.1 ($[Co(bpy)(ala)]^+$, 28%).

$[Co(bpy)_2(val)](ClO_4)_2$

A mixture of diastereoisomers was present in the crude product. A diastereoisomerically pure product was obtained by recrystallising the crude product from dilute $HClO_4$ several times. ^1H NMR of the Λ-*S*/Δ-*R* isomer (DMSO-d_6): δ 0.60 (d, 3H, CH_3), 0.96 (d, 3H, CH_3), 2.08 (br m, 1H, methine H), 3.77 (br m, α-H, 1H), 5.04 (br t, 1H, NH), 7.03 (br m, NH overlapping bpy H, 2H), 7.60-7.71 (m, 3H), 8.15 (br s,

2H), 8.40-8.46 (br m, 3H), 8.68-8.72 (m, 2H), 8.87-9.00 (m, 3H), 9.07 (d, 1H), 9.27 (d, 1H). ^{13}C NMR of Λ-*S*/Δ-*R* isomer (DMSO-d_6): δ 15.80, 18.06 (both CH_3), 30.54 (methine C), 61.34 (α-C), 124.67, 124.81, 125.52, 125.96, 128.48, 128.96, 129.42, 129.79, 142.08 (2C), 142.72, 143.23, 149.14, 150.73, 152.94, 153.55, 156.44, 156.67, 156.94, 157.70, 180.54 (COO). Anal. Calcd. for $[CoC_{25}H_{26}N_5O_2](ClO_4)_2$: C, 43.75; H, 3.82; N 10.20. Found: C, 43.44; H, 3.90; N, 9.86. UV-vis: 483 nm (99). MS (FAB): (m/z) 586.2 ($[Co(bpy)_2(val)(ClO_4)]^+$, 18%), 487.1 ($[Co(bpy)_2(val)^{2+} - H^+]^+$, 27%), 331.1 ($[Co(bpy)(val)^{2+} - H^+]^+$, 71%).

$[Co(bpy)_2(cpg)](ClO_4)_2 \cdot H_2O$

^{1}H NMR of the Λ-*S*/Δ-*R* (major) diastereoisomer (DMSO-d_6): δ 0.40-0.70 (br m, cyclopropyl CH_2's, 4H), 0.75-0.85 (br m, cyclopropyl CH, 1H), 3.01-3.09 (m, α-H, 1H), 6.00-6.06 (br m, 1H NH), 7.08 (d, 1H), 7.13-7.19 (br m, 1H, NH), 7.59-7.67 (m, 3H), 8.11-8.21 (m, 2H), 8.36-8.43 (m, 2H), 8.49 (d, 1H), 8.63-8.74 (m, 2H), 8.86-8.91 (m, 2H), 8.96-9.04 (m, 2H), 9.12 (d, 1H). ^{1}H NMR of Λ-*R*/Δ-*S* (minor) isomer (DMSO-d_6): δ 0.40-0.70 (br m, cyclopropyl CH_2's, overlapping with resonances of the major isomer), 1.18 (br m, cyclopropyl CH, 1H), 2.62 (m, α-H, 1H), 6.38 (br m, NH, 1H), 6.62 (br m, NH, 1H). Most of the bpy resonances were coincident with those of the major isomer except; δ 9.35 (d, 1H, J = 5.3 Hz). ^{13}C NMR of Λ-*S*/Δ-*R* isomer (DMSO-d_6): δ 2.91, 4.93 (both cyclopropyl CH_2's) 14.95 (cyclopropyl CH), 60.45 (α-C), 124.63, 124.72, 125.48, 126.06, 128.55, 128.92, 129.89, 129.92, 142.03 (2C), 142.65, 143.09, 148.72, 150.66, 152.57, 153.40, 156.33 (2C), 156.90, 156.26, 180.12 (COO). ^{13}C NMR of Λ-*R*/Δ-*S* isomer (DMSO-d_6): A few peaks were distinguishable from those of the Λ-*S*/Δ-*R* diastereoisomer; δ 5.70, 14.12, 180.65 (COO). Anal. Calcd. for $[CoC_{25}H_{24}N_5O_2](ClO_4)_2 \cdot H_2O$: C, 42.75; H, 3.73; N, 9.97. Found: C, 42.71; H, 3.75; N, 10.01. UV-vis: 479 nm (105). MS (FAB): (m/z) 584.2 ($[Co(bpy)_2(cpg)(ClO_4)]^+$, 12%), 485.2 ($[Co(bpy)_2(cpg)^{2+} - H^+]^+$, 21%), 329.1 ($[Co(bpy)(cpg)^{2+} - H^+]^+$, 56%).

$[Co(bpy)_2(pgly)](ClO_4)_2 \cdot H_2O$

Assignment of the ^1H NMR signals was aided by (i) recrystallisation to give a diasteromerically pure product, and (ii) the acquisition of COSY and TOCSY spectra. ^1H NMR (DMSO-d_6): δ 4.99 (br m, 1H, α-H), 6.09 (br t, 1H, NH), 7.10 (d, 1H, bpy), 7.22 (br s, 2H, phenyl), 7.35 (br s, 3H, phenyl), 7.63-7.73 (m, 4H, NH and 3 bpy), 8.22-8.34 (m, 2H, bpy), 8.36-8.45 (m, 2H, bpy), 8.69-8.76 (m, 3H, bpy), 8.83 (d, 1H, bpy), 8.90 (d, 1H, bpy), 9.01-9.07 (m, 2H, bpy), 9.46 (d, 1H, bpy). ^{13}C NMR (DMSO-d_6): δ 59.65 (α-C), 124.58, 124.80, 125.57, 126.00, 128.53 (3C), 128.97, 129.40 (2C), 129.93, 130.11, 137.23, 142.00, 142.08, 142.68, 143.19, 148.90, 150.76, 153.02, 153.38, 156.48, 156.59, 156.95, 157.68, 179.89 (COO). Anal. Calcd. for $[CoC_{28}H_{25}N_5O_2](ClO_4)_2 \cdot H_2O$: C, 45.57; H, 3.52; N, 9.49. Found: C, 45.42; H, 3.35; N, 9.41. UV-vis: 483 nm (111). MS (FAB): (m/z) 521 ($[Co(bpy)_2(pgly)^{2+} - H^+]^+$, 4%), 365 ($[Co(bpy)(pgly)^{2+} - H^+]^+$, 6%).

$[Co(bpy)_2(aib)](ClO_4)_2.H_2O$

^1H NMR (DMSO-d_6): δ 0.99, 1.33 (both s, total 6 H, CH_3's), 6.08 (d, 1H, NH), 6.59 (d, 1H, NH), 7.01 (d, 1H), 7.61 (t, 1H), 7.68 (t, 1H), 7.84 (d, 1H), 8.14 (t, 1H), 8.22 (t, 1H), 8.37-8.43 (m, 3H), 8.70 (m, 2 H), 8.87 (m, 2H), 8.98 (d, 1H), 9.06 (d, 1H), 9.50 (d, 1H). ^{13}C NMR (DMSO-d_6): δ 27.50, 28.38 (both CH_3's), 58.75 (α-C), 124.73, 124.94, 125.59, 126.31, 128.52 (2C), 128.91, 129.54, 142.07, 142.13, 143.01, 143.33, 149.26, 150.82, 152.42, 153.59, 156.66, 156.81, 157.31, 157.78, 184.49 (COO). Anal. Calcd for $[CoC_{24}H_{24}N_5O_2](ClO_4)_2 \cdot H_2O$: C, 41.76; H, 3.80; N, 10.14. Found: C, 41.58; H, 4.07; N, 9.86. UV-vis: 482 nm (99). MS (FAB): (m/z) 572.1 ($[Co(bpy)_2(aib)(ClO_4)]^+$, 13%), 473.2 ($[(Co(bpy)_2(aib)^{2+} - H^+]^+$, 35%).

Steady state photolysis of $[Co(bpy)_2(aa)]^{2+}$ complexes

General method

Millimolar D_2O solutions of the complexes were placed in NMR tubes and submerged in ice-water in a quartz bath. They were irradiated for around 60 minutes with filtered light (254 nm Pyrex transmission filter, Corning 7-54) from a 200W high pressure mercury lamp. Following photolysis, the solutions were acidified with DCl and ^1H NMR spectra obtained immediately.

Photolysis of $[Co(bpy)_2(ala)](ClO_4)_2$

^1H NMR (D_2O/DCl): Free alanine; δ 1.59 (d, 3H, CH_3, J = 7.3 Hz), 4.12 (m, 1H, α-H). Acetaldehyde; δ 2.23 (br s, 3H, CH_3), 9.66 (br s, 1H,). Hydrated acetaldehyde; δ 1.31 (d, 3H, CH_3), 5.23 (d, 1H). Free bipyridine; δ 7.98 (m, 2H), 8.52 (m, 4H), 8.91 (m, 2H). $[Co(bpy)_3]^{3+}$; δ 7.51 (d), 7.83 (t), 8.58 (t), 8.88 (d).

Photolysis of $[Co(bpy)_2(val)](ClO_4)_2$

^1H NMR (D_2O/DCl): Free valine; δ 0.97-1.04 (m, 6H, both CH_3's), 2.26 (m, 1H, CH), 4.04 (d, 1H, α-H, J = 2.5 Hz). 2-Methylpropanal; δ 0.89 (d, CH_3's), 1.71 (m, CH), 9.57 (d, 1H, J = 1.4 Hz). Hydrated 2-methylpropanal; δ 1.08 (d, CH_3's), 2.61 (m, 1H, CH), 4.71 (d, 1H, J = 5.4 Hz). Free bipyridine; δ 7.98 (m, 2H), 8.52 (m, 4H), 8.91 (m, 2H). $[Co(bpy)_3]^{3+}$; δ 7.51 (d), 7.83 (t), 8.58 (t), 8.88 (d).

Photolysis of $[Co(bpy)_2(cpg)](ClO_4)_2$

^1H NMR (D_2O/DCl): Free cyclopropylglycine; δ 0.50-0.85, 1.15, 3.11 (peaks assigned in section 1(b)). Cyclopropanecarboxaldehyde; δ 1.38 (br m, cyclopropyl CH_2's, 4H), 1.95 (br m, 1H, cyclopropyl CH), 8.79 (d, 1H, J = 7.4 Hz). Free bipyridine; δ 7.98 (m, 2H), 8.52 (m, 4H), 8.91 (m, 2H). $[Co(bpy)_3]^{3+}$; δ 7.51 (d), 7.83 (t), 8.58 (t), 8.88 (d). The D_2O photolysate was extracted with $CDCl_3$. ^1H NMR of extract ($CDCl_3$):

Cyclopropanecarboxaldehyde; δ 1.08 (m, 4H), 1.84 (br m, 1H), 8.91 (d, 1H, J = 5.8 Hz). ^{13}C NMR of extract ($CDCl_3$): Cyclopropanecarboxaldehyde; δ 7.29, 22.66, 201.33.

Photolysis of $[Co(bpy)_2(pgly)](ClO_4)_2$

^1H NMR (D_2O/DCl): Benzaldehyde; δ 7.60-7.78 (m, 4H), 7.96 (d, 2H), 9.94 (s, 1H). Free phenylglycine; δ 5.22 (s, 1H), 7.51-7.55 (m, 5H). Free bipyridine; δ 7.98 (m, 2H), 8.52 (m, 4H), 8.91 (m, 2H). $[Co(bpy)_3]^{3+}$; δ 7.51 (d), 7.83 (t), 8.58 (t), 8.88 (d). The photolysate was extracted with $CDCl_3$. ^1H NMR of extract ($CDCl_3$): Benzaldehyde; δ 7.55-7.70 (m, 3H), 7.90-7.94 (m, 2H), 10.05 (s, 1H).

Photolysis of $[Co(bpy)_2(aib)](ClO_4)_2$.

^1H NMR (D_2O/DCl): Free aminoisobutyric acid; δ 1.61 (s, 6H). Acetone; δ 2.23 (s). Free bipyridine; δ 7.98 (m, 2H), 8.52 (m, 4H), 8.91 (m, 2H). $[Co(bpy)_3]^{3+}$; δ 7.51 (d), 7.83 (t), 8.58 (t), 8.88 (d).

Dry N_2 was used to de-oxygenate the solution to check the oxygen-dependence of the photolysis products. There was little change in the product distribution (see text).

For the photolysis experiments in the presence of TEMPO, two ratios of the radical trap to the $[Co(bpy)_2(aib)]^{2+}$ complex were used (1:1 and 1:10). These solutions were also de-oxygenated by N_2. There was little change in the product distribution (see text).

CHAPTER FOUR

A POLYDENTATE FRAMEWORK

Introduction

$[Co(bpy)_2(aa)]^{2+}$ complexes which contain α-alkyl substituted amino acid ligands, do not yield stable three membered chelates upon photolysis, as established in Chapter 3. This was a displeasing observation, especially given that the crucial radical clock experiment involved an amino acid with a cyclopropyl substituent. There was no *direct* evidence for the formation of a metallacycle and the conclusions which were drawn from this experiment rested upon the nature of the decomposition products, and upon Poznyak's low-temperature photolysis results.

If a Co–C–N three membered chelate can be conclusively identified following photolysis of an alkyl-substituted aminoacidato complex, it would demonstrate that alkyl-substitution does not *prevent* the formation of these chelates, rather it just compromises their stability This would bolster the conclusions from the radical clock experiment in Chapter 3 as the possibility that a metallacycle does not actually form in the photolysis of $[Co(bpy)_2(cpg)]^{2+}$ would effectively be eliminated.

Apart from their possible contribution to the mechanistic investigation, the Co–C–N structure is an inherently interesting structural motif, very few examples of which have been well-characterised. Furthermore, those which have substituents on the carbon atom have very poor thermal stability and consequently have not been adequately characterised.[27,73]

This chapter details the results of incorporating the aminoacidato chelates in a polydentate framework. The synthesis and photochemical behavior of a range of closely related complexes is described.

Design considerations

The incorporation of an amino acid into a framework of higher denticity can be achieved by substitution at either of two positions: the nitrogen centre, or the α-carbon. Given that one aim of this work was to include a cyclopropyl moiety at the α-position, the potential of attaching chelating arms at this position was not explored.

The primary consideration in selecting suitable polydentate ligands was the potential to stabilise the Co–C–N metallacycle. There are certain conformational restrictions placed upon the whole complex when such a chelate is formed, and the remainder of the complex must be able to cope with these distortions. This is well illustrated by the following example (Fig 4.1).

Photolysis of the complex **4.1a**, which contains a six-membered β-aminoacidato chelate, was found to be facile, and yields a stable metallacycle (**4.1b**). On the other hand, complex **4.1c** is much less reactive.[39] It appears that this unreactivity is associated with the structural demands of the incipient four-membered chelate. The complex (**4.1c**) must isomerise before it can form a stable metallacycle (**4.1d**). If the four-membered chelate was to develop co-planar with one of the ethylenediamine arms (ie directly replace the aminoacidato chelate), a massive geometrical deformation must occur at either the tertiary nitrogen centre, or to the ethylenediamine ring. In order to achieve a more stable conformation in the organometallic product, the complex can rearrange its geometry to take the four-membered ring out of the plane of the ethylenediamine chelate. Complex **4.1a** can form the metallacycle directly as the aminoacidato chelate is normal to the attached ethylenediamine ring. These results suggest that to maximise the chances of isolating a stable metallacycle, the aminoacidato chelate should not be coplanar with another chelating arm.

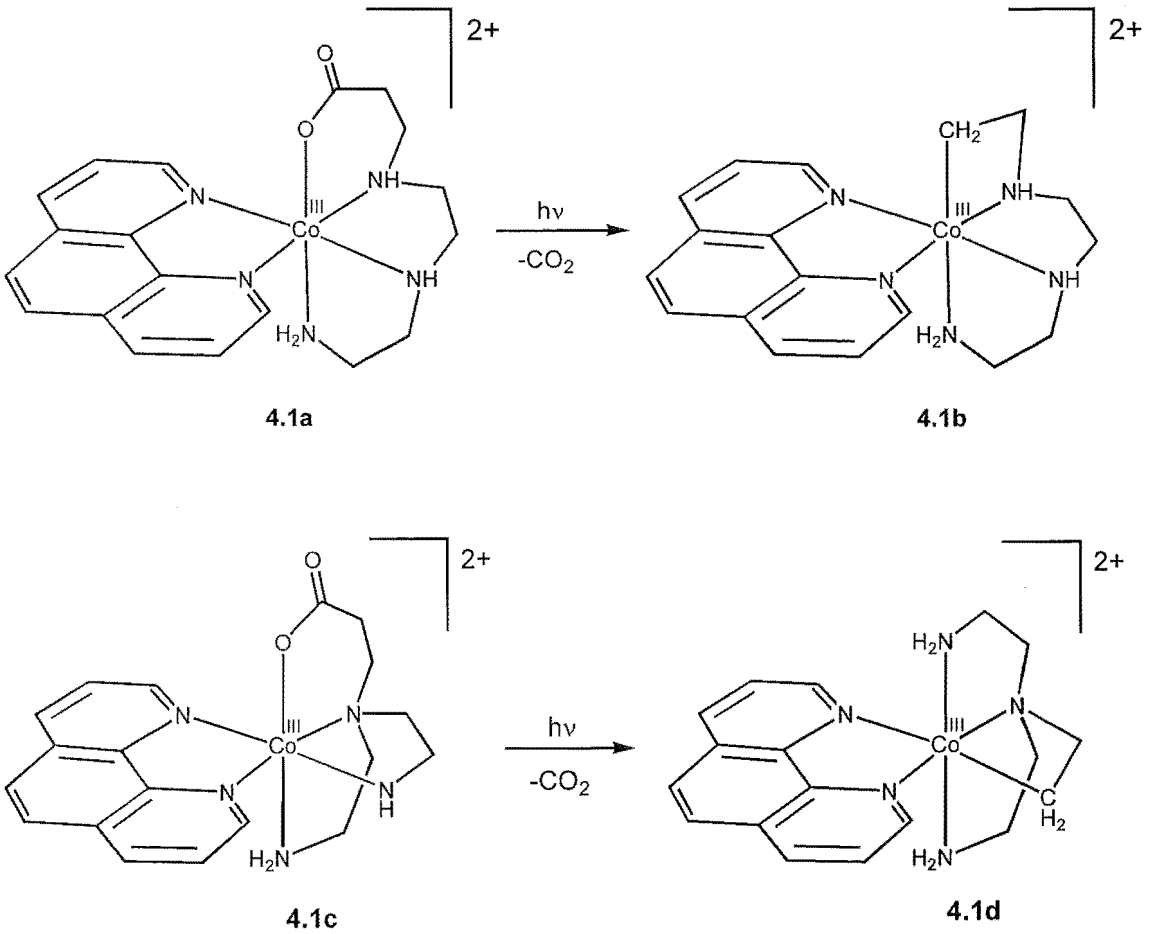

Figure 4.1. Photochemistry observed for two related Co(III)-aminocarboxylato complexes. Note that 4.1c must isomerise before it can form a stable organometallic product.

The carbon atom of the metallacycle is a strongly electron-donating centre. This excess electron density can be alleviated by the presence of π-acidic ligands, such as bpy or phen. A notable illustration of this point is provided by the $[Co(gly)(en)(bpy)]^{2+}$ complex which, in contrast to $[Co(bpy)_2(gly)]^{2+}$, does not form a stable metallacycle upon photodecarboxylation. This instability has been ascribed to the inclusion of the en ligand which is not able to remove excess electron density from the cobalt centre.[24,28] With respect to the construction of complexes which may enhance the stability of Co–C–N chelates, it appears that π-acidic ligands are especially useful auxiliary ligands.

In summary, in order to maximise the chance of producing a stable Co–C–N metallacycle from an aminoacidato chelate which is incorporated in a polydentate framework, the complex should have the following characteristics. The geometrical arrangement of the chelate ring should allow the metallacycle to form normal to the attached chelate(s), the polydentate framework should be flexible enough to cope with the contraction of the animoacidate chelate ring, and π-acidic ligands should fill as many other coordination sites as possible. Figure 4.2 depicts two suitable possibilities which were formulated with these considerations in mind.

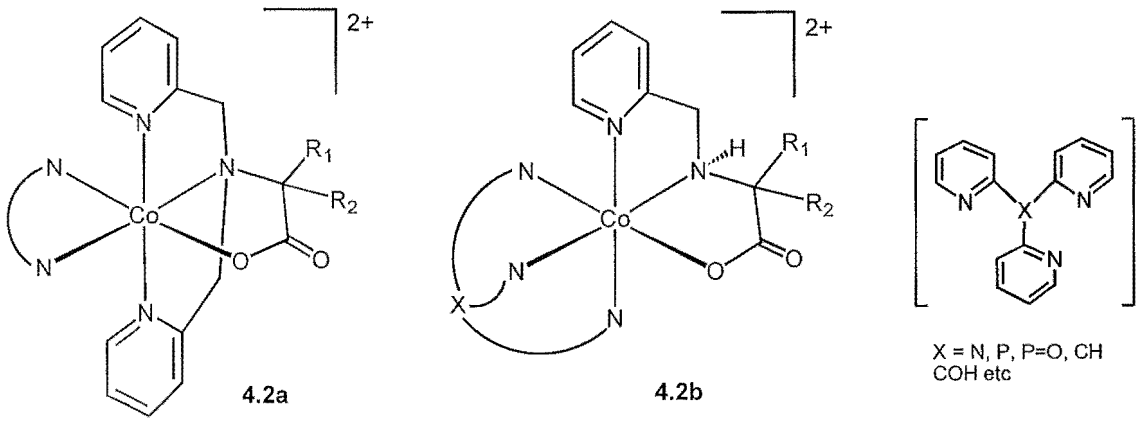

Figure 4.2. Two complexes which are potential precursors to stable Co-C-N metallacycles.

Complex **4.2a** has the aminoacidato ligand tethered by two pyridylmethyl arms. Phen or bpy would be well-suited to filling the remaining two coordination sites. The complex has two possible geometrical isomers, as the two pyridyl groups can be arranged either *cis* or *trans* (the *trans* configuration is pictured). R_1 and R_2 in **4.2a** are enantiotopic, which means that there will not be diastereoismers if chiral amino acid is used to prepare the complex. This contrasts with the $[Co(bpy)_2(aa)]^{2+}$ complexes where the corresponding groups are diastereotopic.

Another potential candidate (**4.2b**) involves attaching just one pyridylmethyl arm to the amino acid. To avoid the unfavourable co-planar arrangement of the pyridyl and

aminoacidato chelates, the *fac* isomer of this complex would be required. In this case, one of the strongly π-acidic, facially-coordinating tris(pyridyl) ligands would be eminently well-suited to filling the three vacant coordination sites.

Given the ready availability of the di-imine co-ligands required by complexes of the type **4.2a**, we chose to study the synthesis and photochemistry of these compounds.

Aminoacidato chelates tethered by two pyridylmethyl arms

Two practical questions had to be addressed before this set of complexes could be deemed suitable candidates for the generation and stabilisation of *alkyl substituted* Co–C–N metallacycles.

(a) Can the *trans*-pyridyl isomer of the complex be synthesised, and in reasonable yield?

(b) Will the glycinato analogue form a stable (unsubstituted) metallacycle upon irradiation?

These answers to these questions could not be found in the literature, as no dipyridylmethyl-aminoacidato complexes of Co(III), such as **4.2a**, have been reported. Hence, a feasibility study was commenced to determine whether this ligand framework had the potential to stabilise substituted Co–C–N chelates. Although the present idea was independently conceived, the photochemistry of a very similar complex has been investigated by Poznyak and Pavlovskii, as mentioned in Chapter 1.[35]

Synthesis of $[Co(dpg)(phen)]^{2+}$

The stepwise nucleophilic displacement of chloride from two equivalents of 2-chloromethylpyridine (**4.3b**) produces bis-N,N-(2-pyridylmethyl)glycine (dpg, **4.3c**) in good yield, as previously reported.[88] It was found that ion-exchange chromatography on Dowex provided an efficient method of separating this product from the mono-alkylated amino acid. The original procedure detailed purification of the product by recrystallisation.

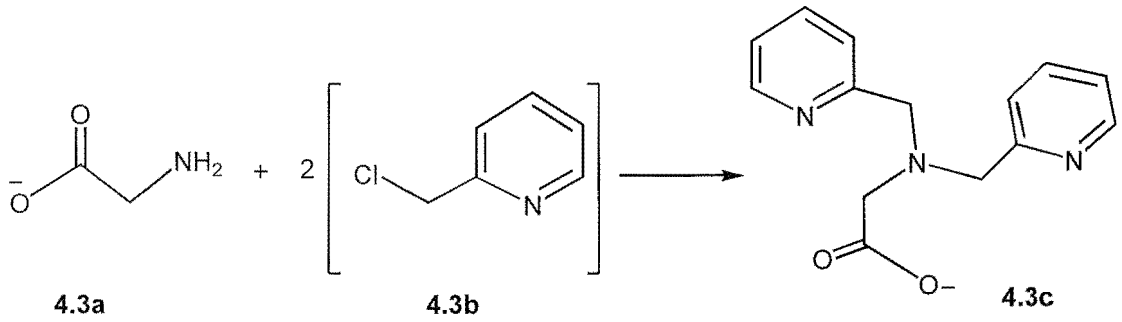

Figure 4.3. The synthetic route to the bis-N,N-(2-pyridylmethyl)glycine (dpg) ligand.

$[Co(dpg)(NO_2)_2]$ (**4.4a**) was prepared by the air oxidation of the free ligand, Co(II), and $NaNO_2$ in buffered aqueous solution. This method was based on a published[89] synthesis of $[Co(NO_2)_3(tacn)]$ and, as the desired $[Co(dpg)(NO_2)_2]$ is a neutral complex, it also has the attractive property of precipitating out of the reaction mixture. The $[Co(dpg)(NO_2)_2]$ complex was characterised by ^1H and ^{13}C NMR spectroscopy. It was pleasing to discover that the complex had the '*trans*-pyridyl' geometry (C_S symmetry).

Nitro complexes of Co(III) are common synthetic intermediates, although the Co–NO_2 bond is usually quite robust.[90] The usual method of replacing nitro ligands in the coordination sphere of Co(III) is to heat the complex with (concentrated) HCl, substituting the nitrite for chloride. The chloro ligands are typically more labile, hence will undergo substitution reactions with 'good' ligands.

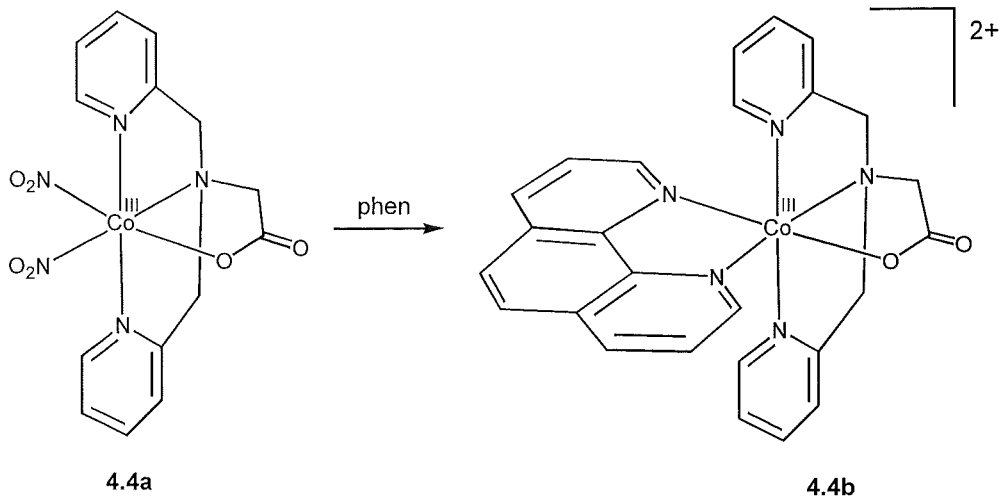

4.4a 4.4b

Figure 4.4. The synthetic route to $[Co(dpg)(phen)]^{2+}$.

In contrast, it was found that both nitro ligands in $[Co(dpg)(NO_2)_2]$ (**4.4a**) were easily displaced when the complex was reacted directly with phen, even under mild reaction conditions. The direct reaction method gave much better yields than those obtained *via* a di-chloro intermediate. This method may avoid the thermally-initiated redox decomposition which has been noted for other Co(III)–NO_2 complexes.[90] The reaction mixture still required separation by ion-exchange chromatography however. The $[Co(dpg)(phen)]^{2+}$ complex ion crystallised readily as the perchlorate salt.

The *trans*-pyridyl geometry is conserved during the formation of the $[Co(dpg)(phen)]^{2+}$ complex (**4.4b**), as indicated by its ^1H and ^{13}C NMR spectra. The complex has C_S symmetry, with the mirror plane described by the phen ligand. Therefore, there are eight signals from the phen, and four from the pyridyl groups, in the aromatic region of the ^1H NMR spectrum. The two sets of peaks are easily distinguished by their relative peak integrals, as, fortuitously, there are no overlapping signals (in DMSO-d_6). The signal from the symmetry-equivalent glycinato protons appear as a singlet, and further downfield, the picolyl methylene protons are split in an AB pattern. (The spectrum is given in Fig 4.11, pp 107)

The UV-vis spectrum exhibits a d-d transition with a peak at 480 nm. Given that the donor set is nearly identical to that for the $[Co(bpy)_2(aa)]^{2+}$ complexes, it is unsurprising

that the absorption maxima are also identical. Intense charge-transfer bands are found below around 400 nm.

$[Co(dpg)(phen)](ClO_4)_2$ was further characterised by mass spectrometry and elemental analysis, and the solid state structure was determined by X-ray crystallography (Fig 4.5).

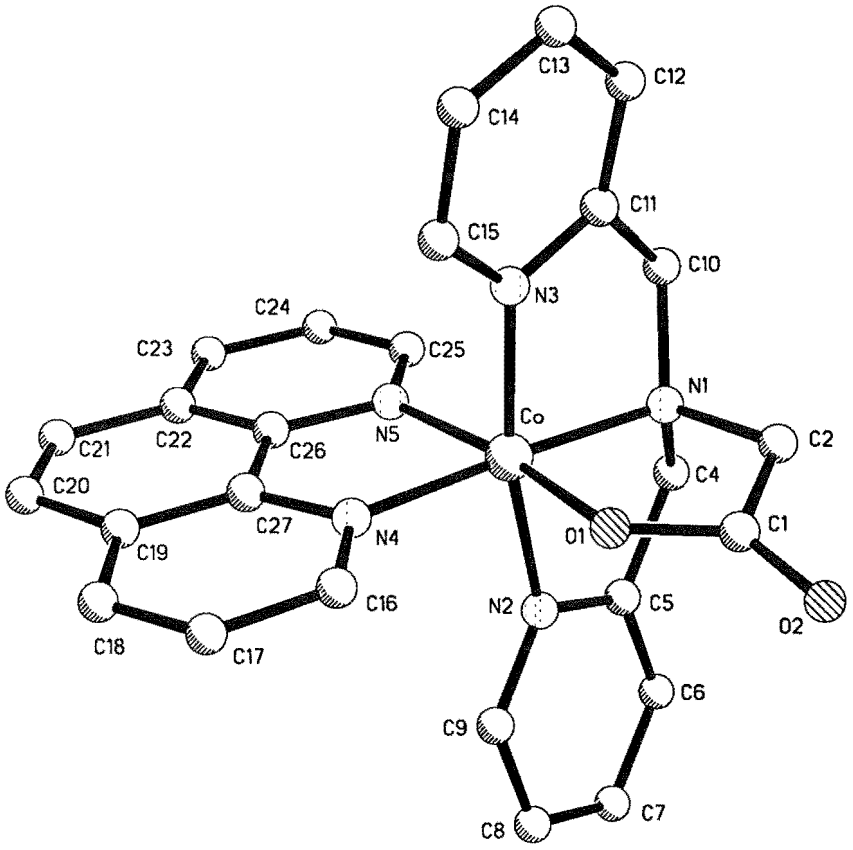

Figure 4.5. Crystal structure of the $[Co(dpg)(phen)]^{2+}$ complex. All hydrogen atoms, and the perchlorate counter anions, have been omitted from the diagram. Selected bond lengths (Å) and angles (°): Co-O(1) 1.880(2); Co-N(1) 1.930(3); Co-N(2) 1.933(3); Co-N(3) 1.921(3); Co-N(4) 1.919(3); Co-N(5) 2.010(3); O(1)-Co-N(1) 87.57(11), N(3)-Co-N(1) 84.73(13); N(3)-Co-N(2) 168.71(12); N(1)-Co-N(2) 84.03(13); N(4)-Co-N(5) 83.01(11); N(1)-Co-N(5) 100.80(11).

The pyridyl donors have adopted a *trans* configuration, as proposed on the basis of NMR spectroscopy, with the aminoacidato chelate and the phen ligand filling the remaining coordination sites. The geometry around the cobalt centre is pseudo-octahedral, with deviations from 90° in all the chelate bite angles. There is a marked difference in the Co–N_{phen} bond lengths; 2.01 Å *trans* to the carboxylate group, and 1.92Å *trans* to the tertiary nitrogen donor, although both fall within the range seen for other similar complexes (*vide infra*). Likewise, the bond lengths between the dpg ligand and the cobalt centre are typical. The glycinato ring is able to assume a favourable planar conformation. (See discussion in Chapter 5). The five-membered picolylamine chelate adopts the common envelope motif, with the picolyl methylene unit slightly out of the plane of the other four atoms.

The closest relative to this type of complex which has been discussed in the literature is a tetranuclear Co(III) complex of N-(2-pyridylmethyl)glycinate (which has a Co_4O_4 core).[91] It was found that the N-(2-pyridylmethyl)glycinato ligand assumes a folded conformation. The Co–N_{py} (average 1.96 Å), Co–N_{amine} (average 1.97 Å), and Co–O (1.94 Å) bond distances are all somewhat longer than those determined for the $[Co(dpg)(phen)]^{2+}$ complex. This is probably a consequence of the non-bonded interactions experienced by the N-(2-pyridylmethyl)glycinato ligands in the former case, as they are "squeezed in" around the tetranuclear core. A series of Co(III) complexes of the tetradentate N-(2-pyridylmethyl)-L-aspartato ligand, with various aminoacidato co-ligands, has also been reported.[92]

Photochemistry of $[Co(dpg)(phen)]^{2+}$

The $[Co(dpg)(phen)]^{2+}$ complex (**4.6a**) is a prototype for the development of polydentate frameworks which may impart stability on C-substituted Co–C–N metallacycles. The first criterion has been filled, that is, the geometry of the complex will allow a metallacycle to form in a plane normal to the appended pyridyl arms. The

second question is whether a stable metallacycle (**4.6b**) can actually be derived from the photo-induced decarboxylation of this complex.

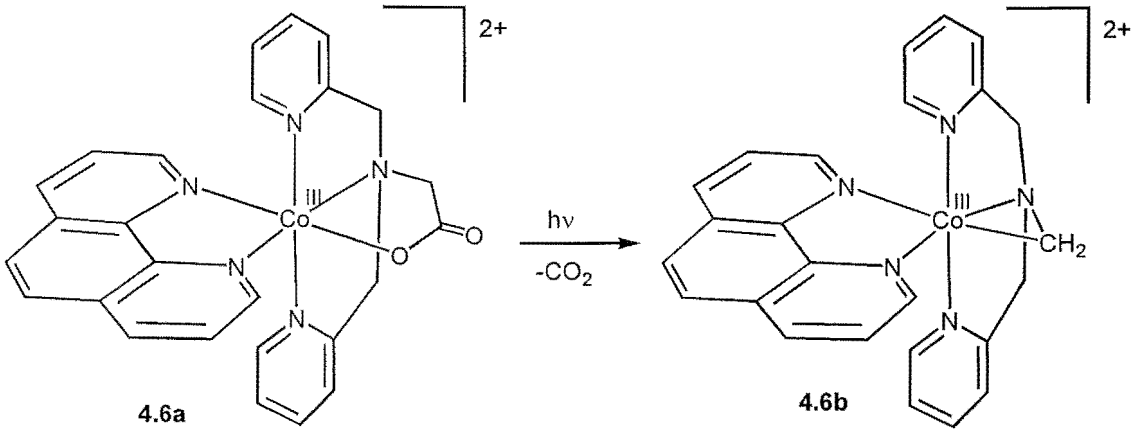

4.6a **4.6b**

Figure 4.6. A possible photochemical reaction of the $[Co(dpg)(phen)]^{2+}$ complex.

The photolysis reaction of $[Co(dpg)(phen)]^{2+}$ was monitored in three different ways, as detailed in the experimental section. The first method involved large-scale photolysis with separation of the photolysis product by ion-exchange chromatography. The other two methods, ^1H NMR and UV-vis spectroscopy, will also be discussed at some length, as the results proved to be invaluable yardsticks for subsequent work.

Photolysis of an aqueous solution $[Co(dpg)(phen)]^{2+}$ with broad spectrum light from an immersable mercury lamp induced a colour change from orange-red to yellow. Ion-exchange chromatography of this photolysate on CM Sephadex, produced two closely-spaced bands upon elution with 0.2 M $NaClO_4$. The band which eluted first was orange-red, and was identified as unchanged $[Co(dpg)(phen)]^{2+}$. The chromatographic behavior of the second band implied that it also had a dipositive charge. The colour of the eluate was noticeably more yellow than the starting material, and upon concentration of the solution on a rotary evaporator, orange crystals deposited. These crystals were of poor quality, however recrystallisation from dilute $HClO_4$, furnished

crystals suitable for X-ray crystallography. The solid state structure of the photolysis product is shown in Fig 4.7.

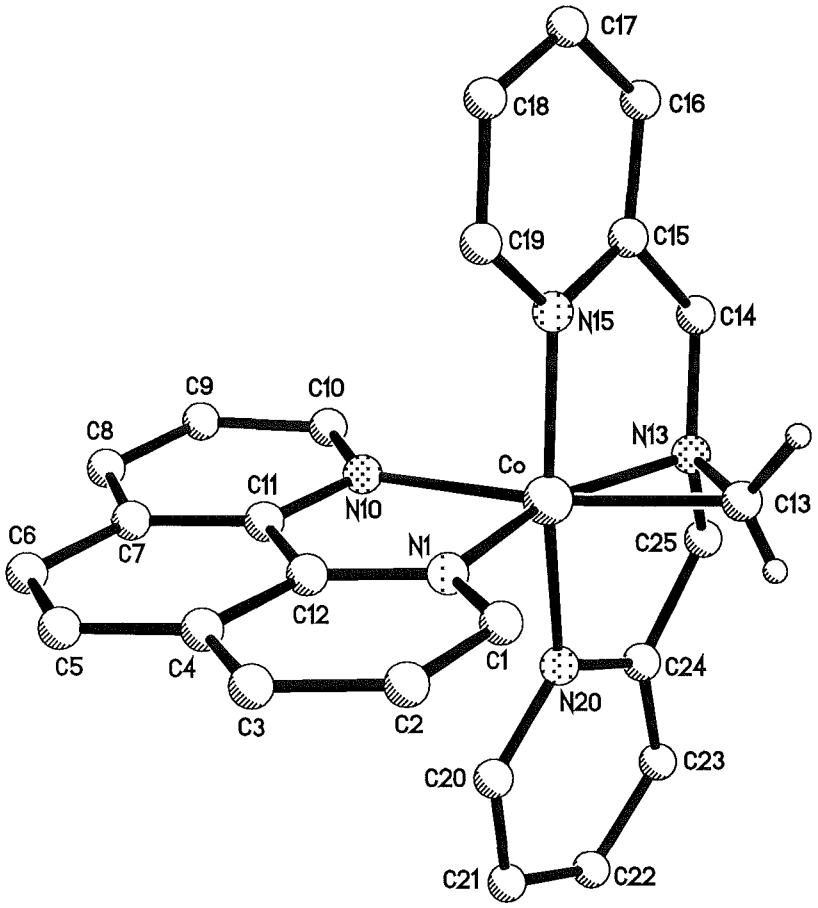

Figure 4.7. Crystal structure of one of the two $[Co(dcm)(phen)]^{2+}$ cations found in the asymmetric unit. Most hydrogens, and the perchlorate counter ions, have been omitted from the diagram. Selected bond lengths (Å) and angles (°): Co-N(13) 1.898(4); Co-C(13) 1.924(6); Co-N(15) 1.931(4); Co-N(20) 1.940(4); Co-N(1) 1.970(4); C(13)-N(13) 1.417(7); Co-N(10) 2.044(4); N(13)-Co-C(13) 43.5(2); N(13)-Co-N(15) 84.31(18); N(13)-Co-N(20) 84.12(17); N(13)-Co-N(1) 157.79(18); N(13)-Co-N(10) 119.13(17); N(1)-Co-N(10) 83.07(17).

It was exciting to find that the photolysis product was a complex which contains a Co–C–N metallacycle. The X-ray diffraction study revealed that carbon dioxide had been

eliminated from the aminoacidato chelate to leave the three-membered metallacyclic ring. The Co–C bond had formed in the coordination site left vacant by the carboxylato ligand, and no geometrical isomerisation had taken place. The formation of a three-membered chelate ring induced some structural changes in the complex, most notably in the deviation from octahedral geometry around the cobalt centre. The bite angle of the new chelate is 43.5°, with bond lengths Co–C = 1.93 Å and Co–N = 1.90 Å. Both hydrogen atoms attached to C(13) were found on a electron density difference map during the refinement. The bond distances between the dipicolylamine portion of the dgm ligand and the cobalt centre remain similar to those in the original complex ($[Co(dpg)(phen)]^{2+}$, Fig 4.5). In both cases, the Co–N_{py} bond lengths fall between 1.92 and 1.94 Å and the chelate bite angles are all clustered around 84-85°. The picolylamine chelate rings retain their envelope configurations in the photolysis product. However, the pyridine rings have been rotated around their Co–N axes. This has important ramifications for the ^{1}H NMR spectra, as will be discussed later.

Rather than viewing the complex as a tortured octahedral Co(III) complex, the structural parameters imply that the complex has significant Co(I) character. In this case, the complex can be viewed as having trigonal bipyramidal geometry, with the C(13)–N(13) fragment π-bound as a η^2-imminium ligand (Fig 4.8).

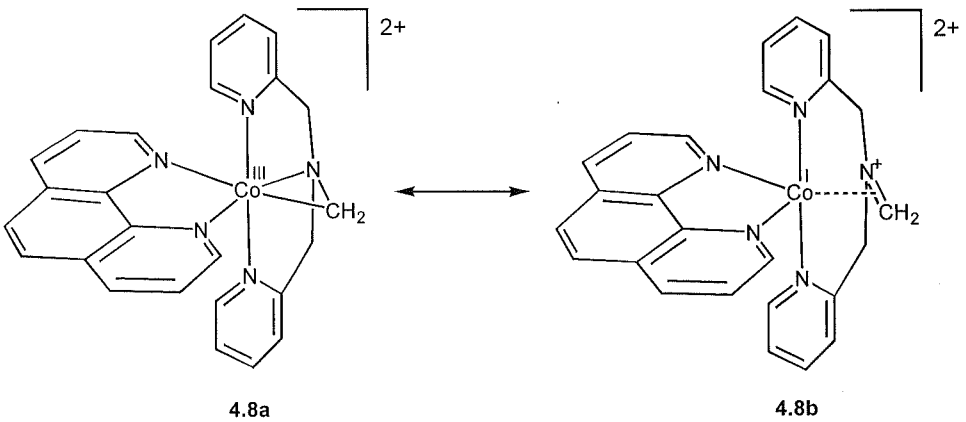

4.8a 4.8b

Figure 4.8. Two resonance forms of the $[Co(dgm)(phen)]^{2+}$ complex.

The C(13)–N(13) bond length (1.42 Å) is midway between that expected for a C–N single bond (1.50 Å), and the C–N bond length found in pyridine[93] (1.34 Å), which represents a bond order of about 1.5. This implies that the C–N bond order is about 1.25, in accordance with partial imine character, as depicted in Fig 4.8. The difference in the Co–N_{phen} bond lengths is around 0.074 Å. For comparison, the analogous difference in the structure of the $[Co(dpg)(phen)]^{2+}$ (**4.5**) cation is 0.091 Å. These figures show that there is only a limited '*trans*-influence'.[Я] Moreover, the smaller difference in the Co–N_{phen} bond lengths in $[Co(dgm)(phen)]^{2+}$ is entirely consistent with partial π character of the bond between the cobalt centre and the N(13)–C(13) unit. The two bonds to the phen ligand are likely to become almost equal in length if the bond was wholly Co(I)-imine in character. Another structural feature which reinforces the notion that the N(13)–C(13) bond has partial double bond character is the geometry around C(13). The angles at C(13) between each of the attached hydrogen atoms and the nitrogen atom (115° and 125°), although lacking in precision due to the low electron density, indicate a shift towards sp^2 hybridisation at C(13), as expected for an imine functionality.

Four other complexes which contain a Co–C–N chelate have been characterised by X-ray crystallography. Two of these have been synthesized photochemically by contraction of an aminoacidato chelate (**4.9a**[94] and **4.9b**[36]), whilst the other two (**4.9c**[95] and **4.9d**[96]) result from intramolecular reactions of macrocyclic complexes.

[Я] A *trans* influence is the lengthening of a metal-ligand bond which is *trans* to a strongly electron-donating ligand. This is discussed further for the specific case of Co-C bonds in ref 86.

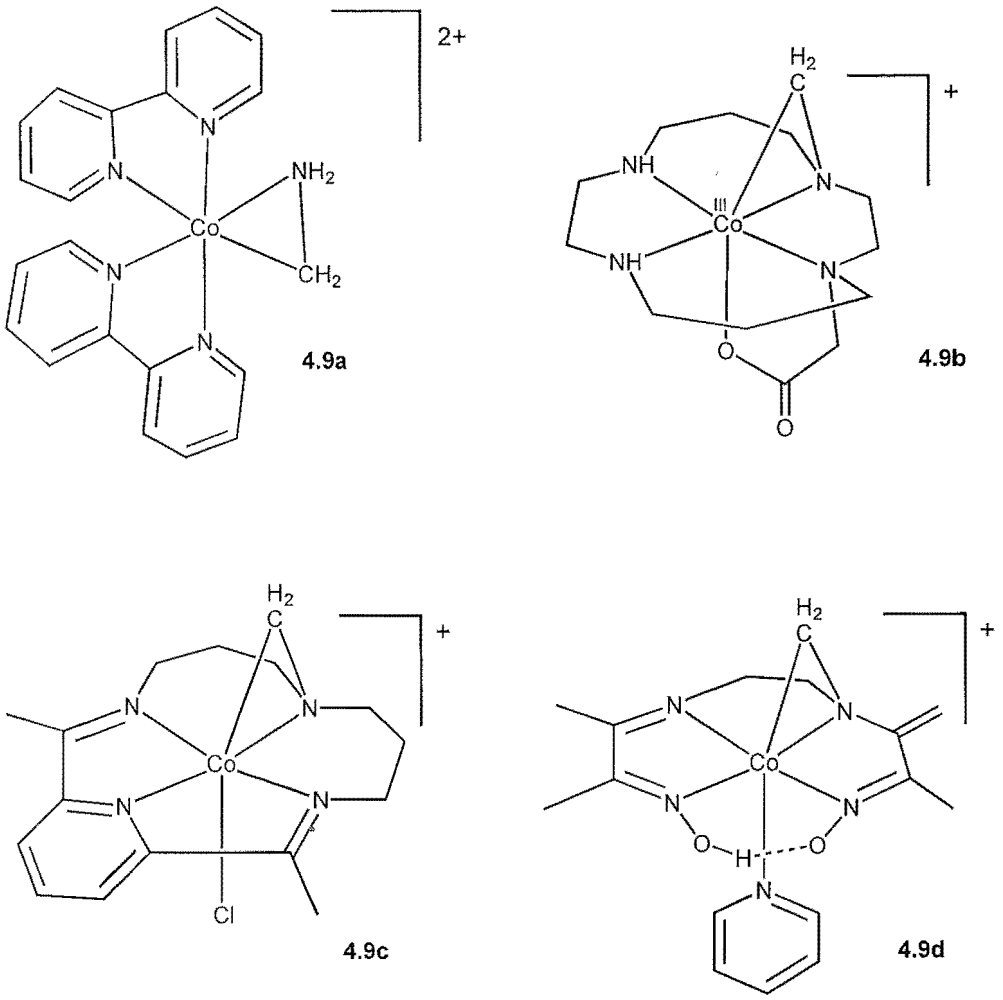

Figure 4.9. The four complexes which contain a Co-C-N chelate ring which have been characterised by X-ray crystallography.

A selection of structural parameters of the cobalt complexes which contain a Co–C–N metallacycle have been collated in Table 4.1. It should be noted that the structures **4.9a** and **4.9c** were not well refined (R = 0.128 and 0.096 respectively).

Table 4.1. Selected Structural Parameters for Complexes With a Co–C–N Chelate.

	$Co–C_{met}$ (Å)	$Co–N_{met}$ (Å)	$C–N_{met}$ (Å)	Co–C–N (°)	$Co–L_{trans}$ (Å)
4.9a	1.86(2)	1.91(1)	1.35(2)	41.9(6)	2.03(1)
4.9b	1.980(3)	1.920(2)	1.447(4)	43.52(12)	1.993(2)
4.9c	1.950(10)	1.942(8)			
4.9d	1.927(5)	1.943(5)	1.44	43.8(2)	2.068(5)
4.7	1.924(6)	1.898(4)	1.417(4)	43.5(2)	2.044

The Co–C bond lengths in η^2-aminomethylene chelates is shorter than that generally observed for the Co–C bond distances in η^1-complexes of sp^3 alkyl ligands.[86] The bond in complex **4.9a** is particularly short. The aminomethylene ligand is not restrained by a polydentate framework. This freedom may account for its relatively close contact with the cobalt centre. The Co–C bond distance of the $[Co(dgm)(phen)]^{2+}$ lies at the short end of the scale, as does the Schiff-base complex **4.9d**. It is difficult to spot a single factor which governs the Co-C bond length, however in general π-acidic ligands, especially *trans* to the C donor, seem to encourage contraction of this bond.

A bond order of around 1.5 has been estimated for the C–N bond in **4.9a** (given that its length is similar to that in pyridine). This is likely to be a consequence of the bipyridyl ligands, which can act as electron density sponges, thereby allowing more Co(I) character in the complex. The aminomethylene ligand will therefore have a greater tendency towards sp^2 hybridisation. It appears that bpy and phen are particularly effective in this role of accepting electron density, as the *trans* pyridyl ligand in **4.9d** does not serve to shorten the C–N bond. This notion of the imine-like behavior of the aminomethylene unit in the $[Co(dgm)(phen)]^{2+}$ complex is developed further with respect to its decomposition reactions.

The geometrical parameters listed above indicate that there is a correlation between the C–N bond length, and the Co–aminomethylene distances. It appears that the chelate bite angle is inflexible, hence constraints will be placed upon the relative values which the C–N, Co–C, and Co–N bond distances can take.

In summary, several broad trends appear to relate the structural parameters of complexes which contain a Co–C–N metallacycle. The presence of strong π-acidic ligands leads to a contraction of the C–N bond within the metallacycle. If such a ligand is trans to the ligating carbon, the Co–C bond distance will also shorten.

Further characterisation of $[Co(dgm)(phen)]^{2+}$

Elemental analysis, mass spectrometry, UV-vis spectroscopy, and ^{1}H NMR and ^{13}C NMR spectroscopy were all consistent with the structure determined by X-ray crystallography. A detailed discussion of the results from two of these methods, UV-vis and ^{1}H NMR spectroscopy, will now be presented since these observations laid the foundation for the characterisation of the photolysis products of the complexes with α-substituted aminoacidato chelates.

UV-vis spectroscopy

UV-vis spectra were obtained periodically during the photolysis of an aqueous solution of $[Co(dgm)(phen)]^{2+}$, and the combined results are presented in Fig 4.10.

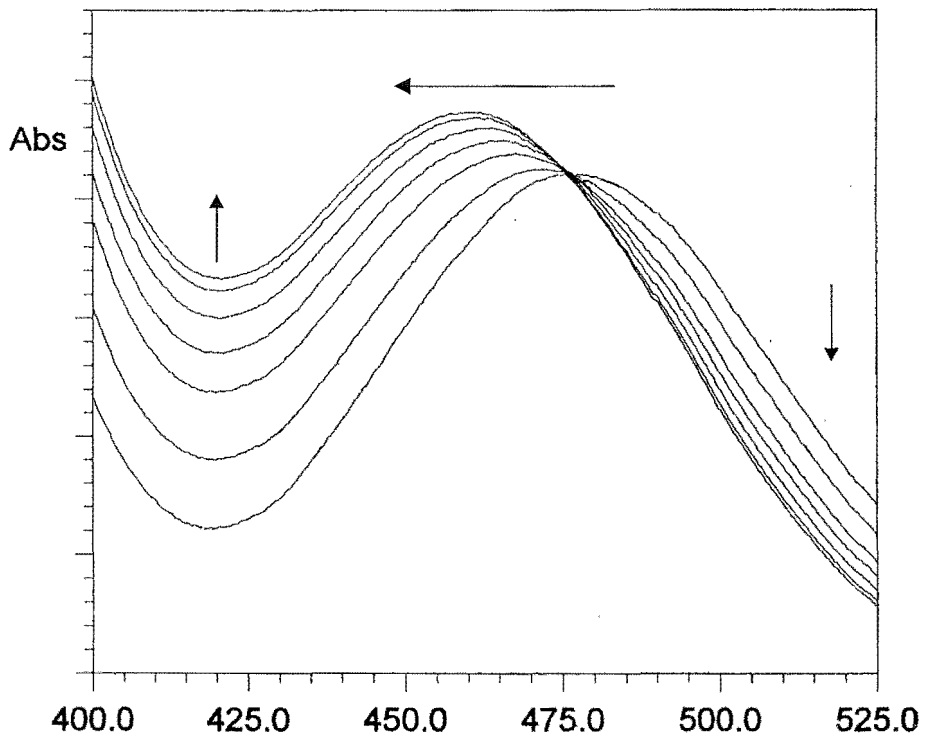

Figure 4.10. The photochemical conversion of $[Co(dpg)(phen)]^{2+}$ (**4.6a**) to $[Co(dgm)(phen)]^{2+}$ (**4.6b**), as monitored by UV-vis spectroscopy.

Of the expected two ligand field bands for $[Co(dpg)(phen)]^{2+}$, one is clearly visible in the absorption spectrum, with a maximum at 480 nm. The other, higher energy, d-d transition is presumably buried under the intense charge-transfer bands in the region 200 - 400 nm. The observable ligand field band shifts to lower wavelengths upon irradiation with UV light. This shift is entirely consistent with the replacement of a carboxylate donor by a strongly basic carbon donor. The rise in absorption in the 400 - 425 nm region can be ascribed to a carbon-to-cobalt charge transfer transition.[86] The spectral changes are similar to those noted in the photolysis of the $[Co(phen)_2(gly)]^{2+}$ complex.[97]

Co(II) ions are often produced by the photo-initiated redox decomposition reactions of Co(III) complexes.[8] $[Co(H_2O)_6]^{2+}$ absorbs very weakly in the visible region of the spectrum, hence this redox process can be easily identified by a 'bleaching' of the solution. It is apparent that this did not occur to any great extent in the present example.

This demonstrates that UV-vis is a reliable guide to the progress of the photolysis reaction of $[Co(dpg)(phen)]^{2+}$. The spectral changes upon irradiation, a shift of the d-d transition to higher energy, and the appearance of a Co–C charge transfer band, are useful indications of the formation of a metallacyclic product.

^{1}H NMR spectroscopy

^{1}H NMR spectroscopy also proved to be a valuable tool for monitoring the photolysis reaction. The ^{1}H NMR spectrum of the C_S-symmetric $[Co(dpg)(phen)]^{2+}$ (Fig 4.11a), clearly shows an AB system for the picolyl methylene groups (5.38 and 6.35 ppm, H_{13} to H_{16}). The singlet for the glycinato protons is partially obscured by the HOD peak. The phen protons resonate at low field, with seven of the eight expected peaks well resolved (8.25-9.90 ppm, H_1 to H_8). The cluster around 8.0 ppm contains the eighth phen proton, along with four protons from the pyridine rings of the dpg ligand. These two pyridyl groups are related by a mirror plane, and give rise to another two sets of signals (7.25 and 7.70 ppm).

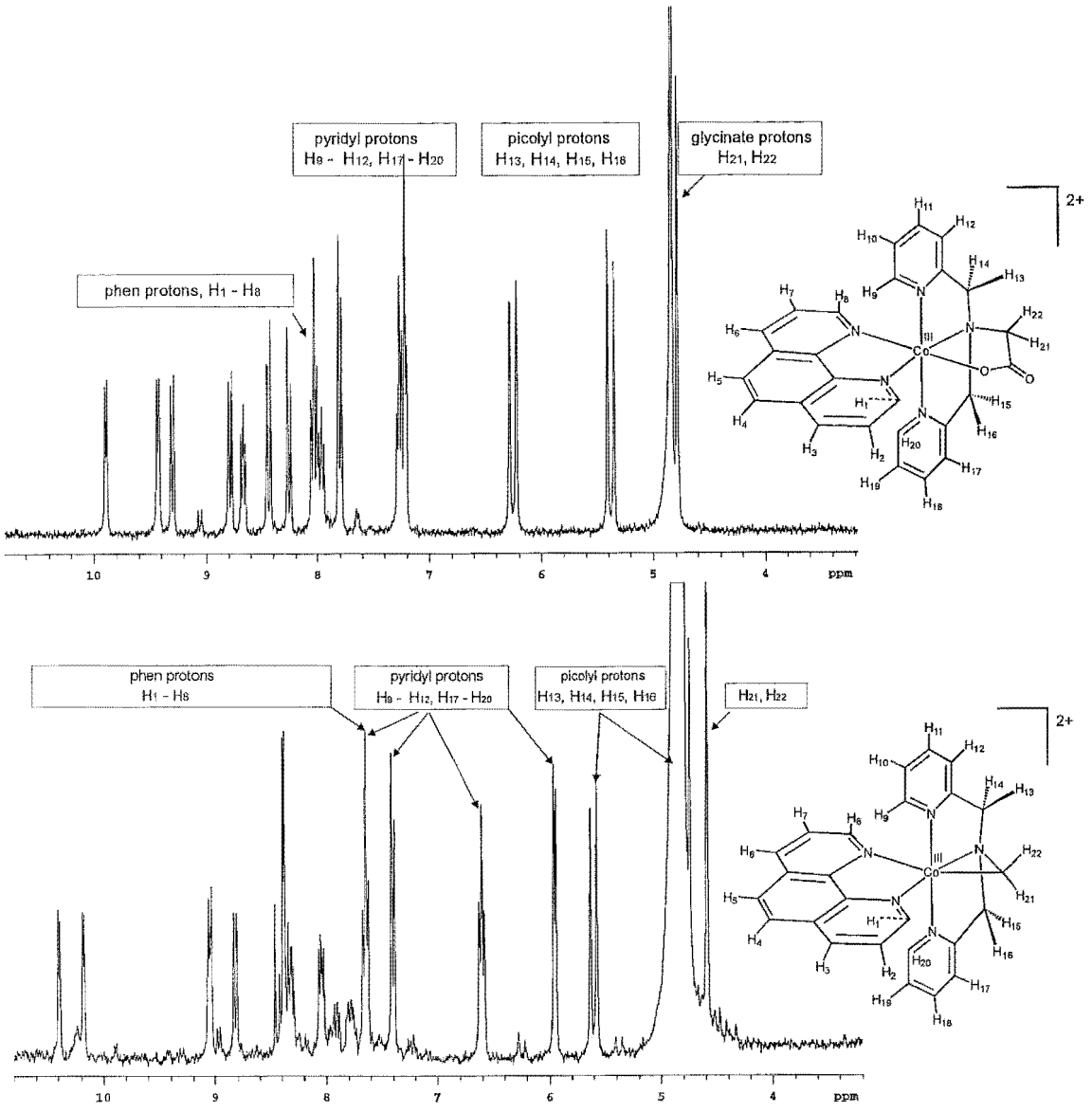

Figure 4.11. ^{1}H NMR (D_2O, 300 MHz) spectra of $[Co(dpg)(phen)]^{2+}$ (top) and its photolysis product, $[Co(dgm)(phen)]^{2+}$ (below). The small peaks visible at 7.65 ppm and 9.05 ppm in the spectrum of $[Co(dpg)(phen)]^{2+}$ are from $[Co(phen)_3]^{3+}$.

The ^{1}H NMR of the same sample following UV irradiation is also displayed in Fig 4.11. The narrow peak widths indicate that the new compound is unlikely to be a Co(II) complex. One of the striking features of the photolysis reaction is the clean conversion to this photolysis product. All the major peaks can be assigned to $[Co(dgm)(phen)]^{2+}$, with few side-products observed by ^{1}H NMR spectroscopy. These assignments were aided by the acquisition of a COSY spectrum.

The solid state structure of $[Co(dgm)(phen)]^{2+}$ indicated that there were significant structural changes associated with the contraction to a three-membered chelate ring. These distortions also seem to be present in solution and lead, for example, to a major shift in the signals for the protons on the pyridine rings. The contraction of the glycinate chelate forces these rings to rotate around their Co–N axis, moving the ortho protons further into the π-electron cloud of the phen ligand. These protons now resonate at 5.96 ppm, an unusually low value for aromatic protons. Another notable shift occurs for two of the phen resonances, which move beyond 10 ppm. These are likely to represent the protons located on the extremity of the phen ligand ie H_1 and H_8. Although a little speculative, this shift is consistent with the idea that the C–N bond of the metallacycle has some π character, with H_1 and H_8 influenced by the resulting magnetic anisotropy. Such effects should also serve to shift the signals of the Co-bound methylene group (H_{22} and H_{23}) downfield. However, this effect may be balanced the upfield shift which would result from these protons being positioned over one face of the pyridine rings. The methylene groups attached to the pyridyl arms (H_{13} to H_{16}) remain as a AB system, one half of which was found under the HOD peak by the COSY spectrum.

This ^1H NMR spectrum of the $[Co(dgm)(phen)]^{2+}$ complex, which was obtained by *direct* photolysis of the D_2O sample of $[Co(dpg)(phen)]^{2+}$, was identical to a spectrum of the photolysis product which was isolated by column chromatography. Photolysis of $[Co(dpg)(phen)]^{2+}$ in DMSO-d_6 also gave a clean conversion to the $[Co(dgm)(phen)]^{2+}$ photolysis product, which again was commensurate with an independent sample. A ^{13}C NMR spectrum of the photolysis product was obtained in DMSO-d_6 due to the greater solubility of the complexes in this solvent.

In summary, a stable complex which contains a Co–C–N metallacycle has been isolated from the photolysis of a glycinato ligand which has been tethered by two chelating pyridylmethyl arms. This success prompted an investigation into the versatility of this

polypyridyl ligand framework. Of particular interest was the potential to produce stable metallacycles with alkyl substituents on the carbon atom.

Photolysis of a tethered alaninato complex - $[Co(dpa)(phen)]^{2+}$

The dpaH ligand was prepared by the reaction of L-alanine with picolyl chloride, in the same fashion as the glycinato analogue. Indeed, the same synthetic route was followed to the $[Co(dpa)(NO_2)_2]$ complex, and further to $[Co(dpa)(phen)]^{2+}$. Again, two geometrical isomers are possible for these complexes, as the pyridyl ligands can be either *trans* to each other (as in $[Co(dpg)(phen)]^{2+}$), or in a *cis* arrangement. These two isomers cannot be distinguished immediately by their ^1H NMR spectra, since in this case, the *trans* isomer does not have a mirror plane. However, the chemical shifts of the protons of the two pyridine rings and those of the picolyl methylene groups, are similar to those observed for $[Co(dpg)(phen)]^{+}$, implying that the complex has the *trans* geometry (**4.12a**). If the *cis* geometry was adopted, the two pyridine rings would be in very different environments, hence chemical shifts of their protons would be quite distinct. In addition, the UV-vis spectrum is very similar to that of the $[Co(dpg)(phen)]^{2+}$ complex.

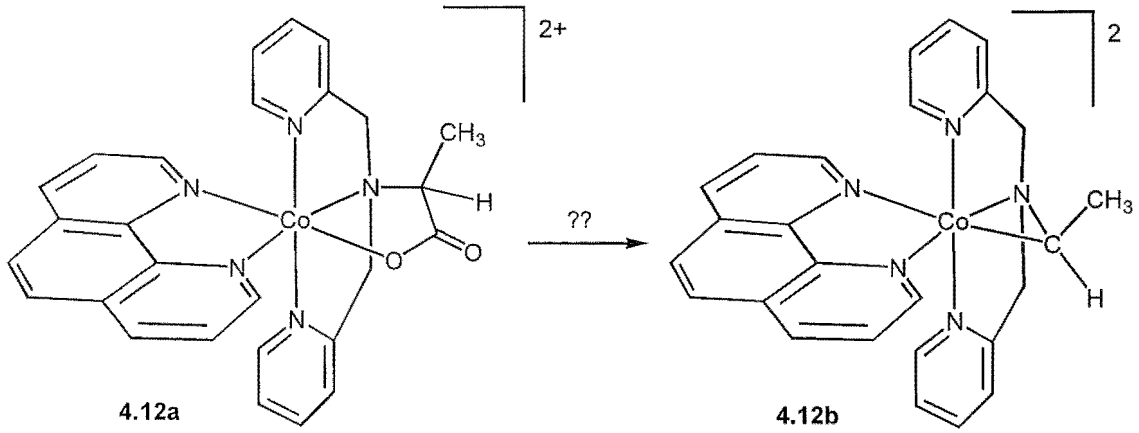

Figure 4.12. Photolysis of the $[Co(dpa)(phen)]^{2+}$ complex.

A major goal of this section of work was to observe the transformation depicted in Fig 4.12, and to fully characterise **4.12b**.

The photolysis of a D_2O solution of $[Co(dpa)(phen)]^{2+}$ was monitored by ^1H NMR spectroscopy. The well-resolved spectrum indicated clean conversion to another diamagnetic Co(III) complex. Many of the spectral changes seen in the photolysis of $[Co(dpg)(phen)]^{2+}$ were repeated in this instance. These changes are consistent with the photolysis product being the $[Co(dam)(phen)]^{2+}$ complex (**4.12b**). For example, two of the phen resonances moved beyond 10 ppm, and a multiplet appeared at 5.95 ppm. The pyridyl ligands will rotate around their Co–N axis and their ortho protons will move further into the phen π-cloud, hence will resonate at higher field. Also, the two phen ortho protons may well be influenced by the anisotropy of the C–N bond in the metallacycle, and may be those which appear above 10 ppm. In addition, the doublet of the methyl group of the alaninato chelate was seen to move from 1.80 to 1.13 ppm. Upon formation of $[Co(dam)(phen)]^{2+}$ (**4.12b**), the alaninato methyl group is expected to move into a shielded region over a pyridine ring, hence will resonate at higher field.

The couplings which were observed in a COSY spectrum were also consistent with the proposed structure **4.12b**. The proton which is attached to the carbon atom of the metallacycle was located under the HOD peak. This spectrum also established that the multiplet just under 6 ppm was indeed due to the pyridyl rings of the dam ligand. The changes in the ^1H NMR and ^{13}C NMR spectra following photolysis in DMSO-d_6 were also consistent with the formation of $[Co(dam)(phen)]^{2+}$. The ^{13}C NMR spectrum obtained in this solvent showed that the signal for the carboxylate carbon had disappeared. The carbon bonded to the cobalt centre was assigned the peak at 46.2 ppm on the basis of the chemical shift of this carbon in the $[Co(dgm)(phen)]^{2+}$ metallacycle.

The photolysis of $[Co(dpa)(phen)]^{2+}$ (**4.12a**) in aqueous solution was also monitored by UV-vis spectroscopy. The d-d transition, initially seen at 481 nm, moved to 462 nm during the photolysis, with a slightly increased absorbance. Furthermore, a rise in absorption in the region 400 - 430 nm, attributed to the tail of a Co–C charge transfer

band in the case of formation of the $[Co(dgm)(phen)]^{2+}$ metallacycle, is also observed during photolysis of $[Co(dpa)(phen)]^{2+}$.

Unfortunately, the photolysis product could not be isolated as a solid, let alone as good quality crystals, although there were promising signs that this crystallisation is possible. To this point, this has prevented a full characterisation of the photolysis product as neither elemental analysis nor X-ray crystallography have been possible. However, on the basis of ^{1}H NMR, ^{13}C NMR and UV-vis spectroscopy, the photolysis product was able to be assigned as the $[Co(dpa)(phen)]^{2+}$ complex (**4.12b**). This was an encouraging result, and paved the way for the investigation into the cyclopropylglycinato analogue, $[Co(dpc)(phen)]^{2+}$.

Photolysis of a tethered cyclopropylglycinato complex

It was hoped that this polypyridyl ligand framework would also be able to stabilise the photolysis product of $[Co(dpc)(phen)]^{2+}$ (**4.13a**). If UV photolysis of this complex induces decarboxylation and formation of **4.13b**, a relative measure of the rate constant k_c can be gained from the observed product distribution. This is the reaction pathway predicted by the currently accepted mechanism. From the radical **4.13b**, a competition will exist between the ring-opening reaction (k_r), and recombination with the cobalt centre (k_c). On the basis of the theoretical results described in Chapter 2, a reasonable estimate is $k_c \approx 10^7 - 10^9\ s^{-1}$. If $k_c >> k_r$, the cyclopropyl group will be retained in the product, perhaps as **4.13d**. (This observation would also be made if the radical is not formed at all). If k_c is significantly smaller than k_r, the rearrangement reaction will proceed, and ring-opened products will be observed (**4.13c**).

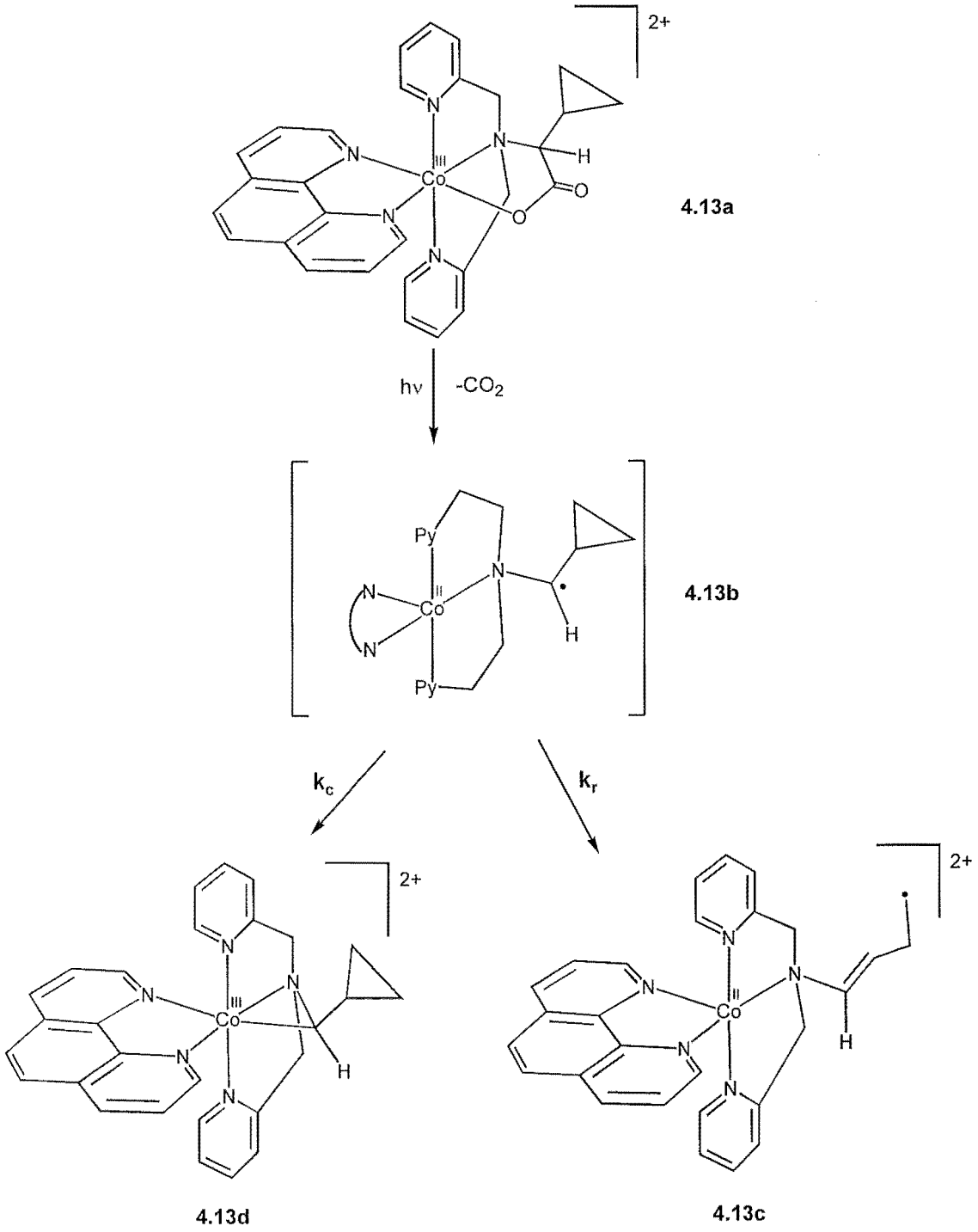

Figure 4.13. Two possible reaction pathways for the $[Co(dpc)(phen)]^{2+}$ complex.

Cyclopropylglycine was derivatised to give dpcH by reaction with picolyl chloride, in the same manner as for the alanine and glycine trailblazers. Synthesis of the $[Co(dpc)(phen)]^{2+}$ complex proceeded as expected, and the complex was characterised

by NMR, UV-vis, and mass spectrometry. Again, the possibility that the complex exists in the *cis*-pyridyl configuration cannot be ruled out, however, the NMR and UV-vis spectra are consistent with *trans*-pyridyl geometry. Ideally, an elemental analysis would have been carried out, however, as only a small quantity of the amino acid was available, the resource of $[Co(dpc)(phen)]^{2+}$ was too limited. This also precluded large-scale photolysis reactions. Hence, ^1H NMR and UV-vis spectroscopy were employed to follow the course of the photolysis reaction.

The two foremost considerations which directed the ^1H NMR investigation of the photolysis reaction of $[Co(dpc)(phen)]^{2+}$ (**4.13a**) were to establish (i) whether a metallacycle was formed, and (ii) whether the cyclopropyl group survived. The results indicate that both of these can be answered in the affirmative.

Upon irradiation of $[Co(dpc)(phen)]^{2+}$ (**4.13a**) with 254 nm light, a clean reaction takes place which, on the basis of the well-resolved ^1H NMR spectrum, produces another Co(III) complex (Fig 4.14). Several of the changes which occur in this spectrum are reminiscent of the transformations seen for the $[Co(dpg)(phen)]^{2+}$ complex (Fig 4.11). For instance, two of the phen signals shift downfield to 10.50 and 10.15 ppm, and two protons which can be assigned to the pyridyl ligands are pushed upfield to around 5.95 ppm. Thus, just by using an inductive argument based on the $[Co(dgm)(phen)]^{2+}$ complex, it appears likely that a similar metallacycle has been formed. A COSY spectrum adds weight to this argument, and allowed the general assignment of all the peaks.

The fate of the cyclopropyl group is clearly revealed by the ^1H NMR and COSY spectra. A broadened set of signals centre around 1 ppm, characteristic of this moiety, is evident in both the reactant and the photolysis product. However the cyclopropyl methine proton (H_{22}) appears at 0 ppm in the product. Construction of a molecular model of $[Co(dcm)(phen)]^{2+}$ indicates that this proton is likely to lie directly over a pyridine ring of the dcm ligand.

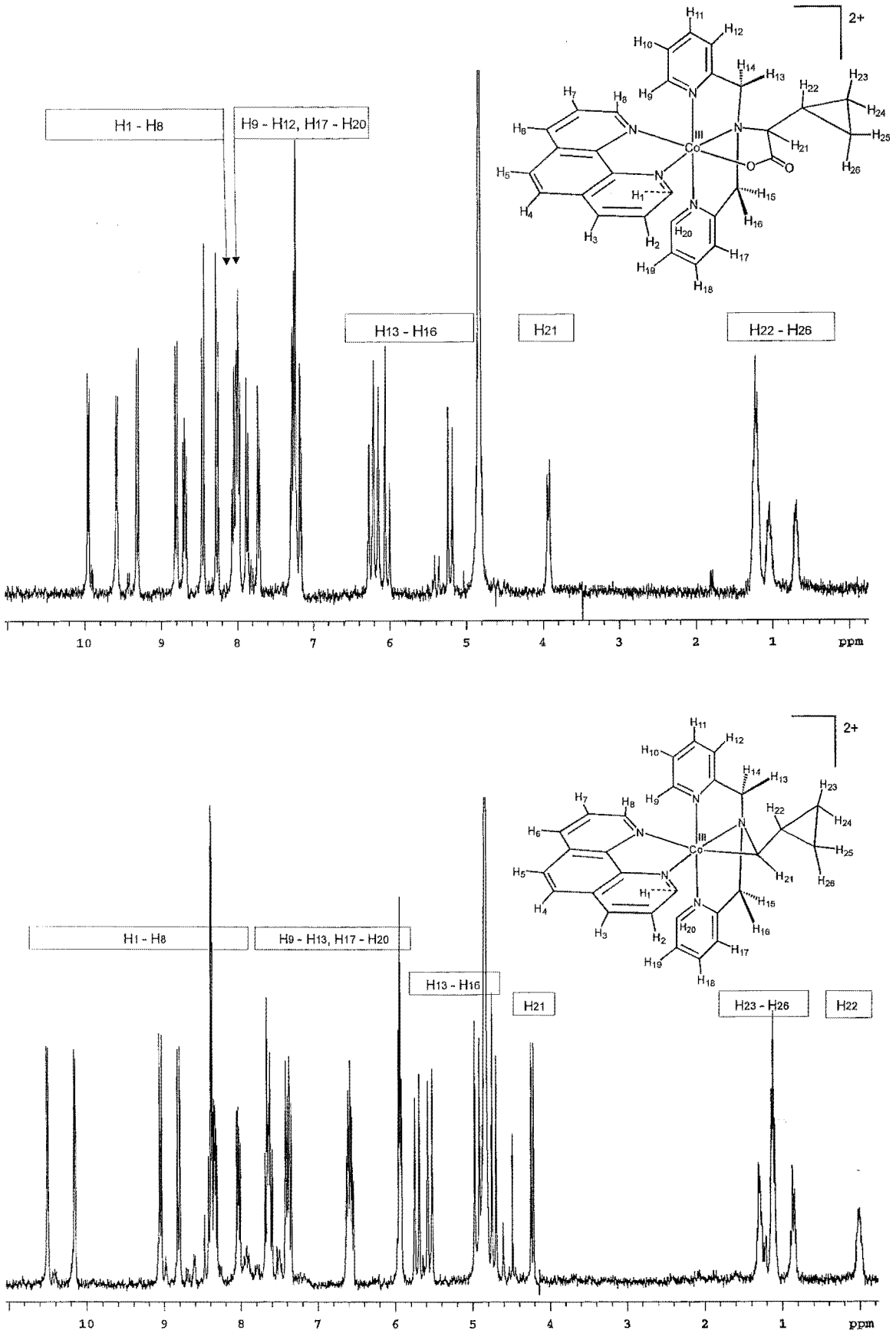

Figure 4.14. ^{1}H NMR spectra of the $[Co(dpc)(phen)]^{2+}$ complex (top), and its photolysis product, $[Co(dcm)(phen)]^{2+}$ (below).

The photolysis was also carried out in DMSO-d_6, and similar spectral changes were observed. A ^{13}C spectrum fully supported the assignment of the photolysis product as **4.13d**.

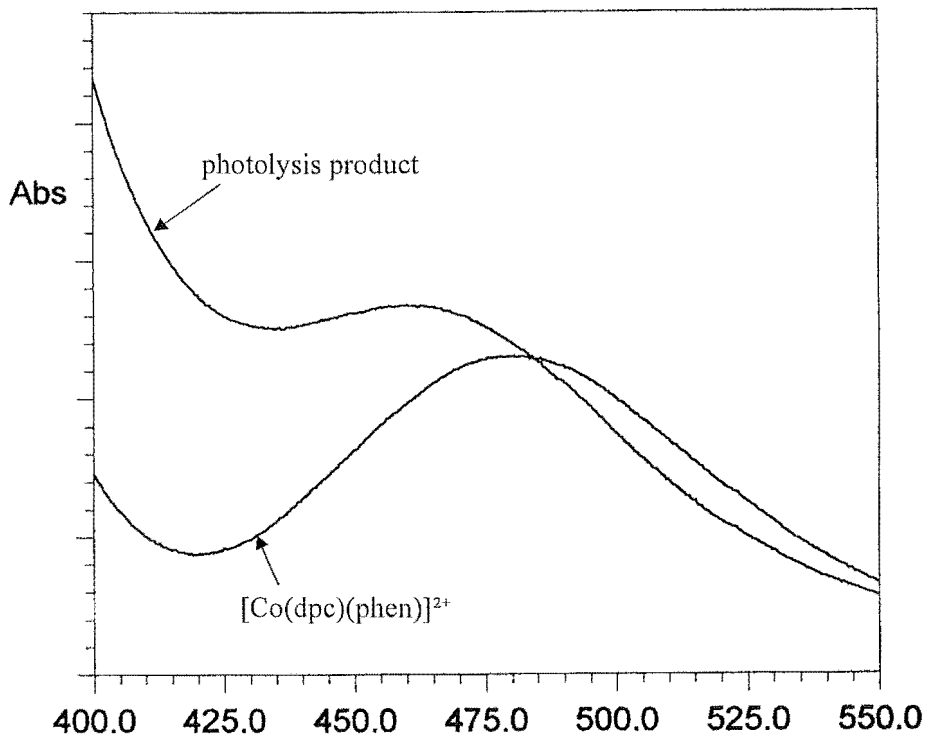

Figure 4.15. A UV-vis spectrum of $[Co(dpc)(phen)]^{2+}$ (**4.13a**) and its photolysis product.

A UV-vis spectrum of $[Co(dpc)(phen)]^{2+}$, and its photolysis product are shown in Fig 4.15. The shift of the d-d absorption peak to shorter wavelengths (462 nm), accompanied by a rise in absorption in the 400 - 430 nm region, is entirely consistent with **4.13d** as the photolysis product.

The implications for the mechanism

Without question, the cyclopropyl ring survives photolysis of the $[Co(dpc)(phen)]^{2+}$ complex, and no ring-opened products are observed. Therefore, if the radical **4.13b** is formed at all, it has a very short lifetime. If the photolysis reaction of $[Co(dpc)(phen)]^{2+}$ proceeds *via* the currently accepted mechanism (Fig 4.13), the rate constant k_c must be around 10^9 s^{-1}.

Decomposition of the photolysis products

Although the characterisation of the alkyl-substituted metallacycles was a particularly pleasing result, their eventual decomposition reactions also proved to be quite informative. This section presents some observations regarding the solution behavior (D_2O, DMSO-d_6, DCl) of these complexes in the hours and days following photolysis. As alluded to earlier, although the alkyl-substituted metallacycles were stable enough to characterise by NMR and UV-vis, they have thus far eluded attempts to isolate them in the solid state.

Decomposition pathways

The decomposition reactions of the $[Co(dgm)(phen)]^{2+}$ (**4.5**), $[Co(dam)(phen)]^{2+}$ (**4.12b**), $[Co(dcm)(phen)]^{2+}$ (**4.13d**), complexes were observed in both neutral and acidified solution, and the evolution of the products was monitored by ^1H NMR. Three reaction modes are possible, which differ according to how the bonding electrons are shared between the alkyl fragment and the cobalt centre. This was discussed more fully in Chapter 3.

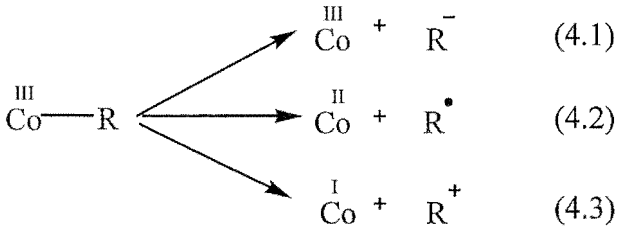

Decomposition *via* Eqtn 4.1 will lead to an α-amino carbanion, which would be expected to extract a deuteron from the solvent (D_2O or DMSO-d_6). Alternatively, a Co(II) complex and an α-amino radical may be formed (Eqtn 4.2). This radical could abstract a hydrogen atom from the α-position of another complex (reactant or metallacycle), or react with another odd-electron species, for example self-termination, or reaction with O_2. The third alternative is the production of a Co(I) complex and a

carbocation (Eqtn 4.3). A carbocation with an adjacent amine group is merely a canonical form of an iminium ion, and hydrolysis of this would give an amine and a carbonyl compound.

Thermal decomposition of the metallacycles

In both D_2O and DMSO-d_6, the $[Co(dcm)(phen)]^{2+}$ (**4.13d**) and $[Co(dam)(phen)]^{2+}$ (**4.12b**) complexes decomposed to give aldehydes (cyclopropanecarboxaldehyde and acetaldehyde respectively, Fig 4.16). In D_2O, these complexes had half-lives of 7-9 hours, and 5 days respectively. Extraction of the resulting D_2O solutions with $CDCl_3$, revealed the presence of free phen and bis(2-pyridylmethyl)amine (bpa, **4.16c**) in both cases. These products were also observed following the thermal decomposition of $[Co(dgm)(phen)]^{2+}$, although this complex had a relatively long half-life in D_2O (> 1 week). Bpa was characterised on the basis of its 1D ^1H NMR and 2D ^1H(COSY) spectra.

These observations strengthen the arguments presented in Chapter 3 regarding the formation of carbonyl compounds from unstable organometallic photolysis products derived from the $[Co(bpy)_2(aa)]^{2+}$ complexes. In that instance, the existence of (unstable) substituted metallacycles, had to be inferred from low-temperature photolysis experiments. A direct link has now been established between substituted metallacycles and the carbonyl compounds. This product distribution is entirely consistent with decomposition of the metallacycle into a Co(I) fragment and an imine (Fig 4.16), as outlined for the photolysis products of $[Co(bpy)_2(aa)]^{2+}$ (Fig 3.10).

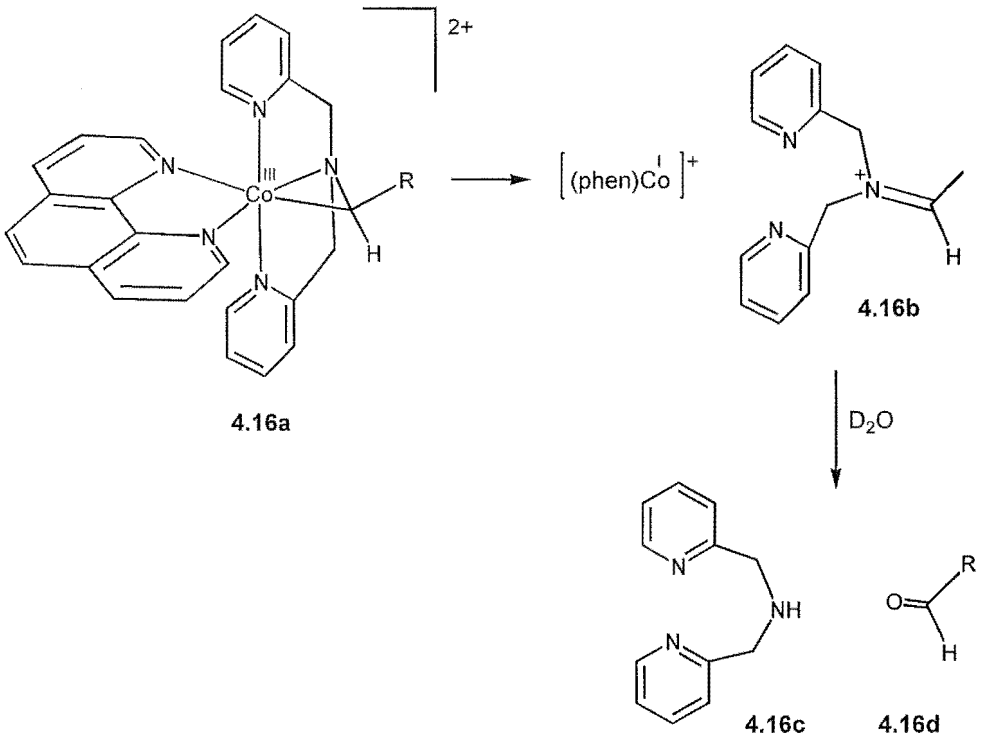

Figure 4.16. A decomposition pathway for the organometallic photolysis products which accounts for the observed products.

It is possible that the imine (**4.16b**) was formed *via* homolytic decomposition (Eqtn 4.2), followed by reaction of the aminoalkyl radical with an oxidant, for example dissolved molecular oxygen. This pathway would also generate the iminium ion **4.16b**. However, this route to the observed carbonyl compounds is unlikely on the following basis. Homolytic dissociation would generate a tridentate aminoalkyl radical coordinated to Co(II). Ligand exchange reactions of the Co(II) centre will occur with a maximum rate constant of 10^6 s^{-1}.[44] The survival of the cyclopropyl group in the decomposition of $[Co(dcm)(phen)]^{2+}$ (**4.13d**) implies that maximum lifetime of any such aminoalkyl radical must significantly less than 10^{-6} s. This precludes any dissociation of the radical from the cobalt centre, and formation of the iminium ion would have to occur whilst the radical is coordinated. It would be possible for dioxygen to react with the radical whilst it was still coordinated, however based on literature precedent, a dioxygen insertion product would probably form.[98] A five-membered peroxo chelate would be the expected product. (See, for example, Fig 1.5)

Most attention has so far been paid to the imine fragment of the metallacycle, with little attention paid to the Co(I) portion, which perhaps remains coordinated to the phen and bpa ligands. Several possibilities can be considered for this species, all of which have the ultimate effect of oxidation to Co(II). Firstly, the complex could abstract a proton to give a Co(III)-hydride complex (or in D_2O, a Co(III)-deuteride complex). Electrophilic attack by another proton (deuteron) on the Co–H(D) may yield H_2 (D_2) and a Co(II) species. Secondly, the Co(I) fragment could reduce a Co(III) complex, perhaps some unchanged starting material, to generate two Co(II) complexes. Circumstantial evidence for this is provided by the following observation. If the $[Co(dpa)(phen)]^{2+}$ complex (**4.12a**) was incompletely photolysed, and the solution of $[Co(dpa)(phen)]^{2+}$ and $[Co(dam)(phen)]^{2+}$ (**4.12b**) was stood at room temperature, ^1H NMR spectroscopy showed that the $[Co(dpa)(phen)]^{2+}$ complex continued to be depleted. Signals which could be assigned to the free dpa ligand, grew into the spectrum. This is consistent with the following process.

$$\left[Co^{I}\right] + \left[Co^{III}(dpa)(phen)\right]^{2+} \rightarrow \quad 2Co^{2+} + dpa + phen \qquad (4.4)$$

An analogous reaction between the Co(I) species and the metallacycle may be hindered due to fact that the reduction potential for **4.12a** will be lower than that for **4.12b**. This line of inquiry was not fully explored in the present study.

If the D_2O solutions of the (decomposing) $[Co(dcm)(phen)]^{2+}$ (**4.13d**) or $[Co(dam)(phen)]^{2+}$ (**4.12b**) metallacycles were allowed to stand at room temperature for prolonged periods, a new grouping of eight aromatic protons appeared in the ^1H NMR spectra. Clearly these signals were due to the formation of a new compound, but it took the fortuitous crystallisation of this complex before its structure was revealed. X-ray crystallography heralded the structure shown in Fig 4.17.

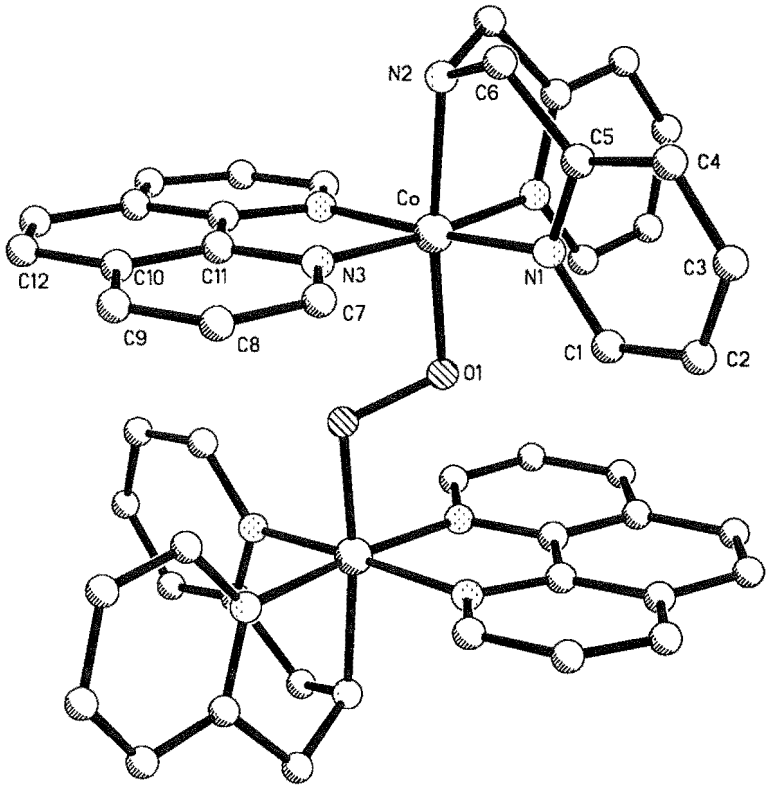

Figure 4.17. X-ray crystal structure of the $[Co(phen)(bpa)(O_2)Co(phen)(bpa)]^{4+}$ complex ion. All hydrogen atoms, and the perchlorate counter ions have been omitted from the diagram. Selected bond lengths (Å) and angles (°): Co-O(1) 1.883(5); Co-N(1) 1.925(4); Co-N(2) 2.004(6); Co-N(3) 1.943(4); N(1)-Co-N(2) 84.20(18); N(3)'-Co-N(3) 84.2(3); N(1)'-Co-N(1) 88.9(2); O(1)'-O(1)-Co 113.0(4).

The complex is a peroxo-bridged dinuclear complex, $[Co(phen)(bpa)(O_2)Co(phen)(bpa)]^{4+}$. Each cobalt centre is coordinated to a phen and bpa ligand, and the two units are linked by an O_2^{2-} bridge. The geometry around each cobalt is identical, with the oxygen ligand occupying a coordination site *trans* to the secondary nitrogen of the folded bpa ligand. This gives a highly symmetrical structure (C_{2h} symmetry), and the atoms which are labeled in Fig 4.17 comprise the asymmetric unit. The remainder of the complex is generated by a mirror plane which bisects the complex normal to the phen ligands, and a centre of inversion, which is located at the midpoint of the O–O bond. The cobalt has near-octahedral geometry, with the largest deviations appearing in the chelate bite angles, as expected.

The complex is best formulated as a μ-peroxo Co(III) dimer, rather than a superoxo species (or one with other cobalt oxidation states). This is consistent with its diamagnetic behavior, the number of perchlorate counter anions (four), the O(1)'–O(1)–Co bond angle (113.0°), and the O(1)–O(1)' bond length (1.436 Å). A cross-section of reported values shows that for binuclear, monobridged peroxo complexes of Co(III), this bond angle generally lies the range 110 - 115°. The bond lengths all took values between 1.38 - 1.53 Å.[99,100]

Of the nine possible geometrical isomers, the dimeric complex has adopted one with the same conformation around each cobalt centre, and with the peroxo ligand *trans* to the secondary nitrogen of the bpa ligand. Steric factors are unlikely to particularly disfavour any of the geometrical arrangements, hence electronic factors probably account for the selectivity. The preference may have come about because the ligating secondary amine is the most basic donor. The bonding interaction with the oxo ligand, that is the filling of the empty O_2 π^* orbitals with electron density from the metal d orbitals,[100] will be maximised when this donor is aligned *trans* to the oxo ligand. The relatively long Co–N(2) bond (2.004 Å) is in keeping with other μ-peroxo dimers which have similar donor sets.[101]

The complexation of molecular oxygen by cobalt complexes has been a fruitful area of research.[90] Most interest has focussed on the development of catalysts for oxidation reactions,[102,103] models for biological systems,[99] and dioxygen storage devices.[104] An enormous number of reports have appeared in the literature detailing many aspects of the chemistry of dioxygen complexes, with μ-peroxo cobalt dimers among the most commonly featured. Many of these contain polydentate ligands which have both pyridyl and amino functionalities.[105,106,107]

The complex featured in the present study does not possess unusual properties or structural features but, to the best of the author's knowledge, this is just the second cobalt complex of the bpa ligand to have been characterised by X-ray crystallography. The other complex was a trinuclear compound with a Co_3O_4 core and was uncovered with a CAS online search.[108] A search of the Cambridge Structural Database did not reveal *any* structures which contained the bpa fragment (even with other metals or no metals at all).

The most common method of synthesis of μ-peroxo complexes is the air oxidation of neutral solutions of Co(II) and the required ligands.[90] Thus, the discovery of the dimer **4.17** in the decomposing photolysates is not suprising given that Co(II), bpa and phen are all characterised by-products from the decomposition reactions of $[Co(dam)(phen)]^{2+}$ and $[Co(dcm)(phen)]^{2+}$. It would make an interesting study to determine whether this complex could be synthesized independently, and whether the geometrical isomer **4.17** is the sole product.

Decomposition in acidic solution

Electrophilic attack of a proton on a Co–C bond will induce heterolytic cleavage and the formation of an alkane, as represented by the general equation 4.1. This reaction is quite general for mono-alkylated Co(III) complexes, which produce the corresponding alkane, however rather forcing conditions (eg heating in conc HCl) are often required.[86] This type of reaction for a η^2-aminomethylene ligand has previously been reported for the complex **4.18a**.[36] The Co–C bond in this complex is cleaved upon warming in dilute HCl. A chloro ligand fills the vacant coordination site, to give **4.18b**, with no apparent change of the cobalt oxidation state.

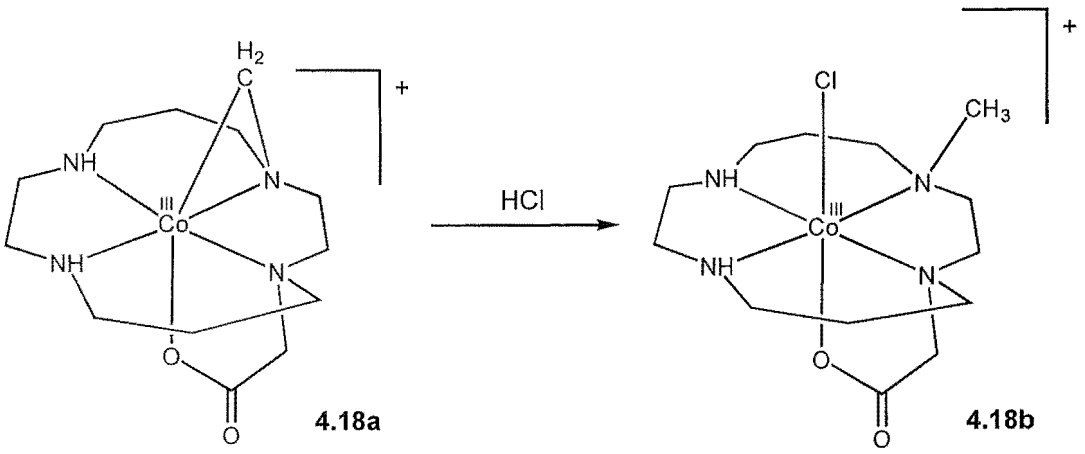

Figure 4.18

Thus, the possibility arises that the presence of acid may alter the decomposition pathway of the $[Co(dgm)(phen)]^{2+}$ and $[Co(dam)(phen)]^{2+}$ complexes, possibly yielding the complexes shown in Fig 4.19. The dependence of the decomposition products of the $[Co(dgm)(phen)]^{2+}$ (**4.19a** R = H) and $[Co(dam)(phen)]^{2+}$ (**4.19a** R = CH_3) on the presence of acid was probed by monitoring DCl solutions ([DCl] ≈ 0.5 M) of these complexes by ^{1}H NMR spectroscopy.

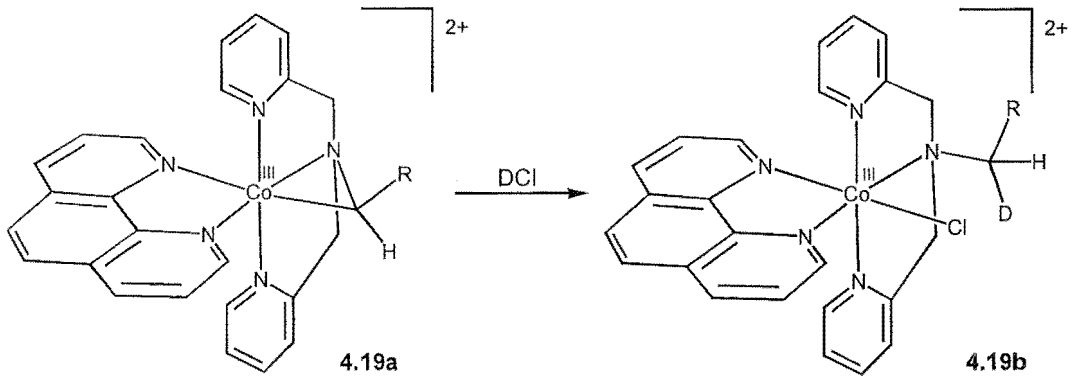

Figure 4.19. The likely result of electrophilic attack of a deuteron on the Co-C bond in $[Co(dgm)(phen)]^{2+}$ (R = H) or $[Co(dam)(phen)]^{2+}$ (R = CH_3).

The ring-opened complexes **4.19b** (R = H or R = CH_3) should be easily detected by ^{1}H NMR spectroscopy. The incorporation of a deuteron on the formerly ligating carbon atom would induce splitting of the signals of the geminal proton(s). In addition, eight new phen resonances and four new peaks will develop for the two pyridine rings.

The actual changes in the ^{1}H NMR spectra indicated that free phen formed upon standing solutions containing $[Co(dgm)(phen)]^{2+}$ and $[Co(dam)(phen)]^{2+}$ at room temperature in DCl. The fate of the pyridine-containing ligand was initially unclear due to the crowding in the aromatic region of the spectra. In the case of the $[Co(dam)(phen)]^{2+}$ complex however, it appeared that the methyl group had been incorporated into acetaldehyde. Following the complete destruction of the original complexes, the solutions were made basic with NaOD, and extracted with $CDCl_3$. The spectra obtained in this solvent were more enlightening and confirmed the suspicion that the decomposition products were analogous to those seen in neutral solution, and in DMSO. The presence of free phen was confirmed, and, more importantly, free bpa was detected. This clearly demonstrates that the C–N bond of the aminoalkyl ligand was cleaved in both instances. This is entirely consistent with the formation of an imine, and subsequent hydrolysis, as in neutral solution.

The difference in the decomposition pathways of **4.19a** (R = H, CH_3) and **4.18a** in the presence of acid can be ascribed to the nature of the bonding in the complexes, and of the auxiliary ligands. Complex **4.18a** was found to have a C–N bond length of 1.447 Å, whilst $[Co(dpg)(phen)]^{2+}$ (**4.19a**, R = H) has this bond length at 1.417 Å, as discussed earlier. This indicates there is somewhat more electron density in the C–N bond in the latter complex, which will render the carbon atom less susceptible to electrophilic attack. Furthermore, the π-acidic co-ligands on this complex will promote the reduction to Co(I), as required to account for the observed products. The strongly σ-donating coordination sphere of the complex **4.18a** would inhibit such a reduction step.

This work may be extended by examining the interactions of other reagents with the aminomethylene ligands in these complexes. It is possible that stronger electrophiles may be able to cleave the Co–C bond to produce novel complexes or ligands. Alternatively, the imine-like character of C–N bond may render it susceptible to nucleophilic attack whilst still coordinated. There is considerable potential for the development of novel synthetic methodologies and for the further exploration of the properties of these metallacycles.

Summary of Chapter 4

This chapter has presented the results of the photolysis of a series of Co(III) complexes of aminoacidato chelates which are tethered by two coordinating pyridylmethyl arms. The tethered glycinato complex, $[Co(dpg)(phen)]^{2+}$, was found to have *trans*-pyridyl geometry, making it an ideal precursor to a Co–C–N metallacycle. Indeed, photodecarboxylation yielded a stable metallacyclic complex which was characterised by X-ray crystallography. The structural parameters imply that the η^2-aminomethylene unit has considerable imine character. The analogous alaninato and cyclopropylglycinato complexes were prepared, and their photochemistry was investigated. Both were found to yield Co–C–N metallacycles, substituted at the carbon atom with methyl and cyclopropyl substituents respectively. These represent the best characterised examples of Co–C–N metallacycles which have substituents on the ligating carbon atom. Unfortunately, neither were able to be characterised by crystallography or elemental analysis. The fact that the cyclopropyl group remains intact during the photolysis has implications for the photolysis mechanism, and sets the rate constant for Co–C bond formation at greater than 10^9 s^{-1}. The eventual decomposition reactions of the substituted metallacycles were monitored, and carbonyl compounds were detected, presumably *via* heterolytic cleavage of the Co–C bond (with both bonding electrons remaining with the cobalt). The decomposition products were found to be identical in acidic solution. In neutral D_2O solution, secondary chemistry of the decomposition products, and dissolved molecular oxygen, was found to produce a novel binuclear peroxo-bridged Co(III) dimer. This was characterised by X-ray crystallography.

Experimental section

For general experimental details, see the experimental section in Chapter 3. The details of the X-ray crystallography are collated in Appendix 2.

N,N-bis(2-pyridylmethyl)aminoacido ligands

General method

The synthesis of this series of ligands was based on a literature method[88] (Fig 4.3) however, the isolation and purification procedure differed from the original account. Following the extraction of the aqueous reaction mixture with CH_2Cl_2, the aqueous portion was acidified and loaded on to Dowex. Elution with 1.5 M HCl gave a yellow band identified as the monoalkylated amino acid. Elution with 2.5 M HCl gave the desired product as a pale yellow eluate which yielded an oily pale yellow material when taken to dryness on a rotary evaporator. Precipitation of the ligand as the trihydrochloride salt was induced by the addition of acetone/isopropanol (1/1), and the off-white solid was filtered, washed with isopropanol and ether, and air-dried.

N,N-Bis(2-pyridylmethyl)glycine (dpgH.3HCl)

^{1}H NMR as the trihydrochloride (D_2O): δ 3.75 (s, 2H, gly CH_2), 4.51 (s, 4H, picolyl CH_2's), 7.99 (t, 2H), 8.03 (d, 2H). 8.55 (t, 2H), 8.76 (d, 2H). ^{13}C NMR (D_2O): δ 55.94 (gly α-C), 56.45 (pyridyl CH_2's), 127.20, 127.86, 142.15, 148.13, 153.33, 175.30 (COO).MS (FAB): m/z 258 ($[H_2dpg]^+$).

N,N-Bis(2-pyridylmethyl)-L-alanine (dpaH.3HCl)

L-Alanine was used in the synthesis. ^{1}H NMR as the trihydrochloride (D_2O): δ 1.50 (d, 3H, CH_3, J = 6.8 Hz), 3.83 (q, 1H, ala α-H), 4.43 (s, 4H, picolyl CH_2's), 7.93 (t, 2H), 8.04 (d, 2H), 8.50 (t, 2H), 8.69 (d, 2H). ^{13}C NMR (D_2O): δ 14.24 (ala CH_3), 54.01

(picolyl CH_2's), 60.57 (ala α-C), 127.20, 127.96, 142.08, 148.18, 153.78, 177.31 (COO). MS (FAB): m/z 272 ($[H_2dpa]^+$).

N,N-Bis(2-pyridylmethyl)cyclopropylglycine (dpcH.3HCl)

^1H NMR as the trihydrochloride (D_2O): 0.46-0.54 (br m, 3H, cyclopropyl CH_2's), 0.62-0.68 (br m, 1H, cyclopropyl CH_2), 1.03-1.09 (br m, 1H, cyclopropyl CH), 2.92 (d, 1H, J = 9.7, α-C), 4.57 (AB, 4H, J = 16.6 Hz, picolyl CH_2's), 7.94 (t, 2H), 8.08 (d, 2H), 8.51 (t, 2H), 8.71 (d, 2H). ^{13}C NMR (D_2O): δ 4.47, 5.50, 12.05, 54.90, 70.69 (cpg α-C), 127.15, 127.91, 141.98, 148.13, 154.02, 176.61 (COO). MS (FAB): m/z 298 ($[H_2dpc]^+$).

Preparation of the $[Co(dpx)(phen)]^{2+}$ complexes

General synthetic procedure

The abbreviation dpx is used as a generic term for this family of ligands.

$Co(NO_3)_2.6H_2O$ (4.64 g, 16 mmol) and $NaNO_2$ (4.96 g, 70 mmol) were dissolved in a buffer solution of glacial acetic acid (3.5 mL) and NaOH (1.2 g) in H_2O (30 mL). To this was added a solution of dpx.3HCl (12 mmol), with NaOH (1.44 g, 36 mmol), in H_2O (10 mL). The solution was aerated overnight. An orange-brown precipitate of $[Co(dpx)(NO_2)_2]$ deposited, which was filtered, washed with ice-cold water, and dried in an oven (50-60°C). These $[Co(dpx)(NO_2)_2]$ complexes were characterised by NMR and mass spectrometry (see below).

$[Co(dpx)(NO_2)_2]$ (2.5 mmol) was suspended in 0.2 M NaCl solution (5 mL) with stirring, and a solution of phen (0.49 g, 2.5 mmol) in methanol (5 mL) was added. Stirring continued at rt for 3 h. Any remaining solid was removed by filtration and the orange filtrate was loaded on to SP Sephadex C25 (H^+ form, 3 × 20 cm). An intense

orange band eluted with 0.25 M HCl, and the eluate was reduced in volume on a rotary evaporator. Conc $HClO_4$ and ethanol were added, and crystalline $[Co(dpx)(phen)](ClO_4)_2$ formed after standing overnight in a refrigerator. Recrystallisation from dilute $HClO_4$ gave an analytically pure product. The yield was generally around 30% from the amino acid.

Characterisation of the dpg complexes

$[Co(dpg)(NO_2)_2]$ (4.4a)

^1H NMR (DMSO-d_6): δ 3.92 (s, 2H, gly CH_2), 4.77 and 5.09 (AB, 4H, picolyl CH_2's), 7.65 (m, 4H), 8.15 (t, 2H), 8.58 (d, 2H). ^{13}C NMR (DMSO-d_6): δ 66.46 (gly CH_2), 67.34 (picolyl CH_2's), 123.64, 125.61, 140.42, 151.05, 162.31, 176.92 (COO). FAB-MS: (m/z) 315 ($[Co(dpg)]^+$).

$[Co(dpg)(phen)](ClO_4)_2$ (4.6a)

^1H NMR (DMSO-d_6): δ 4.68 (s, 2H, gly CH_2), 5.32 and 6.19 (AB, 4H, picolyl CH_2's, J = 17.5 Hz), 7.16 (d, 2H, dpg), 7.31 (t, 2H, dpg), 7.81 (d, 2H dpg), 7.99 (t, 1H, phen), 8.08 (t, 2H, dpg), 8.38 and 8.57 (AB, 2H, phen), 8.74 (m, 1H, phen), 8.92 (d, 1H, phen), 9.42 (d, 1H, phen), 9.62 (d, 1H, phen), 9.75 (d, 1H, phen). ^1H NMR (D_2O): δ 4.79 (s, partially obscured by HOD peak, gly CH_2), 5.38 and 6.25 (AB, 4H, J = 17.6 Hz, picolyl CH_2's), 7.20-7.27 (m, 4H), 7.80 (d, 2H), 7.95-8.06 (m, 3H), 8.25 and 8.45 (AB, 2H, J = 8.8 Hz), 8.79 (m, 1H), 8.79 (d, 1H), 9.30 (d, 1H), 9.43 (d, 1H), 9.89 (d, 1H). ^{13}C NMR (DMSO-d_6): δ 67.58 (picolyl CH_2's), 70.76 (gly CH_2), 125.23 (dpg), 127.52 (dpg), 127.71, 128.07, 128.47, 129.22, 130.63, 131.44, 141.14, 141.55 (dpg), 141.98, 145.16, 146.45, 150.99 (dpg), 153.68, 155.11, 163.50 (dpg), 177.10 (COO). Anal. Calcd for $[CoC_{26}H_{22}N_5O_2](ClO_4)_2$: C, 44.98; H, 3.19; N, 10.09. Found: C, 44.67; H, 3.04; N, 10.09. UV-vis: 480 nm (220). λ_{min} 420 nm (71). FAB-MS: m/z 594 ($[Co(dpg)(phen)(ClO_4)]^+$, 3%), 495 ($[Co(dpg)(phen)]^+$, 23%).

Characterisation of the dpa complexes

$[Co(dpa)(NO_2)_2]$

^{1}H NMR (DMSO-d_6): δ 1.28 (d, 3H, CH_3, J = 6.8 Hz), 3.57 (m, obscured by H_2O peak), 4.74-4.92 and 5.10-5.16 (overlapping AB quartets, total 4H), 7.60-7.80 (m, 4H), 8.14 (br s, 2H), 8.37 (d, 1H), 8.75 (d, 1H). ^{13}C NMR (DMSO-d_6): δ 13.56 (CH_3), 59.22, 66.70, 67.12, 122.63, 123.89, 125.62, 125.69, 140.47, 140.71, 151.11, 151.26, 162.17, 162.71, 178.05 (COO). MS (FAB): m/z 329 ($[Co(dpa)]^+$).

$[Co(dpa)(phen)](ClO_4)_2 \cdot H_2O$ (4.12a)

^{1}H NMR (DMSO-d_6): δ 1.61 (d, 3H, CH_3, J = 6.8 Hz), 4.40 (m, 1H, α-H), 5.32 (apparent t, 2H, picolyl CH_2), 6.03-6.11 (m, 2H, dpa picolyl CH_2), 7.13 (m, 2H, dpa), 7.30 (d, 2H, dpa), 7.72 (d, 1H, dpa), 7.93-8.12 (m, 4H, dpa pyridyl H (3H), and phen (1H)), 8.38 (d, 1H, phen), 8.57 (d, 1H, phen), 8.74 (m, 1H, phen), 8.92 (d, 1H, phen), 9.43 (d, 1H, phen), 9.75 (m, 2H, phen). ^{1}H NMR (D_2O): δ 1.80 (d, 3H, CH_3, J = 7.8 Hz), 4.63 (q, partially obscured by HOD peak), 5.33 and 6.10 (AB, 2H, J = 16.9 Hz), 5.48 and 6.15 (AB, 2H, J = 18.6 Hz), 7.15-7.28 (m, 3H), 7.76 (d, 1H), 7.87 (d, 1H), 7.97-8.08 (m, 2H), 8.28 (d, 1H), 8.46 (d, 1H), 8.70 (m, 1H), 8.81 (d, 1H), 9.32 (d, 1H), 9.56 (d, 1H), 9.92 (d, 1H). ^{13}C NMR (DMSO-d_6): δ 13.60, 59.03, 66.43, 71.19, 124.28, 125.52, 127.58 (2C), 127.76, 128.08, 128.53, 129.19, 130.64, 131.48, 141.14, 141.57, 142.01 (2C), 145.16, 146.50, 151.18 (2C), 153.54, 155.54, 163.16, 163.90, 178.08 (COO). Anal Calcd. for $[CoC_{27}H_{24}N_5O_2](ClO_4)_2 \cdot H_2O$: C, 44.66; H, 3.58; N, 9.64. Found: C, 44.56; H, 3.38; N, 9.66. UV-vis: 481 nm (187), 262 nm (31000), 227 (53200), 204 nm (58800). MS (FAB): m/z 608 ($[Co(dpa)(phen)(ClO_4)]^+$, 10%), 509 ($[Co(dpa)(phen)]^+$, 34%).

Characterisation of the dpc complexes

$[Co(dpc)(NO_2)_2]$

This crude complex was rather impure, as shown by its ^1H NMR spectrum, but was not further purified before being used in the reaction to give the phen complex. A ^{13}C NMR spectrum was not acquired due to the small amount of complex which was isolated and the difficulty in recovering it from DMSO. ^1H NMR (DMSO-d_6): δ 0.37-0.42 (br m, 1H), 0.60-0.95 (br m, 4H), 3.02 (d, obscured by H_2O peak, α-H), 4.66 (d, 1H), 4.97-5.35 (m, 3H), 7.58-7.83 (m), 8.10-8.16 (m), 8.45 (d), 8.63 (d). The major unassigned peaks in the ^1H NMR were: δ 1.22 (s), 7.50 (m), 8.00 (m), 8.60 (d), 8.82 (d). MS (FAB): m/z 355 ($[Co(dpc)]^+$).

$[Co(dpc)(phen)](ClO_4)_2$ (4.13a)

^1H NMR (DMSO-d_6): δ 0.60-0.65 (br m, 1H, cyclopropyl CH_2), 0.82-0.87 (br m, 1H, cyclopropyl CH_2), 1.02-1.08 (br m, 2H, cyclopropyl CH and CH_2), 1.14-1.19 (br m, 1H, cyclopropyl CH_2), 3.85 (d, 1H, α-H, J = 8.8 Hz), 5.17 and 6.15 (AB, 2H, J = 17.6 Hz), 5.80 and 6.19 (AB, 2H, J = 18.1 Hz), 7.13 (m, 2H, dpc pyridyl), 7.30 (m, 2H, dpc pyridyl), 7.75 (d, 1H, dpc picolyl), 7.99-8.10 (m, 4H, dpc pyridyl (1H) and phen (3H)), 8.39 (d, 1H), 8.57 (d, 2H), 8.76 (m, 1H), 8.93 (d, 1H), 9.44 (d, 1H), 9.78-9.82 (m, 2H). ^1H NMR (D_2O): δ 0.68-0.74 (br m, 1H), 1.03-1.08 (br m, 1H), 1.19-1.25 (br m, 3H), 3.92 (d, 1H, J = 9.3 Hz), 5.21 and 6.20 (AB, 2H, J = 17.6 Hz), 6.03 and 6.24 (AB, 2H, J = 18.6 Hz), 7.15-7.29 (m, 4H), 7.72 (d, 1H), 7.86 (d, 1H), 7.96-8.07 (t, 3H), 8.26 (d, 1H), 8.44 (d, 1H), 8.68 (m, 1H), 8.80 (d, 1H), 9.31 (d, 1H), 9.58 (d, 1H), 9.95 (d, 1H). ^{13}C NMR (DMSO-d_6): δ 3.42, 5.28, 11.44, 60.25, 67.38, 79.46, 124.31, 125.54, 127.54 (2C), 127.68, 128.04, 128.50, 129.19, 130.63, 131.43, 141.11, 141.39, 141.94 (2C), 145.16, 146.44, 150.85, 151.08, 153.50, 155.44, 163.41, 163.76, 176.90 (COO). UV-vis: 481 nm. MS (FAB): m/z 634 ($[Co(dpc)(phen)(ClO_4)]^+$, 1%), 535 ($[Co(dpc)(phen)]^+$, 9%).

Photolysis of N,N-bis(2-pyridylmethyl)aminoacido complexes

Method 1 - NMR scale photolysis

Milligram amounts of the complexes were dissolved in deuterated NMR solvents (D_2O or DMSO-d_6). They were photolysed with a high-pressure mercury lamp equipped with a 254 nm transmission Pyrex filter (Corning, 7-54). The samples were cooled by immersion in a quartz ice-water bath. This method allowed the progress of the reactions to be followed by NMR spectroscopy.

Method 2 - Large scale photolysis and chromatographic isolation of photolysis products

Aqueous solutions of the complexes (approximately millimolar concentration) were photolysed with an immersable Jelight PS-3004-30 mercury lamp for around 80 mins. The solutions were kept below 20°C by flowing ice-cold water through a jacket around the cell. Typically, several 60 mL batches were combined and chromatographed on CM Sephadex C25 (Na^+, 3 × 25 cm). Elution with 0.2 M $NaClO_4$ developed two bands - an orange band of the unchanged starting material, and an intense orange-yellow band of the photolysis product. This second eluate was concentrated on a rotary evaporator (<30 °C) until an orange crystalline solid deposited. This solid was filtered, washed with ethanol and ether, and air dried.

Method 3 - UV-vis monitoring of the photolysis reaction

Aqueous solutions of the complexes, with concentrations in the range 1.0-1.5 mM, were photolysed in quartz cuvettes. A 200W high-pressure mercury lamp, equipped with a 254 nm transmission filter (Pyrex, Corning, 7-54), was used as the light source. Two water-filled 1 cm quartz cuvettes served as IR filters.

Photolysis of $[Co(dpg)(phen)](ClO_4)_2$ - production of $[Co(dgm)(phen)]^{2+}$

NMR scale photolysis

Samples of $[Co(dpg)(phen)](ClO_4)_2$ were photolysed in both DMSO-d_6 and D_2O. The ^1H NMR spectra of the resulting solutions were identical to those described below for the isolated metallacycle.

Large-scale photolysis - isolation of $[Co(dgm)(phen)]^{2+}$ (4.6b)

A crude red-orange precipitate of $[Co(dgm)(phen)]^{2+}$, obtained by the large-scale photolysis procedure detailed above, was recrystallised from warm, dilute $HClO_4$. This pure material was characterised by NMR, UV-vis and microanalysis. Yield: approx 15% at 70% conversion. ^1H NMR (D_2O): d 4.60 (s, Co-CH_2, partially obscured by HOD peak), 4.80 and 5.59 (AB, the peak at 4.80 ppm was hidden by the HOD signal, J = 17.1 Hz, dgm picolyl CH_2), 5.96 (d, 2H, dgm), 7.41 (d, 2H, dgm), 7.66 (m, 2H, dgm), 8.04-8.09 (m, 1H, phen), 8.37-8.8.46 (m, 3H, phen), 8.83 (d, 1H, phen), 9.06 (d, 1H, phen), 10.20 (d, 1H, phen), 10.40 (d, 1H, phen). ^1H NMR (DMSO-d_6): δ 4.51 (s, 2H), 4.50 (s, 2H, CH_2), 4.73 and 5.75 (AB, 4H, J = 16.6 Hz), 5.91 (d, 2H), 6.71 (t, 2H), 7.53 (d, 2H), 7.74 (t, 2H), 8.20 (m, 1H, phen), 8.43 - 8.57 (m, 3H, all phen), 9.00 (d, 1H, phen), 9.22 (d, 1H, phen), 10.47 (d, 1H, phen), 10.51 (d, 1H, phen). ^{13}C NMR (DMSO-d_6): δ 46.17 (Co-CH_2), 60.63, 123.13 (dgm), 124.54 (dgm), 126.96, 127.75, 127.99, 128.25, 130.52, 131.08, 139.17, 139.42 (dgm), 140.12, 145.14, 147.22, 148.95 (dgm), 154.71, 157.89, 159.99 (dgm). Anal. Calcd for $[CoC_{25}H_{22}N_5](ClO_4)_2 \cdot H_2O \cdot 0.25NaClO_4$: C, 42.96; H, 3.43; N, 10.02. Found: C, 42.98; H, 3.11; N, 9.74. UV-vis: 460 nm (180), 296 nm (sh, 9000), 274 nm (25600), 254 nm (20800), 222 nm (36000). λ_{min} 422 nm (142). MS (FAB): m/z 550 ($[Co(dgm)(phen)(ClO_4)]^+$, 25 %), ($[Co(dgm)(phen)]^+$, 22 %).

Photolysis of $[Co(dpa)(phen)](ClO_4)_2$ - production of $[Co(dam)(phen)]^{2+}$

NMR-scale photolysis

The complex was photolysed in D_2O to yield the $[Co(dam)phen]^{2+}$ metallacycle (Fig 4.12). ^1H NMR (D_2O): δ 1.13 (d, 3H, CH_3, J = 6.4 Hz), α-H hidden by HOD peak, 5.56 (half of AB system - remainder hidden by HOD peak, 1H, J = 16.6 Hz), 5.72 (half of picolyl CH_2 AB system - remainder hidden by HOD peak, 1H, J = 17.6 Hz), 5.87-5.92 (m, 2H, dam pyridyl), 6.53-6.65 (m, 2H, dam pyridyl), 7.36-7.42 (m, 2H, dam pyridyl), 7.89-7.94 (m, 1H), 8.00-8.05 (m, 2H, , dam pyridyl and phen), 8.30-8.47 (m, 2H, phen), 8.81 (d, 1H, phen), 9.03-9.08 (m, 2H, phen), 10.17 (d, 1H, phen), 10.44 (d, 1H, phen).

An sample of $[Co(dpa)(phen)]^{2+}$ was photolysed in DMSO-d_6, also yielding $[Co(dam)(phen)]^{2+}$. The ^1H NMR assignments were aided with a COSY spectrum. ^1H NMR (DMSO-d_6): δ 1.02 (d, 3H, J = 6.3 Hz), 4.65-4.79 (m, 3H, α-H and 2 picolyl CH_2's), 5.71 (d, 1H, CH_2, J = 17.1 Hz), 5.82-5.92 (m, 3H, 1 picolyl CH_2 and 2 aromatic dam pyridyl), 6.66-6.70 (m, 2H, dam pyridyl), 7.50-7.56 (m, 2H, dam pyridyl), 7.71-7.74 (m, 2H, dam pyridyl), 8.18-8.21 (m, 1H, phen), 8.42-8.57 (m, 3H, phen), 8.99 (d, 1H, phen), 9.22 (d, 1H, phen), 10.49 (br m, 2H, phen). ^{13}C NMR (DMSO-d_6): δ 14.52 (CH_3), 52.71 (Co-CH_2), 57.65, 61.13, 121.31, 123.21, 124.18, 124.87, 126.89, 127.72, 127.96, 128.25, 130.43, 131.07, 139.08, 139.41, 139.74, 139.89, 140.07, 147.28, 148.58, 148.77, 154.19, 157.55, 159.95, 161.79.

Photolysis of $[Co(dpc)(phen)](ClO_4)_2$ - production of $[Co(dcm)(phen)]^{2+}$

NMR scale photolysis (Fig 4.13, 4.14)

^{1}H NMR of $[Co(dcm)(phen)]^{2+}$ (DMSO-d_6): δ –0.27 - –0.22 (br m, 1H, CH), 0.72-0.77, 0.95-1.00, 1.18-1.23, 1.38-1.43 (all br m, total 4H, cyclopropyl CH_2's), 4.21 (d, 1H, J = 9.0 Hz, α-H), 4.70 and 5.69 (AB, 2H, J = 17.1 Hz), 4.74 and 5.90 (AB, downfield doublet obscured by dcm aromatic H's, upfield peak overlapping with other dcm CH_2 peak), 5.90 (m, 2H, dcm pyridyl), 6.63-6.72 (m, 2H, dcm pyridyl H's), 7.42-7.57 (m, 3H, dcm pyridyl (2H) and phen (1H)), 7.66-7.77 (m, 2H, dcm pyridyl), 8.17-8.21 (m, 1H, phen), 8.46-8.57 (m, 2H), 8.99 (d, 1H), 9.22 (d, 1H), 10.39 (d, 1H), 10.47 (d, 1H). ^{1}H NMR (D_2O): δ –0.03 - 0.05 (br m, 1H, cyclopropyl CH), 0.85 (m, cyclopropyl CH_2), 1.09-1.13 (m, 2H, cyclopropyl CH_2), 1.27-1.31 (m, 1H, cyclopropyl CH_2), 4.23 (d, 1H, J = 9.3 Hz, α-H), 4.73 and 5.55 (AB, 2H, J = 16.8 Hz), 4.94 and 5.72 (AB, 2H, J = 17.1 Hz), 5.90-5.96 (m, 2H, dcm pyridyl), 6.52-6.63 (m, 2H, dcm pyridyl), 7.34-7.42 (m, 2H, dcm pyridyl), 7.59-7.68 (m, 2H, dcm pyridyl), 8.00-8.05 (m, 1H), 8.30-8.47 (m, 3H), 8.81 (d, 1H), 9.05 (d, 1H), 10.15 (d, 1H), 10.50 (d, 1H). ^{13}C NMR (DMSO-d_6): δ 5.75 (2C, cyclopropyl CH_2's), 10.24 (cyclopropyl CH), 58.10 (Co-C), 61.09 and 61.21 (dcm picolyl CH_2's), 121.4, 123.08, 123.16, 123.59, 124.13, 124.90, 126.87, 127.90, 128.22, 130.38, 137.31, 139.01, 139.23, 139.76, 140.05, 147.31, 148.65, 148.95, 154.03, 157.46, 159.93, 161.83. Some peaks which were disregarded as thermal decomposition products. An ^{1}H NMR taken following the acquisition of this ^{13}C spectrum confirmed that the decomposition products remained as minor components (see spectrum following full thermal decomposition given below): δ 6.50, 50.00.

Decomposition of $[Co(dpx)(phen)]^{2+}$ photolysis products

Decomposition in neutral solutions

The NMR-scale photolysates (see above) were stood for prolonged periods at room temperature and the appearance of decomposition products was monitored by NMR spectroscopy over several days.

Decomposition of $[Co(dgm)(phen)]^{2+}$

This complex has a half-life of around 1 week in D_2O at rt. After three weeks, the solution was basified with NaOD, and extracted into $CDCl_3$. ^1H NMR ($CDCl_3$): Bis(2-pyridylmethyl)amine; δ 3.97 (s), 7.16-7.19 and 7.34-7.37 (both m, obscured by residual $CHCl_3$), 7.63 (m, obscured by phen), 8.56 (d). Phen; δ 7.60-7.65 (m), 7.81 (s), 8.27 (d), 9.20 (d).

Decomposition of $[Co(dam)(phen)]^{2+}$

^1H NMR after standing at rt for 5 days (D_2O): Acetaldehyde; δ 2.25 (d), 9.66 (m). $[Co(phen)(bpa)(O_2)Co(phen)(bpa)]^{4+}$: 7.50-7.53 (m, 8H), 7.58-7.61 (m, 8H), 7.73-7.79 (m, 16 H), 7.95 (d, 8H), 8.06 (t, 8H), 8.27 (d, 8H), 8.97 (d, 8H). $[Co(phen)_3]^{3+}$; δ 7.65 (d), 7.92 (m), 8.47 (s), 9.05 (d). The D_2O solution was basified with NaOD and extracted with $CDCl_3$. ^1H NMR ($CDCl_3$): Bis(2-pyridylmethyl)amine; δ 3.97 (s), 7.16-7.19 and 7.34-7.37 (both m, obscured by residual $CHCl_3$), 7.63 (m, obscured by phen), 8.56 (d). Phen; δ 7.60-7.65 (m), 7.81 (s), 8.27 (d), 9.20 (d).

^1H NMR after standing at rt for 72 hours (DMSO-d_6): Acetaldehyde; δ 2.11 (d, 3H, J = 2.9 Hz), 9.63 (m, 1H). The peaks for the metallacycle ($[Co(dam)(phen)]^{2+}$) still dominated the spectrum.

Decomposition of Co(dcm)(phen)]$^{2+}$

This photolysis product has a half-life of around 8-9 hours in D_2O at room temperature. Cyclopropanecarboxaldehyde was detected after standing overnight in both D_2O and DMSO. ^{1}H NMR (D_2O): Cyclopropanecarboxaldehyde; δ 1.19-1.24 (m, 4H), 1.76-1.80 (m, 1H), 8.70 (d, 1H), [Co(phen)(bpa)(O_2)Co(phen)(bpa)]$^{4+}$: 7.50-7.53 (m, 8H), 7.58-7.61 (m, 8H), 7.73-7.79 (m, 16 H), 7.95 (d, 8H), 8.06 (t, 8H), 8.27 (d, 8H), 8.97 (d, 8H). The D_2O sample was extracted with $CDCl_3$. ^{1}H NMR ($CDCl_3$): Cyclopropanecarboxaldehyde; δ 1.07-1.10 (m, 4H, cyclopropyl CH_2's), 1.85 (m, 1H, cyclopropyl CH), 8.90 (d, 1H, J = 5.9 Hz, aldehyde H). The $CDCl_3$ solution was too dilute to record a ^{13}C spectrum.

^{1}H NMR after 3 days at rt (DMSO-d_6): δ 1.03 and 1.05 (m, 4H, cyclopropyl CH_2's), 1.71-1.77 (m, 1H, cyclopropyl CH), 8.73 (d, 1H, J = 6.5 Hz, aldehyde H). The ratio of aldehyde: Co(dcm)(phen)]$^{2+}$ was approximately 1:2 at this point. ^{13}C NMR following complete decomposition of [Co(dcm)(phen)]$^{2+}$ (DMSO-d_6): δ 6.52, 50.08, 123.17, 123.62, 127.81, 137.34, 148.98, 151.74, 157.49.

Decomposition in acidic solution

[Co(dgm)(phen)]$^{2+}$

DCl (1 M) was added to D_2O photolysate of [Co(dpg)(phen)]$^{2+}$ to give a concentration of approximately 0.5 M DCl. The ^{1}H NMR of this solution was monitored periodically.

The peaks of the [Co(dgm)(phen)]$^{2+}$ complex disappeared over a period of weeks. ^{1}H NMR after 21 days (DCl): Phen; δ 8.05 (m, 2H), 8.21 (s, 2H), 8.94 (d, 2H), 9.21 (d, 2H). Some minor unidentified peaks were also present; δ 1.48 (d), 4.45 (s). The solution was basified with NaOD and extracted with $CDCl_3$. ^{1}H NMR ($CDCl_3$): Bis(2-pyridylmethyl)amine; δ 3.97 (s), 7.16-7.19 and 7.34-7.37 (both m, obscured by residual

$CHCl_3$), 7.63 (m, obscured by phen), 8.56 (d). Phen; δ 7.60-7.65 (m), 7.81 (s), 8.27 (d), 9.20 (d).

[Co(dam)(phen)]$^{2+}$

DCl (1 M) was added to a D_2O photolysate of [Co(dpa)(phen)]$^{2+}$ to give a concentration of approximately 0.5 M DCl. The ^{1}H NMR of this solution was monitored periodically.

The peaks of the [Co(dam)(phen)]$^{2+}$ complex disappeared with a half-life of around 24 hours. The acetaldehyde was present in a low concentration due to evaporation, and only the methyl group could be identified with certainty. ^{1}H NMR after 3 days (DCl): Acetaldehyde; δ 2.25 (d, CH_3). Phen; δ 8.05 (m, 2H), 8.21 (s, 2H), 8.94 (d, 2H), 9.21 (d, 2H). Some minor unidentified peaks were also present; δ 1.48 (d), 4.45 (s). The solution was basified with NaOD and extracted with $CDCl_3$. ^{1}H NMR ($CDCl_3$): Bis(2-pyridylmethyl)amine; δ 3.97 (s), 7.16-7.19 and 7.34-7.37 (both m, obscured by residual $CHCl_3$), 7.63 (m, obscured by phen), 8.56 (d). Phen; δ 7.60-7.65 (m), 7.81 (s), 8.27 (d), 9.20 (d). No unidentified peaks were present in the aromatic region, however peaks at δ 2.61 (s) and δ 1.25 (s) remained unassigned.

CHAPTER FIVE

FURTHER EXPLORATIONS OF THE PHOTOLYSIS MECHANISM

Introduction

One of the primary conclusions from the earlier sections of this thesis was that the proposed mechanism for the photolysis of $[Co(bpy)_2(aa)]^{2+}$ complexes is wrong or, at least, the rate-determining step has been incorrectly assigned. The emphasis of the remainder of the thesis has been the development of experiments which may allow a re-formulation of the reaction mechanism.

One approach adopted in the current study has been to attempt to divert the normal course of the reaction by introducing variations in the amino acid fragment. Any changes subsequently induced in the photolysis products may shed some light on the nature of transient reaction intermediates. Specifically, this chapter presents the results of attempts to:

(i) detect the photo-isomerisation of polydentate Co(III)-aminocarboxylato complexes;

(ii) obtain evidence for the presence of a Co(I) intermediate by an intramolecular nucleophilic substitution reaction.

The possible photo-isomerisation of Co(III)-aminocarboxylato complexes

Background

The coordination chemistry of linear polydentate aminocarboxylate ligands has historically been an intensive field of research, especially throughout the 1970s.[109] In particular, kinetically inert Co(III) ion complexes of these ligands were found to be useful probes for investigating areas such as the stereochemistry and optical activity of coordination compounds.

This section will concentrate on a particular class of polydentate aminocarboxylato ligands, namely tetradentate ligands with N,N',O,O' donor sets. The members of this set differ only in the length of the diamine backbone, or of the carboxylate arms.

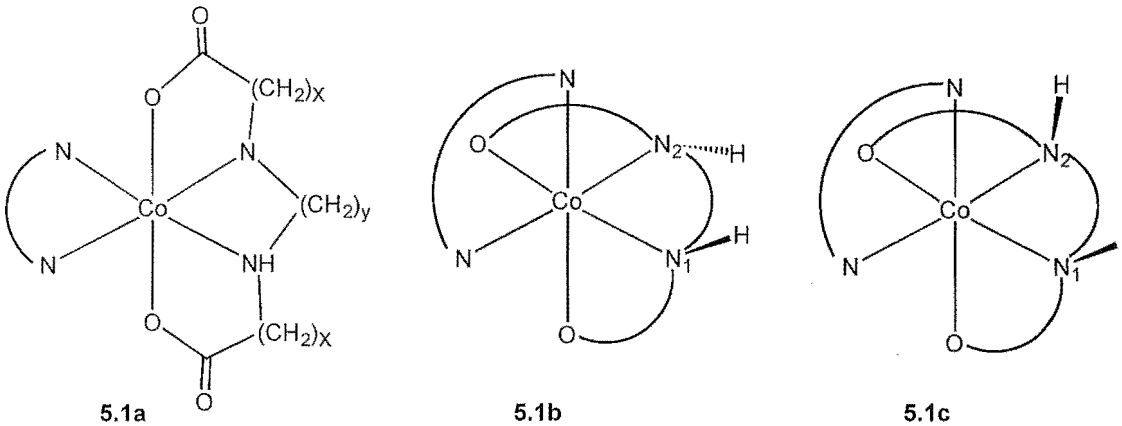

Figure 5.1. Schematic representation of the Δ-α (**5.1a**), Λ-β-e(1) (**5.1b**), and Λ-β-e(2) (**5.1c**) geometrical isomers of a Co(III) complex of a linear tetradentate ligand with a N,N',O,O' donor set. The polydentate ligands are as follows: (i) edda x =1, y = 2; (ii) pdda x= 1, y = 3; (iii) eddp x = 2, y = 2. A bidentate auxiliary ligand fills the remaining two coordination sites.

Symmetrical tetradentate aminocarboxylato ligands can adopt two distinct geometrical configurations, as depicted in Fig 6.1. These are often labeled α and β. The α isomer is C_2-symmetric, and has the carboxylato donors arranged *trans* to each other. The β isomer has a *cis*(O)*cis*(N) configuration. The α and β isomers are dissymmetric, and will therefore each exist as a pair of enantiomers (Λ and Δ). The stereochemistry of this family of complexes, with numerous examples for a variety of multidentate ligands, is discussed in a review article by Radanovic.[110]

Further stereochemical considerations involve the secondary nitrogen centres of the chelating tetradentate ligands which are also asymmetric. For the α isomer, the ligand folds at both these nitrogen centres, and only one configuration is possible. However, for the β isomer, the proton on the 'in-plane' secondary nitrogen (N(2) in Fig 6.1) can sit in either of two orientations (**5.1a** and **5.1b**). ("In-plane" refers to the chelate lying in the same plane as the diamine backbone.) Isomers which differ by their configuration at these nitrogen centres are termed 'epimers'.

Henceforth, these epimers will be referred to by non-systematic nomenclature in the text. The β-e(1) isomer (**5.1b**) has the proton on the in-plane secondary nitrogen atom directed *away* from the auxiliary ligand. The β-e(2) has this proton directed *towards* the auxiliary ligand. This nomenclature avoids the confusion introduced by conventional notation as the Cahn-Ingold-Prelog labels, *R* and *S*, are dependent on the identity of the ligand. For instance, an *R* configuration for an edda ligand is equivalent to the *S* configuration for the pdda ligand.

Polydentate aminocarboxylato complexes of cobalt(III) – photochemistry

An outline of the plethora of literature reports which feature the photolysis of polydentate aminocarboxylato complexes of cobalt(III) was presented in the introduction. Indeed, research into the photochemistry of the $[Co(edta)]^-$ complex was a forerunner to much of the work on bidentate aminoacidato complexes. In general, the four-membered Co–C–C–N metallacycles, formed by the photodecarboxylation of six-membered aminoacidato chelates, are more robust than their three-membered analogues.

One particular report, which came to our attention midway through the project, sparked an idea for investigating the reversibility of the proposed first step in the photolysis of the Co(III)-aminoacidato complexes. In 1995 Kawaguchi's group published their observations concerning the photodecarboxylation reactions of a family of optically active $[Co(eddp)(en)]^+$ isomers.[41] One aspect of their report is presented in Fig 5.2.

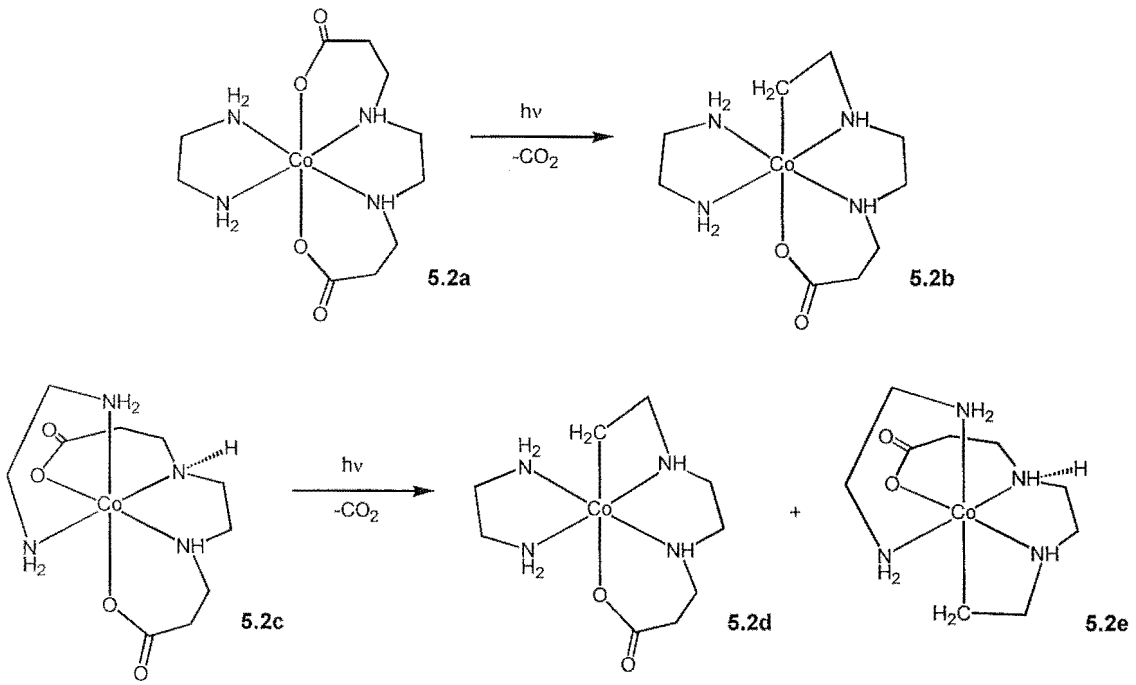

Figure 5.2. The major photolysis products of the α-$[Co(eddp)(en)]^+$ (**5.2a**) and β-e(1)-$[Co(eddp)(en)]^+$ (**5.2c**).

Photolysis of α-[Co(eddp)(en)]$^{+}$ (**5.2a**) gives the α-isomer of the metallacycle with retention of the stereochemistry of the cobalt centre (**5.2b**). On the other hand, photolysis of β-e(1)-[Co(eddp)(en)]$^{+}$ (**5.2c**) was found to give predominantly the α isomer of the photolysis product (**5.2d**). A lesser amount of the β isomer (**5.2e**) was found. The transformation of β-e(1)-[Co(eddp)(en)]$^{+}$ to the α-isomer isomer of the photolysis product was rationalised in the following manner. The 'in-plane' propionato arm will react preferentially because this chelate is more strained than its out-of-plane counterpart. However, a large amount of strain would accompany the formation of a four-membered chelate ring co-planar with the ethylenediamine backbone. The notion of 'coordination-site exchange' was invoked to account for the geometrical change. Similar observations have been reported following photolysis for the [Co(edda)(en)]$^{2+}$ complex.[111]

These results can be equally well rationalised by separating the geometrical rearrangements from the decarboxylation step (Fig 5.3). Photolysis of β-e(1)-[Co(eddp)(en)]$^{2+}$ (**5.3a**) may induce homolysis of the 'in-plane' Co–O bond to generate a Co(II)-acyloxyl radical intermediate (**5.3b**). This intermediate may undergo a geometrical interconversion, *without decarboxylation*, and reform the Co–O bond to give α-[Co(eddp)(en)]$^{+}$ (**5.3c**). This complex could then yield the α isomer of the photolysis product directly, to give the observed product **5.2d**.

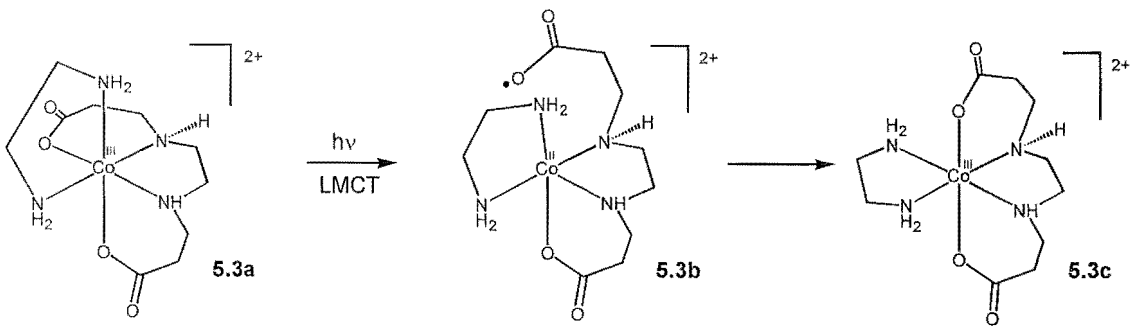

Figure 5.3. A photochemical pathway converting β-e(1)-[Co(eddp)(en)]$^{+}$ (**5.3a**) to α-[Co(eddp)(en)]$^{+}$ (**5.3c**).

Evidence for a pre-decarboxylation isomerisation step, *viz* the observation of α-[Co(eddp)(en)]$^+$ (**5.3c**) during UV irradiation of β-e(1)-[Co(eddp)(en)]$^+$ (**5.3a**), would strongly suggest that the initial Co–O bond homolysis step is reversible. However, if the isomerisation is to be observed at all, decarboxylation of the coordinated acyloxyl radical *must* be significantly slower than the isomerisation of the Co(II) complex intermediate **5.3b**.

In order for this experiment to be performed reliably, several criteria should ideally be met. Firstly, the β-e(1) isomer of the desired complex should be isolated. This isomer will allow the isomerisation step to proceed more readily than the β-e(2) isomer. For the conversion of the β-e(2)-isomer to the α-isomer, inversion at a nitrogen centre would be required. Given the neutral, low-temperature reaction conditions of this experiment, such an inversion would entail cleavage of the Co-N bond of the inverting nitrogen *or* a lifetime sufficient to allow ligand exchange on the Co(II) centre. Secondly, the α-isomer shall have been independently prepared and characterised. This will enable the rapid and reliable characterisation of any α-isomer which may be formed in the photolysate. Moreover, if the α-isomer is not formed in the *synthesis* of these complexes, it is unlikely to form in significant quantities during the photolysis. Finally, the α-isomer should not be significantly more photoreactive than the β-isomer, or it will not build up to the concentration required to detect it by ^{1}H NMR spectroscopy.

Preparation, characterisation, crystallography of a range of Co(III)-aminocarboxylato complexes.

At the outset, this investigation was focussed on an attempt to observe the β-e(1) to α-isomerisation for the [Co(eddp)(en)]$^+$ complex, and to determine whether this conversion might be seen for other complexes of tetradentate aminocarboxylate complexes of Co(III) with various co-ligands. In reality however, what was initially considered as a minor part of the investigation, the preparation and characterisation of a variety of isomers of the desired complexes, has become the major contribution to this section of the thesis.

The synthesis of α- and β-$[Co(eddp)(en)]^+$, β-$[Co(eddp)(bpy)]^+$, α- and β-$[Co(edda)(en)]^+$, α- and β-$[Co(edda)(bpy)]^+$, and β-$[Co(pdda)(phen)]^+$, were carried out *via* literature methods, or straightforward derivations thereof (as detailed in the experimental section). Ion-exchange chromatography proved to be a valuable tool for the separation of the geometrical isomers where required.

As previously mentioned, the β geometrical isomers will exist as either of two 'epimers' depending on the configuration at the in-plane nitrogen centre. However, many of the literature reports on these complexes do not assign these isomers. Given the importance of the configuration with respect to the possible photo-isomerisations, the first task was to assign the configuration of specifically, the β-$[Co(eddp)(bpy)]^+$, β-$[Co(edda)(bpy)]^+$, and β-$[Co(pdda)(phen)]^+$ complexes. In all of these cases, only one epimer was formed. The configurations of the β-$[Co(eddp)(en)]^+$ epimers were previously assigned by X-ray crystallography.[41]

One simple method of determining the configuration at the nitrogen centre, once all the peaks in the ^1H NMR spectrum of the complex have been assigned, was to make use of the nuclear Overhauser effect (nOe). These experiments enable the identification of protons which are close in space by the observation of NMR signal enhancements which are induced by magnetisation transfer.

Examination of models for the β-e(2) isomers of complexes with phen or bpy, suggests that the proton on the secondary nitrogen will be proximate to an ortho proton of the di-imine ligand, and that an nOe interaction may well be observable (see Fig 5.1). Conversely, for the β-e(1) isomer, the nitrogen proton will be distal to the di-imine proton, and nOe enhancements would not be expected. The same reasoning can be applied to the complexes of en, whereby nOe interactions may occur between an NH_2 proton and the polydentate nitrogen proton.

Upon irradiation of the appropriate amine proton resonances in both the β-[Co(eddp)(bpy)]$^+$ and β-[Co(edda)(bpy)]$^+$ complex, nOe enhancements appeared for a bipyridyl signal. In both cases, the e(2) conformation could be assigned. This approach also proved to be both successful and convenient for the assignment of β-e(2)-[Co(edda)(en)]$^+$. Furthermore, the observed nOe enhancements for both configurations of β-[Co(eddp)(en)]$^+$ were entirely consistent with the previous crystallographic assignments. DMSO-d_6 was used as the solvent, rather than the commonly used D_2O, to preclude the exchange of the amine protons for deuterons.

Only one epimer of the β-[Co(pdda)(phen)]$^+$ complex was isolated. No nOe correlations were observed between the amine protons and the phen ligand in this complex. However, one cannot infer from the *absence* of nOe enhancements that the protons are distant in space. In order to establish the configuration of this complex, we turned to X-ray crystallography. The solid state structures α- and β-[Co(edda)(bpy)]$^+$ were also investigated with this technique.

Crystallography of β-[Co(pdda)(phen)]$^+$, α-[Co(edda)(bpy)]$^+$, and β-[Co(edda)(bpy)]$^+$

The solid state structure determination of the β-[Co(pdda)(phen)]Cl complex demonstrates that the complex has the e(1) configuration (Fig 5.4). In systematic nomenclature, this amounts to the Δ-*SS*/Λ-*RR* configuration, where *R* and *S* refer to the stereochemistry of the asymmetric N atoms. The protons on N(2) and C(19) are included in Fig 5.4. This highlights the reason why no nOe interactions were seen between these protons as they are well-separated in space.

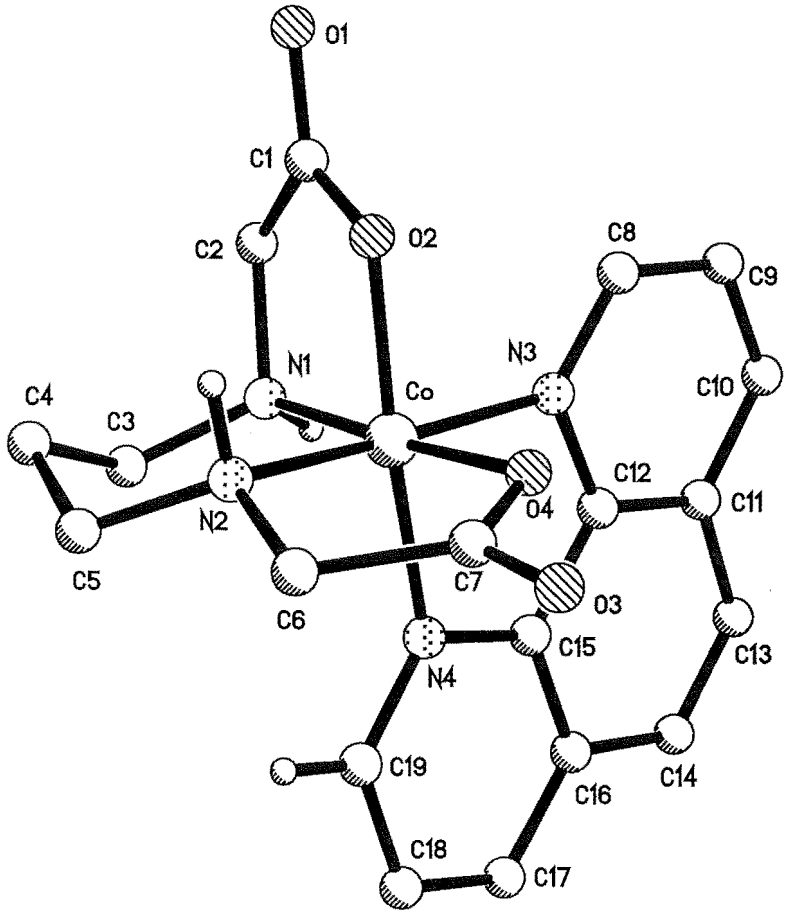

Figure 5.4. The X-ray crystal structure of the Δ-*SS*-β-[Co(pdda)(phen)]$^+$ cation. Most hydrogen atoms and the chloride counter anion have been omitted for clarity. Selected bond lengths (Å) and angles (°): Co-O(2) 1.909(3); Co-O(4) 1.910(3); Co-N(1) 1.961(4); Co-N(2) 1.972(3); Co-N(3) 1.974(4); Co-N(4) 1.996(4); O(2)-Co-N(1) 86.54(15); O(4)-Co-N(2) 84.22(14); N(1)-Co-N(2) 96.32(15); N(3)-Co-N(4) 83.84(14).

The geometry around the trivalent cobalt centre is marginally distorted from octahedral. The six-membered trimethylenediamine chelate unit adopts the well-known, stable chair-like conformation. This geometry at N(2) has the advantage of preventing any steric interactions between the proton on N(2) and the proton on C(19). The inflexible phen chelate constricts the N(3)-Co-N(4) angle to 83.8°, and the other chelates impose distortions of a similar magnitude. The slightly distorted octahedral geometry is reminiscent of other β-[Co(III)-aminocarboxylato] complexes, for example

[Co(edda)(pyridine-2-carboxylato)],[112] [Co(edda)(R-1,2-diaminopropane)]$^{+}$.[113] In addition, the coordination sphere around the cobalt centre is very similar to that for the β-[Co(edda)(bpy)]$^{+}$ complex, which was also structurally characterised in the present study (*vide infra*). The bond lengths around the cobalt centre tend to be slightly longer in the pdda complexes compared to the edda complexes.

It is surprising that the pdda ligand has featured in only two other published crystal structures, [Cr(pdda)(mal)]$^{-}$,[114] and [CrF_2(pdda)]$^{-}$.[115] The same chair-like conformation was observed for the trimethylenediamine unit in the β-[Co(pdda)(mal)]$^{-}$ complex.

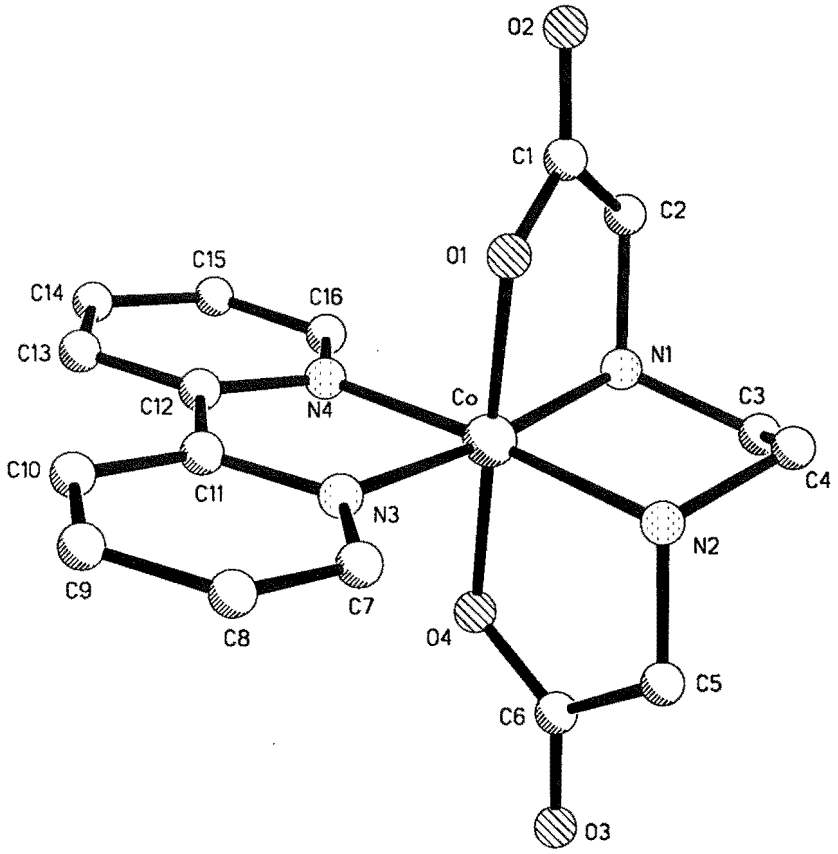

Figure 5.5. X-ray crystal structure of the α-[Co(edda)(bpy)]$^{+}$ complex cation. All hydrogen atoms, and the perchlorate counter-ion have been omitted for clarity. Selected bond lengths (Å) and angles (°): Co-O(1) 1.883(2); Co-O(4) 1.883(2); Co-N(1) 1.946(3); Co-N(2) 1.955(3); Co-N(3) 1.952(3); Co-N(4) 1.955(3); O(1)-Co-N(1) 86.29(11); N(3)-Co-N(4) 82.84(12); O(4)-Co-N(2) 86.72(11); N(1)-Co-N(2) 85.83(12).

The solid state structure of the C_2-symmetric α-[Co(edda)(bpy)]$^+$ complex is shown in Fig 5.5. In this complex, the glycinato rings are free to assume favourable planar configurations, whilst the ethylenediamine unit adopts the common envelope motif.

The solid-state structure of the β-[Co(edda)(bpy)]$^+$ cation$^{\phi}$ clearly demonstrates that the complex has the e(2) configuration, which equates to the Δ-*RR*/Λ-*SS* isomer. The origin of the nOe interaction between the C(7) bpy proton and the proton on the 'in-plane' nitrogen (N(2)) of the edda ligand, is clearly illustrated in Fig 5.6.

A worthwhile comparison of the location of strain in these Co(III)-aminocarboxylato complexes can be made using the methodology reported for the analysis of the β-[Co(edda)(R,S-pn)]$^+$ and [Co(edta)]$^-$ complexes[113,116] for which for the strain in each chelate ring was assigned a numerical value. This value is given as the deviation of the sum of the internal bond angles from its 'ideal value'. The ideal internal bond angles, which sum to 538.4°, allow the glycinato chelates to lie nearly planar. However, in the [Co(edta)]$^-$ complex (**1.6a**) for example, the in-plane glycinato chelate is significantly strained (bond angle sum = 523.5°), whilst the out-of-plane glycinato ring (bond angle sum = 537.8°) assumes a near-ideal conformation.

$^{\phi}$ The refinement of this structure suffers from a very poor goodness-of-fit figure (0.41) due to difficulties with finding a suitable weighting scheme. However, the R-factor (0.035) indicates that the identities and positions of the atoms in this structure are reliable.

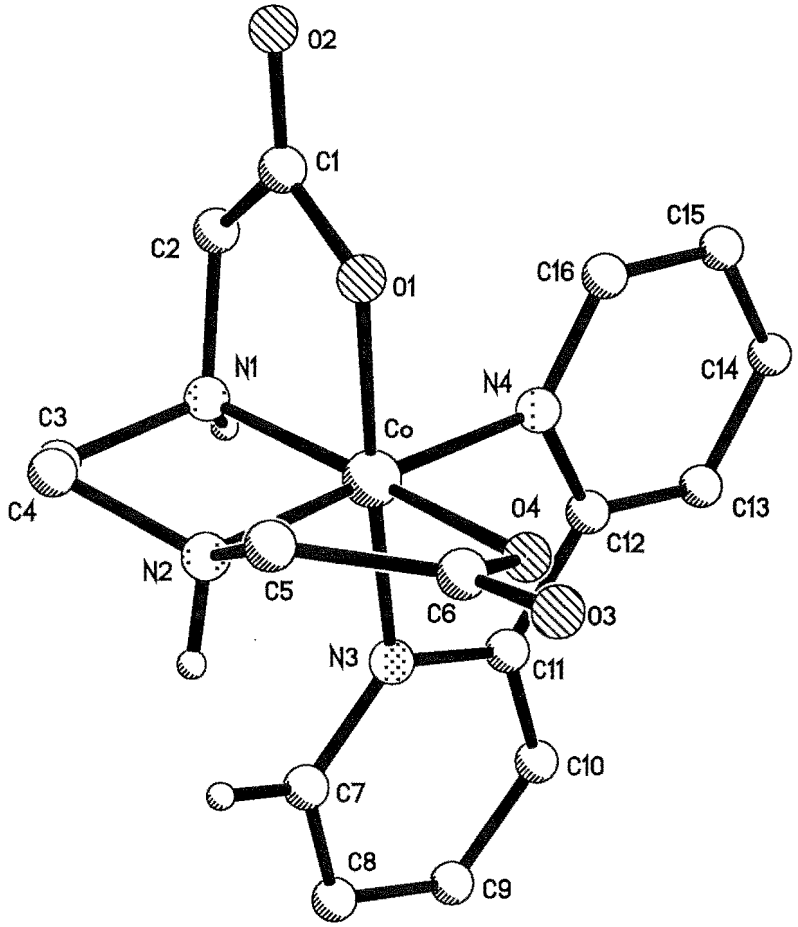

Figure 5.6. X-ray crystal structure of the Δ-*RR*-β-[Co(edda)(bpy)]$^+$ complex cation. Most hydrogen atoms, and the perchlorate counter-ion have been omitted for clarity. Selected bond lengths (Å) and angles (°): Co-O(1) 1.892(50; Co-O(4) 1.922(4); Co-N(1) 1.939(6); Co-N(2) 1.920(5); Co-N(3) 1.967(5); Co-N(4) 1.937(6); N(1)-Co-N(1) 84.6(2); N(1)-Co-N(2) 86.5(2); N(2)-Co-O(4) 85.3(2); N(3)-Co-N(4) 82.7(2).

There is little strain in the glycinato rings of α-[Co(edda)(bpy)]$^+$ (**5.5**), as indicated by the sum of the internal bond angles (537.9°). The difference in disposition of the glycinato rings in the β-[Co(edda)(bpy)]$^+$ cation (**5.6**) leads to significant differences in the internal angles in the two chelate rings: 532.7° for the out-of-plane (α-like) ring, and 528.6° for the in-plane ring. The internal angles for β-[Co(eddp)(phen)]$^+$, on the other hand, are significantly closer to their ideal values, 537.3° for the out-of-plane ring, and 534.3° in-plane.

Igi and Douglas, who originally prepared the β-$[Co(pdda)(phen)]^+$ complex, noted that the trimethylene chain exerts considerable influence on the distribution of geometrical isomers as, unlike analogous edda complexes, the α-isomer does not form.[117] The results of the X-ray crystallography presented here may help rationalise this observation.

The rationalisation rests on the premise that there is an electronic preference for the *cis* arrangement of the carboxylato donor groups in the complexes of eddp and edda. There is good empirical evidence for this, including some of the results presented in Chapter 6. $[Co(aa)_2(bpy)]^+$ complexes can assume one of three geometries: *trans*(N); *cis*(O)*cis*(N); and *trans*(O). However, the *trans*(O) geometry is not generally observed for complexes with bpy or phen in the remaining coordination sites.[@] Generally a mixture of *trans*(N)- and *cis*(O)*cis*(N)- complexes results when these complexes are prepared.[118,119] There is a similarity in the ratio of *trans*(N)- and *cis*(O)*cis*(N)- isomers formed in the synthesis of $[Co(gly)_2(bpy)]^+$ and $[Co(aib)_2(bpy)]^{2+}$. This suggests that the steric properties of the aminoacidato ligands have a rather limited influence on the geometrical configuration. Therefore, it is likely that electronic effects will primarily determine this selectivity, as they are likely to outweigh steric considerations.

As illustrated by discussion above, the glycinate chelates in the α-isomer of the $[Co(edda)(bpy)]^+$ incur less strain than those in the β-isomer. This probably accounts

[@] The examples presented in Chapter 6 are the gly, ala, and aib complexes of the type $[Co(aa)_2(bpy)]^+$. Literature reports for the $[Co(L\text{-}pro)_2(phen)]^+$ $[Co(\beta\text{-}ala)_2(phen)]^+$, and $[Co(L\text{-}ser)_2(phen)]^+$ make no mention of *trans*(O) complexes. See Chapter 6 for details.

for the preferential formation of the α-isomer. The energy penalty due to the strain in the glycinato chelates of the β-isomer can be alleviated by adding an extra methylene unit into the diamine backbone, as evidenced by the bond-angle sums for the β-$[Co(pdda)(phen)]^+$ complex. For this complex, the α-isomer is not formed. This may be because the *electronic* demands for a *cis* arrangement of the carboxylate donors overrides the conformational preference for the α-configuration.

Photolysis results and discussion

Isomerisation reactions

The main goal in this section of work was to detect a possible photo-induced conversion of certain β isomers of cobalt(III) complexes of tetradentate aminocarboxylato complexes to their α-isomer counterparts.

Of all the complexes prepared, only the β-e(1)-$[Co(eddp)(en)]^+$ met the criteria outlined above for being suitable for such an experiment, that is, it has the correct conformation at the 'in-plane' nitrogen centre, and the α-$[Co(eddp)(en)]^+$ has been isolated and characterised.

A sample of this complex in D_2O was photolysed with broad spectrum light from a mercury lamp. The sample was cooled in an ice-water bath during the irradiation to minimise the possibility of thermal isomerisation reactions. The ^1H NMR spectrum of the photolysate was monitored regularly.

The observed changes in the ^1H NMR spectrum were not consistent with the formation of any α-$[Co(eddp)(en)]^+$. New peaks did appear in the spectrum, however, these are probably due to the formation of decarboxylated photoproducts, as described by Kawaguchi *et al.*[41] This cannot be stated with complete certainty, as their report did not detail the ^1H NMR spectra of these products, *and* these products were not isolated in the present study.

In hindsight, decarboxylation of the acyloxyl radical **5.3b** is probably *very* rapid, in which case isomerisation step will be unable to compete with this process. The rate of the decarboxylation step is discussed in more detail in Chapter 7.

Another possible explanation for the isomerisation of the polydentate complexes is that the β-metallacycle **5.2c** is photochemically isomerised to the α-isomer following the decarboxylation. If the Co–C bond in **5.2c** is cleaved homolytically, isomerisation and subsequent Co–C recombination could occur to produce **5.2d**.

Testing for Co(I) as a possible intermediate

Introduction- the behavior of Co(I)

During the course of this project, among the multitude of possible mechanisms which were considered for the photolysis of $[Co(bpy)_2(aa)]^{2+}$, and the decomposition of the metallacyclic products, were some involving a Co(I) complexes as a reaction intermediates. This speculation would gain some credence if it were possible to divert the course of the photolysis reaction by intercepting the Co(I) species.

Univalent cobalt complexes are known to be strongly nucleophilic. Indeed, a popular method of preparing Co(III)-alkyl complexes is *via* the reaction of a Co(I) complex with an alkyl halide. Much of this synthetic work has been prompted by the desire to create vitamin B analogues. This biological cofactor is a macrocyclic cobalt complex, which contains a Co–C bond in certain forms. Methyl B_{12} is formed *in vivo via* enzymatic reduction to give a Co(I)-corrinoid complex, followed by alkylation of the cobalt by nucleophilic attack of the Co(I) centre on S-adenosyl methionine (Fig 5.7).[120]

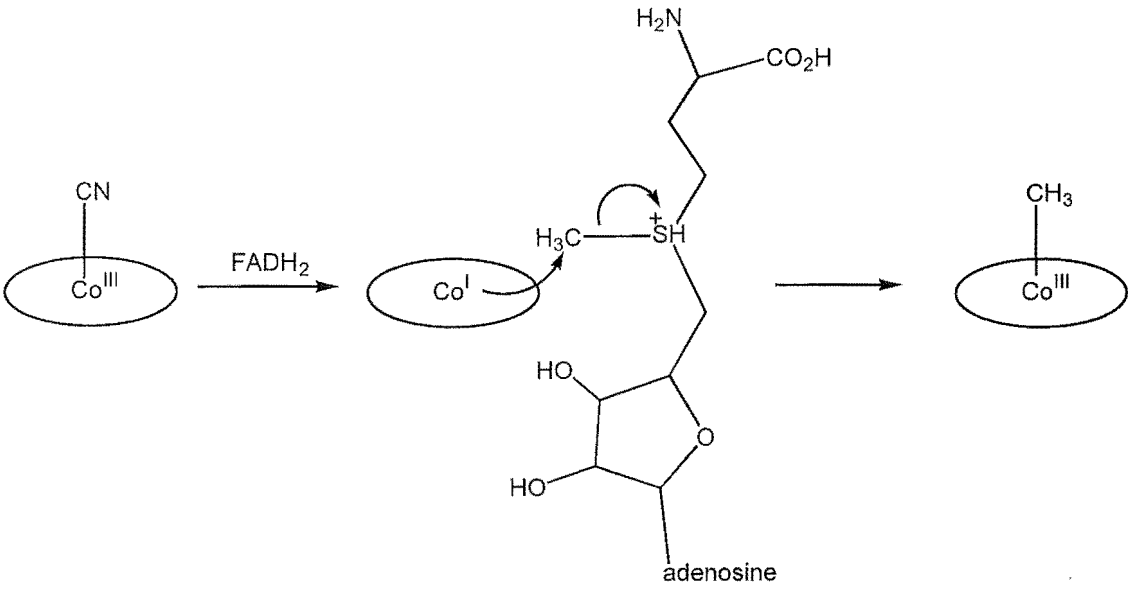

Figure 5.7. The biological production of methyl B_{12}.

In particular, the reaction of Co(I) complexes with alkyl iodides is known to be a facile, S_N2 process. For example, the reaction of $[Co^I(dmg)_2(pyr)]^-$ (dmg = dimethylglyoximato, pyr = pyridine) with MeI was found to occur with a rate constant of 1.8×10^4 $M^{-1}s^{-1}$.[121]

If there is a reasonably long-lived Co(I) intermediate in the photolysis pathway of $[Co(bpy)_2(aa)]^{2+}$ complexes, the presence of an alkyl iodide may lead to a deviation from the standard reaction. For example, if methyl iodide was added to the photolysis solution, a Co(III)–CH_3 complex may be formed. Alternatively, if an alkyl iodide fragment is actually *incorporated* into the complex, entropic factors would promote the substitution reaction, and the formation of a chelate ring may bestow extra kinetic stability upon the resulting Co(III)-alkyl complex. A straightforward method of functionalising the complex in this way is to introduce an alkyl iodide unit at the α-position of the amino acid. To this end, a complex of 2-amino-4-iodobutyrate (iod) was prepared.

Preparation of $[Co(bpy)_2(iod)]^{2+}$

A literature method[122] was followed to prepare the required amino acid by the ring opening of α-aminobutyrolactone with hydroiodic acid (Fig 5.8).

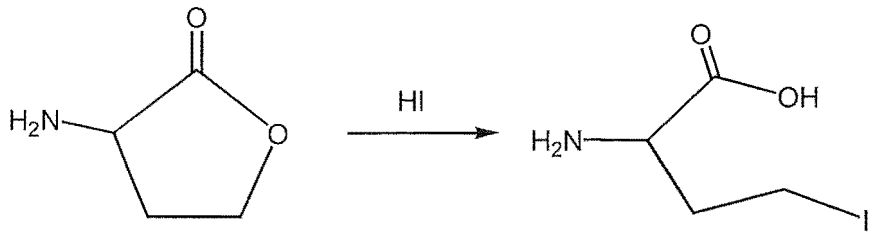

Figure 5.8.

The $[Co(bpy)_2(iod)]^{2+}$ complex (**5.9a**) was prepared from $[Co(bpy)_2Cl_2]^{2+}$, in a manner similar to that of the other amino acid complexes. We were wary of the possibility of hydrolysis of the iodo group and kept solutions of the complex below pH 5 during the reaction work-up. The presence of the iodo group in the product, while difficult to establish with certainty by NMR, was confirmed by elemental analysis.

Two diastereoisomers were formed and they both persisted upon recrystallisation with a ratio of around 5:2 (by ^{1}H NMR spectroscopy). The peaks of the two compounds were not well separated in the ^{1}H NMR spectrum, which made the assignment of configurations difficult. On the basis of the results for the related $[Co(bpy)_2(aa)]^{2+}$ complexes however, it is likely that the Λ-*S*/Δ-*R* isomer will predominate, a conjecture which is in keeping with the chemical shifts of the readily distinguishable NH protons.

Photolysis of $[Co(bpy)_2(iod)]^{2+}$

A Co(I) intermediate species such as **5.9c** could be formed directly following photolysis of $[Co(bpy)_2(iod)]^{2+}$ (**5.9a**), or it could result from thermal decomposition product of an unstable metallacycle (**5.9b**) (Chapter 3). If this Co(I) intermediate is able to undergo nucleophilic substitution, two products would be formed; an iodide ion and a novel Co(III)-alkyl complex (**5.9f**). If **5.9f** is prone to thermal decomposition, the deuterated aldehydes (**5.9g** or **5.9h**) may be formed.

On the other hand, 3-iodopropanal (**5.9d**) would be observed if the substitution reaction is unable to proceed and the iminium ion in **5.9c** diffuses from the vicinity of the cobalt. This was the decomposition pathway proposed for similar alkyl-substituted complexes in Chapter 3.

Photolysis results

The photolysis reaction of $[Co(bpy)_2(iod)]^{2+}$ was performed in D_2O with filtered (254 nm) light from a mercury lamp. ^1H NMR spectroscopy was used to monitor the reaction directly. Upon the complete disappearance of the $[Co(bpy)_2(iod)]^{2+}$ complex, the $CDCl_3$ extract of the photolysate was also analysed. A qualitative test for iodide was carried out by oxidising the photolysate with acidified potassium nitrite, and detecting for the presence of iodine.

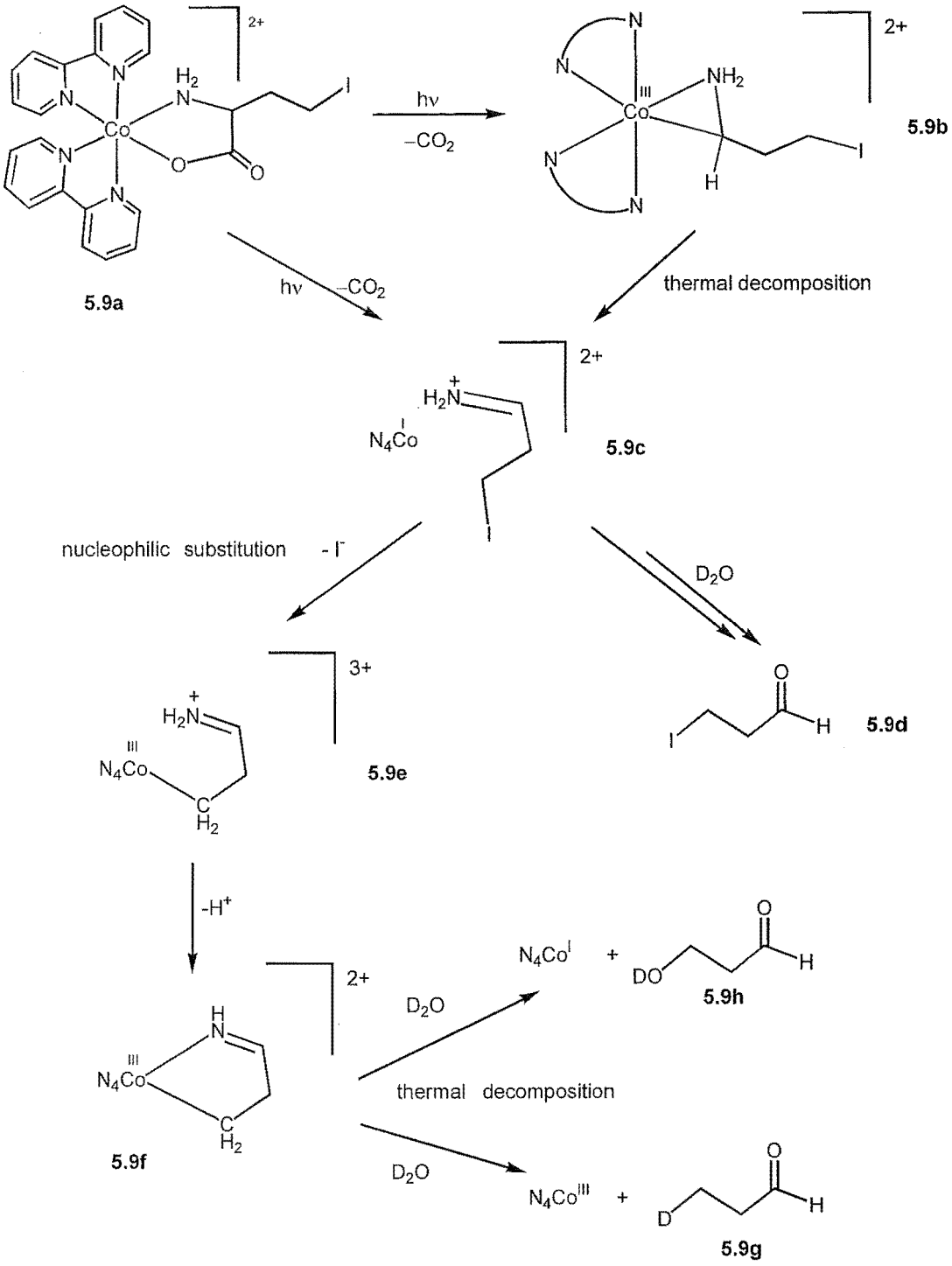

Figure 5.9. Some possible photochemical reaction pathways of the $[Co(bpy)_2(iod)]^{2+}$ complex.

The test for the iodide ion gave a negative result. Following oxidation of the photolysate, iodine was not detected by either a starch test or by extraction into $CHCl_3$.[▽]

The aromatic region of the ^1H NMR spectrum would become rather crowded if another 16 inequivalent protons were added by the formation of a $[Co(bpy)_2(alkyl)]^{2+}$ complex (eg **5.9f**) during photolysis of $[Co(bpy)_2(iod)]^{2+}$. Instead, however, the spectrum becomes simplified in this domain upon photolysis in D_2O, and peaks corresponding to free bipyridine and the $[Co(bpy)_3]^{3+}$ cation are the only prominent changes. A peak is seen at an aldehyde-like chemical shift (10.55 ppm). The upfield region is less clear-cut. The signals for the free amino acid were the only recognisable feature.

The aldehyde peak was 'extracted' into the $CDCl_3$ spectrum along with a pair of triplets at 3.16 and 3.32 ppm, altogether assigned as 3-iodopropanal (**5.9d**). This assignment is somewhat tentative as, unfortunately, no corroborating characterisation was carried out. The $CDCl_3$ solution was too dilute for the recording of a ^{13}C NMR spectrum. However, the chemical shifts and peak integrals in the ^1H NMR spectrum are fully consistent with the proposal. A literature search for a ^1H NMR spectrum of this compound proved fruitless, however the chemical shifts which were observed are very close to those reported for 3-iodopropanoic acid.[123] The fact that the aldehyde proton is observed as a singlet implies there is little, if any, coupling between this proton and the closest methylene protons. The departure of the aldehyde from the aqueous photolysate left only two unidentified peaks in the ^1H NMR spectrum in D_2O: multiplets at 3.68 and 3.82 ppm.

[▽] Iodine and starch form an intensely blue-black coloured complex, while iodine has a characteristic violet colour in $CHCl_3$.

In summary, neither a stable Co(III)-alkyl complex, nor free iodide, were observed in the photolysis of the $[Co(bpy)_2(iod)]^{2+}$ complex. The photolysis products mirror those of other aminoacidato complexes, the appended alkyl iodide arm seemingly imparting little influence on the course of the reaction. Accordingly, no definitive comments regarding the formation of a Co(I) intermediate can be made.

Outlook

The failure to observe the intramolecular nucleophilic displacement of iodide by Co(I) tells us that either the Co(I) complex could not displace the iodide, or that it was not formed at all. If alternative evidence of the intermediacy of Co(I) is obtained, it may be worthwhile revisiting this experiment with a tethered amino acid ligand.

A pyridylmethyl derivative of the amino acid, analogous to those presented in Chapter 4, would be a candidate. In this case, the nitrogen donor would be tri-substituted. Hence, if an imine analogous to **5.9e** is generated, the nitrogen could not re-coordinate to the metal centre *via* its lone pair. The happiest medium perhaps lies with a amino acid ligand which is tethered by just one pyridylmethyl arm. A tridentate, facially coordinating ligand could fill the remaining three coordination sites (**5.10a**). An ideal co-ligand would be a tris(2-pyridyl) moiety, such as tris(2-pyridyl)phosphine which has been shown to stabilise the univalent oxidation state for cobalt (Fig 5.10).

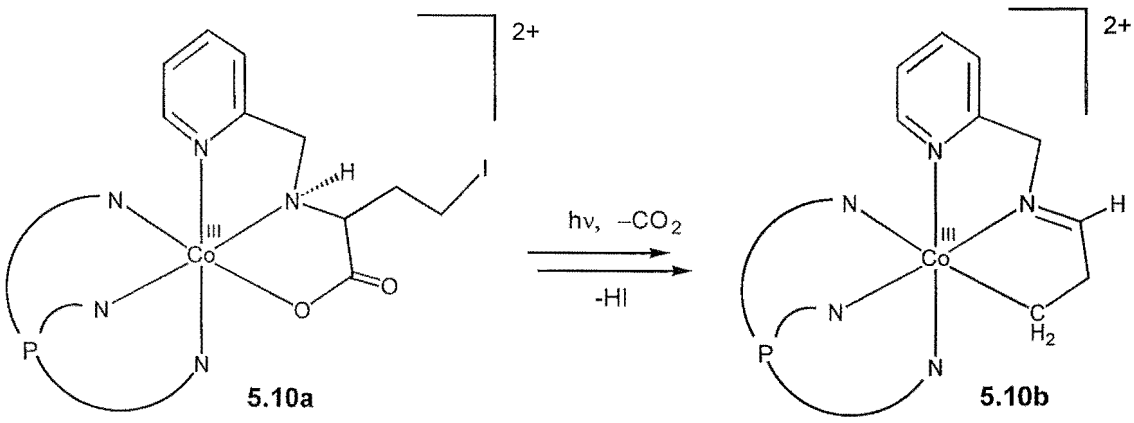

Figure 5.10. A possible photodecarboxylation-induced intramolecular substitution reaction.

Summary of Chapter 5

In the first section of this chapter, a number of polydentate aminocarboxylato complexes of Co(III) were prepared. Some evidence was being sought for the reversibility of the Co–O bond homolysis step in the photolysis of Co(III)-aminoacidato complexes. Unfortunately, most of the complexes were unsuitable for the investigation of this photoisomerisation reaction. The sole complex which was suitable for this experiment, did not show any signs of isomerisation *before* the decarboxylation step, which would have made good evidence for the reversibility of the Co–O cleavage.

The second section of this chapter outlined a strategy for intercepting any Co(I) intermediates which may feature on the reaction pathway of $[Co(bpy)_2(aa)]^{2+}$ complexes. It was disappointing to note that the incorporation of this "Co(I) trap" had no influence on the outcome of the photolysis reaction. Should this idea be revisited in the future, an alternative complex was suggested.

Experimental section

For general experimental details, see the experimental section in Chapter 3. The X-ray crystallography details are given in Appendix 2.

Complexes of ethylenediamine-N,N'-diacetic acid (edda)

[Co(edda)(bpy)]Cl

The α and β isomers of this complex were prepared *via* the method of Kuroda and Watanabe who reported UV-vis and microanalytical data for the perchlorate salts.[117] In

the present study, the isomers were separated on SP Sephadex C25 ion-exchange resin (Na^+, 3 × 35cm), with 0.1 M NaCl as the eluent. The eluates were individually desalted on Sephadex G-10. The α-isomer was precipitated by concentrating this eluate on a rotary evaporator. $HClO_4$ was added to the β-isomer to induce crystallisation. Douglas *et al* have previously reported the ^{13}C NMR for both isomers in D_2O.[124]

α-[Co(edda)(bpy)]Cl·3H$_2$O

^1H NMR (DMSO-d_6): δ 2.86 and 3.21 (AB, 4H, J = 7.8 Hz), 3.35 and 4.30 (ABX pattern obscured by H_2O peak), 8.01 (t, 2H), 8.29 (br s, NH, 2H), 8.50 (t, 2H), 8.84 (d, 2H), 9.95 (d, 2H). ^{13}C NMR (DMSO): δ 52.68, 54.55, 124.51, 128.38, 141.74, 153.84, 156.81, 180.42 (COO). Anal. Calcd for $[CoC_{16}H_{18}N_4O_4]Cl·3H_2O$: C, 40.16; H, 5.02; N, 11.70. Found: C, 40.11; H, 4.77; N, 11.37. UV-vis: 538 (129), 374 (sh, 130).

Δ*RR*/Λ*SS*-β-[Co(edda)(bpy)]ClO$_4$

^1H NMR (DMSO-d_6): δ 2.69-2.73 (m, 1H), 2.94-2.99 (m, 2H), 3.18-3.32 (m, 3H), 3.38-3.54 (2H), 6.71 (br s, IH, NH), 7.57 (br s, 1H, NH), 7.90 (t, 1H), 8.06 (t, 1H), 8.46 (t, 1H), 8.53 (t, 1H), 8.61 (d, 1H), 8.79 (d, 1H), 8.87 (d, 1H), 9.19 (d, 1H). An nOe experiment displayed an interaction between a NH signal (δ 7.57) and a bpy proton (δ 9.19). ^{13}C NMR (D_2O): δ 50.61, 55.10, 56.94, 58.11, 125.30, 125.65, 129.26, 129.87, 143.39, 143.50, 151.38, 152.49, 183.44, 184.46. UV-vis: 499 nm (183).

[Co(edda)(en)]ClO$_4$

The α and β isomers of this complex were prepared *via* a published procedure, which reported UV-vis and analytical data.[125] The ^1H NMR,[126] and ^{13}C NMR[124] spectra were entirely consistent with published data.

Δ*RR*/Λ*SS*-β-[Co(edda)(en)]ClO_4

^{1}H NMR (DMSO-d_6): δ 2.30-2.38 (br m, 1H), 2.52-3.02 (m, 6H), 3.14-3.35 (m, 4H), 3.88-3.96 (m, 1H), 4.42 (br s, 1H, en NH), 4.84 (br s, 1H, en NH), 5.54 (br s, 1H, en NH), 5.68 (br s, 1H, en NH), 6.09 (br s, 1H, edda NH), 7.52 (br s, 1H, edda NH). An nOe interaction was observed between an en NH proton (δ 4.84) and an NH proton on the edda ligand (δ 6.09).

Complexes of propanediamine-N,N'-diacetic acid (pdda)

Propanediamine-N,N'-diacetic acid

The free ligand was prepared according to a literature method.[127] ^{1}H NMR (D_2O): δ 2.14-2.25 (br m, $CH_2CH_2CH_2$, 2H), 3.26 (t, NH_2CH_2, 4H), 3.98 (s, gly CH_2's, 4H). ^{13}C NMR (D_2O): δ 25.22, 47.19, 50.40, 171.64 (COO).

[Co(pdda)(phen)]Cl

The β-isomer of this complex was prepared *via* a published method.[127]

Δ-*SS*/Λ*RR*-β-[Co(pdda)(phen)]Cl

^{1}H NMR (D_2O): δ 2.10 (m, 1H), 2.24 (d, 1H), 2.40 (m, 1H), 2.64 (m 1H), 3.06 (m, 1H), 3.57 (m, 1H), all six signals are those of the propane backbone protons, 3.25 and 3.71 (AB, 2H, J = 18.3 Hz, out-of-plane gly), 3.79 and 4.21 (AB, 2H, J = 17.1 Hz, in-plane gly), 8.12 -8.17 (m, 2H), 8.26-8.36 (m, 4H), 8.94-8.98 (m, 2H), 9.04 (d, 1H), 9.11 (d, 1H). ^{13}C NMR (a list of peaks was not given in reference 127) (D_2O): δ 23.20, 46.77, 49.07, 55.37, 56.56, 127.90, 127.99, 128.86, 128.95, 131.94, 132.08, 142.15, 142.34, 148.41, 148.66 151.94, 155.34, 182.24 and 184.67 (both COO).

Complexes of ethylenediamine-N, N'-dipropionic acid (eddp).

The free ligand was prepared *via* the hydrolysis of (β-cyanoethyl)ethylenediamine, according to the method of Haydock and Mullholland.[128] ^{1}H NMR (D_2O): 2.91 (t, 4H), 3.45 (t, 4H), 3.57 (s, 4H). ^{13}C NMR (D_2O): δ 30.97, 44.10, 44.24, 174.76.

[Co(eddp)(en)]ClO_4

The α and β isomers of this complex were synthesized *via* a literature method[129]. It was found that the perchlorate salts were easier to handle. The complexes were isolated as the perchlorate salts in the following manner. The isomers were separated on SP Sephadex C25 (H^+) by elution with 0.1 M HCl. The eluates were taken to dryness on rotary evaporator, and the crystallisation induced by the addition of conc $HClO_4$/ethanol (1/1). The UV-vis and ^{13}C NMR spectra agreed with those in the original report.

α-[Co(eddp)(en)]$ClO_4 \cdot 2H_2O$

^{1}H NMR (D_2O): δ 2.50-3.47 (m, 8H), 5.45 (br s, NH), 7.13 (br s, NH). Anal Calcd for $[CoC_{10}H_{26}N_4O_4](ClO_4)\cdot 2H_2O$: C, 26.31; H, 5.70; N, 12.27. Found: C, 26.53; H, 5.89; N. 12.21.

Λ*SS*/Δ*RR*-β-[Co(eddp)(en)]$ClO_4 \cdot H_2O$

The ^{1}H NMR of the crude product spectra indicated that a mixture of epimers was present. The major Λ*SS*/Δ*RR* isomer was obtained as the sole product by recrystallisation from dilute $HClO_4$. ^{1}H NMR (D_2O): δ 2.44-3.21 (br m, 8H), 4.45 (br s, 1H, NH), 5.32 (br s, 2H, NH), (br s, 2H, NH), 6.75 (br s, 1H, NH). ^{1}H NMR of e(2) epimer (D_2O): 2.50-2.95 (br m, 5H), 3.06-3.31 (br m, 3H), 4.23, 4.65, 5.39, 5.63, 5.90, 7.14 (all br s, 1H, NH). Anal. Calcd for $[C_{10}H_{22}CoN_4O_4](ClO_4)\cdot H_2O$: C, 27.39; H, 5.47; N, 12.77. Found: C, 27.17; H, 5.76; N, 12.48.

[Co(eddp)(bpy)]ClO_4

Only the β-isomer of this complex was observed. An alternative preparative method for this compound can be found in the literature,[130] although no spectral data were reported for the complex.

Δ-*SS*/Λ-*RR*-β-[Co(eddp)(bpy)]$ClO_4 \cdot 3.5H_2O$

H_2eddp.2HCl (2 g, 7.2 mmol) was dissolved in distilled water (150 mL) and $CoCl_2.6H_2O$ (1.71 g, 7.2 mmol) was added along with bpy (1.12 g, 7.2 mmol) in ethanol (20 mL). The pH was raised to 8 by the addition of NaOH solution (1 M). PbO_2 (4 g) was added to the reaction mixture which was warmed (45°C) with stirring for 1 hour. The solution was filtered, diluted with distilled water and loaded on to Sephadex (H^+ form, 5 × 20 cm). A violet band washed out with distilled water, and then a crimson band was collected with 0.1 M HCl. This solution was concentrated on a rotovap, a few drops of conc $HClO_4$ were added, and the solution was refrigerated. A crimson solid developed which was filtered, washed with ethanol and ether, then air dried. This crude product was recrystallised from hot, dilute $HClO_4$. ^{1}H NMR (D_2O): δ 2.35-2.40 (m, 1H), 2.63-2.70 (m, 1H), 2.80-2.91 (br m, 5H), 3.03-3.20 (m, 2H), 3.33-3.54 (m, 3H), 7.97 (t, 1H), 8.11 (t, 1H), 8.47 (t, 1H), 8.65-8.75 (m, 2H), 8.81 (d, 1H, J = 5.8 Hz), 9.04 (d, 1H, J = 6.4 Hz). ^{1}H NMR (DMSO-d_6): δ 2.22-2.38 (m, 6H), 2.64-2.87 (m, 4H), 3.16-3.35 (m, partially obscured by the H_2O peak), 6.68 (br s, 1H, NH), 7.11 (br s, 1H, NH), 7.84 (t, 1H), 8.03 (t, 1H), 8.38 (t, 1H), 8.50 (t, 1H), 8.67 (d, 1H), 8.75 (d, 1H), 8.82 (d, 1H), 9.11 (d, 1H). An nOe interaction was observed between an NH proton (δ 7.11) and a bpy proton (δ 9.11). ^{13}C NMR (D_2O): 30.67, 35.03, 48.18, 48.62, 53.00, 55.23, 125.30, 127.16, 129.40, 129.96, 143.46, 143.54, 151.47, 151.84, 157.50, 159.00, 178.52, 180.72. Anal. Calcd for $[C_{18}H_{22}CoN_4O_4](ClO_4) \cdot 3.5H_2O$: C, 37.30; H, 5.00; N, 9.66. Found C, 37.06; H, 4.64; N, 9.62. UV-vis: 508 nm (234).

Attempted photo-isomerisation of the Λ*SS*/Δ*RR*-β-[Co(eddp)(en)]$^+$ complex.

A millimolar solution of this complex in D_2O was irradiated in an NMR tube which was submerged in a quartz ice-water bath. A 200W high pressure mercury lamp was used as the light source. The solution was monitored regularly by ^{1}H NMR spectroscopy.

New peaks appeared in the NMR spectrum at δ 2.19-2.40 (m), 2.75-2.85 (m), 3.25-3.40 (m), 4.10-4.25 (m).

Preparation of [Co(bpy)$_2$(iod)](ClO$_4$)$_2$

α-Amino-γ-iodobutyric acid (iod)

2-Amino-4-iodobutyric acid (iod) was prepared by the reaction of HI with α-aminobutyrolactone according to the method of Frankel and Knobler.[122] The amino acid was characterised by NMR spectroscopy: ^{1}H NMR (D_2O): δ 2.23-2.47 (m, 2H), 3.21-3.35 (d, 2H), 3.79 (t, 1H).

The complex was prepared *via* the standard preparative route for [Co(bpy)$_2$(aa)]$^{2+}$ complexes, as detailed in Chapter 3. ^{1}H NMR of Λ-*R*/Δ-*S* (major) isomer (DMSO-d$_6$): δ 1.97-2.35 (br m), 3.62 (br m, 2H), 3.82 (br t, α-H), 6.07 (br m, 1H, NH), 7.10 (d, 1H), 7.59-7.66 (m, 2H), 7.78 (d, 1H), 8.13-8.17 (m, 2H), 8.37-8.52 (m, 3H), 8.64-8.72 (m, 2H), 8.91-9.11 (m, 4H), 9.80 (d, 1H). ^{1}H NMR of Δ-*R*/Λ-*S* (minor) isomer with only two peaks identifiable (DMSO-d$_6$): δ 6.08 and 6.70 (both NH). ^{13}C NMR of major isomer (DMSO-d$_6$): δ 1.97, 38.78, 57.11, 124.84, 124.95, 125.76, 128.81, 129.04, 129.80, 130.22, 142.19, 142.26, 143.02, 143.33, 149.00, 151.03, 152.33, 153.75, 156.23, 156.42, 157.00, 157.27, 179.77 (COO). ^{13}C NMR of minor isomer (DMSO-d$_6$):

δ 2.10, 37.54, 53.72, 126.05, 128.64, 129.97, 142.86, 150.91, 152.45, 157.17 (most of the bpy peaks were indistinguishable from those of the major isomer), 181.17 (COO). Anal. Calcd. for $[CoC_{24}H_{23}IN_5O_2](ClO_4)_2$: C, 36.11; H, 2.88; N, 8.77. Found: C, 35.85; H, 2.59; N, 8.52. UV-vis: 482 nm (102).

Photolysis of $[Co(bpy)_2(iod)](ClO_4)_2$

A saturated solution of the complex in D_2O was photolysed with a high-pressure mercury lamp equipped with a 254 nm transmission filter (Pyrex, Corning 7-54). The solution was cooled in a quartz ice-water bath during the irradiation. A ^1H NMR was run following acidification with DCl. The spectrum was too noisy for the accurate calculation of integrals. ^1H NMR (D_2O/DCl): 3-Iodopropanal; δ 2.09 (m), 3.23 (t), 10.60 (br m). Free α-amino-γ-iodobutyric acid; δ 2.36-2.39 (m), 2.50-2.54 (m), 4.15 (t). Free bpy; δ 7.98 (m, 2H), 8.52 (m, 4H), 8.91 (m, 4H). $[Co(bpy)_3]^{3+}$; δ 7.51 (d), 7.83 (t), 8.58 (t), 8.88 (d). Unidentified peaks; δ 3.68 (m) and 3.82 (m). The D_2O photolysate was extracted with $CDCl_3$: ^1H NMR: 3-Iodopropanal; δ 3.16 (t, 2H), 3.32 (t, 2H), 9.68 (s, 1H). Free bpy; 7.32 (t, 2H), 7.81 (t, 2H), 8.39 (d, 2H), 8.68 (d, 2H). No nOe correlations were seen between any of the 3-iodopropanal protons. The solution was too dilute to see any peaks in the ^{13}C NMR spectrum.

The D_2O photolysate was then tested for the presence of iodide.[131] This test is reported to be sensitive to 2.5 μg of I_2 and has a concentration limit of 1 in 20 000. Potassium nitrite solution, acidified with H_2SO_4, was added to the photolysate and the presence of iodine was tested for in two ways. Firstly, the oxidised solution was dropped on to starch powder, resulting in no observable changes. Secondly, the solution was shaken with $CHCl_3$. The organic layer remained colourless.

CHAPTER SIX

THE PHOTOLYSIS OF $[Co(bpy)_2(aa)]^{2+}$ COMPLEXES IN DMSO

Introduction

Although risking understatement of the case, it can be said that photophysical and photochemical processes are greatly dependent on the nature of the surrounding medium. For transition metal complexes, the sphere of influence of the solvent extends widely, for example perturbing the position of absorption bands and their molar absorptivities, altering deactivation processes, or affecting the outcome of photochemical reactions.[8,22a] Furthermore, photochemical process can be initiated by CTTS (charge-transfer-to-solvent) excitations,[132, 2] or *via* photoreactions of the solvent itself.[133]

Any changes which may be induced by a switch in solvent may provide significant insights into the photolysis mechanism of the $[Co(bpy)_2(aa)]^{2+}$ complexes. For this reason, an investigation of the photochemistry of a series of these complexes in DMSO - a polar, aprotic solvent - was initiated. A range of spectroscopic, electrochemical, and synthetic techniques have been employed in order to identify the complex ions which are formed, and to help understand the role that the solvent plays in their formation.

No detailed literature reports have appeared regarding the photochemistry of $[Co(bpy)_2(aa)]^{2+}$ complexes in non-aqueous media. In fact, it appears that very little work has been done on the non-aqueous photochemistry of Co(III)-aminoacidato complexes in general. The only reference to this subject in the literature is a comment that charge-transfer irradiation of Co(III) complexes with two bidentate amine ligands and an aminoacidato chelate, led to transient Co(III)-alkyl complexes which subsequently reacted with dissolved molecular oxygen.[134]

Steady state photolysis of $[Co(bpy)_2(aa)]^{2+}$

Photolysis of $[Co(bpy)_2(aib)]^{2+}$

UV irradiation (254 nm) of $[Co(bpy)_2(aib)]^{2+}$ [**6.1a**] in DMSO was found to produce (i) *trans*(N)-$[Co(aib)_2(bpy)]^{+}$ [**6.1b**], (ii) acetone [**6.1c**], (iii) uncomplexed amino acid, (iv) uncomplexed bipyridine, and (v) Co(II).

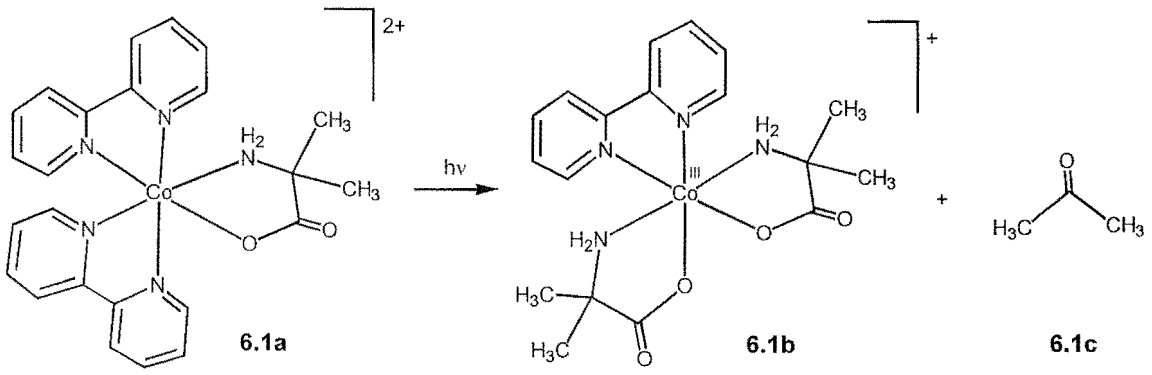

Figure 6.1. The $[Co(bpy)_2(aib)]^{2+}$ and its observed photolysis products in DMSO

The products (except Co(II)) were detected by ^1H NMR spectroscopy. Poor signal to noise ratios and poorly resolved peaks were generally encountered when NMR spectra of the DMSO-d_6 photolysates were obtained directly. However dilution with DCl

alleviated this problem. The difficulties in obtaining a direct spectrum of the photolysate directly may well be caused by the presence of paramagnetic Co(II) ions. The interaction of Co(II) with the proton containing species would be mitigated by the addition of DCl. The identities of all the products was confirmed by spiking the photolysate with authentic samples.

The high solubility of the $[Co(bpy)_2(aib)]^{2+}$ complex in DMSO-d_6 makes them, and their photolysis products, amenable to characterisation by ^{13}C NMR spectroscopy. The presence of acetone and *trans*(N)-$[Co(aib)_2(bpy)]^+$ was confirmed by this method. Ion exchange chromatography of a large scale photolysis experiment confirmed the presence of cobalt(II).

The relative product yields were ascertained by integration of ^1H NMR resonances. In general, it was difficult to obtain a reliable mass balance following irradiation of $[Co(bpy)_2(aib)]^{2+}$. The samples were ice-cooled during the photolysis, and NMR spectra promptly recorded, in order to prevent the evaporation of volatile products. It is possible that the paramagnetic cobalt(II) ions in solution continued to interact with the 'uncomplexed' amino acid and bipyridine, despite the addition of DCl to the NMR samples. This may reduce the intensities of the NMR resonances of these species.

A typical one hour irradiation of $[Co(aib)(bpy)_2]^{2+}$ in DMSO gave the following product distribution for the aib fragment: acetone 25%; aib 40%. The aib figure represents both complexed amino acid, *trans*(N)-$[Co(aib)_2(bpy)]^+$, and uncomplexed amino acid. The amount of *trans*(N)-$[Co(aib)_2(bpy)]^+$ was found to increase over time, at the expense of the free amino acid. Neither the *cis*(O)*cis*(N)-, nor the *trans*(O), isomer was detected by ^1H NMR spectroscopy.

It should be noted that the product ratios stated above for photolysis of the $[Co(bpy)_2(aib)]^{2+}$ complex do not represent the photoproducts of solely the

$[Co(bpy)_2(aib)]^{2+}$ ion. The *trans*(N)-$[Co(aib)_2(bpy)]^+$ ion, which is formed during the irradiation, is also photoreactive, and will itself yield acetone and free amino acid upon photolysis. For example, a one hour irradiation of the *trans*(N)-$[Co(aib)_2(bpy)]^+$ ion, under the same conditions, decomposed 29% of the complex with 5% being found as acetone and 24% as free amino acid. The influence of this process on the observed product distribution is likely to be small, however, as the complex is in low concentration, and these experiments indicated that it reacts more slowly than the $[Co(bpy)_2(aib)]^{2+}$ complex.

$[Co(bpy)_3]^{3+}$ was not detected in the DMSO photolysate of $[Co(bpy)_2(aib)]^{2+}$. Spiking experiments demonstrated that it could have been detected if it had been formed, in spite of the broadening of the peaks in the ^{1}H NMR spectra. It was noted, however, that this complex was rapidly formed when the DMSO photolysate was added to DCl, and that its concentration increased over time.

Photolysis of $[Co(bpy)_2(gly)]^{2+}$ and $[Co(bpy)_2(ala)]^{2+}$

UV irradiation of $[Co(bpy)_2(gly)]^{2+}$ in DMSO gave a similar product distribution to the aib complex. Although formaldehyde could not be detected, signals attributable to *trans*(N)-$[Co(gly)_2(bpy)]^+$, uncomplexed amino acid, and bipyridine were identified in the ^{1}H NMR spectrum. There was no evidence of the $[Co(bpy)_2(H_2C–NH_2)]^{2+}$ metallacycle, which can be isolated following the photolysis of $[Co(bpy)_2(gly)]^{2+}$ in aqueous solution. It has previously been noted that this complex is unstable in a number of other non-aqueous solvents.[73]

Following photolysis of the $[Co(bpy)_2(ala)]^{2+}$ complex, signals due to acetaldehyde were clearly evident in the ^{1}H NMR spectrum. *Trans*(N)-$[Co(ala)_2(bpy)]^+$ is also formed in the photolysate (spiking experiments), although the congested ^{1}H-NMR spectrum made it difficult to rule out the possibility that other geometrical isomers are also present.

The carbonyl compounds

The appearance of carbonyl compounds upon UV irradiation of a number of $[Co(bpy)_2(aa)]^{2+}$ complexes, including $[Co(bpy)_2(ala)]^{2+}$ and $[Co(bpy)_2(aib)]^{2+}$, was also observed in aqueous solution (Fig 3.10). Those observations were rationalised by suggesting that photodecarboxylation generates an intermediate containing a Co–C–N chelate, which subsequently cleaves to give a $[Co^{I}(bpy)_2]^{+}$ complex and an iminium ion. Hydrolysis of the latter fragment will give the observed carbonyl compound. The same reasoning can be applied to the appearance of carbonyl compounds in DMSO, with residual H_2O accounting for the hydrolysis of the imine. Again, electron transfer from the Co(I) species to a molecule of $[Co(bpy)_2(aa)]^{2+}$ could produce the Co(II), free amino acid, and free bpy, although no direct evidence for this reaction has been gathered. The origin of the Co(II), and the carbonyl compounds, in the DMSO photolysates was not further investigated in the present study. Instead, most effort was directed towards the investigation of some other interesting secondary chemistry in the DMSO photolysate - the production of *trans*(N)-$[Co(aa)_2(bpy)]^{+}$ complexes.

Independent Synthesis and Crystallography of $[Co(aa)_2(bpy)]^{+}$ complexes

Synthesis

The initial photochemical experiments in DMSO solution led us to the conclusion that photolysis of the $[Co(bpy)_2(aa)]^{2+}$ complexes was giving rise to a single but different complex of the amino acids. The ^{1}H and ^{13}C NMR data were consistent with the compounds being complexes of the type *trans*(N)-$[Co(aa)_2(bpy)]^{+}$. A range of these complexes were synthesized, along with the *cis*(O)*cis*(N)- geometrical isomers, to use as authentic samples for characterisation of the photolysates. The syntheses followed the methods of Yasui and Douglas,[135] who prepared the *trans*(N)-$[Co(aa)_2(bpy)]^{2+}$ complexes of gly, (*S*)-ala, (*S*)-hydroxyprolinate, and (*S*)-allohydroxyprolinate, and separated the diastereoisomers of the complexes which contained optically active amino

acids by fractional crystallisation. A subsequent publication from Yasui[119] detailed the characterisation of the *trans*(N)- and *cis*(O)*cis*(N)- geometrical isomers of the complexes of glycine and β-alanine, and four diastereoisomers (Δ-(*S*)-*trans*(N), Λ(*S*)-*trans*(N), Δ-(*S*)-*cis*(O)*cis*(N), Λ-(*S*)-*cis*(O)*cis*(N)) of the L-serinato system, and two (Λ-(L)-*trans*(N) and Δ-(L)-*trans*(N)) of the prolinato system.

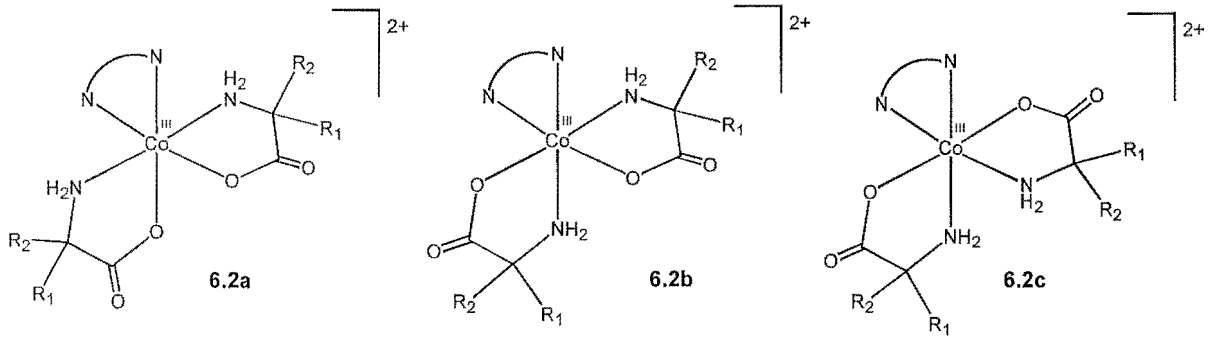

Figure 6.2 **(a)** *Trans*(N)-$[Co(aa)_2(bpy)]^+$, **(b)** *cis*(O)*cis*(N)-$[Co(aa)_2(bpy)]^+$, and **(c)** *trans*(O)-$[Co(aa)_2(bpy)]^+$.

Three diastereoisomers are possible for $[Co(bpy)(aa)_2]^{2+}$ complexes which have achiral aminoacidato ligands (**6.2a**, **6.2b**, **6.3c**). Each of them also has an enantiomer that arises from the dissymmetry of an octahedral tris(chelate) system. Six diastereoisomers are possible if one hand of a chiral amino acid is used, but none of their enantiomers will be present. Finally, ten diastereoisomers are possible if racemic amino acid is employed, with each of them having an enantiomer.

Following the preparative method of Yasui[119] we were able to synthesize the $[Co(gly)_2(bpy)]^+$, $[Co(ala)_2(bpy)]^+$, and $[Co(aib)_2(bpy)]^+$ complexes *via* the PbO_2 oxidation of Co(II), amino acid, and bipyridine in H_2O. Ion-exchange chromatography was used to separate the various components of reaction mixture, and all complexes were characterised by NMR and UV-Vis spectroscopy.

The UV-Vis spectra of the *trans*(N)- and *cis*(O)*cis*(N)-$[Co(gly)_2(bpy)]^+$ complexes were consistent with published data,[119] and these complexes were further characterised by ^1H and ^{13}C NMR spectroscopy. The characterisation of the aminoisobutyrato complexes was relatively straightforward. The first band which eluted from the ion exchange column exhibited a ^1H NMR spectrum indicative of C_2 symmetry. The UV-vis spectrum was similar to that of the glycinato complex with *trans*(N)- geometry, and this configuration was confirmed by X-ray crystal structure analysis. The complex was further characterised by ^{13}C NMR spectroscopy and microanalysis. The second, crimson, band from the ion-exchange column was assigned the *cis*(O)*cis*(N) configuration the basis of its ^1H and ^{13}C NMR spectra, and by comparison of its UV-vis spectrum with that of the analogous glycinato complex. The *trans*(N)- to *cis*(O)*cis*(N)-$[Co(aib)_2(bpy)]^+$ ratio was approximately 5.5:1 and the combined yield of these complexes was around 40%. This ratio of isomers indicates that the *trans*(N)-$[Co(aib)_2(bpy)]^+$ isomer is slightly more favoured in comparison to the analogous glycinato and serinato (ser) complexes where *trans*(N):*cis*(O)*cis*(N) ratios of around 4.3:1 were reported.[119] The failure to observe any *trans*(O)-$[Co(aa)_2(bpy)]^+$ complexes contrasts with analogous ethylenediamine and oxalato complexes, $[Co(aa)_2(en)]^+$ [136] and $[Co(aa)_2(ox)]^-$, [137] where all three geometrical isomers have been characterised.

In contrast, the numerous isomers of the D,L-alaninato complex made separation and characterisation somewhat more difficult. Only the *trans*(N)-$[Co(ala)_2(bpy)]^+$ geometrical isomer, of which there are three possible diastereoisomers, was isolated. The reaction mixture was chromatographed on SP Sephadex ion-exchange resin. The chromatographic behavior of the most intense red band was consistent with it containing singly-charged complexes. A UV-vis spectrum of the eluate implied the complex had the *trans*(N) geometry. Analysis of the ^1H NMR spectrum indicated that a mixture of diastereoisomers was present, and a COSY spectrum supported this conclusion, showing that at least two compounds were present. Successive recrystallisation removed most of one diastereoisomer from the crude mixture. The major remaining

component was assigned the Δ-*SS*/Λ-*RR* configuration on the basis of the ^{1}H NMR chemical shift of the protons on the amino acid ligands. From an inspection of a molecular model, it can be seen that, for this configuration, the methyl groups are directed away from the bipyridine ligand, and would not therefore be expected to be strongly affected by its anisotropic magnetic field. These methyl protons resonate at 1.33 ppm. On the other hand, the Δ-*RR*/Λ-*SS* configuration has the methyl groups located in a shielded environment out of the plane of the aromatic rings, thereby resonating at higher field (1.15 ppm). This conclusion is supported by the reversal of the relative positions of the aminoacidato α-protons. In the case of the Δ-*SS*/Λ-*RR* isomers this proton is somewhat shielded and resonates downfield (3.11 ppm) from that of the Δ-*RR*/Λ-*SS* diastereoisomer (3.48 ppm). It is possible that some Δ-*RS*/Λ-*SR* diastereoisomer is also formed. Although this complex is unsymmetrical it would be difficult to detect by ^{1}H NMR in the presence of the other diastereoisomers as the NMR spectrum of this complex is likely to be similar to a superposition of the spectra of the other diastereoisomers. The separation of such diastereoisomers has precedent,[119] although was not pursued in the present study.

The solid state structures of two of the complex products - $[Co(ala)_2(bpy)]^+$ and $[Co(aib)_2(bpy)]^+$ - were determined by X-ray crystallography. The *trans*-(N)- geometry which was proposed for both of these complexes, on the basis of UV-Vis and ^{1}H NMR spectroscopy, was confirmed by this technique.

Of the various possible diastereoisomers of the *trans*(N)-$[Co(ala)_2(bpy)]^+$ complex, the crystal chosen for the diffraction study was found to have the Δ-*SS*/Λ-*RR* configuration. The coordination sphere of the C_2-symmetric Δ-*SS*/Λ-*RR*-*trans*(N)-$[Co(ala)_2(bpy)]^+$ complex cation has a distorted octahedral geometry, the most significant deviations being the chelate bite angles of the amino acid (85.7°), and the bipyridine (83.2°). The Co-O (1.89 Å) and Co-N bond lengths (1.94 Å) are similar to those previously found for the $[Co(aa)_2(phen)]^+$ complexes of gly,[138] ala,[139] and L-pro.[118] A water molecule was

found in the crystal lattice for the ala complex. Short contacts of this molecule with the carbonyl oxygen of an aminoacidato ligand (2.9 Å) and with two oxygen atoms of the perchlorate counter anion (2.9 Å) are indicative of hydrogen bonding interactions.

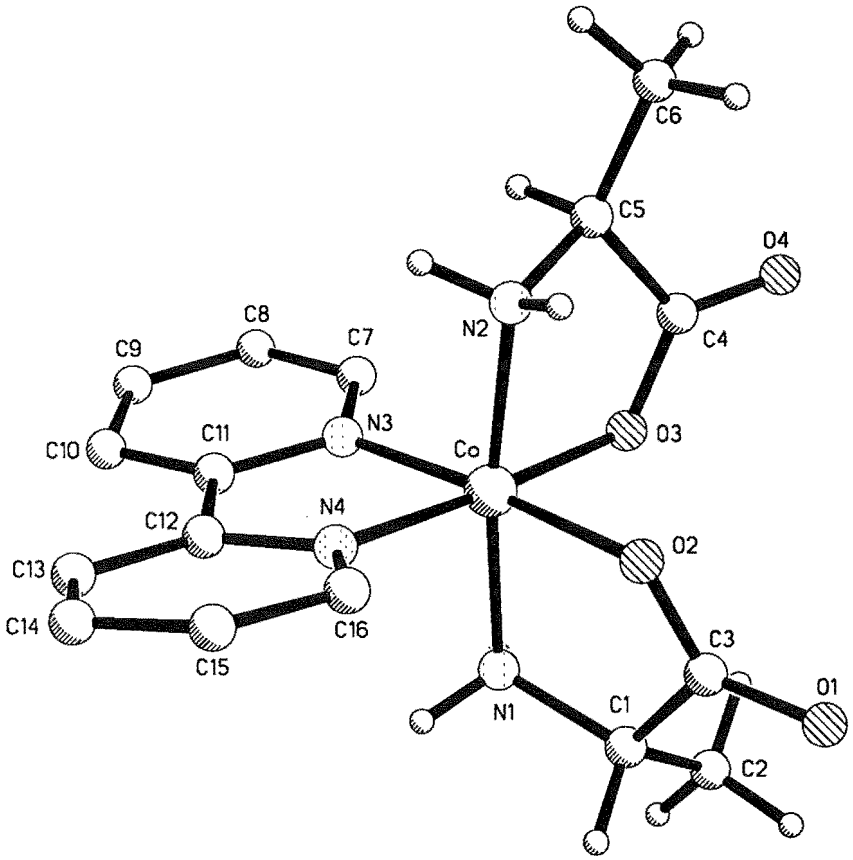

Figure 6.3. X-ray crystal structure of the (Δ-*SS*/Λ-*RR*)-*trans*(N)-$[Co(ala)_2(bpy)]^+$ complex ion. Selected bond lengths (Å) and angles (°): Co-N(1) 1.940(5); Co-O(3) 1.891(4); Co-N(2) 1.939(5); N(1)-C(1) 1.478(7) Co-N(3) 1.917(5); C(1)-C(3) 1.529(8); Co-N(4) 1.912(4); C(3)-O(1); 1.221(6); Co-O(2) 1.889(4); C(3)-O(2) 1.290(7). N(1)-Co-O(2) 85.7(2); N(1)-Co-N(4) 93.7(2); N(2)-Co-N(3) 94.3(2); N(1)-Co-O(3) 88.7(2); N(3)-Co-N(4) 83.1(2); N(1)-Co-N(2) 172.1(2); N(4)-Co-N(2) 92.1(2); Co-O(2)-C(3) 115.2(3).

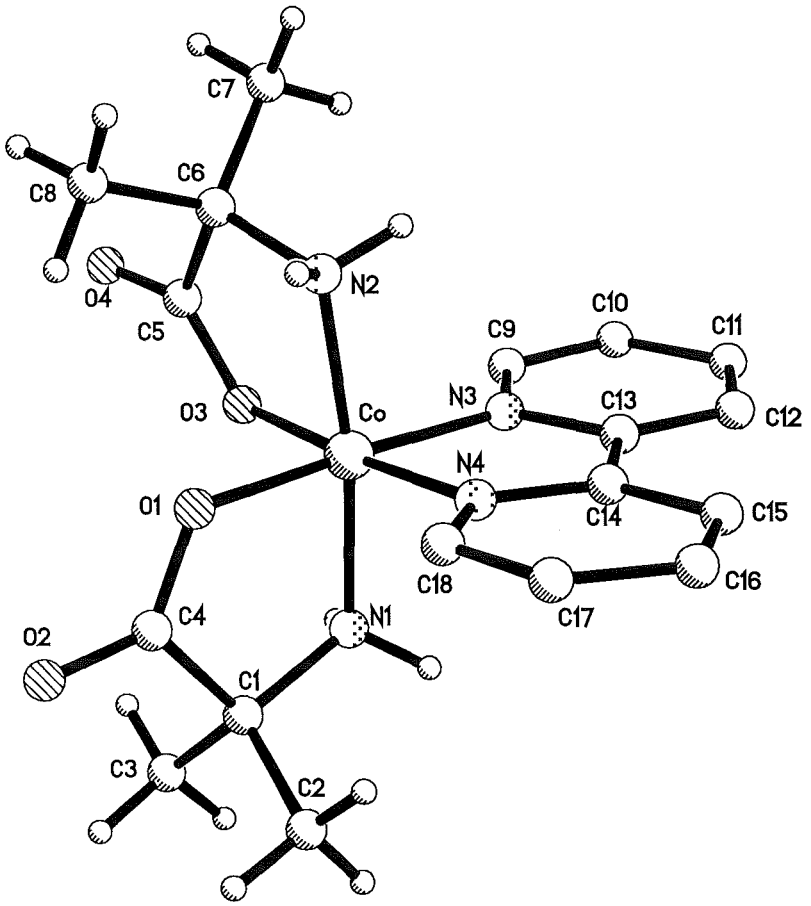

Figure 6.4. X-ray crystal structure of the *trans*(N)-$[Co(aib)_2bpy]^+$ cation. Selected bond lengths (Å) and angles (°): Co-N(1) 1.940(4); Co-O(3) 1.894(3); Co-N(2) 1.947(4); N(1)-C(1) 1.497(6); Co-N(3) 1.930(4); C(1)-C(4) 1.534(7); Co-N(4) 1.916(4); C(4)-O(1) 1.291(6); Co-O(1) 1.869(3); C(4)-O(2) 1.223(6). N(1)-Co-O(1) 86.2(2); N(2)-Co-N(3) 94.5(2); N(2)-Co-O(3) 85.9(2); N(1)-Co-N(3) 91.9(2); N(3)-Co-N(4) 83.2(2); N(2)-Co-O(1) 87.7(2); Co-O(1)-C(4) 117.1(3); N(1)-Co-N(2) 171.8(2).

The structure of *trans*(N)-$[Co(aib)_2(bpy)]^+$ is rather similar to its alaninato analogue with a slightly distorted octahedral geometry around the cobalt centre and similar Co-O (1.87 Å) and Co-N (1.94 Å) bond lengths for the aminoacidato ligands. These bond lengths are typical for Co(III)-aminocarboxylato complexes (*vide infra*). The '*trans*(N)' bond angle, N(1)-Co-N(2) = 171.8°, also deviates from strict octahedral geometry (cf 172.1° for the alaninato analogue). Sodium perchlorate was found to co-crystallise with

the complex. The sodium ion is positioned closer to the two carbonyl oxygen atoms of the amino acid ligands (2.2 - 2.4 Å) than the perchlorate oxygen atoms (2.4 - 2.6 Å). One of the perchlorate anions was disordered over two sites (2:3) which differ by rotation about one of the Cl-O bonds.

Further investigations

The formation of *trans*(N)-$[Co(aa)_2(bpy)]^+$ following photolysis of $[Co(bpy)_2(aa)]^{2+}$ in DMSO, presented an opportunity and demanded an explanation:

(i) Can a selective synthesis be designed for *trans*(N)-$[Co(aa)_2(bpy)]^+$ complexes based on our observations?

(ii) Why is the product distribution dependent on the solvent?

We employed the $[Co(aib)(bpy)_2]^{2+}$ complex to make a detailed study of this system as: (a) the uncomplexed photolysis products, acetone, aib, and bipyridine, are easily detected by NMR spectroscopy; (b) the $[Co(aib)_2(bpy)]^+$ complex can only form *geometrical* isomers; and (c) both the *trans*-(N)- and *cis*-(O)*cis*-(N)- geometrical isomers are easily prepared and characterised for use as authentic samples.

A selective synthesis of *trans*(N)-$[Co(aa)_2(bpy)]^+$ in DMSO?

The $[Co(aib)_2(bpy)]^+$ ion is formed in the DMSO photolysate of $[Co(aib)(bpy)_2]^{2+}$, and only the *trans*(N)- isomer was detected, as discussed previously. Further, no $[Co(bpy)_3]^{3+}$ was identified by ^1H NMR prior to the addition of D_2O. This is significant because the separation of unwanted $[Co(aa)_x(bpy)_y]^{(3-x)+}$ complexes is necessitated by conventional procedures employed to prepare $[Co(aa)_2(bpy)]^+$. For this reason, a selective synthetic route to *trans*(N)-$[Co(aa)_2(bpy)]^+$ complexes would be of great value.

The DMSO photolysate of $[Co(aib)_2(bpy)]^{2+}$ contains Co(II), free bipyridine and free, anionic amino acid. This mixture was simulated on a preparative scale by combining anhydrous $CoCl_2$, the sodium salt of aminoisobutyrate, and bipyridine in dry DMSO (1:2:1 ratio). Dry air was bubbled through this solution and the reaction mixture was chromatographed on SP-Sephadex ion-exchange resin. The products were characterised by ^1H NMR spectroscopy, and the yields ascertained by UV-vis spectroscopy.

It was found that this synthetic procedure did indeed lead to the formation of the $[Co(aib)_2(bpy)]^+$ ion, predominantly as the *trans*(N) isomer (approximately 40% based on Co). $[Co(bpy)_3]^{3+}$ (25%) and *cis*(O)*cis*(N)-$[Co(aib)_2(bpy)]^+$ (3%) and were also detected, and occasionally a small amount of a violet, uncharged material (possibly $[Co(aib)_3]$) was seen during the chromatography. The remainder of the cobalt was found as unchanged Co(II). Reactions performed in CH_3CN gave similar results to the DMSO experiments, although the same reaction in H_2O produced almost exclusively $[Co(bpy)_3]^{3+}$.

Following photolysis of $[Co(bpy)_2(aib)]^{2+}$ in both DMSO and H_2O, the photolysate contains the 'starting materials' for the formation of $[Co(bpy)_x(aa)_y]^{(3-y)+}$ complexes, namely Co(II), amino acid, bipyridine, and an oxidant; dissolved molecular oxygen. When replicated on a synthetic scale, air oxidation of these mixtures gave product distributions similar to those obtained in the photochemical experiments, *viz* predominantly *trans*(N)-$[Co(aa)_2(bpy)]^+$ in DMSO, and $[Co(bpy)_3]^{3+}$ in H_2O. (Note, however, that ratio of reactants was changed from that in the photolysate to 1:2:1 Co(II):aib:bpy).

However, the DMSO synthesis also produced small amounts of $[Co(bpy)_3]^{3+}$ and *cis*(O)*cis*(N)-$[Co(aa)_2(bpy)]^+$, although both were invisible in the DMSO photolysate. A possible reason for the appearance of $[Co(bpy)_3]^{3+}$ lies with the method of separation. The product distributions from the synthetic reactions were determined following

separation by ion exchange chromatography in aqueous solution. $[Co(bpy)_3]^{3+}$ forms rapidly in aqueous solutions containing cobalt(II), bipyridine and an oxidant, such as dissolved oxygen. The observed $[Co(bpy)_3]^{3+}$ complex may therefore result from reactions that occur after the reaction mixture is diluted with water. Some support for this hypothesis can be drawn from the observation that this complex was observed by ^1H NMR spectroscopy in the photochemical experiments only after addition of DCl/D_2O. Spiking experiments showed that it could have been detected if it was present in the photolysate prior to the addition of DCl/D_2O.

The results from the large-scale synthesis experiment suggests that *cis*(O)*cis*(N)-$[Co(aib)_2(bpy)]^{2+}$ should form in the DMSO photolysate. However, due its slow formation, low concentration and/or the low intensity of its ^1H NMR peaks (spread over four resonances), it was not detected by ^1H NMR spectroscopy.

As noted above, *trans*(N)-$[Co(aa)_2(bpy)]^{2+}$ complexes are easily synthesised for a variety of amino acids by the PbO_2 oxidation of Co(II), amino acid and bipyridine, in the presence of charcoal. From a practical perspective, the DMSO method is an inferior preparative route to *trans*(N)-$[Co(aa)_2(bpy)]^{+}$ complexes as it is somewhat less convenient to set up, and the product still requires purification by ion exchange chromatography.

Why $[Co(bpy)_2(aa)]^{2+}$ in DMSO, and $[Co(bpy)_3]^{3+}$ in D_2O?

It has been outlined in previous sections that there are similarities and differences between the photolysis products of $[Co(bpy)_2(aa)]^{2+}$ in DMSO and in D_2O. Carbonyl compounds, free amino acid, free bpy, and Co(II) are produced in both solvents. The difference lies in the nature of the complex ions which are formed. On one hand, large amounts of $[Co(bpy)_3]^{3+}$ form in aqueous solution, while on the other hand, *trans*(N)-$[Co(aa)_2(bpy)]^{2+}$ dominates in the DMSO solutions.

It appears that secondary (thermal) chemistry of the photolysis products is responsible for the appearance of the $[Co(aa)_2(bpy)]^{2+}$ complexes in DMSO. These complexes can be independently synthesized in good yield in DMSO by the air oxidation of a 1:1:2 mixture of Co(II), bipyridine and aib. However, given that the DMSO photolysate of $[Co(aib)(bpy)_2]^{2+}$ will contain *more than twice* as much free bipyridine as free amino acid, it is somewhat surprising that the *trans*(N)-$[Co(aib)_2bpy]^{2+}$ complex is the predominant secondary product. Furthermore, the formation of $[Co(bpy)_3]^{3+}$ in the air-oxidation of a 1:1:2 mixture of Co(II), bipyridine and aib is also "anti-stoichiometric".

As such, an explanation regarding the diverse product distributions observed in the DMSO and H_2O photolysates essentially reduces to a rationalisation of the solvent dependence of the products of air oxidation of a mixture of Co(II), amino acid and bipyridine. The outcome of these reactions will depend on the equilibria which will exist between the substitutionally labile cobalt(II) complexes, the solvent dependence of the ease of oxidation of such complexes, and the relative oxidising ability of dioxygen in aqueous solution and in DMSO.

Electrochemistry of $[Co(bpy)_x(aib)_y]^{z+}$ complexes

Cyclic voltammograms of a series of $[Co(aib)_x(bpy)_y]^{(3-x)+}$ complexes were recorded in both aqueous and non-aqueous solvents. The data from these experiments are summarised Table 6.1. All potentials are reported versus the ferrocinium/ferrocene (Fc^+/Fc) couple (see experimental section). For the electrochemistry in aqueous solution, both glassy carbon and mercury working electrodes had to be used as, unfortunately, neither was compatible with all the complexes studied.

It should be stressed that the data in Table 6.1 refer to the peak cathodic currents, that is, the potential for the reduction of $[Co(aib)_x(bpy)_y]^{(3-x)+}$ to $[Co(aib)_x(bpy)_y]^{(2-x)+}$. Where

distinct anodic (re-oxidation) current peaks could be observed, the anodic and cathodic peak separations are given.

Table 6.1. Potentials for reduction of $[Co(aib)_x(bpy)_y]^{(3-x)+}$ to $[Co(aib)_x(bpy)_y]^{(2-x)+}$. [a]

	H_2O		DMSO		CH_3CN	
	E_{pc}	E_{pc}–E_{pa}	E_{pc}	E_{pc}–E_{pa}	E_{pc}	E_{pc}–E_{pa}
$[Co(bpy)_3]^{3+}$	–125	70	–230	160	–100	110
$[Co(aib)(bpy)_2]^{2+}$	–280	b	–575	b	–380	120
Trans(N)-$[Co(aib)_2bpy]^{+}$	–535	b	–1210	b	–935	b
Cis(O)cis(N)-$[Co(aib)_2bpy]^{+}$	–605	b	–990	b	–770	b

(a) All data are reported in millivolts. (b) No anodic peak observed.

The potentials at which the $[Co(aib)_x(bpy)_y]^{(3-x)+}$ complexes are reduced to $[Co(aib)_x(bpy)_y]^{(2-x)+}$ follow a distinct pattern in all three solvents. The ease of reduction of these complexes correlates with the number of bipyridine ligands. That is, $[Co(bpy)_3]^{3+}$ is most easily reduced, and *trans*(N)-$[Co(aib)_2(bpy)]^{+}$ is hardest to reduce. This seems reasonable as the π-acidic bipyridyl ligands should favour the lower oxidation state, and replacement by aminoacidato ligands should render reduction of the cobalt centre more difficult.

The redox potentials which we observed for the $[Co(bpy)_3]^{3+/2+}$ couple in H_2O and CH_3CN, agree well with those found by Maki[140] and Anson.[141] The trend in reduction potential with the number of π-acid ligands is similar to that observed by Maki.

Of particular note are the differences in spread of the reduction potentials in the various solvents. For example, the difference between the reduction potentials of $[Co(bpy)_3]^{3+}$ and *trans*(N)-$[Co(aib)_2(bpy)]^{+}$ in DMSO (780 mV) is much greater than that seen in H_2O (480 mV). Therefore, the differences in the ease of *oxidation* of the related Co(II)

complexes will be greater in the organic solvents than in water, and may allow selective oxidation under appropriate conditions.

Non-reversibility

Most of the complexes did not exhibit reversible redox behavior, with anodic (re-oxidation) peaks often completely absent from the voltammograms. Although these oxidation peaks could not be observed, it is reasonable to infer that, of the Co(II) complexes under consideration, *trans*(N)-$[Co^{II}(aib)_2(bpy)]$ is easiest complex to oxidise. Accordingly, $[Co^{II}(bpy)_3]^{2+}$ would be the most difficult to oxidise.

Upon repeated cycling of the voltage, new oxidation waves appeared in the voltammograms. Some of these new peaks could be assigned to other $[Co(aib)_x(bpy)_y]^{(3-x)+}$ complexes. For example, following the reduction of *trans*(N)-$[Co(aib)_2(bpy)]^+$ in H_2O, a reversible wave was seen at a potential expected for the $[Co(bpy)_3]^{3+/2+}$ couple. Also, a new cathodic peak appeared following repeated cycling of the DMSO voltammogram of $[Co(aib)(bpy)_2]^{2+}$. The position of this peak coincided with that independently measured for the reduction of *trans*(N)-$[Co(aib)_2(bpy)]^+$. Thus, it appears that the Co(II) complexes which are formed at the electrode, are undergoing secondary ligand exchange reactions. This would account for the lack of reversibility in the cyclic voltammograms.

There are several reports in the literature which pertain to similar transformations of reduced or oxidised species at the electrode surface. For example, Bond *et al*[142] have observed the isomerisation of electrochemically produced *fac*-$[Mn(CO)_3dpmX]^+$ (dpm = $Ph_2PCH_2CH_2PPh_2$, X = Cl, Br) to *mer*-$[Mn(CO)_3dpmX]^+$. Maki[140] noted that reduction of $[Co(CN)_2(bpy)_2]^+$ in aqueous solution is followed by ligand exchange reactions. It was inferred that this process yields $[Co(CN)_4(bpy)]^{2-}$ and $[Co(OH_2)_2(bpy)_2]^+$. Similar behavior has previously been observed for the $[Co(ida)_2]^-$ ion (ida = iminodiacetato), which was interpreted in terms of a *cis-trans* isomerisation of the Co(II) species.[143]

The solvent dependence of the secondary chemistry

Aqueous solution

In aqueous solution, oxidation of a mixture of Co(II), an amino acid and bpy (1:2:1 ratio), gives primarily the $[Co(bpy)_3]^{3+}$ complex. Intuitively, two factors would appear to work against this:

(i) The $[Co^{II}(bpy)_3]^{2+}$ complex is harder to oxidise than any of the mixed ligand complexes;

(ii) The ratio of reactants will disfavour this stoichiometry.

However, the observations can be rationalised in the following manner. Stability constant data indicates that bpy is a significantly better ligand for Co(II) than gly. The overall formation constant for $[Co(bpy)_3]^{2+}$ is $\log\beta_3 = 17.6$, whilst for $[Co(gly)_3]^{3+}$, $\log\beta_3 = 10.8$.[144] Water is better able to solvate the aminoisobutyrate ions than bipyridine, thus it will be enthalpically (though not entropically) preferable to bind the bipyridine to the metal ion. Furthermore, the polar medium can easily solvate the dipositive charge on $[Co^{II}(bpy)_3]^{2+}$. Therefore, production of the $[Co(bpy)_3]^{3+}$ complex may be favoured in aqueous solution merely due to the fact that it dominates the equilibria of the $[Co^{II}(aib)_x(bpy)_y]^{(2-x)+}$ complexes.

Some experimental evidence has been gathered in support of this notion. A 1:1:2 mixture of Co(II), bpy, and aib^- was prepared in H_2O, and the voltammograms of the solution was recorded. Firstly, the potential was scanned anodically, but no distinct oxidation peaks were observed. A subsequent cathodic scan produced a distinct reduction current peak is seen for the $[Co(bpy)_3]^{3+/2+}$ couple (–145 mV). Presumably therefore, $[Co^{II}(bpy)_3]^{2+}$ is the only complex oxidised in the oxidation scan. If a significant amount of another Co(II) complex was present, it would have been oxidised before the $[Co(bpy)_3]^{2+}$, and should have been observed in the return reduction scan.

The DMSO solution

The electrochemical oxidation experiment for a 1:1:2 mixture of Co(II), bpy, and aib^- was repeated in DMSO. Again, no oxidation waves are seen distinctly, however a subsequent large reduction wave (–1200 mV) can be assigned to the *trans*(N)-$[Co(aib)_2(bpy)]^+$ complex. No redox activity of the $[Co(bpy)_3]^{3+/2+}$ couple is observed, which may indicate that there was little $[Co^{II}(bpy)_3]^{2+}$ in solution to be oxidised.

This observation is reasonable given that, in the less polar solvent, the equilibria of Co(II) complexes is expected to shift towards the neutral species, $[Co^{II}(aib)_2(bpy)]$. This will be oxidised to give the observed *trans*(N)-$[Co(aib)_2(bpy)]^+$. The *cis*(O)*cis*(N)-$[Co(aib)_2(bpy)]^+$ is not observed under the conditions of the electrochemical oxidation, which suggests that the *trans*(N)- complex is the predominant geometrical isomer of $[Co^{II}(aib)_2(bpy)]$.

With respect to the "anti-stoichiometric" formation of *trans*(N)-$[Co(aib)_2(bpy)]^+$ in the DMSO photolysate, three factors can account for its predominance. Firstly, of the related Co(II) complexes it is the most easily oxidised. Secondly, on the basis of the electrochemical oxidation experiments, it appears to be favoured in the equilibria of the Co(II) complexes. Thirdly, the larger spread of oxidation potentials may aid the selectivity.

Another consideration adds weight to the above arguments. Dioxygen is a more powerful oxidant in protic solvents, than in aprotic solvents.[145] In water, the oxidising power of dioxygen may be sufficient to remove an electron from any of the $[Co(aib)_x(bpy)_y]^{(2-x)+}$ species. Hence, the fact that $[Co^{II}(bpy)_3]^{2+}$ is relatively difficult to oxidise will be of limited consequence, and the product distribution may closely reflect the distribution of Co(II) complexes. In aprotic solvents, such as DMSO, the weaker oxidising power of O_2 may allow it to react only with the most easily oxidised species, *viz* $[Co^{II}(aib)_2(bpy)]$ (and perhaps $[Co(aib)_3]^-$ if it is present).

Summary

In aqueous solution, the high concentration of $[Co^{II}(bpy)_3]^{2+}$ appears to balance its handicap of being relatively difficult to oxidise and $[Co(bpy)_3]^{3+}$ is the predominant oxidation product. Its formation may also be aided by the fact that O_2 is a relatively powerful oxidant in H_2O. In DMSO, $[Co^{II}(aib)_2(bpy)]$ is the most easily oxidised species *and* also seems to dominate the equilibria of the possible Co(II) complexes. The greater spread of reduction potentials may enhance the selectivity of oxidation in DMSO.

It follows that reactions which give rise to mixtures of the various stereoisomers of the $[Co(aib)_x(bpy)_y]^{(3-x)+}$ complexes are likely to be performed under kinetic control, employing relatively strong oxidants. In these cases, the differences in ease of oxidation of the various cobalt(II) precursors become less significant. The literature methods which were used to prepare the various isomer mixtures use PbO_2 for this purpose.

Summary of Chapter 6

The products from the steady-state UV photolysis of several $[Co(bpy)_2(aa)]^{2+}$ complexes have been established. In many respects, the product distribution reflects that of photolysis in aqueous solution, *viz* free amino acid, free bpy, and a carbonyl compound are seen in both solvents. The most notable difference is ascribed to the solvent dependence of secondary, non-photochemical, reactions between the products of the photolysis. The predominance of *trans*(N)-$[Co(aa)_2(bpy)]^+$ in DMSO, which contrasts with the ascendancy of $[Co(bpy)_3]^{3+}$ in H_2O, appears to result from the differences in the speciation of the various Co(II) complexes and their electrochemical properties. The larger differences between the reduction potentials of the $[Co(aib)_x(bpy)_y]^{(3-x)+}$ complexes in DMSO, and the behavior of dioxygen in the different solvents, may also exert significant influence on the product distribution.

Experimental section

For the general details of the experimental methods, see the experimental section in Chapter 3. Details of the X-ray crystallography are given in Appendix 2.

Preparation of the $[Co(bpy)_2(aa)]^{2+}$ complexes

These complexes were prepared and characterised as detailed in Chapters 3, except for $[Co(bpy)_2(gly)](ClO_4)_2$. This complex was prepared in the sane manner as the other complexes.

$[Co(bpy)_2(gly)](ClO_4)_2 \cdot H_2O$

^{1}H NMR (DMSO): δ 3.15-3.32 and 3.75-3.85 (AB, α-H, 2H), 6.16 (br m, NH, 1H), 6.64 (br m, NH, 1H), 7.18 (d, 1H), 7.62 (m, 3H), 8.22 (m, 2H), 8.41 (m, 2H), 8.57 (d, 1H), 8.73 (m, 2H), 8.89 (t, 2H), 9.03 (d, 2H), 9.20 (d, 1H). ^{13}C NMR (DMSO): δ 44.46 (α-C), 124.84, 125.70, 126.14, 128.81, 129.07, 139.93, 130.08, 142.17, 142.89, 143.22, 149.54, 150.99, 152.32, 153.48, 155.94, 156.38, 156.70, 156.95, 180.67 (COO). Anal. Calcd for $[CoC_{22}H_{26}N_5O_2](ClO_4)_2 \cdot H_2O$: C, 39.90; H, 3.35; N, 10.57. Found: C, 39.67; H, 3.00; N, 10.34. UV-vis: 486 nm (93). MS (FAB): (m/z) 544.1 ($[Co(bpy)_2(gly)(ClO_4)]^+$, 3%), 445.1 ($[Co(bpy)_2(gly)]^+$, 8%), 289.1 ($[Co(bpy)(gly)]^+$, 21%).

Photolysis of $[Co(bpy)_2(aa)]^{2+}$ complexes in DMSO

General procedure

Millimolar solutions of each complex in DMSO-d_6 were irradiated in an NMR tube, or quartz cuvette, which was submerged in a quartz ice-bath. A 200W high pressure mercury lamp was used as the light source. After about one hour of photolysis, a portion of the photolysate was added to 0.025 M DCl for the recording of ^{1}H NMR spectra. In some cases, reasonable quality NMR spectra of the photolysate could be obtained after standing the photolysate for about 48 hours. ^{13}C NMR spectra were more easily acquired in this manner. In the quantitative experiments the DMSO-d_5 line was used to standardise the NMR integrals. All products were identified by spiking the NMR solutions with authentic samples.

Photolysis of $[Co(bpy)_2(gly)](ClO_4)_2$

^{1}H NMR (D_2O/DCl): Free glycine; δ 3.92. *Trans*(N)-$[Co(gly)_2(bpy)]^+$; δ 3.48-3.55 (m), 3.71-3.79 (m), the bipyridyl peaks coincide with the free bipyridine. Free bipyridine; δ 7.93 (t), 8.41-8.52 (m), 8.87 (d). $[Co(bpy)_3]^{3+}$; δ 7.47 (d), 7.78 (t), 8.54 (t), 8.83 (d). ^{13}C NMR (DMSO-d_6): Free glycine; δ 45.20, 179.44. Free bipyridine; δ 122.96, 126.80, 140.92, 150.38, 156.34. The $[Co(gly)_2(bpy)]^+$ was invisible in the ^{13}C spectrum due to its relatively low concentration.

Photolysis of $[Co(bpy)_2(ala)](ClO_4)_2$

^{1}H NMR (D_2O/DCl): Free alanine; δ 1.59 (d), 4.17 (q). Acetaldehyde and hydrated acetaldehyde; δ 1.18 - 1.34 (m, CH_3's of both), 5.23 (q, hydrated form, partially obscured by HOD peak), 9.67 (q, aldehyde). (Δ-*SS*/Λ-*RR*)-*Trans*(N)-$[Co(ala)_2(bpy)]^+$; δ 1.52 (d), 3.60 (m), 5.79 - 5.90 (br m), the bipyridyl peaks were obscured by the free bipyridine. (Δ-*RR*/Λ-*SS*)-*Trans*(N)-$[Co(ala)_2(bpy)]^+$; δ 1.33 (d), 3.90 (m), 6.50 (br m), the bpy peaks were obscured by free bipyridine. Free bipyridine; δ 7.93 (t), 8.41-8.52

(m), 8.87 (d). $[Co(bpy)_3]^{3+}$; δ 7.47 (d), 7.78 (t), 8.54 (t), 8.83 (d). ^{13}C NMR (DMSO-d_6): Free alanine; δ 19.10, 51.90, 179.60. Free bipyridine; δ 122.96, 126.80, 140.92, 150.38, 156.34.

Photolysis of $[Co(bpy)_2(aib)](ClO_4)_2$

^1H NMR (D_2O/DCl): Acetone; δ 2.22 (s). Free aminoisobutyric acid; δ 1.61 (s). *Trans*(N)-$[Co(aib)_2(bpy)]^+$; δ 1.21 (s), 1.58 (s), 5.40 (d, NH), 6.14 (d, NH), the bipyridyl peaks are obscured by free bipyridine. Free bipyridine; δ 7.93 (t), 8.41-8.52 (m), 8.87 (d). $[Co(bpy)_3]^{3+}$; δ 7.47 (d), 7.78 (t), 8.54 (t), 8.83 (d). ^{13}C NMR (DMSO-d_6): Acetone; δ 30.22, 206.02. Free aminoisobutyric acid; δ 30.10, 55.80, 179.36. *Trans*(N)-$[Co(aib)_2(bpy)]^+$; δ 27.03, 27.47, 57.87, 122.70, 123.56, 126.05, 140.59, 150.06, 157.24, 187.20.

Independent preparation and spectroscopy of the $[Co(aa)_2(bpy)]^+$ complexes

The method of Yasui[119] was followed for the preparation of the $[Co(aa)_2(bpy)](ClO_4)$ complexes. The crude reaction mixtures were separated on SP Sephadex C25 (Na^+), desalted on G-10 Sephadex, and isolated by the addition of concentrated $NaClO_4$ solution. The crude solids were recrystallised from a minimum volume of hot, dilute $HClO_4$. The resulting precipitates were filtered, washed with ethanol and ether, and air dried. The NMR spectra are reported here for the first time.

***Trans*(N)-$[Co(gly)_2(bpy)](ClO_4)\cdot 1.5H_2O$**

^1H NMR (DMSO-d_6): δ 3.08-3.27 (m, 4H), 5.65 (br m, 1H, NH), 6.04 (br m, 1H, NH), 7.88 (t, 2H), 8.37 (m, 4H), 8.71 (d, 2H). ^1H NMR: (D_2O) δ 3.48-3.56 (m, 2H, CH), 3.71-3.79 (m, 2H, CH), 5.28 - 5.37 (br m, 2H, NH), 5.99-6.05 (br m, 2H, NH), 7.90 (t, 2H), 8.42 (t, 2H), 8.51-8.56 (m, 4H). ^{13}C NMR (DMSO-d_6): δ 45.80, 123.80, 127.41,

141.49, 150.98, 157.01, 182.27. ^{13}C NMR (D_2O): δ 47.08 (α-C), 125.17, 129.08, 143.22, 151.77, 157.53, 187.03 (COO). Anal. Calcd for $[CoC_{14}H_{16}N_4O_4](ClO_4)\cdot 1.5H_2O$: C, 34.33; H, 3.88; N, 11.44. Found: C, 34.03; H, 3.51; N, 11.39. The UV-vis spectrum agreed quantitatively with that previously reported[119] for *trans*(N)-$[Co(gly)_2(bpy)]Cl_2$: 481 nm (110), 309 nm (19000), 300 nm (sh, 23000), 221 nm (63000).

Cis(O)_cis_(N)-$[Co(gly)_2(bpy)](ClO_4)$

^{1}H NMR (D_2O): δ 3.18-3.30 (br m, 1H), 3.42-3.55 (br m, 1H), 3.75-3.92 (br m, 1H), 4.89-4.97 (br m, 1H), 5.02 (br m, 1H, NH), 5.62 (br m, 1H, NH), 6.04 (br m, 1H, NH), 6.38 (br m, 1H, NH), 7.88 (t, 1H), 8.00 (t, 1H), 8.39 (t, 1H), 8.50 (t, 1H), 8.58-8.63 (m, 2H), 8.73 (d, 1H), 8.82 (d, 1H). ^{13}C NMR (D_2O): δ 46.48 and 46.99 (both α-C's), 125.33, 125.54, 129.40, 129.51, 143.23, 143.39, 151.00, 152.97, 157.86, 158.29, 185.27, 185.51 (both COO). ^{13}C NMR (DMSO-d_6): δ 44.66, 46.21 (both α-C's), 123.56, 123.68, 126.99, 127.09, 141.19 (2C), 149.40, 153.53, 156.75, 156.85, 180.68, 181.65 (both COO). The complex appeared to decompose during the acquisition of this spectrum and several other peaks appeared in the spectrum. A satisfactory microanalysis could not be obtained for this compound however the UV-vis spectrum was in qualitative agreement with that reported earlier for the *cis*(O)*cis*(N)-$[Co(gly)_2(bpy)]Cl_2$ compound.[119]

(Δ-_SS_/Λ-_RR_)-_Trans_(N)-$[Co(ala)_2(bpy)](ClO_4)_4\cdot H_2O$

^{1}H NMR (DMSO-d_6): δ 1.33 (d, 3H, CH_3, J = 7.3 Hz), 3.11 (q, 1H, α-H), 5.72 (br m, 1H, NH), 5.96 (br m, 1H, NH), 7.90 (d), 8.40 (m), 8.70 (d). ^{1}H NMR (D_2O): δ 1.52 (d, 3H, CH_3), 3.60 (br m, 1H, α-H), 5.75-5.90 (br m, NH), 7.87 (m), 8.36-8.53 (m). ^{13}C NMR (DMSO-d_6): δ 19.03 (CH_3), 32.29 (α-C), 123.46, 127.15, 141.28, 150.84, 157.24, 183.35 (COO).

(Δ-*RR*/Λ-*SS*)-*Trans*(N)-[Co(ala)$_2$(bpy)](ClO$_4$)·H$_2$O

^{1}H NMR (DMSO-d$_6$): δ 1.15 (d, 3H, CH$_3$, J = 6.9 Hz), 3.48 (q, 1H, α-H), 5.14 (br m, 1H, NH), 6.46 (br m, 1H, NH), 7.90 (d), 8.40 (m), 8.70 (d). ^{1}H NMR (D$_2$O): δ 1.33 (d, 3H, CH$_3$), 3.88 - 3.96 (br m, 1H, α-H), 5.02-5.08 (br m, NH), 6.44-6.55 (br m, NH), 7.87 (m), 8.36-8.53 (m). ^{13}C NMR (DMSO-d$_6$): δ 18.91 (CH$_3$), 52.55 (α-C), 123.39, 127.25, 141.28, 150.69, 156.98, 183.45 (COO). The microanalysis was performed on a mixture of Δ-*RR*- and Λ-*SS*-*trans*(N)-[Co(ala)$_2$(bpy)](ClO$_4$). Anal. Calcd. for [CoC$_{16}$H$_{20}$N$_4$O$_4$](ClO$_4$)·H$_2$O: C, 38.09; H, 4.36; N, 11.01. Found: C, 38.02; H, 4.32; N, 10.91.

***Trans*(N)-[Co(aib)$_2$(bpy)](ClO$_4$)·NaClO$_4$·0.5H$_2$O**

^{1}H NMR (DMSO-d$_6$): δ 1.01 (s, 3H, CH$_3$), 1.39 (s, 3H, CH$_3$), 5.41 (d, 2H, NH), 6.07 (d, 2H, NH), 7.88 (t, 2H), 8.35-8.40 (m, 4H), 8.69 (d, 2H). ^{1}H NMR (D$_2$O): δ 1.22, 1.58 (both s, 3H, CH$_3$), 5.32 (d, 2H, NH), 6.15 (d, 1H, NH), 7.87 (t, 2H), 8.36-8.53 (m, 6H). ^{13}C NMR (DMSO-d$_6$): δ 27.58 (CH$_3$), 27.99 (CH$_3$), 58.28 (*C*(CH$_3$)$_2$), 123.14, 126.50, 141.02, 150.58, 157.75, 185.59 (COO). ^{13}C NMR: (D$_2$O) δ 27.53 (CH$_3$), 27.96 (CH$_3$), 61.37 (*C*(CH$_3$)$_2$), 125.07, 128.98, 143.26, 151.51, 157.88, 191.38 (COO). Anal. Calcd for [CoC$_{18}$H$_{24}$N$_4$O$_4$](ClO$_4$)·NaClO$_4$·0.5H$_2$O: C, 33.25; H, 3.84; N, 8.61. Found: C, 33.51; H, 3.76; N, 8.34. UV-vis: 478 nm (126), 308 nm (1300), 258 nm (1190), 238 nm (sh, 1060).

***Cis*(O)*cis*(N)-[Co(aib)$_2$(bpy)](ClO$_4$)·2H$_2$O**

^{1}H NMR (DMSO): δ 0.83, 1.38, 1.42, 1.45 (all s, 3H, CH$_3$), 5.22 (br d, 1H, NH), 5.38-5.52 (br m, 2H, NH), 5.66 (br d, 1H, NH), 7.89 (t, 1H), 8.03 (t, 1H), 8.42 (t, 1H), 8.51 (t, 1H), 8.62 (d, 1H), 8.75-8.83 (m, 3H). ^{1}H NMR (D$_2$O): δ 1.03 (s, 3H, CH$_3$), 1.50 (s, 3H, CH$_3$), 1.60 (s, 3H, CH$_3$), 1.63 (s, 3H, CH$_3$), 7.88 (t, 1H), 8.00 (t, 1H), 8.40 (t, 1H), 8.49 (t, 1H), 8.57-8.64 (m, 2H), 8.70 (d, 1H), 8.78 (d, 1H). ^{13}C NMR (DMSO-d$_6$): δ 27.10, 28.02, 28.11, 28.63 (all CH$_3$), 58.26, 59.67 (both α-C), 123.90, 124.14, 127.41,

127.48, 141.69, 141.89, 150.45, 152.63, 157.75, 157.81, 184.76 (2 COO). ^{13}C NMR (D_2O): δ 27.22, 27.90, 28.08, 28.69 (all CH_3's), 60.75, 62.13 (both α-C), 125.67, 125.96, 129.53 (2C), 143.61, 143.81, 151.46, 152.89, 158.25, 158.50, 189.32 (2 peaks, both COO). Anal. Calcd for $[CoC_{18}C_{24}N_4O_4](ClO_4)\cdot 2H_2O$: C, 38.96; H, 5.05; N, 10.09. Found: C, 38.69; H, 5.08; N, 10.10. UV-vis: 518 nm (171), 307 nm (17000), 224 nm (54000).

Synthesis of $[Co(aib)_2(bpy)]^+$ in DMSO

Methods

Sodium aminoisobutyrate was prepared in the following manner. Equimolar quantities of aibH and NaOH were dissolved in H_2O. The solvent was removed on a rotary evaporator, and the resulting white solid was oven-dried (60°).

Blue anhydrous $CoCl_2$ (30 mg, 0.23 mmol) was dissolved in dry (rated by manufacturer at < 0.05% H_2O) DMSO (30 mL). To this solution was added sodium aminoisobutyrate (0.46 mmol) and bipyridine (0.23 mmol) to give a yellow-brown solution. Air, dried by passing through conc H_2SO_4 and 4Å molecular sieves, was slowly bubbled through the stirred solution overnight. The orange reaction mixture was then diluted with distilled H_2O, and quickly loaded on to SP-Sephadex (H^+, 3 × 20 cm). Occasionally an uncharged violet band was seen. A red band eluted with 0.05 M HCl and was identified as *trans*(N)-$[Co(aib)_2(bpy)]^+$. A small amount of the *cis*(O)*cis*(N) isomer followed closely. A pink band, Co(II), eluted with 0.1 M HCl, and a yellow band eluted with 0.5 M HCl which was identified as $[Co(bpy)_3]^{3+}$. UV-vis spectroscopy was used to quantify all the products.

Electrochemistry

General procedure

Most of the cyclic voltammograms were recorded with a EG&G Princeton Applied Research 173 potentiostat driven by a EG&G PAR 175 Universal Programer. A standard three-electrode setup was used; including a glassy carbon working electrode and Pt wire auxiliary electrode. In aqueous solutions, a saturated calomel electrode was used as the reference electrode. In CH_3CN and DMSO, a reference electrode of Ag/AgCl in CH_3CN was employed. For the *trans*(N)- and *cis*(O)*cis*(N)-$[Co(aib)_2(bpy)]^{2+}$ complexes, a dropping mercury electrode was employed (EG&G PAR 303A drop generator equipped with a EG&G PAR 174A Polarographic Analyser). For these cases an Ag/AgCl reference electrode was used.

The concentration of the complexes was typically 1 mM. $NaClO_4$ (0.1 M) was used as the supporting electrolyte in H_2O. $(Bu_4N)(PF_6)$ (0.1 M) was used in the non-aqueous solvents. These solvents were dried over molecular sieves prior to use. All solutions were degassed by bubbling with N_2 gas, and all solutions were kept under a N_2 atmosphere during the scans. The scan rate was 0.1 Vs^{-1}.

Reporting of electrochemical data

It has been found that the reduction potential of ferrocene is rather insensitive to solvent.[146] Under the conditions of these experiments, the Fc^+/Fc couple was consistently found to exhibit fully reversible behavior with peak separations of around 60 mV. For the purposes of direct comparison of electrochemical data between the three solvents, ferrocene was added as an internal reference to all the solutions, *except* for those with a dropping mercury electrode in H_2O. For this system, the potentials with respect to the Fc^+/Fc couple were inferred by measuring a cyclic voltammogram of the $[Co(bpy)_2(aib)]^{2+}$ complex at *both* the carbon electrode, with a Fc internal reference, **and** at the dropping mercury electrode (ie the $[Co(bpy)_2(aib)]^{3+/2+}$ couple was an used as a secondary reference).

CHAPTER SEVEN

OUTLOOK

Chapters 2, 3, and 4 presented the most significant sections of research which contributed to this thesis. These results raised some questions regarding the photolysis mechanism, hence it is worthwhile considering alternative possibilities. One such scheme is presented forthwith. Also, the results have opened some doors to the synthesis of some novel and interesting compounds. Some possibilities for future research in this direction are outlined.

The radical clock experiment in Chapters 2 and 3, and our skepticism regarding the published mechanism, is based on the experimental observation that the rate constant for the formation of the $[Co(bpy)_2(CH_2–NH_2)]^{2+}$ metallacycle is 4×10^3 s^{-1}. Unfortunately, a crucial experiment – a re-examination of the kinetics – was hampered by unforseen hardware problems. It is vital that this experiment is repeated as soon as possible to establish the integrity of the original kinetic study.

The mechanisms for formation and decomposition of the metallacycles

In Chapter 3, it was concluded that the rate determining step in the formation of a Co–C–N metallacycle following photolysis of a $[Co(bpy)_2(aa)]^{2+}$ complex, *cannot* be Co–C bond formation. The possibility that another step in the proposed mechanism (Fig 2.1) is rate determining ($k \approx 10^3\ s^{-1}$) was considered. The loss of carbon dioxide from the coordinated aminoacyloxyl radical (**2.1b**) is probably not responsible for determining the kinetics. The decarboxylation rates of free aminoacyloxyl radicals ($H_2NCR_2CO_2^{\bullet}$) have not been measured experimentally as a consequence of the difficulties involved in generating the unpaired spin at the oxygen centre (the ionisation energy of the nitrogen centre is lower).[147] However, this decarboxylation of the protonated glycyloxyl radical ($H_3N^+CH_2CO_2^{\bullet}$) has been *calculated* to be exergonic by *ca.* 160 $kJmol^{-1}$.[148] Decarboxylation of acyloxyl radicals ($CR_3CO_2^{\bullet}$) are known to be very fast.[149,150] In some cases, it is believed that decarboxylation may even take place from the geminate radical pair, in other words, a discrete acyloxyl radical is not ever formed. Thus, it appears that decarboxylation of **2.1b** could not be as slow as $10^3\ s^{-1}$. The rate of loss of CO_2 could be measured experimentally by (laser) flash photolysis with infra-red monitoring. This would allow one to determine whether CO_2 was lost *before* or *after* the rate-limiting step for the formation of the metallacycle. That is, if CO_2 is lost at approximately the same rate as the product is formed, then the rate-determining step must be either the decarboxylation itself, or an event which precedes it. The experiment was not able to be performed with the resources available locally.

An alternative mechanism, which covers both the formation and decomposition of the organometallic photolysis products, is illustrated in Fig 7.1. Although the discussion should be taken *con granulo salis*, it does account for much of the photochemical behavior of the $[Co(bpy)_2(aa)]^{2+}$ complexes.

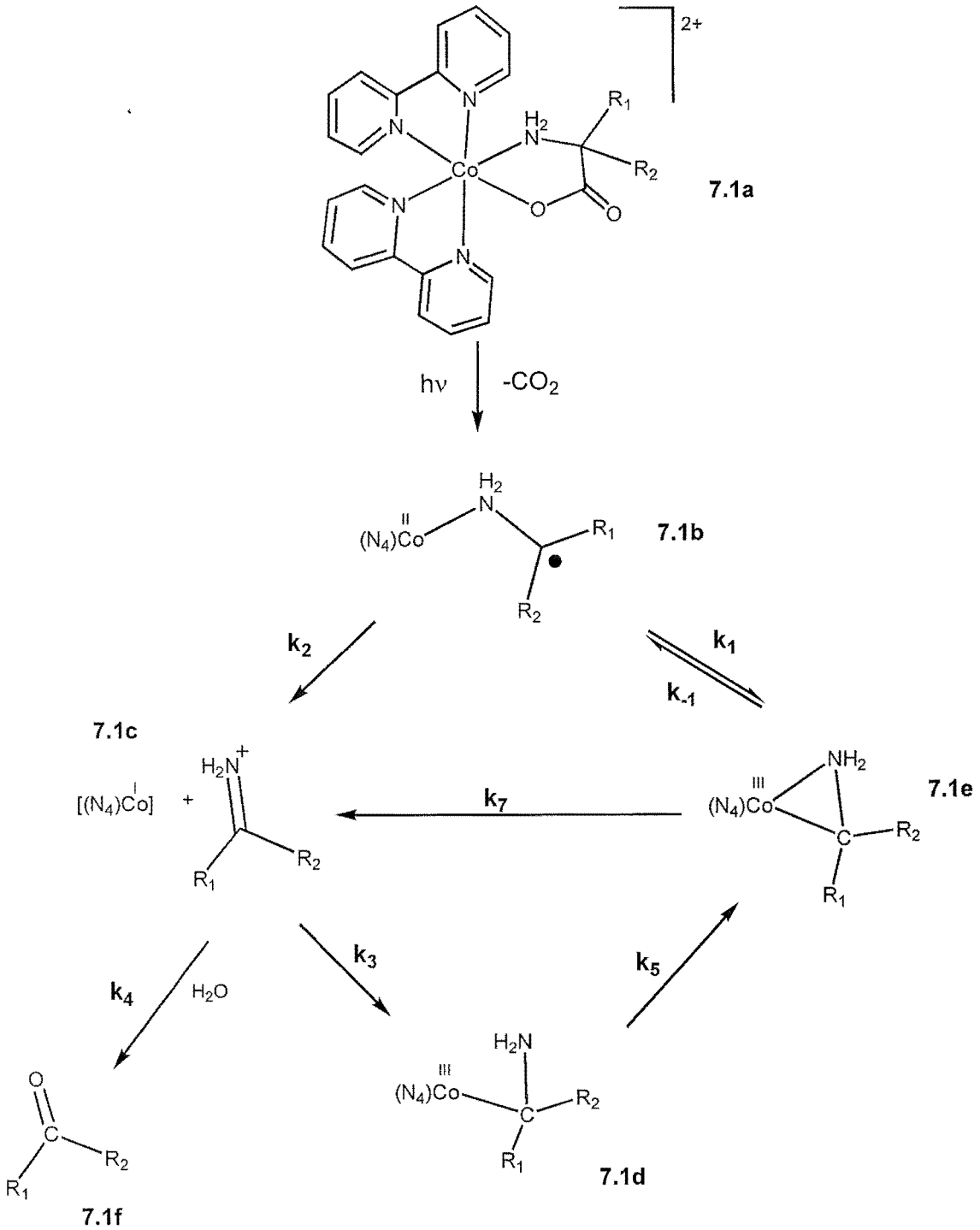

Figure 7.1. Some mechanistic food for thought.

Formation of the metallacycle

The coordinated aminoalkyl radical **7.1b**, formed *via* the LMCT-induced decarboxylation step, will be a powerful reductant. For example, a reduction potential for the $H_3CSCH_2CH_2\dot{C}HNH_3^+$ radical has been deduced experimentally to be around –0.7 V (vs NHE).[151] The deprotonated radical was found to be an even more powerful reductant (E_0 less than –0.94 V vs NHE), a conclusion which has been supported by a more recent theoretical investigation.[152] The reduction potential for the $[Co(bpy)_3]^{2+}/[Co(bpy)_3]^+$ couple is around –0.73 (vs NHE).[141]

This suggests that the alkyl radical in **7.1b** will have the ability to *reduce* the Co(II) centre (k_2) if it dissociates from the metal centre. This redox step would occur at the expense of the direct formation of the metallacycle (k_1, **7.1c**), and would yield **7.1c**: an iminium ion and a $[Co^I(bpy)_2]^+$ complex, probably still in a solvent cage. This step could also be a β-scission reaction (Fig 7.2), which are well known (and fast) reactions for radicals.[153] In this case, the Co–N bond would be cleaved homolytically (Fig 7.2).

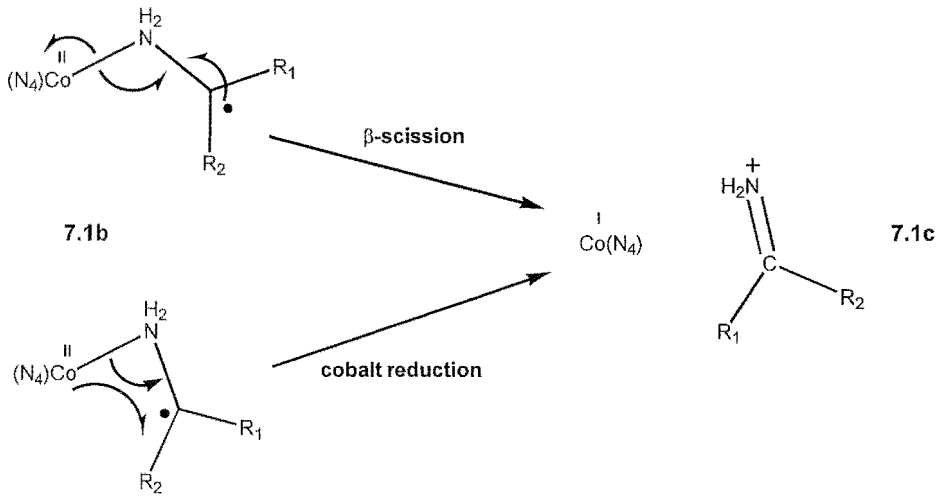

Figure 7.2. A close up of two possible pathways linking 7.1b and 7.1c.

Both of these pathways would generate a $[Co^I(bpy)_2]^+$ complex and an iminium ion (**7.1c**). This pair could combine to form a metallacycle (**7.1e**), perhaps in a stepwise

fashion *via* the η^1 organometallic product **7.1d**. Co(I) complexes are known to be strongly nucleophilic,[86] hence attack at the carbon atom of the iminium ion can be envisaged. Co–N bond formation *may* represent the rate determining step in the production of the metallacycle (that is, $k_5 \approx 10^3\ s^{-1}$). If this really represents the reaction's *modus operandi*, one would expect a dependence of the rate constant k_5 on the nature of R_1 and R_2. Originally, such an investigation, using laser flash photolysis, was planned for this thesis. It is hoped that this investigation will proceed in the near future. Whilst on the subject of kinetics, although the required set-up is not available locally, a time-resolved spectroscopic study of this reaction may well prove to be very illuminating.

Decomposition of the metallacycle

The thermal decomposition of this metallacycle may proceed *via* **7.1c**, as already proposed in Fig 3.10. This could happen either by direct dissociation of **7.1e** to **7.1c** (k_7), or through the transient formation of **7.1b**, with a subsequent reduction or β-scission step (k_{-1} then k_2). With respect to the earlier discussion regarding the possible avenues for Co–C bond cleavage, it can now be seen that homolytic cleavage (Eqtn 3.2) could give the same outcome as the heterolytic cleavage (Eqtn 3.3).

Upon formation of **7.1c**, there may be a competition between Co–C bond formation (k_3) to eventually regain the **7.1e**, and dissociation (k_4), to give **7.1f** irreversibly. Thus, the photolysis product may *cycle* between the metallacycle (**7.1e**), and the Co(I)–iminium pair (**7.1c**).

The lifetime of the photolysis product would, within this cycle, be dependent on the values of several rate constants. If the rate constant(s) which link **7.1c** and **7.1e** is (are) large, there will be more opportunity for the (irreversible) dissociation of the iminium ion from **7.1c**. The relative values of k_3 and k_4, will determine exactly what fraction of **7.1c** goes down this path each time it is formed. If $k_3 > k_4$, the lifetime of the

metallacycle will be enhanced as it will be readily reformed from **7.1d**. On the other hand, if k_3 is rather small, the Co(I) complex and the iminium ion will able be to diffuse apart, and the lifetime of the metallacycle will be correspondingly short.

These speculations are consistent with the observation that Co–C–N metallacycles were not observable following photolysis of the alkyl-substituted aminoacidato complexes. The presence of electron-donating alkyl groups on the carbon centre will hinder the nucleophilic reaction (k_3), both sterically and electronically. Hence, k_4 will be promoted, and each time **7.1c** is formed, there would be a greater chance of irreversible dissociation.

Rate constants for the decomposition reactions can be deduced following flash photolysis. Indeed, the aforementioned planned laser flash photolysis experiments could be combined with a study of the decay kinetics to place any mechanistic propositions on a firmer (quantitative) basis.

Possible future experiments

Besides the large scope for flash photolysis experiments, there are numerous other possibilities for extending the work presented in this thesis, of which a few examples will be given presently.

The potential for improving the yields of the photodecarboxylation reactions, or for isolating products of low thermal stability by immobilising the reactant complex has not yet been explored. This could include photolysis of the complexes in the solid-state, bound to ion-exchange resins, or in frozen solutions. This latter method has found application by other research groups. The potential benefits of this approach include limiting the dissociative decomposition reaction and precluding the possible intermolecular redox reactions of the decomposition products.

The incorporation of the aminoacidato chelate into a polypyridyl framework was successful for stabilising the organometallic photolysis product. However, in order to have full confidence in the identity of the product, an X-ray crystal structure or elemental analysis is required. A further measurement which would be very informative is the optical rotatory dispersion spectrum of the optically active $[Co(dpa)(phen)]^{2+}$ complex *and* that of its photolysis product, $[Co(dam)(phen)]^{2+}$. If the optical activity is indeed retained in the product, there may be some scope for stereoselective reactions at the ligating carbon atom.

This polydentate framework could be used to synthesize numerous related complexes, which could be perhaps further utilised as intermediates for the synthesis of other complexes. An example of an interesting possibility is given below. A compound which is closely related to those discussed in Chapter 4, but with a chelating arm actually attached to the α-carbon, is depicted in Fig 7.3. Decarboxylation of the aminoacidato chelate may produce a metallacycle which is tethered at both the nitrogen and carbon centres.

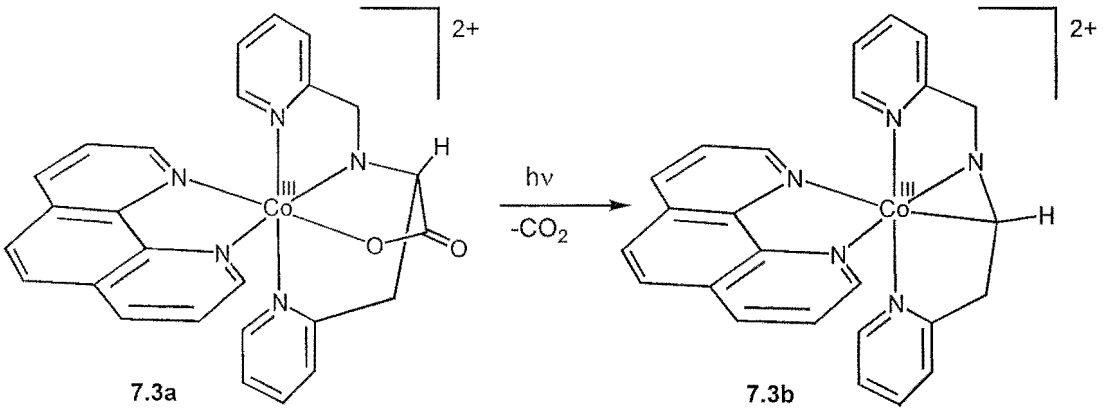

7.3a 7.3b

Figure 7.3. A possible photolysis experiment.

APPENDIX 1

RATE CONSTANT CALCULATIONS

This appendix contains an introduction to *ab initio* quantum mechanics, an outline of density functional theory, and an overview of transition-state theory. Particulars of the *ab initio* calculations which are presented in this thesis, namely calculated energies, geometries, and spin densities, are also included.

The beginner's guide to quantum chemistry

The main property of interest in quantum chemistry is the energy of a system, given by the solution of the Schrodinger equation.

$$\hat{H}\psi = E\psi \qquad \text{(A1.1)}$$

The time-independent Hamiltonian ($\hat{H}$) operates on the eigenfunction ψ to yield the energy levels (E) as eigenvalues of ψ. The Hamiltonian is composed of kinetic (T) and potential energy (V) terms.

$$\hat{H} = -\frac{\hbar}{2m}\nabla^2\psi + V\psi \qquad \text{(A1.2)}$$

The *Born-Oppenheimer approximation* separates the nuclear and electronic contributions to the kinetic energy. The electrons are treated as reacting instantaneously to changes in nuclear coordinates. In a physical sense this is justified by noting that electrons have much lower mass than nuclei, hence will move much faster. The kinetic energy of the nuclei is omitted, and electronic Hamiltonian (H^{elec}) becomes:

$$H^{elec} = T^{elec} + V^{nucl\text{-}elec} + V^{elec} + V^{nucl} \qquad \text{(A1.3)}$$

This equation can be solved analytically only for very simple systems (eg the hydrogen atom), but the introduction of a few assumptions, especially for the problematic issue of electron-electron correlation, allows the energies of complex molecular systems to be evaluated.

A note on basis sets and levels of theory

MO methods are based on the expression of the wavefunction, or equivalent, as a linear combination of a certain set of *basis functions*. In practice, these functions are associated with each nucleus and are derived from the analytical solutions to the Schrödinger equation for the hydrogen atom. Common basis sets include Slater-type atomic orbitals and Gaussian-type atomic orbitals. The present investigation utilised solely the 6-31G* basis set, which is a common Gaussian-type basis set with d-orbital polarisation functions on the non-hydrogen atoms. Increasing the basis set size, for example to 6-311G**, increases the accuracy of the model by allowing the orbitals greater flexibility, along with exponentially increasing the computer resources required. The choice of a particular basis set is often a dilemma, requiring a balance of the desired accuracy against the available disk space and computation time.

Shorthand descriptions of the levels theory used for a particular calculation combine the basis set and an abbreviation of the theoretical method. For example, HF/6-31G* signifies that the computation employed Hartree-Fock theory with a 6-31G* basis set. Occasionally, reference to a basis set is omitted, as it is implied by the method - usually so-called compound methods, which consist of a number of pre-defined components eg G2, CBS-Q. Single-point energy calculations for a geometry which has been optimised at a lower level of theory are abbreviated as, for example, PMP2/6-31G*//UHF/6-31G* indicates that a single point energy calculation using PMP2 with a 6-31G* basis set was performed on the UHF/6-31G* optimised geometry

Density Functional Theory- An Introduction

DFT methods have been propelled by significant improvements in the last decade, and often are more efficient than Hatree-Fock techniques because electronic exchange effects are better accommodated. Also, in many cases, DFT provides a more economical return on computer time. An overview, albeit brief, of the DFT approach is given here, while the interested reader is directed to more comprehensive accounts.[154]

The core concept of DFT methods is that molecular energies, and indeed all properties of a molecular system, can be expressed as a function of the electron density (ρ). The foundations were laid by Hohenberg and Kohn[155] in 1964 when they demonstrated the

existence of a unique functional of ρ (which, of course is dependent on R, the nuclear coordinates) which yields the exact ground state energy of the system.[∅]

$$E = E[\rho, R_\alpha] \qquad \text{(A1.4)}$$

Fortunately for quantum chemists the form of this functional could not be given and the development of approximations to the true solution has kept many of their families from starving.

The energy comprises three terms: a kinetic energy term; a coulombic energy term; and a exchange-correlation or "many-body" term.

$$E = T[\rho] + U[\rho] + E_{XC}[\rho] \qquad \text{(A1.5)}$$

The kinetic energy component is equates to the kinetic energy of a system of non-interacting particles with the same electron density as the real system, while the Coulombic term accounts for the classical electrostatic interactions between nuclei and electrons. All exchange and correlation effects are represented by the many-body term which stems from the desire of the electrons to both maximise their attraction to the nucleus whilst minimising their repulsion to each other. This is formally described as the exchange-correlation hole: the zone around each electron into which no other electron is allowed.

The full electron density can be formulated from single-particle densities, derived from one-particle wavefunctions ψ_i with the important property that the sum of the squares of the occupied orbitals represents the true electron density of the system.

$$\rho(r) = \sum_{occ} |\psi_i(r)|^2 \qquad \text{(A1.6)}$$

Application of the variational principle, minimizing the energy with respect to the electron density, led Kohn and Sham[156] to propose that the exact energy was represented by a Schrödinger equation.

[∅] A functional is a function whose definition is itself a function.

$$\left[-\tfrac{1}{2}\nabla^2 + V_c(r) + \mu_{XC}(r)\right]\psi_i = \varepsilon_i\psi_i \quad \text{(A1.7)}$$

The bracketed term in this equation is a one-electron Hamiltonian, composed of a kinetic energy operator ($-½\nabla^2$), a Coulombic potential operator ($V_c(r)$), and an exchange-correlation potential operator ($\mu_{XC}(r)$). The eigenfunctions of the Hamiltonian operator (ψ_i) are commonly expressed as a linear combination of a set of basis functions.[c]

$$\psi_i = \sum_p c_{ip} g_p \quad \text{(A1.8)}$$

DFT methods converge to a solution by improving the exchange-correlation operator, by definition also improving the exchange-correlation energy.

$$\mu_{XC}(r) = \frac{\partial E_{XC}[\rho]}{\partial \rho(r)} \quad \text{(A1.9)}$$

Approximations are required to find a solution to this exchange-correlation functional which although universal, is of unknown form. As such, DFT methods are distinct from HF methods as they solve an *approximate* many-body Hamiltonian with an *exact* wavefunction, whereas the HF approach combines an exact Hamiltonian with an adjustable wavefunction.

The quest to find accurate approximations to the unknown $\mu_{XC}(r)$ is an area of intense activity. The first generation of functionals invoked the local density approximation (LDA). These include a Dirac functional for exchange in conjunction with simple models for correlation. The second generation of functionals employ both the electron density and its gradient - generalised gradient approximations (GGAs) - whereby a gradient-corrected energy functional is generated. More sophisticated third generation functionals give more accurate results, of course at increased computational cost, by incorporating a DFT-type exchange (LDA + GGA) with a HF-type exchange calculated from the orbitals. The most popular of these hybrid functionals is the B3LYP functional, employed in the present study, which blends HF exchange, local Dirac

[c] This basis set is also used for expressing the electron density and the exchange-correlation potential.

exchange, the B88[157] gradient correction to the exchange energy, and the LYP[158] gradient corrected correlation functional.

Partition functions

Evaluation of the TST expression (A1.10) for a unimolecular reaction requires the calculation of the partition function of both the reactant (Q) and of the TS ($Q^{\ddagger}$).

$$k = \frac{kT}{h}\frac{Q^{\ddagger}}{Q}\exp\left(-\frac{E_0}{kT}\right) \qquad \text{(A1.10)}$$

A partition function links quantum mechanical energy states with a macroscopic system and its thermodynamic variables. The general form of a canonical (ie N, V, T constant) molecular partition function is given by a summation over all the energy states ε_i, of degeneracy g_i.

$$Q(N,V,T) = \sum_i g_i \exp\left(-\frac{\varepsilon_i(N,V)}{kT}\right) \qquad \text{(A1.11)}$$

The values for ε_i are solutions of the Schrodinger equation:

$$\hat{H}\psi = E\psi \qquad \text{(A1.12)}$$

Fortunately, these equations have analytical solutions for the energy levels of unhindered rotors and harmonic oscillators. If we assume separability of the Hamiltonians, the partition function can be written as a product of translational, vibrational, and rotational terms:

$$Q = Q_{trans} \times Q_{vib} \times Q_{rot} \qquad \text{(A1.13)}$$

The evaluation of these individual terms will now be considered in more detail with special attention paid to the peculiarities of the reactions of interest; the ring-opening rearrangements of the aminocyclopropylmethyl radical and its protonated form.

The translational partition function

The translational partition function of an ideal gas is given by:

$$Q_{trans} = V\left(\frac{2\pi mkT}{h^2}\right)^{3/2} \qquad \text{(A1.14)}$$

where V is the reference volume and m is the mass of the translating molecule. If we reflect upon the form of the TST expression (A1.10), it becomes apparent that, for a

unimolecular reaction, the net contribution of this partition function will be 1, ($Q^{\ddagger}_{trans}=Q_{trans}$), and can be disregarded.

The rotational partition function

The contribution of molecular rotation to the partition function can be expressed as:

$$Q_{rot} = \frac{\pi^{1/2}}{\sigma}\left(\frac{8\pi^2 kT}{h^2}\right)^{3/2}(I_a I_b I_c)^{1/2} \qquad \text{(A1.15)}$$

where I_a, I_b, and I_c are the principle moments of inertia. In practice, these are easily calculated once the equilibrium geometry has been ascertained. The symmetry number, denoted by σ, is a factor which accounts for any rotational symmetry of the molecule.

Computationally, all stationary point geometries are arrived at by calculating all the forces on the molecule at a given geometry and "tweaking" the structure until the forces lie below a certain threshold value close to zero. However, this procedure does not distinguish between minima and saddle points. This task is completed by the frequency calculation (see below).

The vibrational partition function

The vibrational contribution to the partition function can be expressed as a product of *i* individual harmonic oscillator partition functions which incorporate the vibrational frequencies, ν_i. In mathematical terms:

$$Q_{vib,i} = \left[1-\exp\left(-\frac{h\nu_i}{kT}\right)\right]^{-1} \qquad \text{(A1.16)}$$

$$Q_{vib} = \prod_i Q_{vib,i} \qquad \text{(A1.17)}$$

Of the 3N degrees of freedom enjoyed by a non-linear, ground state molecule, the subtraction of three translational and three rotational modes, leaves 3N-6 *vibrational* modes, where N is the number of atoms. The transition state is restricted to 3N-5 vibrational modes as one degree of freedom becomes the *imaginary frequency* (see below). These vibrational frequencies are routinely evaluated with the help of *ab initio* techniques which provide a detailed knowledge of the potential energy surface. Specifically, the evaluation of the second derivative of the energy with respect to the nuclear coordinates (the Hessian matrix), yields the information required to compute the frequencies.

The frequency analysis also enables the first order saddle points to be distinguished from the energy minima. These transition states have one negative eigenvalue in the Hessian matrix, an imaginary vibrational frequency which corresponds to motion along the reaction coordinate; that is, a geometric distortion which leads to a *lowering* of the potential energy. This frequency is omitted from the partition function.

The form of the vibrational partition function is such that low frequency vibrations make the greatest contribution. Such modes are often associated with torsional motions of the molecule and are not particularly well represented by the harmonic oscillator approximation. This point will be addressed later.

The sensitivity of the partition function to the low frequency vibrations, and the significant differences in the vibrational modes of the reactant and TS, gives the $Q^{\ddagger}_{vib}/Q_{vib}$ ratio the dominating hand in shaping the overall partition function ratio $Q^{\ddagger}/Q$ for a unimolecular reaction.

Calculation of the reaction barrier

The reaction barrier is defined as the energy difference between the reactant and the transition state at 0 K. *Ab initio* quantum mechanical calculations can provide the energies for these two points on the potential surface, however, a *zero-point energy* correction must be applied. This correction accounts for the vibrational energy of the molecule which persists even at 0 K, and has a simple relationship with the vibrational frequencies:

$$E = E_{calc} + ZPE = E_{calc} + \tfrac{1}{2}\sum_i h\nu_i \qquad \text{(A1.18)}$$

Fortunately, an frequency analysis is a routine part of calculations directed toward the TST equation as they are required to assess the vibrational partition function.

In the present investigation, TST enabled the construction of Arrhenius expressions for the ring opening, and closing, of the two aminocyclopropylmethyl radicals. The Arrhenius equation is generalised by:

$$k_{rxn} = A\exp\left(-\frac{E_a}{RT}\right) \qquad \text{(A1.19)}$$

The *activation energy* contains the enthalpic contribution to the rate constant, and is related to the reaction barrier.[53]

$$E_{act} = E_0 - k\frac{\partial \ln\left(\frac{Q^{\ddagger}}{Q}\right)}{\partial \mathrm{T}^{-1}} + k\mathrm{T} \qquad \text{(A1.20)}$$

The second term in this equation corresponds to a thermal correction to the activation enthalpy.

The Arrhenius frequency factor can be expressed as:

$$A = \frac{ekT}{h}\exp\left(\frac{\Delta S^{\ddagger}}{\mathrm{k}}\right) \qquad \text{(A1.21)}$$

Hence, the frequency factor contains the entropic contribution to the rate coefficient, and is a cousin of the first term in the TST expression as:

$$\Delta S^{\ddagger} = k\ln\left(\frac{Q^{\ddagger}}{Q}\right) - \frac{k}{\mathrm{T}}\frac{\partial \ln\left(\frac{Q^{\ddagger}}{Q}\right)}{\partial \mathrm{T}^{-1}} \qquad \text{(A1.22)}$$

Co-ordinates and atomic spin densities computed at the B3-LYP/6-31G* level

1. The aminocyclopropylmethyl radical (2.11a)

	Label	Spin	x	y	z
1	C2	0.086	1.325306	0.811870	-0.331872
2	C3	-0.066	0.293063	-0.008525	0.453411
3	H3	0.012	0.194253	0.288032	1.500327
4	C1	0.014	1.628185	-0.604914	0.074210
5	C4	0.834	-0.945975	-0.511740	-0.160349
6	H2a	0.007	1.838293	1.620293	0.184346
7	H2b	-0.003	1.108766	1.011397	-1.377487
8	H1a	0	1.631402	-1.367980	-0.700877
9	H1b	0	2.357291	-0.776542	0.861569
10	N1	0.152	-2.123390	0.251962	-0.031977
11	H(N1)	0	-2.968155	-0.268266	-0.250518
12	H4	-0.03	-0.878979	-1.078714	-1.086975
13	H(N2)	0	-2.222610	0.687906	0.881053

2. Transition state for ring opening of the aminocyclopropylmethyl radical (2.11b).

	Label	Spin	x	y	z
1	C1	-0.010	1.523904	-0.645055	0.054580
2	C2	0.609	1.683805	0.799548	-0.252323
3	C3	-0.198	0.173731	-0.152663	0.456960
4	H2a	-0.026	1.497214	1.165898	-1.254009
5	H2b	-0.024	2.128424	1.477090	0.467663
6	C4	0.562	-0.983547	-0.326782	-0.293870
7	H1a	0.003	1.525048	-1.316613	-0.807428
8	H5	0.010	0.082158	0.235853	1.469044
9	H1b	0	2.145149	-1.051118	0.855904
10	H(N1)	0.010	-2.825632	0.460954	-0.689019
11	H4	-0.029	-0.958586	-0.863596	-1.238301
12	N	0.090	-2.251248	0.141142	0.085127
13	H(N2)	0	-2.222402	0.853244	0.808173

3. The ring-opened aminocyclopropylmethyl radical (2.11c).

	Label	Spin	x	y	z
1	N1	0	-2.439960	-0.161655	0.002551
2	C4	0.005	-1.136142	0.302596	-0.214098
3	H(N1)	0	-2.482396	-1.055890	0.480787
4	H(N2)	0	-3.014991	-0.181356	-0.832546
5	C3	0.012	-0.022654	-0.121867	0.399509
6	H4	0	-1.089632	1.141800	-0.907795
7	H3	0	-0.077142	-0.966475	1.088082
8	C1	-0.080	1.336279	0.505383	0.207976
9	C2	1.090	2.371141	-0.450564	-0.297928
10	H1a	0.013	1.692108	0.949105	1.151838
11	H1b	0.058	1.233566	1.361623	-0.485924
12	H2a	-0.050	2.103827	-1.211439	-1.024996
13	H2b	-0.051	3.422638	-0.319066	-0.060060

4. The protonated aminocyclopropylmethyl radical (2.14a).

	Label	Spin	x	y	z
1	C1	0.0348	-1.697051	-0.610093	0.072907
2	C3	-0.0538	-0.329223	-0.033255	0.433864
3	H2a	0.0060	-0.173551	0.206780	1.485076
4	H2b	0.005	-1.288546	1.078644	-1.306848
5	C4	0.889	0.833384	-0.462690	-0.298600
6	H1a	0.002	-2.343358	-0.847813	0.912144
7	H1b	0	-1.725632	-1.336110	-0.734924
8	C2	0.152	-1.451046	0.811056	-0.267289
9	H3	0.004	-1.889815	1.592069	0.346622
10	H4	-0.039	0.814453	-0.824747	-1.319828
11	N1	-0.039	2.145513	0.144733	0.066859
12	H(N1)	.0047	2.252148	0.198126	1.088962
13	H(N2)	.0389	2.269960	1.106677	-0.294301
14	H(N3)	.0026	2.929370	-0.416862	-0.290209

5. The transition state for ring-opening of the protonated aminocyclopropylmethyl radical (2.14b).

	Label	Spin	x	y	z
1	C1	-0.027	-1.614316	-0.623956	0.037739
2	C3	-0.117	0.232782	-0.212647	0.448594
3	H3	0.007	-0.114475	0.135473	1.472991
4	H2a	-0.029	-1.515369	1.229425	-1.200723
5	C4	0.540	0.879987	-0.400250	-0.338039
6	H1a	0.008	-2.227056	-1.019298	0.847585
7	H1b	0.007	-1.655488	-1.260094	-0.846648
8	C2	0.6621	-1.711349	0.830605	-0.212403
9	H2b	-0.027	-2.072339	1.508257	0.553252
10	H4	0.026	0.896325	-0.810632	-1.338868
11	N1	0.025	2.175163	0.218896	0.056895
12	H(N1)	0	2.179286	0.456188	1.057104
13	H(N2)	0.023	2.390146	1.088951	-0.457191
14	H(N3)	0.004	2.963594	-0.423056	-0.101117

6. The ring-opened protonated aminocyclopropylmethyl radical (2.14c).

	Label	Spin	x	y	z
1	H(N1)	0.000	-3.055648	0.394096	0.252593
2	N1	-0.001	-2.337746	-0.305692	0.016337
3	C4	0.039	-1.021640	0.327391	-0.293179
4	H(N2)	0.002	-2.700575	-0.852304	-0.778081
5	H(N3)	0.000	-2.261420	-0.946200	0.817077
6	C3	0.03	0.059804	0.037738	0.424853
7	H4	-0.001	-1.076383	1.006837	-1.134989
8	H3	0.000	-0.004701	-0.669136	1.253689
9	C1	-0.068	1.434788	0.594386	0.134881
10	H1a	0.006	1.806623	1.085187	1.042367
11	H1b	0.024	1.363334	1.361217	-0.647445
12	C2	1.067	2.351554	-0.518514	-0.277299
13	H2a	-0.050	3.087113	-0.923793	0.407522
14	H2b	-0.049	2.258848	-0.962069	-1.262628

APPENDIX 2

X-RAY CRYSTALLOGRAPHY

Details of data collection, structure solution and refinement, and atomic coordinates

General

A variety of people provided invaluable help with the crystallography, and the collaborators are listed for each particular structure. Two different setups were used for the data collection and refinement, as a CCD detector was installed, and the diffractometer computer software upgraded, during the course of the project.

Setup 1. The X-ray data were collected with a Siemens P4 four circle diffractometer with graphite monochromated Mo-K_α (λ = 71073 Å) radiation. The unit cell parameters were determined from an initial measurement of 15-30 strong reflections. The intensities of several check reflections were monitored during the data collection and data weighted accordingly if crystal decay was demonstrable. The structure solution and refinement made use of XSCANS[159] and the SHELXTL software package.[160] Absorption was corrected for as detailed for individual structures, and Lorentz and polarisation corrections were applied to the raw data. Neutral scattering factors and anomalous dispersion corrections for non-hydrogen atoms were taken from the literature.[161] Hydrogen atoms were treated as detailed for the individual structures.

Setup 2. The X-ray data were collected with a Siemens P4 four circle diffractometer, equipped with a Siemens SMART 1K CCD area detector, using graphite monochromated Mo-K_α (λ = 71073 Å) radiation. The data collection was controlled by the SMART programme.[162] The crystal to detector distance was 6.0 cm. Data processing was carried out with the help of SAINT[163] which applied Lorentz and Polarisation corrections to three-dimensionally integrated diffraction spots. SADABS[164] was employed to scale the diffraction data, to apply an empirical absorption correction based on redundant reflections, and to apply a decay correction where appropriate. Neutral scattering factors and anomalous dispersion corrections for non-hydrogen atoms were taken from the literature. The structure refinement, based on F^2 with anisotropic thermal displacement parameters for all non-hydrogen atoms, made use of SHELXTL. Hydrogen atoms were treated as detailed for the individual structures.

A2.1 $[Co(bpy)_2(cpg)](ClO_4)_2$ (Fig 3.4)

A single crystal suitable for X-ray analysis was obtained by the slow cooling of a warm saturated solution of the complex in dilute $HClO_4$/MeOH (8:1). The initial unit cell determination used 17 strong reflections in the range $4.876 \geq 2\theta \geq 12.486$. The intensities of three standard reflections, measured every 297 reflections, showed little decay. The hydrogen atoms were placed in calculated positions and refined with isotropic thermal parameters based on the attached atom.

Collaborator	Prof Ward Robinson
Setup	1
Empirical formula	$C_{25}H_{24}Cl_2CoN_5O_{10}$
Formula weight	700.32
Colour	Orange
Temperature	168(2) K
Crystal system	Monoclinic
Space group	P2(1)/c
Unit cell dimensions	a = 12.512(3) Å, α= 90°.
	b = 17.657(4) Å, β= 92.06(2)°.
	c = 12.285(3) Å, γ = 90°.
Volume	2712.4(10) $Å^3$
Z	4
Density (calculated)	1.286 Mg/m^3
Absorption coefficient	0.677 mm^{-1}
F(000)	1074
Crystal size	0.5 × 0.25 × 0.22 mm^3
Theta range for data collection	2.02 to 24.00°.
Index ranges	$1 \geq h \geq -14$, $20 \geq k \geq 0$, $14 \geq l \geq -14$
Reflections collected	4559
Independent reflections	4255 [R(int) = 0.0317]
Completeness to theta = 24.00°	99.9 %
Absorption correction	Empirical (ψ scans)
Max. and min. transmission	0.43107 and 0.49705
Refinement method	Full-matrix least-squares on F^2
Data / restraints / parameters	4255 / 0 / 442
Goodness-of-fit on F^2	1.022
Final R indices [$I > 2\sigma(I)$]	R1 = 0.0650, wR2 = 0.1277
R indices (all data)	R1 = 0.1322, wR2 = 0.1554
Largest diff. peak and hole	0.927 and -0.326 $e.Å^{-3}$
Solution method	Direct methods

Table A2.1. Atomic coordinates (x 10^4) and equivalent isotropic displacement parameters ($Å^3$ x 10^3) for $[Co(bpy)_2(cpg)](ClO_4)_2$.

	x	y	z	U(eq) [165]
Co	2631(1)	248(1)	2293(1)	32(1)
N(1)	4132(4)	372(3)	2702(4)	34(1)
N(2)	2445(4)	1281(3)	2771(4)	37(1)
N(3)	2176(4)	14(4)	3744(4)	37(2)
N(4)	1169(4)	97(3)	1779(4)	32(1)
N(5)	2788(4)	-791(3)	1807(4)	36(2)
C(1)	4009(5)	691(4)	739(6)	38(2)
C(2)	4760(6)	540(6)	1736(6)	62(3)
C(3)	5591(8)	1084(11)	1916(8)	63(6)
C(3')	5690(30)	400(40)	1650(30)	40(20)
C(4)	6602(7)	845(8)	2569(8)	68(3)
C(5)	6657(6)	1046(9)	1387(8)	69(3)
C(6)	2676(6)	1916(5)	2229(7)	49(2)
C(7)	2658(7)	2620(5)	2699(8)	68(3)
C(8)	2357(7)	2694(6)	3746(8)	71(3)
C(9)	2055(6)	2057(6)	4299(7)	58(2)
C(10)	2130(5)	1359(5)	3811(6)	46(2)
C(11)	1904(5)	645(5)	4324(6)	42(2)
C(12)	1461(6)	560(6)	5334(6)	61(3)
C(13)	1250(6)	-149(7)	5712(7)	67(3)
C(14)	1524(6)	-783(6)	5123(7)	59(2)
C(15)	1995(5)	-670(5)	4130(5)	43(2)
C(16)	377(5)	600(5)	1831(5)	39(2)
C(17)	-660(5)	438(5)	1471(5)	42(2)
C(18)	-883(5)	-265(5)	1065(5)	41(2)
C(19)	-83(5)	-793(5)	994(5)	39(2)
C(20)	958(5)	-597(4)	1362(5)	33(2)
C(21)	1878(5)	-1103(4)	1342(5)	34(2)
C(22)	1875(5)	-1801(4)	874(5)	37(2)
C(23)	2811(6)	-2215(4)	850(6)	47(2)
C(24)	3727(6)	-1908(5)	1319(6)	48(2)
C(25)	3692(5)	-1215(4)	1799(5)	39(2)
O(1)	2993(3)	557(3)	893(3)	36(1)
O(2)	4341(4)	891(3)	-121(4)	48(1)
Cl(1)	334(2)	-2380(1)	3248(1)	45(1)

O(11)	-6(4)	-1610(3)	3127(4)	63(2)
O(12)	168(5)	-2775(3)	2236(4)	67(2)
O(13)	-254(4)	-2743(3)	4086(4)	58(2)
O(14)	1451(4)	-2390(3)	3546(4)	57(2)
Cl(2)	5176(1)	-3550(1)	-513(2)	47(1)
O(21)	6020(30)	-3910(30)	-1030(30)	98(13)
O(21')	5600(30)	-4170(20)	-930(30)	159(14)
O(22)	5000(50)	-2898(15)	-910(20)	150(20)
O(22')	5520(30)	-2915(16)	-1104(17)	151(13)
O(23)	4360(30)	-4050(20)	-600(30)	130(19)
O(23')	4088(13)	-3540(30)	-701(18)	175(17)
O(24)	5430(4)	-3470(3)	617(4)	65(2)

A2.2 [Co(dpg)(phen)](ClO$_4$)$_2$ (Fig 4.5)

Crystals suitable for the diffraction study were obtained by the slow cooling of a hot solution of the complex in dilute $HClO_4$. All hydrogen atoms were placed at calculated positions and refined with a riding model.

Collaborator	Dr Jan Wikiara/Julian Adams
Setup	2
Empirical formula	$C_{26}H_{22}Cl_2CoN_5O_{10}$
Formula weight	694.32
Temperature	293(2) K
Crystal description	Orange block
Crystal system	Monoclinic
Space group	P2(1)/c
Unit cell dimensions	a = 11.620(8) Å, α= 90°.
	b = 24.487(13) Å, β= 114.54(3)°.
	c = 10.296(6) Å, γ = 90°.
Volume	2665(3) Å^3
Z	4
Density (calculated)	1.298 Mg/m^3
Absorption coefficient	0.687 mm^{-1}
F(000)	1062
Crystal size	0.40 × 0.20 × 0.18 mm^3
Theta range for data collection	2.10 to 23.51°.
Index ranges	12≥h≥–12, 27≥k≥–27, 7≥l≥–11
Reflections collected	26963
Independent reflections	3873 [R(int) = 0.0509]
Completeness to theta = 23.51°	98.0 %
Absorption correction	Empirical (SADABS)
Refinement method	Full-matrix least-squares on F^2
Data / restraints / parameters	3873 / 0 / 397
Goodness-of-fit on F^2	0.940
Final R indices [I > 2σ(I)]	R1 = 0.0351, wR2 = 0.0888
R indices (all data)	R1 = 0.0560, wR2 = 0.0933
Largest diff. peak and hole	0.855 and -0.429 e.Å^{-3}
Solution method	Direct methods

Table A2.2. Atomic coordinates (x 10^4) and equivalent isotropic displacement parameters ($Å^2$ x 10^3) for $[Co(dpg)(phen)](ClO_4)_2$.

	x	y	z	U(eq)
Co	2094(1)	1412(1)	3751(1)	18(1)
N(1)	923(3)	1563(1)	1810(3)	19(1)
N(2)	3367(3)	1584(1)	3063(3)	19(1)
N(3)	599(3)	1285(1)	4067(3)	22(1)
N(4)	3267(3)	1313(1)	5705(3)	20(1)
N(5)	2365(3)	606(1)	3636(3)	20(1)
O(1)	2041(2)	2160(1)	4129(2)	22(1)
O(2)	1569(3)	2965(1)	3027(3)	34(1)
C(1)	1473(3)	2471(2)	3014(4)	22(1)
C(2)	635(3)	2168(1)	1707(4)	25(1)
C(4)	1574(3)	1425(2)	868(3)	22(1)
C(5)	2945(3)	1582(1)	1640(4)	21(1)
C(6)	3718(3)	1731(2)	979(4)	26(1)
C(7)	4941(3)	1903(2)	1791(4)	29(1)
C(8)	5353(3)	1928(1)	3244(4)	24(1)
C(9)	4555(3)	1761(1)	3846(4)	22(1)
C(10)	-266(3)	1247(2)	1525(4)	24(1)
C(11)	-476(3)	1252(1)	2864(3)	21(1)
C(12)	-1635(4)	1227(1)	2910(4)	28(1)
C(13)	-1710(4)	1230(2)	4208(4)	33(1)
C(14)	-627(4)	1262(2)	5428(4)	31(1)
C(15)	511(4)	1287(1)	5324(4)	27(1)
C(16)	3714(3)	1699(2)	6714(4)	23(1)
C(17)	4589(3)	1570(2)	8067(4)	24(1)
C(18)	4997(3)	1046(2)	8415(4)	26(1)
C(19)	4540(3)	633(1)	7394(3)	23(1)
C(20)	4898(4)	70(2)	7622(4)	29(1)
C(21)	4447(4)	-297(2)	6557(4)	30(1)
C(22)	3587(3)	-141(1)	5161(4)	23(1)
C(23)	3103(3)	-503(2)	4008(4)	28(1)
C(24)	2260(4)	-306(1)	2729(4)	28(1)
C(25)	1914(3)	242(2)	2587(4)	27(1)
C(26)	3198(3)	405(1)	4921(3)	20(1)

C(27)	3685(3)	791(1)	6043(3)	18(1)
Cl(1)	7824(1)	2025(1)	7957(1)	29(1)
O(11)	8312(6)	2512(2)	7789(5)	140(2)
O(12)	8738(4)	1605(2)	8249(3)	81(1)
O(13)	6791(3)	1880(2)	6722(3)	93(1)
O(14)	7460(3)	2067(1)	9120(3)	57(1)
Cl(2)	-1966(1)	-174(1)	1208(1)	35(1)
O(21)	-1677(4)	-181(2)	2661(3)	78(1)
O(22)	-2567(3)	332(1)	619(3)	62(1)
O(23)	-848(3)	-225(1)	948(3)	59(1)
O(24)	-2821(3)	-608(1)	488(4)	63(1)

A2.3 [Co(dgm)(phen)](ClO$_4$)$_2$·H$_2$O (Fig 4.7)

X-ray quality crystals were produced by a recrystallisation from H_2O/ethanol (50/50). Two independent molecules were present in the asymmetric unit. The hydrogen atoms bound to the carbon atom of the metallacycle (C(13)) were found on a difference electron density map and were refined isotropically. Other hydrogen atoms were placed in calculated positions and refined with a riding model.

Collaborators	Dr Jan Wikiara/Julian Adams
Setup	2
Empirical formula	$C_{25}H_{22}Cl_2CoN_5O_{10}$
Formula weight	666.31
Crystal description	Orange-red
Crystal system	Orthorhombic
Temperature	159(2) K
Space group	Pbcm
Unit cell dimensions	a = 18.158(5) Å, α= 90°.
	b = 8.978(2) Å, β= 90°.
	c = 34.173(9) Å, γ = 90°.
Volume	5571(2) Å^3
Z	8
Density (calculated)	1.589 Mg/m^3
Absorption coefficient	0.870 mm^{-1}
F(000)	2720
Crystal size	0.1 × 0.3 × 0.65 mm^3
Theta range for data collection	2.24 to 27.65°
Index ranges	23≥h≥–23, 11≥k≥–4, 42≥l≥–44
Reflections collected	42616
Independent reflections	11940 [R(int) = 0.0489]
Completeness to theta = 27.65°	95.6 %
Absorption correction	Empirical (SADABS)
Refinement method	Full-matrix least-squares on F^2
Data / restraints / parameters	11940 / 1 / 773
Goodness-of-fit on F^2	0.882
Final R indices [I > 2σ(I)]	R1 = 0.0431, wR2 = 0.1006
R indices (all data)	R1 = 0.0763, wR2 = 0.1077
Absolute structure parameter	0.326(17)
Largest diff. peak and hole	0.751 and -0.447 e.Å^{-3}
Solution method	Direct methods

Table A2.3. Atomic coordinates (x 10^4) and equivalent isotropic displacement parameters ($Å^2$ x 10^3) for $[Co(dgm)(phen)](ClO_4)_2 \cdot H_2O$.

	x	y	z	U(eq)
Co(1)	1144(1)	2504(1)	4563(1)	34(1)
N(1)	401(2)	2613(4)	4983(1)	40(1)
C(1)	-295(3)	2130(5)	4975(2)	46(1)
N(1')	2875(2)	2479(4)	2138(1)	37(1)
C(1')	2175(3)	2933(6)	2154(2)	49(1)
C(2)	-760(4)	2324(7)	5296(2)	61(2)
Co(2)	3634(1)	2547(1)	2543(1)	33(1)
C(2')	1694(3)	2813(7)	1844(2)	57(2)
C(3)	-510(4)	2967(7)	5639(2)	60(2)
C(3')	1934(4)	2121(7)	1510(2)	58(2)
C(4)	219(3)	3478(5)	5656(2)	49(1)
C(4')	2650(3)	1628(5)	1470(2)	47(1)
C(5)	542(4)	4187(6)	5981(2)	62(2)
C(5')	2955(4)	875(6)	1126(2)	62(2)
C(6)	1259(5)	4615(8)	5986(2)	72(2)
C(6')	3674(4)	399(7)	1123(2)	54(2)
C(7)	1733(3)	4402(6)	5644(2)	48(1)
C(7')	4148(3)	688(5)	1449(1)	43(1)
C(8)	2473(5)	4764(6)	5628(2)	54(2)
C(8')	4909(5)	318(7)	1453(2)	50(2)
C(9)	2869(3)	4438(6)	5301(2)	48(1)
C(9')	5324(3)	605(5)	1779(2)	45(1)
N(10)	1812(2)	3415(4)	4981(1)	33(1)
C(10)	2507(3)	3762(4)	4974(1)	38(1)
N(10')	4271(2)	1655(4)	2111(1)	34(1)
C(10')	4981(3)	1290(5)	2103(2)	39(1)
C(11)	1418(3)	3706(5)	5318(1)	35(1)
C(11')	3860(3)	1379(5)	1780(1)	38(1)
C(12)	663(3)	3250(5)	5315(1)	41(1)
C(12')	3106(3)	1827(5)	1789(1)	37(1)
N(13)	1536(2)	2101(4)	4060(1)	38(1)
C(13)	789(3)	1651(6)	4083(2)	43(1)
N(13')	4055(2)	2911(4)	3045(1)	35(1)

C(13')	3306(3)	3361(6)	3032(2)	42(1)
C(14)	2112(3)	937(5)	4068(2)	46(1)
C(14')	4623(3)	4080(5)	3040(2)	44(1)
N(15)	1521(2)	555(4)	4692(1)	40(1)
C(15)	2010(5)	3(5)	4423(3)	42(2)
N(15')	4012(2)	4515(5)	2415(1)	40(1)
C(15')	4470(5)	5049(5)	2690(3)	43(2)
C(16)	2348(3)	-1363(5)	4475(2)	57(2)
C(16')	4845(3)	6400(5)	2633(2)	55(2)
C(17')	4697(4)	7201(5)	2294(2)	65(2)
C(17)	2239(3)	-2133(5)	4815(2)	57(2)
C(18)	1745(4)	-1581(6)	5092(2)	59(2)
C(18')	4205(3)	6668(5)	2024(2)	60(2)
C(19)	1392(5)	-258(6)	5023(2)	50(2)
C(19')	3875(4)	5305(7)	2094(2)	49(2)
N(20)	949(2)	4465(4)	4348(1)	34(1)
C(20)	556(3)	5568(5)	4516(2)	37(1)
N(20')	3436(2)	572(4)	2756(1)	36(1)
C(20')	3049(3)	-517(5)	2583(2)	39(1)
C(21)	467(3)	6953(5)	4341(2)	41(1)
C(21')	2948(3)	-1882(5)	2768(2)	45(1)
C(22)	784(3)	7174(5)	3974(2)	44(1)
C(22')	3233(3)	-2128(6)	3129(2)	55(2)
C(23)	1175(3)	6049(5)	3793(2)	44(1)
C(23')	3653(3)	-1017(6)	3303(2)	48(1)
C(24)	1255(3)	4715(6)	3986(2)	34(1)
C(24')	3752(4)	333(7)	3105(2)	40(1)
C(25)	1703(3)	3464(5)	3826(2)	42(1)
C(25')	4236(3)	1565(5)	3259(2)	46(1)
Cl(1)	509(1)	2039(2)	456(1)	79(1)
O(11)	1153(4)	1354(7)	408(4)	237(6)
O(12)	671(5)	2814(9)	832(2)	157(3)
O(13)	-69(3)	1115(8)	546(2)	142(3)
O(14)	365(3)	3273(7)	229(2)	115(2)
Cl(2)	6970(1)	2890(2)	1636(1)	79(1)
O(21)	6793(4)	2257(9)	1261(2)	145(3)
O(22)	6322(4)	3606(6)	1759(3)	177(4)
O(23)	7520(4)	3925(7)	1590(2)	154(3)
O(24)	2119(4)	-1687(6)	1863(2)	120(2)

Cl(3)	3700(1)	5317(2)	4079(1)	41(1)
O(31)	3012(2)	5931(4)	3940(1)	58(1)
O(32)	4296(2)	5959(5)	3868(1)	63(1)
O(33)	3782(3)	5587(5)	4487(1)	65(1)
O(34)	3684(3)	3725(4)	4010(1)	67(1)
Cl(4)	6200(1)	-306(2)	3005(1)	39(1)
O(41)	5572(2)	-989(4)	3182(1)	72(1)
O(42)	6199(3)	1196(5)	3114(2)	107(2)
O(43)	6858(2)	-1020(5)	3138(1)	77(1)
O(44)	6178(3)	-429(7)	2590(1)	97(2)
OW1	3848(3)	1009(6)	4439(2)	122(2)
OW2	6338(3)	3933(6)	2647(2)	120(2)

A2.4 $[Co(bpa)(phen)(O_2)Co(bpa)(phen)](ClO_4)_4$ (Fig 4.17)

Small orange-brown crystals developed in an NMR tube during the thermal decomposition of $[Co(dcm)(phen)]^{2+}$ at room temperature. All hydrogen atoms were included in calculated positions, and were refined using a riding model.

Collaborators	Dr Peter Steel/Dr Jan Wikiara
Setup	2
Empirical formula	$C_{48}H_{42}Cl_4Co_2N_{10}O_{18}$
Formula weight	1306.58
Crystal description	Orange block
Temperature	168(2) K
Crystal system	Monoclinic
Space group	C2/m
Unit cell dimensions	a = 21.652(10) Å, α= 90°
	b = 11.320(5) Å, β= 114.142(6)°
	c = 12.352(6) Å, γ = 90°
Volume	2763(2) $Å^3$
Z	2
Density (calculated)	1.571 Mg/m^3
Absorption coefficient	0.875 mm^{-1}
F(000)	1332
Crystal size	0.04 × 0.05 × 0.2 mm
Theta range for data collection	2.07 to 24.00°.
Index range	24≥h≥–24, 5≥k≥–12, 13≥l≥–14
Reflections collected	6574
Independent reflections	2287 [R(int) = 0.0743]
Completeness to theta = 24.00°	99.8 %
Absorption correction	None
Refinement method	Full-matrix least-squares on F^2
Data / restraints / parameters	2287 / 0 / 199
Goodness-of-fit on F^2	0.823
Final R indices [I>2σ(I)]	R1 = 0.0497, wR2 = 0.1017
R indices (all data)	R1 = 0.1033, wR2 = 0.1109
Largest diff. peak and hole	0.588 and -0.429 $e.Å^{-3}$
Solution method	Direct methods

Table A2.4. Atomic coordinates (x 10^4) and equivalent isotropic displacement parameters ($Å^2$ x 10^3) for $[Co(bpa)(phen)(O_2)Co(bpa)(phen)]ClO_4)_4$.

	x	y	z	U(eq)
Co	918(1)	0	1752(1)	23(1)
O(1)	21(2)	0	595(4)	30(1)
N(1)	704(2)	1190(4)	2657(4)	28(1)
N(2)	1830(3)	0	3119(5)	27(2)
N(3)	1213(2)	1151(4)	895(3)	26(1)
C(1)	79(3)	1646(5)	2389(5)	45(2)
C(2)	-35(3)	2493(6)	3084(6)	61(2)
C(3)	505(3)	2895(5)	4075(6)	57(2)
C(4)	1131(3)	2430(5)	4370(5)	40(2)
C(5)	1222(3)	1580(4)	3638(5)	29(1)
C(6)	1905(2)	1111(4)	3799(5)	35(1)
C(7)	1174(2)	2325(4)	868(5)	32(1)
C(8)	1390(3)	3008(5)	156(5)	41(2)
C(9)	1656(3)	2487(5)	-557(5)	39(2)
C(10)	1703(2)	1259(5)	-565(5)	31(1)
C(11)	1476(2)	625(4)	171(4)	24(1)
C(12)	1943(2)	590(5)	-1315(5)	42(2)
Cl(1)	1533(1)	5000	-2788(2)	35(1)
O(4)	1445(3)	5000	-1703(5)	65(2)
O(3)	1906(2)	6030(3)	-2837(3)	55(1)
O(2)	889(3)	5000	-3754(6)	71(2)
Cl(2)	1796(1)	5000	-6925(2)	40(1)
O(8)	1655(3)	5000	-5885(5)	52(2)
O(7)	2182(2)	3955(3)	-6915(3)	57(1)
O(6)	1176(3)	5000	-7970(5)	71(2)

A2.5 α-[Co(edda)bpy]Cl·3H_2O (Fig 5.5)

Crystals suitable for the X-ray diffraction study were grown by recrystallising the crude complex from H_2O/ethanol (1/1). The initial unit cell determination used 11 strong reflections in the range $31.528 \geq 2\theta \geq 9.682$. Three check reflections were recorded every 97 reflections and they showed a decay of 12.0 %. Hydrogen atoms were placed in calculated positions and refined as riding atoms, except those of the free H_2O molecules. These were discarded from the refinement as no convincing model for them could be found.

Collaborator	Prof Ward Robinson
Setup	1
Empirical formula	$C_{16}H_{24}ClCoN_4O_7$
Formula weight	478.77
Temperature	293(2) K
Crystal description	Red trapezoidal prism
Crystal system	Triclinic
Space group	P-1
Unit cell dimensions	a = 8.6731(19) Å, α= 100.884(10)°.
	b = 11.5541(14) Å, β= 110.08(2)°.
	c = 11.702(2) Å, γ = 104.88(3)°.
Volume	1013.7(3) $Å^3$
Z	2
Density (calculated)	1.569 Mg/m^3
Absorption coefficient	1.025 mm^{-1}
F(000)	4963
Crystal size	0.2 × 0.5 × 0.6 mm^{-3}
Theta range for data collection	2.28 to 24.00°.
Index ranges	7≥h≥–9, 12≥k≥–12, 12≥l≥–13
Reflections collected	5998
Independent reflections	3133 [R(int) = 0.0270]
Completeness to theta = 24.00°	98.5 %
Absorption correction	Semi-empirical (ellipsoid)
Min. and max. transmission	0.51837and 0.61303
Refinement method	Full-matrix least-squares on F^2
Data / restraints / parameters	3133 / 0 / 264
Goodness-of-fit on F^2	1.059
Final R indices [$I > 2\sigma I$)]	R1 = 0.0384, wR2 = 0.1044
R indices (all data)	R1 = 0.0465, wR2 = 0.1064
Largest diff. peak and hole	0.755 and -0.440 e.$Å^{-3}$
Solution method	Direct methods

Table A2.5. Atomic coordinates (x 10^4) and equivalent isotropic displacement parameters ($Å^2$ x 10^3) for α-[Co(edda)bpy]Cl·$3H_2O$.

	x	y	z	U(eq)
Co(1)	8755(1)	8145(1)	6371(1)	18(1)
Cl(1)	-2487(2)	1607(1)	-365(1)	43(1)
O(1)	7407(3)	7720(2)	7294(2)	23(1)
O(2)	5194(4)	8032(3)	7678(3)	37(1)
O(3)	12829(3)	9515(3)	5698(2)	32(1)
O(4)	10120(3)	8598(2)	5467(2)	22(1)
N(1)	8136(4)	9654(3)	6462(3)	21(1)
N(2)	10846(4)	9167(3)	7927(3)	21(1)
N(3)	9157(4)	6554(3)	6320(3)	22(1)
N(4)	6784(4)	7136(3)	4739(3)	22(1)
C(1)	6350(5)	8330(3)	7297(3)	25(1)
C(2)	6583(5)	9429(4)	6778(4)	27(1)
C(3)	9669(5)	10755(3)	7415(3)	26(1)
C(4)	10552(5)	10309(3)	8499(3)	26(1)
C(5)	12366(5)	9466(4)	7581(3)	27(1)
C(6)	11764(5)	9186(3)	6152(3)	23(1)
C(7)	10421(5)	6320(4)	7192(4)	30(1)
C(8)	10490(6)	5140(4)	7100(4)	37(1)
C(9)	9233(6)	4136(4)	6088(4)	38(1)
C(10)	7920(6)	4352(4)	5186(4)	33(1)
C(11)	7906(5)	5568(3)	5321(3)	24(1)
C(12)	6586(5)	5909(3)	4411(3)	25(1)
C(13)	5260(5)	5060(4)	3286(4)	35(1)
C(14)	4096(6)	5473(4)	2475(4)	40(1)
C(15)	4328(5)	6730(4)	2792(4)	38(1)
C(16)	5690(5)	7538(4)	3922(4)	31(1)
OW1A	5134(18)	7368(18)	9805(11)	73(3)
OW1B	4620(20)	6750(20)	9458(15)	25(6)
OW2	246(5)	3896(4)	-421(4)	74(1)
OW3A	13155(11)	4116(11)	9186(11)	57(3)
OW3B	12714(13)	3413(14)	8564(14)	62(4)

A2.6. Δ-*RR*/ Λ-*SS*-β-[Co(edda)(bpy)](ClO$_4$) (Fig 5.6)

Crystals suitable for the diffraction study were produced by recrystallisation of the crude material from dilute $HClO_4$. All hydrogen atoms were placed in calculated positions and refined with a riding model. The refinement suffers from a very poor goodness-of-fit figure.

Collaborator	Prof Ward Robinson
Setup	1
Empirical formula	$C_{16}H_{18}ClCoN_4O_8$
Formula weight	488.72
Temperature	293(2) K
Wavelength	0.71073 Å
Crystal system	Monoclinic
Space group	P2(1)/c
Unit cell dimensions	a = 7.544(2) Å, α= 90°.
	b = 23.065(6) Å, β= 94.12(3)°.
	c = 10.963(4) Å, γ = 90°.
Volume	1902.7(10) Å^3
Z	4
Density (calculated)	1.706 Mg/m^3
Absorption coefficient	1.098 mm^{-1}
F(000)	1000
Crystal size	0.5 x 0.12 x 0.1 mm^3
Theta range for data collection	2.06 to 22.49°.
Index ranges	1≥h≥–8, –12≥k≥12, –11≥l≥–11
Reflections collected	2992
Independent reflections	2480 [R(int) = 0.0549]
Completeness to theta = 22.49°	100.0 %
Absorption correction	Empirical (ψ scans)
Min. and max. transmission	0.83156 and 0.91714
Refinement method	Full-matrix least-squares on F^2
Data / restraints / parameters	2480 / 0 / 271
Goodness-of-fit on F^2	0.410
Final R indices [I>2sigma(I)]	R1 = 0.0353, wR2 = 0.0478
R indices (all data)	R1 = 0.1234, wR2 = 0.0600
Largest diff. peak and hole	0.289 and -0.212 e.Å^{-3}
Solution method	Direct methods

Table A2.6. Atomic coordinates (x 10^4) and equivalent isotropic displacement parameters ($Å^2$ x 10^3) for β-[Co(edda)(bpy)](ClO_4).

	x	Y	z	U(eq)
Co	4407(1)	6124(1)	2305(1)	18(1)
O(1)	4835(6)	6275(2)	656(4)	23(1)
N(1)	2382(7)	6634(2)	1991(5)	20(2)
N(2)	5752(7)	6810(2)	2738(6)	22(2)
N(3)	3756(7)	5914(2)	3954(5)	17(2)
N(4)	3234(7)	5398(3)	1872(6)	20(2)
O(4)	6645(6)	5726(2)	2525(4)	19(1)
C(1)	3570(10)	6509(3)	-35(7)	25(2)
C(2)	1966(9)	6628(3)	646(6)	25(2)
C(3)	2852(9)	7214(3)	2505(7)	27(2)
C(4)	4767(9)	7327(3)	2276(7)	23(2)
C(5)	7608(8)	6719(3)	2309(7)	23(2)
C(6)	7978(9)	6081(4)	2419(6)	22(2)
C(7)	4011(8)	6222(3)	4994(6)	21(2)
C(8)	3555(9)	6026(4)	6108(6)	33(2)
C(9)	2809(9)	5482(3)	6161(7)	30(2)
C(10)	2525(9)	5156(3)	5103(7)	25(2)
C(11)	2980(9)	5382(3)	4005(6)	18(2)
C(12)	2679(9)	5087(3)	2828(7)	17(2)
C(13)	1974(10)	4547(3)	2684(7)	29(2)
C(14)	1775(10)	4306(3)	1517(7)	38(2)
C(15)	2282(10)	4634(3)	554(7)	35(2)
C(16)	3001(9)	5173(3)	757(7)	24(2)
O(2)	3574(7)	6590(2)	-1118(4)	38(2)
O(3)	9512(6)	5894(2)	2394(5)	27(1)
Cl	8817(3)	6882(1)	5453(2)	29(1)
O(5)	8253(6)	6319(2)	5014(4)	35(2)
O(6)	10495(6)	7028(2)	4971(5)	50(2)
O(7)	9049(7)	6877(2)	6767(4)	48(2)
O(8)	7536(7)	7313(2)	5014(5)	41(2)

A2.7 Δ-SS/Λ-RR-β-[Co(pdda)phen]Cl·3H_2O (Fig 5.4)

Slow cooling of a hot 0.1 M HCl solution of a sample of the crude complex produced crystals which were suitable for the diffraction study. The initial unit cell determination employed 25 reflections in the range $32.332 \geq 2\theta \geq 9.722$. Three check reflections were measured every 97 and the showed an abnormally large decay of 38.6 %. The intensities were adjusted to compensate for this. All hydrogen atoms were placed at calculated positions except those of the water molecules which were found on the electron difference density map. The interatomic distance of those atoms were restrained to sensible values.

Collaborator	Prof Ward Robinson
Setup	1
Empirical formula	$C_{19}H_{26}ClCoN_4O_7$
Formula weight	516.82
Temperature	293(2) K
Crystal description	Red block
Crystal system	Monoclinic
Space group	P2(1)/c
Unit cell dimensions	a = 8.715(6) Å, α= 90°.
	b = 10.229(5) Å, β= 96.17(4)°.
	c = 25.007(12) Å, γ = 90°.
Volume	2216(2) $Å^3$
Z	4
Density (calculated)	1.549 Mg/m^3
Absorption coefficient	0.944 mm^{-1}
F(000)	1072
Crystal size	0.63 × 0.40 × 0.25 mm^3
Theta range for data collection	2.15 to 24.99°.
Index ranges	3≥h≥–10, 12≥k≥0 29≥l≥–29
Reflections collected	5618
Independent reflections	3829 [R(int) = 0.0293]
Completeness to theta = 24.99°	98.3 %
Absorption correction	Empirical
Max. and min. transmission	0.27259 and 0.19964
Refinement method	Full-matrix least-squares on F^2
Data / restraints / parameters	3829 / 18 / 307
Goodness-of-fit on F^2	1.025
Final R indices [I > 2σ(I)]	R1 = 0.0413, wR2 = 0.1027
R indices (all data)	R1 = 0.0706, wR2 = 0.1291
Largest diff. peak and hole	0.935 and -0.707 $e.Å^{-3}$
Solution method	Direct methods

Table A2.7 Atomic coordinates (x 10^4) and equivalent isotropic displacement parameters ($Å^2$ x 10^3) for Δ-*SS*/Λ-*RR*-β-[Co(pdda)(phen)]Cl·$3H_2O$.

	x	y	z	U(eq)
Co	3665(1)	7008(1)	3447(1)	19(1)
O(1)	669(4)	6638(4)	2163(1)	45(1)
O(2)	2805(3)	6516(3)	2741(1)	25(1)
O(3)	7865(4)	5713(3)	3293(1)	33(1)
O(4)	5341(3)	5824(3)	3404(1)	24(1)
N(1)	1884(4)	8176(3)	3457(1)	23(1)
N(2)	4956(4)	8233(3)	3082(1)	23(1)
C(1)	1393(5)	6933(5)	2594(2)	29(1)
C(2)	695(5)	7787(5)	2999(2)	30(1)
C(3)	2163(6)	9615(4)	3481(2)	30(1)
C(4)	3094(6)	10104(5)	3032(2)	32(1)
C(5)	4776(6)	9689(4)	3114(2)	32(1)
C(6)	6604(5)	7790(4)	3173(2)	25(1)
C(7)	6670(5)	6347(5)	3294(2)	25(1)
N(3)	2496(4)	5604(3)	3764(1)	22(1)
N(4)	4412(4)	7405(3)	4213(1)	21(1)
C(8)	1609(5)	4674(4)	3520(2)	29(1)
C(9)	854(6)	3740(5)	3806(2)	36(1)
C(10)	1030(6)	3756(4)	4361(2)	31(1)
C(11)	1972(5)	4713(4)	4636(2)	24(1)
C(12)	2712(5)	5611(4)	4318(2)	21(1)
C(13)	2265(6)	4826(4)	5217(2)	29(1)
C(14)	3250(6)	5746(4)	5447(2)	29(1)
C(15)	3725(5)	6588(4)	4560(2)	19(1)
C(16)	4033(5)	6660(4)	5128(2)	23(1)
C(17)	5087(6)	7613(5)	5339(2)	30(1)
C(18)	5799(6)	8404(4)	4994(2)	29(1)
C(19)	5427(5)	8284(4)	4433(2)	25(1)
Cl	264(2)	3042(1)	618(1)	36(1)
OW1	4968(5)	3142(3)	3082(1)	39(1)
OW2	1817(5)	5698(4)	364(2)	51(1)
OW3	7329(5)	1765(4)	3648(2)	51(1)

A2.8. Δ-*SS*/Λ-*RR*-*Trans*(N)-[Co(ala)$_2$(bpy)](ClO$_4$)·H$_2$O (Fig 6.3)

Single crystals for the diffraction study were produced by the slow cooling of a hot saturated solution of the complex in dilute $HClO_4$. The initial unit cell determination used 27 strong reflections in the range $27.937 \geq 2\theta \geq 5.745$. The intensities of three standard reflections, measured every 97 reflections, showed no decay. The hydrogen atoms were placed in calculated positions and refined using a riding model with isotropic displacement parameters based on the U_{eq} of their attached atoms.

Collaborator	Prof Ward Robinson
Setup	1
Empirical formula	$C_{16}H_{22}ClCoN_4O_9$
Formula weight	508.76
Colour	Orange
Temperature	144(2) K
Crystal system	Monoclinic
Space group	P2(1)/c
Unit cell dimensions	a = 10.556(7) Å, α= 90°.
	b = 10.345(7) Å, β= 99.06(8)°.
	c = 18.62(3) Å, γ = 90°.
Volume	2008(3) Å^3
Z	4
Density (calculated)	1.683 Mg/m^3
Absorption coefficient	1.047 mm^{-1}
F(000)	1048
Crystal size	0.70 × 0.25 × 0.20 mm^3
Theta range for data collection	2.22 to 25.00°.
Index ranges	2≥h≥–12, 12≥k≥0, 22≥l≥–22
Reflections collected	3872
Independent reflections	3531 [R(int) = 0.0902]
Absorption correction	Empirical (ψ scans)
Max. and min. transmission	0.8179 and 0.5277
Refinement method	Full-matrix least-squares on F^2
Data / restraints / parameters	3531 / 0 / 294
Goodness-of-fit on F^2	1.035
Final R indices [I > 2σ(I)]	R1 = 0.0595, wR2 = 0.1116
R indices (all data)	R1 = 0.1134, wR2 = 0.1300
Largest diff. peak and hole	0.749 and -0.637 e.Å^{-3}
Solution method	Patterson

Table A2.8 Atomic coordinates (x 10^4) and equivalent isotropic displacement parameters ($Å^2$ x 10^3) for Δ-*SS*/Λ-*RR*-*trans*(N)-[Co(ala)$_2$(bpy)](ClO$_4$)·H$_2$O.

	x	y	z	U_{eq}
Co	8011(1)	8472(1)	1493(1)	21(1)
N(1)	9031(4)	7453(4)	2246(2)	28(1)
N(2)	7140(4)	9688(4)	791(2)	23(1)
O(2)	8024(3)	9754(3)	2217(2)	25(1)
O(3)	9547(3)	9194(4)	1268(2)	29(1)
C(1)	9515(6)	8272(6)	2881(3)	41(2)
C(2)	10920(6)	8321(7)	3036(5)	68(3)
C(3)	8883(5)	9603(5)	2786(3)	26(1)
C(4)	9391(6)	10149(6)	826(3)	35(2)
C(5)	8074(7)	10237(9)	368(5)	73(3)
C(6)	7727(6)	11405(6)	-47(3)	41(2)
O(1)	9158(4)	10432(4)	3251(2)	33(1)
O(4)	10253(4)	10898(4)	739(2)	43(1)
N(3)	7963(4)	7086(4)	806(2)	21(1)
N(4)	6424(4)	7734(4)	1664(2)	22(1)
C(7)	8770(5)	6902(5)	334(3)	28(1)
C(8)	8681(5)	5866(6)	-126(3)	30(1)
C(9)	7742(6)	4950(6)	-89(3)	30(1)
C(10)	6900(6)	5104(5)	400(3)	30(1)
C(11)	7023(5)	6203(5)	833(3)	22(1)
C(12)	6109(5)	6595(5)	1327(3)	24(1)
C(13)	4995(5)	5949(6)	1402(3)	33(1)
C(14)	4155(6)	6523(7)	1804(3)	38(2)
C(15)	4436(5)	7709(6)	2118(3)	36(2)
C(16)	5611(5)	8284(6)	2052(3)	29(1)
Cl	5292(1)	7963(1)	-948(1)	33(1)
O(5)	5386(5)	7946(5)	-176(3)	62(2)
O(6)	4027(4)	7568(5)	-1261(2)	58(1)
O(7)	5492(5)	9247(4)	-1181(3)	69(2)
O(8)	6212(4)	7125(4)	-1188(3)	57(1)
O(1W)	7728(6)	5570(6)	3023(3)	47(1)

A2.9 Trans(N)-$[Co(aib)_2bpy](ClO_4)\cdot NaClO_4\cdot 0.5H_2O$ (Fig 6.4)

X-ray quality crystals were produced by recrystallisation of the crude complex from dilute $HClO_4$. The initial unit cell determination used 15 strong reflections in the range $24.909 \geq 2\theta \geq 3.782$. The intensities of three standard reflections, measured every 497 reflections, showed 7.88% decay. Hydrogen atoms were placed in calculated positions and refined with a riding model.

Collaborator	Prof Ward Robinson
Setup	1
Empirical formula	$C_{18}H_{25}Cl_2CoN_4NaO_{12.5}$
Formula weight	650.24
Description	Red plates
Temperature	168(2) K
Crystal system	Triclinic
Space group	P-1
Unit cell dimensions	a = 8.776(3) Å, α= 76.904(14)°.
	b = 11.218(2) Å, β= 79.31(3)°.
	c = 14.186(3) Å, γ = 79.08(3)°.
Volume	1320.6(6) $Å^3$
Z	2
Density (calculated)	1.635 Mg/m^3
Absorption coefficient	0.937 mm^{-1}
F(000)	666
Crystal size	0.08 × 0.28 × 0.8 mm^3
Theta range for data collection	2.16 to 28.00°
Index ranges	$1 \geq h \geq -14$, $14 \geq k \geq -14$, $18 \geq l \geq -18$
Reflections collected	7521
Independent reflections	6367 [R(int) = 0.0590]
Completeness to theta = 28.00°	99.9 %
Absorption correction	None
Refinement method	Full-matrix least-squares on F^2
Data / restraints / parameters	6367 / 0 / 405
Goodness-of-fit on F^2	1.010
Final R indices [$I > 2\sigma(I)$]	R1 = 0.0704, wR2 = 0.1096
R indices (all data)	R1 = 0.1596, wR2 = 0.1371
Largest diff. peak and hole	0.581 and -0.450 $e.Å^{-3}$
Solution method	Direct methods

Table A2.9 Atomic coordinates (x 10^4) and equivalent isotropic displacement parameters ($Å^2$ x 10^3) for *trans*(N)-[Co(aib)$_2$(bpy)](ClO$_4$)·NaClO$_4$·0.5H$_2$O.

	x	y	z	U(eq)
Co	14771(1)	3220(1)	2849(1)	16(1)
O(1)	15638(4)	4541(3)	3020(2)	23(1)
O(2)	17048(5)	5119(3)	3934(3)	36(1)
O(3)	13009(4)	3643(3)	3773(2)	19(1)
O(4)	10930(4)	5056(3)	3998(2)	25(1)
N(1)	15812(5)	2236(3)	3928(3)	20(1)
N(2)	13649(5)	4390(4)	1877(3)	19(1)
C(1)	16800(6)	2973(5)	4253(4)	22(1)
C(2)	18541(6)	2486(5)	3958(4)	33(1)
C(3)	16456(7)	2880(5)	5363(4)	35(1)
C(4)	16469(6)	4326(4)	3719(4)	22(1)
C(5)	12026(6)	4597(4)	3451(3)	19(1)
C(6)	12248(6)	5138(4)	2350(3)	18(1)
C(7)	10785(6)	5050(6)	1959(4)	31(1)
C(8)	12533(7)	6480(4)	2188(4)	32(1)
N(3)	14000(5)	1801(4)	2663(3)	21(1)
N(4)	16454(5)	2767(4)	1862(3)	23(1)
C(9)	12666(7)	1414(5)	3099(4)	31(1)
C(10)	12195(8)	387(5)	2909(5)	40(2)
C(11)	13199(10)	-263(5)	2259(5)	53(2)
C(12)	14590(9)	126(6)	1815(5)	43(2)
C(13)	14973(7)	1178(5)	2015(4)	27(1)
C(14)	16362(7)	1740(5)	1555(4)	29(1)
C(15)	17510(8)	1305(6)	838(4)	46(2)
C(16)	18755(9)	1942(8)	454(5)	56(2)
C(17)	18818(7)	3018(7)	753(4)	48(2)
C(18)	17642(6)	3405(6)	1462(4)	33(1)
Na	8529(2)	6138(2)	4441(1)	24(1)
Cl(1)	7864(2)	8963(1)	3976(1)	43(1)
O(5)	8051(6)	9955(4)	3175(3)	51(1)
O(6)	9088(12)	8352(10)	4394(7)	45(2)
O(6')	9507(18)	8145(14)	3928(14)	65(6)
O(7)	7255(17)	8056(10)	3549(9)	91(5)

O(7')	6781(18)	8278(14)	4190(12)	62(5)
O(8)	6582(12)	9387(8)	4661(8)	85(4)
O(8')	8010(30)	9554(14)	4803(11)	129(9)
Cl(2)	6599(2)	6963(1)	10282(1)	32(1)
O(9)	7377(5)	7205(4)	9290(3)	36(1)
O(10)	5639(7)	8056(4)	10503(4)	74(2)
O(11)	7745(6)	6489(5)	10919(3)	64(1)
O(12)	5620(6)	6027(4)	10345(3)	56(1)
OW1	8746(14)	8426(10)	11510(8)	93(4)

References

[1]Ciamician G., *Science* **1912**, *36*, 385.

[2]Sýkora J., Sima J., *Coord. Chem. Rev.* **1990**, *107*.

[3]Balzani V., Bolleta F., Gandolfi M.T., Maestri M., *Top. Curr. Chem.* **1978**, *75*, 1.

[4]Vogler A., Kunkley H., *Angew. Chem. Int. Ed. Eng.* **1982**, *31*, 209.

[5]Cervone E., Diomedi-Camassei F., Giannini I., Sýkora J., *J. Photochem.* **1979**, *11*, 321.

[6](a) Scandola F. in *Rearrangements in Ground and Excited States (Vol. 3)*; Bernal (Ed), Academic Press: New York, 1980. (b) Scandola F., Bartocci C., Scandola A., *J. Am. Chem. Soc.* **1973**, *95*, 7898.

[7]Balzani V., Moggi L., *Coord. Chem. Rev.* **1990**, *97*, 313 and refs therein.

[8]Balzani V., Carassiti V., *Photochemistry of Coordination Compounds*; Academic Press: London, 1970.

[9]*J. Chem. Ed.* **1983**, *60*, 784-910.

[10]Porter G., *J. Chem. Soc. Faraday Trans. (II)* **1986**, *82*, 2445.

[11]Vanquickenborne L.G., Ceulemans A., *Coord. Chem. Rev.* **1983**, *48*, 157.

[12](a) *Coord. Chem. Rev.* **1991**, *111*, 1 - 348. (b) *Coord. Chem. Rev.* **1993**, *125*, 1 - 360. (c) *Coord. Chem. Rev.* **1994**, *132*, 1 - 264. (d) *Coord. Chem. Rev.* **1997**, *159*, 1 - 428. (e) *Coord. Chem. Rev.* **1998**, *171*, 1 - 491.

[13]Balzani V., Credi A., Venturi M., *Coord. Chem. Rev.* **1998**, *171*, 3.

[14]Balzani V., Scandola F., *Supramolecular Photochemistry*; Ellis Horwood: Chichester, UK, 1991.

[15]*Coord. Chem. Rev.* **1998**, *177*, 1 - 418.

[16]Fremy E., *Ann. Chem. Phys.* **1852**, *25*, 257.

[17](a) Werner A., *Zeits. Anorg. Chem.* **1893**, *3*, 267. (b) Kauffmann G.B., *Classics In Coordination Chemistry Part I: The Selected Papers of Alfred Werner*; Dover: New York, 1968.

[18]Shibata M., *Top. Curr. Chem.* **1983**, *110*, 1.

[19](a) Hipps K.W., Crosby G.A., *Inorg.Chem.* **1974**, *13*, 1543. (b) Miskowski V.M., Gray H.B., Wilson R.B., Solomon E.I., *Inorg.Chem.* **1979**, *18*, 1410. (c) Ford P.C., *Coord. Chem. Rev.* **1982**, *44*, 61.

[20]Langford C.H., Malkhasian A.Y.S., Sharma D.K., *J. Am. Chem. Soc.* **1984**, *44*, 61.

[21]McCusker J.K., Walda K.N., Magde D., Hendrickson D.N., *Inorg. Chem.* **1993**, *32*, 394.

[22](a) Endicott J.F., In *Concepts in Inorganic Photochemistry*; Adamson A.W., Fleischauer P., (Eds); Wiley: New York, 1975. (b) Langford C.H., *Acc. Chem. Res.* **1984**, *17*, 96.

[23]Manfrin M.F., Varani G., Moggi L., Balzani V., *Mol. Photochem.* **1969**, *1*, 387.

[24]Poznyak A.L., Pavlovskii V.I., *Angew. Chem. Int. Ed. Engl.* **1988**, *27*, 789.

[25](a) Poznyak A.L., Pavlovskii V.I., Chuklanova E.B., Polynova T.N., Porai-Koshits M.A., *Monatsh. Chem.* **1982**, *113*, 561. (b) Poznyak A.L., Pavlovskii V.I., Chuklanova E.B., Polynova T.N., Porai-Koshits M.A. *Koord. Khim.* **1988**, *14*, 103.

[26]Poznyak A.L., Stel'mashok V.E., *Zh. Neorg. Khim.* **1989**, *34*, 97.

[27]Poznyak A.L., Pansevich V.V., *Russ. J. Inorg. Chem.* **1991**, *36*, 1425.

[28]Natarajan E., Natarajan P., *Inorg. Chem.* **1992**, *31*, 1215.

[29]Kojima M., Akhter F. MD., Nakajima K., Yoshikawa Y., *Bull. Chem. Soc. Jpn.* **1996**, *69*, 2889.

[30]Pavlovskii V.I., Poznyak A.L., *Z. Chem.* **1989**, *29*, 6.

[31](a) Natarajan P., Endicott J.F., *J. Am. Chem. Soc.* **1973**, *95*, 2470. (b) Natarajan P., Endicott J.F., *J. Phys. Chem.* **1973**, *77*, 2049. (c) Langford C.H., Quance G.W., *Can. J. Chem.* **1977**, *55*, 3133.

[32]Poznyak A.L., Stel'mashok V.E., *Russ. J. Inorg. Chem.* **1981**, *26*, 1324.

[33]Poznyak A.L., Stel'mashok V.E., *Russ. J. Inorg. Chem.* **1991**, *36*, 806.

[34]Poznyak A.L., Pavlovskii V.I., *Z. Chem.* **1985**, *25*, 447.

[35]Pavlovskii V.I., Poznyak A.L., *Koord. Khim.* **1988**, *14*, 801.

[36]Tonei D.M.,Baker L.J., Brothers P.J., Clark G.R., Ware D.C., *Chem. Comm.* **1998**, 2953.

[37]Poznyak A.L., *Koord. Khim.* **1991**, *17*, 1261.

[38]Poznyak A.L., Stopolyanskaya L.V., *Russ. J. Inorg. Chem.* **1995**, *40*, 1080.

[39]Shkol'nikova L.M., Poznyak A.L., *Russ. J. Inorg. Chem.* **1995**, *40*, 582.

[40]Yonemura T., Kawaguchi H., Shibuya K., Murakami K., Ama T., Yasui T., Okamoto K., Hidaka J., *Bull. Chem. Soc. Jpn.* **1995**, *68*, 2287.

[41]Kawaguchi H., Yoshida M., Yonemura T., Ama T., Okamoto K., Yasui T., *Bull. Chem. Soc. Jpn.* **1995**, *68*, 874.

[42]Downs A.J., Greene T.M., *Adv. Inorg. Chem.* **1999**, *46*, 101.

[43](a) Meyerstein D., Schwarz H., *J. Chem. Soc. Faraday Trans(I)* **1988**, *84*, 2933 and refs therein. (b) Cohen H., Meyerstein D., Sorek Y., *J. Chem. Soc. Faraday Trans(I)* **1989**, *85*, 1169. (c) Endicott J.F., Roche T.S., *J. Am. Chem. Soc.* **1972**, *94*, 8622. (d) Mok C.Y., Endicott J.F., *J. Am. Chem. Soc.* **1978**, *100*, 123. (e) Tait A.M., Hoffman M.Z., Hayon E., *Int. J. Radiat. Phys. Chem.* **1976**, *8*, 691.(f) Bakac A., Espenson J.H. *J. Am. Chem. Soc.* **1984**, *106*, 5197. (g) Woska D.C., Wayland B.B., *Inorg. Chim. Acta* **1998**, *270*, 197.

[44]Simic M., Lilie J., *J. Am. Chem. Soc.* **1976**, *98*, 6516.

[45]Newcomb M., Glenn A.G. *J. Am. Chem. Soc.* **1989**, *111*, 275.

[46]Schmid P., Griller D., Ingold K.U., *Int. J. Chem. Kinet.* **1979**, *11*, 333.

[47](a) Griller D., Ingold K.U., *Acc. Chem. Res.* **1980**, *13*, 317. (b) Newcomb M., *Tetrahedron* **1993**, *49*, 1151.

[48] He M., Dowd P., *J. Am. Chem. Soc.* **1998**, *120*, 1133.

[49]Smith D.M., Nicolaides A., Golding B.T., Radom L., *J. Am. Chem. Soc.* **1998**, *120*, 10223.

[50]Martinez F.N., Schlegel H.B., Newcomb M., *J. Org. Chem.* **1996**, *61*, 8547.

[51]Martinez F.N., Schlegel H.B., Newcomb M., *J. Org. Chem.* **1998**, *63*, 3618.

[52]Horner J.H., Tanaka N., Newcomb M., *J. Am. Chem. Soc.* **1998**, *120*, 10379.

[53]Gilbert R., Smith S.C., *Theory of Unimolecular and Rearrangement Reactions*; Blackwell: Oxford, 1990.

[54]Laidler K.J., *Theories of Chemical Rection Rates*; McGraw-Hill: New York, 1969.

[55]Heuts J.P.A., PhD Thesis, University of New South Wales, 1996.

[56]For a review of the current status of TST, see: Truhlar D.G., Garret B.C., Klippenstein S.J., *J. Phys. Chem.* **1996**, *100*, 12771.

[57]Heuts J.P.A., Gilbert R.G., Radom L., *Macromolecules* **1995**, *28*, 8771.

[58]Bowry V.W., Lusztyk J., Ingold K.U., *J. Am. Chem. Soc.* **1991**, *113*, 5.

[59]Frisch M.J., Trucks G.W., Schlegel H.B., Gill P.M.W., Johnson B.G., Robb M.A., Cheeseman J.R., Keith T., Petersson G.R., Montgomery J.A., Raghvachari K., Al-Laham M.A., Zakrzewski V.G., Ortiz J.V., Foresman J. V., Cioslowski J., Stefanov B.B., Nanayakkara A., Challacombe M., Peng C.Y., Alaya P.Y., Chen W., Wong M.W., Andres J.L., Replogle E.S., Gomperts R., Martin R.L., Fox D.J., Binkley J.S., Defrees D.J., Baker J., Stewart J. P., Head-Gordon M., Gonzalez C., Pople J.A., GAUSSIAN94 (Rev. B.1); Gaussian Inc.: Pittsburgh, 1995.

[60]Scott A.P., Radom L., *J. Phys. Chem.* **1996**, *100*, 16502.

[61]Armstrong D.A., Rauk A., Yu D., *J. Am. Chem. Soc.* **1993**, *115*, 666, and refs therein.

[62]Nelson S.F., in *Free Radicals (Vol II)*; Kochi J. (Ed.); Wiley-Interscience: New York, 1973.

[63]Chow Y.L., Danen W.C., Nelsen F.S., Rosenblatt D.H., *Chem. Rev.* **1978**, *78*, 243.

[64]Carbanions are generally sp^3-hybridised. See: March J., *Advanced Organic Chemistry*; McGraw-Hill: New York, 1968.

[65]Newcomb M., Horner J.H., Emanuel C.J., *J. Am. Chem. Soc.* **1997**, *119*, 7147.

[66]Truhlar D.A., *J. Comput. Chem.* **1991**, *12*, 266.

[67]McQuarrie D.A., *Statistical Mechanics*; Harper & Row; New York, 1976.

[68]Bell R.L., Taveras D.L., Truong T.N., Simons J., *Int. J. Quant. Chem.* **1997**, *63*, 861.

[69]Glukhovtsev M.N., Bach R.D., Pross A., Radom L., *Chem. Phys. Lett.* **1996**, *260*, 550.

[70]Adam W., Heil M., *J. Am. Chem. Soc.* **1991**, *113*, 1730.

[71]Beckwith A.L.J., Bowry V.W., *J. Am. Chem. Soc.* **1994**, *116*, 2710.

[72]Newcomb M., Horner J.H., Filipkowski M.A., Ha C., Park S-U., *J. Am. Chem. Soc.* **1995**, *117*, 3.

[73]Poznyak A.L., Pavlovskii V.I., *Z. Anorg. Allg. Chem.* **1982**, *485*, 225.

[74]Lawson P.J., McCarthy M.G., Sargeson A.M., *J. Am. Chem. Soc.* **1982**, *104*, 6710.

[75]Tatehata A., *Inorg. Chem.* **1982**, *21*, 2497.

[76]Pavlovskii V.I., Poznyak A.L., *Russ J. Inorg. Chem.* **1980**, *25*, 422.

[77]Boone D.R., Kust R.N., Monroe M.B., *Polyhedron* **1989**, *3*, 49.

[78]Maki N., *Bull. Chem. Soc. Jpn.* **1969**, *42*, 2275.

[79]Buckingham D.A., Durham L., Sargeson A.M., *Aust. J. Chem.* **1967**, *20*, 257.

[80]Chuklanova E.B., Pavlovskii V.I., Polynova T.V., Porai-Koshits M.A., Poznyak A.L., *Koord. Khim.* **1988**, *14*, 103.

[81]Ji L.N., Ye B.H., Zeng T.X., *Polyhedron* **1994**, *13*, 2185.

[82](a) Bruce M.I., *Angew. Chem. Int. Ed. Eng.* **1977**, *16*, 73. (b) R.L. Sweany, In *Comprehensive Organometallic Chemistry (2nd Ed.)*; Abel E.W., Stone F.G.A., Wilkinson G. (Eds); Pergamon: Oxford, 1995.

[83] (a) Pouchert C.J., *The Aldrich Library of NMR Spectra, Ed.(II)*; Aldrich Chemical Co. Inc.: Milwaukee, Wisconsin, 1983. (b) Khusid A.K., Kryshtal G.V., Dombrovsky V.A., Kucherov V.F., Yanovskaya L.A., Kadentsev V.I., Chizhov O.S., *Tetrahedron* **1977**, *33*, 77.

[84] Poznyak A.L., Stelmashok V.E., *Inorg. Chim. Acta* **1984**, *83*, L59.

[85] Balzani V., Carassiti V., Moggi L., Sabbatini N., *Inorg. Chem.* **1965**, *4*, 1247.

[86]Toscano P.J., Marzilli L.G., In *Progress in Inorganic Chemistry*; Lippard S.J. (Ed); Interscience: New York, 1984.

[87]Hancock M.P., Josephsen J., Schäffer C.E., *Acta. Chem. Scand.* **1976**, *30*, 79.

[88]Iikura H., Nagata T., *Inorg. Chem.* **1998**, *37*, 4702.

[89]Okamoto M.S., Barefield E.K., *Inorg. Chim. Acta* **1976**, *17*, 91.

[90]Buckingham D.A., Clark C.R., In *Comprehensive Coordination Chemistry (Vol. 4)*; Wilkinson G. (Ed.); Pergamon: Oxford, 1987.

[91]Ama T., Okamoto K., Yonemura T., Kawaguchi H., Takeuchi A., Yasui T., *Chem. Lett.* **1997**, 1189.

[92]Meiske L.A., Angelici R.J., *Inorg. Chem.* **1980**, *19*, 3783.

[93]Albert A., *Heterocyclic Chemistry (2nd Ed.)*; Athlone Press: London, 1968.

[94]Chuklanova E.B., Polynova T.N., Porai-Koshits M.A., Poznyak A.L., Pavlovskii V.I., *Koord. Khim.* **1986**, *14*, 103.

[95]Poon C-K., Wan W-K., Liao S.S.T., *J. Chem. Soc. Dalton Trans.* **1977**, 1247.

[96]Polson S.M., Hansen L., Marzilli L.G., *J. Am. Chem. Soc.* **1996**, *118*, 4804.

[97]Poznyak A.L., Pavlovskii V.I., *Russ. J. Inorg. Chem.* **1981**, *26*, 292.

[98](a) Fontaine C., Duong K.N.V., Merienne C., Gaudemer A., Gianotti C., *J. Organomet. Chem* **1972**, *38*, 167. (b) Roewer G., Kempe G., Kolle B., Just R., *J. Prakt. Chem.* **1982**, *324*, 53. (c) Ramamurthy P., Natarajan P., *Inorg. Chem.* **1986**, *25*, 3554.

[99]Niederhoffer E.C., Timmons J.H., Martell A.E., *Chem. Rev.* **1984**, *84*, 137.

[100]Ref. 90, pp 775-789.

[101](a) Timmons J.H., Niswander R.H., Clearfield A., Martell A.E. *Inorg. Chem.* **1979**, *18*, 1042. (b) Timmons J.H., Niswander R.H., Clearfield A., Martell A.E. *Inorg. Chem.* **1979**, *18*, 2977.

[102]Sheldon R.A., Kochi J.K., *Metal-Catalysed Oxidations of Organic Componds*; Academic: New York, 1981.

[103]*Selective Hydrocarbon Activation*; Davies J.A., Watson P.L., Liebman J.F., Greenburg A., (Eds.); VCH: New York, 1990.

[104]Adduchi A.J., *CHEMTECH* **1976**, *6*, 575.

[105]Seo J.S., Hynes R.C., Williams D., Chin J., *J. Am. Chem. Soc.* **1998**, *120*, 9943.

[106]Kayatani T., Hayashi Y., Suzuki M., Uehara A., *Bull. Chem. Soc. Jpn.* **1994**, *67*, 2980.

[107]Suzuki M., Kanatomi H., Murase I., *Bull. Chem. Soc. Jpn.* **1984**, *57*, 36.

[108]Ama T., Okamoto K., Yonemura T., Kawaguchi H., *Chem. Lett.* **1997**, 29.

[109]Brubaker G.R., Schaeffer D.P., Worrell J.H., Legg J.I., *Coord. Chem. Rev.* **1971**, *7*, 161.

[110]Radanovic D.J., *Coord. Chem. Rev.* **1984**, *54*, 159.

[111]Poznyak A.L., Stel'mashok V.E., *Koord. Khim.* **1979**, *5*, 1670.

[112]Billing D.G., Carlton L., Dobson S.M., and Pattrick G., *Acta Cryst. C* **1991**, *47*, 1964.

[113]Caputo R.E., Halloran L.J., Legg J.I. & Willett R.D., *Inorg. Chem.* **1975**, *14*, 1762.

[114]Douglas B.E., Grujic S.A., Maricondi C., Parvez M., Radanovic D.J., Trifunovic S.R., *Inorg. Chim. Acta* **1989**, *137*, 33.

[115]Bianchini R.J., Geiser U., Legg J.I., Kaizaki S., Morita Y., Place H., *Inorg. Chem.* **1986**, *25*, 2129.

[116]Weakleim H.A., Hoard J.L., *J. Am. Chem. Soc.* **1959**, *81*, 549.

[117]Kuroda K., Watanabe K., *Bull. Chem. Soc. Jpn.* **1971**, *44*, 1034.

[118]Ye B-H., Zeng T-X., Han P., Ji L-N., *Transition Met. Chem.* **1993**, *18*, 515.

[119]Yasui T., *Bull. Chem. Soc. Jpn.* **1975**, *48*, 454.

[120]Cowan J.A., *Inorganic Biochemistry* (2*nd Ed.*); Wiley: New York, 1997.

[121]Pearson R.G., Figdore P.E., *J. Am. Chem. Soc.* **1980**, *102*, 1541.

[122]Frankel M., Knobler Y., *J. Am. Chem. Soc.*, **1958**, *80*, 3147.

[123]Pouchert C.J., Behnke J. (Eds), *Aldrich Library of FT-NMR Spectra* (*Ed .I*); Aldrich Chemical Company Inc.: USA, 1993.

[124]Gailey K.D., Igi K, Douglas B.E., *Inorg. Chem.* **1975**, *14*, 2956

[125]Kawaguchi H., Uchiyama N., Ama T., Yasui T., *Bull. Chem. Soc. Jpn.* **1990**, *63*, 3535.

[126](a) Legg J.I., Cooke D.W., Douglas B.E., *Inorg.Chem.* **1970**, *9*, 941. (b) Legg J.I, Cooke D.W., *Inorg. Chem.* **1965**, *4*, 1576.

[127]Igi K, Douglas B.E., *Inorg. Chem.* **1974**, *13*, 475

[128]Haydock D.B., Mullholland T.P.C., *J.Chem.Soc.(C)*, **1971** 2389.

[129]Kawaguchi H., Maruyama N., Ama T., Yasui T., *Bull. Chem. Soc. Jpn.* **1992**, *65*, 175.

[130]Shkolnikova L.M., Gasparayan A.V., Belskii V.K., Stel'mashok V.E., Poznyak A.L., Dyatlova N.M., *Kood. Khim.* **1987**, *13*, 823.

[131]Vogel A.I., *Qualitative Inorganic Analysis* (*7th Ed.*); Longman: London, 1996.

[132]Balzani V., Bolletta F., Gandolfi M.T., Maestri M., *Top. Curr. Chem.* **1978**, *75*, 1.

[133]Hoggard P.E., *Coord. Chem. Rev.* **1997**, *159*, 235.

[134]Natarajan E., Ramamurthy P., Natarajan P., *Proc. Indian Acad. Sci. (Chem. Sci.)* **1990**, *102*, 319. A PhD thesis was cited and no further details were given.

[135]Douglas B.E., Yasui T., *Inorg. Chem.* **1971**, *10*, 97.

[136]Matsuoka N., Hidaka J., Shimura Y., *Bull. Chem Soc. Jpn.* **1967**, *40*, 1868.

[137]Matsuoka N., Hidaka J., Shimura Y., *Inorg. Chem.* **1970**, *9*, 719.

[138]Ye B.H., Zeng T.H., Ping H., Ji L.N, Zhuang H.H., *Chinese Chem. Lett.* **1991**, *2* 529,

[139]Ye B., Zeng T., Han P., *Chem. Res. Chinese Univ.* **1993**, *9*, 220. (*Chem. Abs. 121,* 147579w)

[140]Maki N. *Electroanal. Chem.* 1974, *51*, 353.

[141]Margel S., Smith W., Anson F.C., *J. Electrochem. Soc.* **1978** *125* 241.

[142]Bond A.M., Colton R., McCormick M.J., *Inorg. Chem.* **1977**, *16*, 155.

[143] Bond A.M., Haddad R.A., *Inorg. Chem.* 1979 *18* 545.

[144]Sillen L.G., Martell A.E., Bjerrum J., *Stability Constants of Metal-Ion Complexes (2nd Ed.)*; Chemical Society: London, 1964.

[145]Cotton F.A., Wilkinson G.; '*Advanced Inorganic Chemistry*' 5th Ed; Wiley and Sons: London, 1988, pp 450-451.

[146]Gritzner G., Kuta J., *Pure Appl. Chem.* **1984**, *56*, 461

[147]Bonifacic M., Štefanic I., Hug G.L., Armstrong D.A., Asmus K-D., *J. Am. Chem. Soc.* **1998**, *120*, 9930 and refs therein.

[148]Armstrong D.A., Rauk A., Yu D., *J. Chem. Soc. Perkin Trans.(2)* **1995**, 553.

[149]Pincock J.A., *Acc. Chem. Res.* **1997**, *30*, 43 and refs therein.

[150]Yokoi H., Hakano T., Fujita W., Ishiguro K., Sawaki Y., *J. Am. Chem. Soc.* **1998**, *120*, 12453 and refs therein.

[151]Killer K-O., Asmus K-D., *J. Phys. Chem.* **1983**, *87*, 3682.

[152]Armstrong D.A., Rauk A., Yu D., *J. Am. Chem. Soc.* **1993**, *115*, 666.

[153](a) Kerr J.A., Loyd A.C., *Q. Rev. London* **1968**, *22*, 549. (b) Ingold K.U., In *Free Radicals (Vol. I)*; Kochi J. (Ed.); Wiley-Interscience: New York, 1973.

[154](a) Wimmer E., in *Density Functional Methods in Chemistry*; Labanowski J.K., Andzelm J.W. (Eds); Springer-Verlag: New York, 1991. (b) Chermette H., *Coord. Chem. Rev.* **1998**, *178-180*, 699. (c) Semenario J.M., Politzer P. (Eds); *Modern Density Functional Theory*; Elsevier: Amsterdam, 1995.

[155]Hohenburg P., Kohn W., *Phys. Rev. A.* **1964**, *136*, 864.

[156]Kohn W., Sham L.J., *Phys. Rev. A.* **1965**, *140*, 1133.

[157]Becke A.D., *Phys. Rev. A.* **1998**, *98*, 3098.

[158]Lee C., Yang C., Parr R.G., *Phys. Rev. B.* **1996** *37*, 785.

[159]*X*-Ray *S*ingle *C*rystal *An*alysis *S*ystem; Version 2.1; Siemens Analytical Instrument Inc.: Madison, Wisconsin, USA.

[160]Sheldrick G.M., *SHELXTL Structure Determination Programs Version 5.03*; Siemens Analytical Instruments Inc.: Madison, Wisconsin, 1994.

[161]Hamilton W.C., Ibers J.A. (Eds), *International Tables for Crystallography (C)*; Kynock Press: Birmingham, 1992.

[162]*SMART Version 5.045*; Data Collection Software; Siemens Analytical Instruments Inc.: Madison, Wisconsin, 1998.

References

[163]*SAINT Version 5.01*; Data Integration Software; Siemens Analytical Instruments Inc.: Madison, Wisconsin, 1998.

[164]Sheldick G.M.; *SADABS Version 5.01*; Programme for Empirical Absorption Correction of Area Detector Data; University of Göttingen, Germany, 1996.

[165]U(eq) is defined as one third of the trace of the orthogonalized U^{ij} tensor.